METABOLIC ENGINEERING OF

CLOSTRIDIUM AUTOETHANOGENUM

FUNG MIN LIEW, MSC

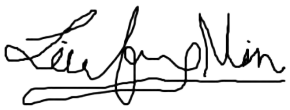
Thesis submitted to the University of Nottingham for the

Degree of Doctor of Philosophy

March 2016

Declaration

Unless otherwise acknowledged, the work presented in this thesis is my own. No part has been submitted for another degree in the University of Nottingham or any other institute of learning.



Fung Min Liew

March 2016

Abstract

Gas fermentation has emerged as a promising technology that converts waste gases containing CO, CO_2 and H_2 (also known as syngas) into fuels and chemical commodities. *Clostridium autoethanogenum* is one of the microorganisms known as acetogens capable of catalyzing such reactions. Employed by LanzaTech Inc. (USA) as a biocatalyst for industrial gas fermentation, this acetogen naturally converts syngas into ethanol, 2,3-butanediol (a platform chemical), acetate, and lactate. Metabolic engineering offers unique opportunities to eliminate side-products, synthesize novel, high-value molecules as diversification strategies, and increase productivities of natural products. However, there had been no scientific reports of genetic manipulation of this acetogen so the overall goal of this PhD project was to develop genetic tools for this gas-utilizing microorganism and construct a hyper-ethanol producing strain via metabolic engineering. The formulation of electroporation and conjugation procedures allowed exogenous DNA to be routinely introduced into the bacterial host. ClosTron mutagenesis and Allele-Coupled Exchange (ACE) techniques were fully exemplified in this bacterium during the construction of knockout, in-frame deletion, and overexpression mutants. Carbon monoxide dehydrogenases (*cooS1*, *cooS2* and *acsA*) were specifically targeted to elucidate their roles in supporting CO oxidation and carbon fixation. In the ethanol formation pathway, inactivation of bi-functional aldehyde/alcohol dehydrogenases (*adhE1* and *adhE2*) impaired growth on pure CO but elevated ethanol titres. Conversely, inactivation of the more highly expressed aldehyde:ferredoxin oxidoreductase (*aor1*), but not the weakly expressed *aor2*, significantly reduced ethanol production, highlighting the importance of *aor1* in autotrophic ethanol formation. A double KO mutant of *aor1* and *aor2* was also generated via ClosTron mutagenesis and *pyrE*-mediated allelic exchange. In an effort to engineer a robust biocatalyst, the native chaperone systems *groESL* and/or *grpE-dnaK-dnaJ* were overexpressed in *C. autoethanogenum*, resulting in enhanced tolerance towards ethanol, heat and salts. In summary, this study demonstrated the genetic tractability of *C. autoethanogenum* and revealed gene targets for future metabolic engineering of a hyper-ethanol producing acetogen.

Acknowledgements

I would like to express my greatest gratitude to LanzaTech Inc. for giving me the wonderful opportunity to pursue a PhD training program at the University of Nottingham, UK. In particular I would like to thank CSO and co-founder Dr. Sean Simpson and CEO Dr. Jennifer Holmgren for pulling the strings to make this happen. Studying in the UK for 4 years has really enriched my experience and broadened my knowledge of the UK and beyond.

At the Synthetic Biology Research Centre (SBRC) of University of Nottingham, my sincerest gratitudes to my academic supervisors Professor Nigel Minton, Associate Professor Klaus Winzer, and Dr. Anne Henstra for their guidance, brilliant ideas and advice. I am particularly grateful that they granted me the freedom to pursue various research avenues and be able to express my research interests, while still providing the support and supervision necessary to ensure progress was made. SBRC is an extraordinarily large, diverse and vibrant academic group, which means I always had access to technical support from post-docs and fellow PhD students. In particular I would like to thank Dr. Jonathan Baker for enlightening me the brave new world of Western Blots, Dr. Carolyn Meaney for enlightening me the procedures for Southern Blots, and Dr. Anne Henstra for his selfless guidance and support. It was also a great pleasure to work with members of the GasChem project: Craig, Bart, Pawel, Pete, James, Rob, Ronja, Florence, Erik, John, Louise, Tomas, Chris, and Sarah.

I am heavily indebted to my industry supervisor Dr. Michael Köpke for his tireless support, encouragements and brilliant advice thoughout this PhD program. Special appreciations to Nigel and Michael for reviewing my thesis despite their packed schedules. I also would like to express my gratitude to Mohammed, Sashini, Bakir, Simon, Rasmus and Naomi from LanzaTech for their support during my (perfectly timed) summer laboratory work in LanzaTech NZ.

Last but not least, I would like to thank my parents for their endless support and encouragements. I am particularly grateful to my fiancée, Lucia, for her cheers, patience and understandings.

Abbreviations

$\Delta G^{o'}$	Standard Gibbs free energy change
µF	Microfarads
µg	Microgram
µL	Microlitre
µM	Micromolar
ABE	Acetone-Butanol-Ethanol
ACE	Alllele-Coupled Exchange
Ack	Acetate kinase
ACS	Acetyl-CoA synthase
AcsA	CODH subunit of bi-functional CODH/ACS complex
AdhE	Bi-functional aldehyde/alcohol dehydrogenase
Aor	Aldehyde:ferredoxin oxidoreductase
asRNA	Antisense RNA
ATCC	American Type Culture Collection
ATP	Adenosine triphosphate
bSECIS	Bacterial selenocysteine insertion sequence
BOF	Blast oven furnace
CBP	Consolidated bioprocessing
CCR	Carbon catabolite repression
CDS	Coding sequence
cfu	Colony forming unit
CIRCE	Controlling inverted repeat of chaperone expression
Cla^R	Clarithromycin resistance
Cm^R	Chloramphenicol resistance
CO	Carbon monoxide
CO_2	Carbon dioxide
CoA	Coenzyme A
codA	Cytosine deaminase
CODH	Carbon monoxide dehydrogenase
CoFeSP	Corrinoid iron-sulfur protein
CRISPR	Clustered Regularly Interspaced Short Palindromic Repeats
dH_2O	Deionised water
DMSO	Dimethylsulfoxide
DNA	Deoxyribonucleic acid
DNase	Deoxyribonuclease
dNTP	Deoxyribonucleoside 5'-triphosphate
DSMZ	Deutsche Sammlung von Mikroorganismen und Zellkulturen (German Collection of Microorganisms and Cell Cultures GmbH)
DTT	Dithiothreitol
EDTA	Ethylenediaminetetraacetic acid
EJ	Exajoule
Em^R	Erythromycin resistance
FC	Fluorocytosine
Fdh	Formate dehydrogenase

FOA	5-Fluoroorotic acid
FRT	FLP recombinase target
fruA	Phosphotransferase system EII subunits for fructose
FTP	Fischer-Tropsch Process
FU	5-fluorouracil
g	Gravity
g	Gram
gDNA	Genomic deoxyribonucleic acid
GHA	Great homology arm
h	Hour
H_2	Hydrogen
HPLC	High-performance liquid chromatography
HrcA	Heat shock regulation at CIRCE elements
HSP	Heat shock protein
IFD	In-frame deletion
kb	Kilo base pair
kDa	Kilo Dalton
KEGG	Kyoto Encyclopedia of Genes and Genomes
KO	Knock-Out
kPa	Kilo Pascal
kV	Kilovolt
L	Litre
LB	Luria-Bertani
LHA	Left homology arm
logP	Octanol-water partition coefficient
M	Molar
MAGE	Multiplex Automated Genome Engineering
Mb	Mega base pair
MEK	Methyl ethyl ketone
MES	2-(N-morpholino)ethane sulphonic acid
MeTr	Methyltransferase
mg	Milligram
min	Minute
mL	Millilitre
mM	Millimolar
mRNA	Messenger ribonucleic acid
N_2	Nitrogen
NADH	Nicotinamide adenine dinucleotide
NCBI	National Centre for Biotechnology Information
NGS	Next generation sequencing
NTA	Nitrilotriacetic acid
NTC	Non-template control
O_2	Oxygen
OD_{600}	Optical density at 600 nm
ORF	Open reading frame
P_{acsA}	Promoter of *Clostridium autoethanogenum* carbon monoxide dehydrogenase

PAGE	Polyacrylamide gel electrophoresis
PBS	Phosphate-buffered saline
PCR	Polymerase chain reaction
PFL	Pyruvate formate lyase
PFOR	Pyruvate:ferredoxin oxidoreductase
P_{pfor}	Promoter of *Clostridium autoethanogenum* pyruvate:ferredoxin oxidoreductase
Pta	Phosphotransacetylase
pyrE	Orotate phosphoribosyl transferase
qRT-PCR	Quantitative reverse-transcriptase polymerase chain reaction
RAM	Retrotransposition activated marker
RBS	Ribosomal binding site
RHA	Right homology arm
RIN	RNA integrity number
RM	Restriction-Modification
RNA	Ribonucleic acid
Rnase	Ribonuclease
Rnf	Rhodobacter nitrogen fixation
RNP	Ribonuclear protein
rpm	Revolutions per minute
SDS	Sodium dodecyl sulfate
sec	Seconds
SHA	Short homology arm
SLP	Substrate level phosphorylation
SOE-PCR	Splicing by overlap extension polymerase chain reaction
T_a	Annealing tempearture
TAE	Tris base-acetic acid-EDTA buffer
THF	Tetrahydrofolate
T_m	Melting temperature
Tm^R	Thiamphenicol resistance
tRNA	Transfer RNA
UTR	Un-translated region
UV	Ultraviolet
v/v	Volume per volume
w/v	Weight per volume
WLP	Wood-Ljungdahl pathway
WT	Wild-type

List of Figures

Figure 1.1. Fluctuations of Brent crude oil and sugar prices between June 2005 and June 2015.. 1
Figure 1.2. Overview of the gas fermentation process. 6
Figure 1.3. Phylogenetic tree of acetogens, solventogenic *Clostridium* species and model bacterium.. 9
Figure 1.4. Wood-Ljungdahl Pathway.. 13
Figure 1.5. Scheme of metabolite production from gas fermentation using native and genetically engineered clostridia.. 19
Figure 2.1. Standard curves of qRT-PCR with various amount of cDNA template for assessments of amplification efficiency of each TaqMan probe and primers.. 57
Figure 2.2. The overall steps involved in the generation of ClosTron insertional mutant using plasmid pMTL007C-E2. 62
Figure 2.3. Vector map of pMTL84151-Δ*pyrE* for the deletion of *pyrE* gene in *C. autoethanogenum*. 64
Figure 3.1. Putative phosphotransferase systems (PTS) in *C. autoethanogenum*.. 76
Figure 3.2. Screening for *C. autoethanogenum fruA*::CTermB-1126s mutants..... 78
Figure 3.3. *C. autoethanogenum fruA* mutants are unable to utilize fructose as substrate.. 79
Figure 3.4. Testing of xylitol and D-mannitol toxicity in *C. autoethanogenum* WT and *fruA* mutant. 81
Figure 3.5. Screening and validation of *C. autoethanogenum pyrE*::CTermB-144s mutants.. 83
Figure 3.6. *C. autoethanogenum pyrE*::CTermB-144s mutants exhibit uracil auxotrophy.. 84
Figure 3.7. *C. autoethanogenum pyrE*::CTermB-144s mutants are resistant to FOA.. 85
Figure 3.8. Screening and validation of *C. autoethanogenum codA*::CTermB-532s mutants.. 86
Figure 3.9. *C. autoethanogenum codA*::CTermB-532s mutants are resistant to FC.... 87
Figure 3.10. Deletion of *pyrE* using ACE in *C. autoethanogenum*..... 89
Figure 3.11. Restoration of *C. autoethanogenum pyrE* mutants..... 91

Figure 4.1. Structures of (A) mono-functional CODH; and (B) bi-functional CODH/ACS complex.. 102
Figure 4.2. Gene arrangement of (A) *cooS1*; (B) *cooS2*; and (C) *acsA* in *C. autoethanogenum*.. 103
Figure 4.3. Screening and validation of ClosTron *cooS1*, *cooS2* and *acsA* mutants.. 105
Figure 4.4. *acsA* ClosTron mutant is unable to grow autotrophically on (A) 2 bar CO; and (B) 1.3 bar H_2 + 0.7 bar CO_2.. 106
Figure 4.5. Growth and metabolite profiles of the complemented *acsA* ClosTron mutant and plasmid control strains on 2 bar CO.. 108
Figure 4.6. Growth and metabolite profiles of *C. autoethanogenum* wild-type (WT) and the *acsA* ClosTron mutant on 10 g/L fructose as the carbon source.. 109
Figure 4.7. The change in biomass, headspace and metabolite levels between start and finish of mixotrophic growth experiment of *acsA* ClosTron mutant and WT on 10 g/L fructose and 2 bar CO.. 112
Figure 4.8. Reverse Wood-Ljungdahl Pathway (WLP) and mixotrophic growth of *acsA* ClosTron mutant.. 113
Figure 4.9. Restriction digest analysis of rescued plasmids pMTL83157 and pMTL83157-*acsA*^{full} from *C. autoethanogenum*.. 114
Figure 4.10. The effect of *acsA* overexpression on growth and metabolite profiles of *C. autoethanogenum* on 2 bar CO.. 115
Figure 4.11. The effect of *acsA* overexpression on growth and metabolite profiles of *C. autoethanogenum* on 10 g/L fructose.. 116
Figure 4.12. Nucleotide alignment of *acsA* and internal stop codon in *C. autoethanogenum*.. 117
Figure 4.13. Restriction digest analysis of rescued *acsA* plasmids from (A) *C. autoethanogenum* transconjugants; (B) *C. acetobutylicum* transformants.. 120
Figure 4.14. Examination of AcsA translation pattern using FLAG-tagged protein in *C. autoethanogenum*, *C. acetobutylicum*, and *E. coli*.. 122
Figure 4.15. Growth and metabolite profiles of *C. autoethanogenum* WT, and ClosTron *cooS1* and *cooS2* mutants on 2 bar CO.. 125
Figure 4.16. Growth and metabolite profiles of *C. autoethanogenum* WT and *cooS1* ClosTron mutant on BOF gas.. 125

Figure 4.17. Growth and metabolite profiles of *C. autoethanogenum* WT and ClosTron *cooS1* and *cooS2* mutants under H_2 + CO_2 conditions..... 126
Figure 4.18. Screening of *cooS2* ClosTron mutants and *cooS1* single crossover in-frame deletion (IFD) mutants.. 128
Figure 4.19. The inactivation of CODH/ACS in *C. autoethanogenum* generates excess reducing equivalents..... 133
Figure 5.1. Gene arrangement of *adhE1* and *adhE2* in *C. autoethanogenum* with predicted catalytic domains, promoter elements, transcriptional terminator, ribosomal binding sites and ClosTron insertion sites. 145
Figure 5.2. Screening and validation of *adhE1a*, *adhE1b*, and *adhE2* ClosTron mutants.. 146
Figure 5.3. Growth and metabolite profiles of *adhE1a, adhE1b* and *adhE2* ClosTron mutants on CO.. 147
Figure 5.4. Growth and metabolite profiles of *C. autoethanogenum* WT and *adhE1a* mutant on BOF gas..... 148
Figure 5.5. Growth and metabolite profiles of *C. autoethanogenum* WT and *adhE* ClosTron mutants growing on fructose.. 149
Figure 5.6. Screening of *C. autoethanogenum* Δ*adhE1*^{mut}, Δ*adhE1* and Δ*adhE1+2* mutants.. 151
Figure 5.7. Growth, metabolite and *adhE2* transcript profiles of *C. autoethanogenum* Δ*pyrE* and Δ*adhE1*^{mut} strains growing on fructose.. 154
Figure 5.8. Growth and metabolite profiles of *C. autoethanogenum* Δ*pyrE* and Δ*adhE1*^{mut} strains on CO.. 155
Figure 5.9. Nucleotide and deduced amino acid alignment of *adhE* between *C. autoethanogenum* and *C. ljungdahlii*. 157
Figure 5.10. Proposed change in metabolic route to ethanol formation in *C. autoethanogenum adhE* mutants under autotrophic conditions.. 162
Figure 6.1. Gene arrangement and alignment of *C. autoethanogenum aor1* and *aor2* 169
Figure 6.2. Screening and validation of *aor1* and *aor2* ClosTron Mutants..... 170
Figure 6.3. Verification of complemented and overexpressed *aor1* mutants.. 171

Figure 6.4. Growth and metabolite profiles of *C.* autoethanogenum WT, *aor1* and *aor2* ClosTron mutants on CO..... 173
Figure 6.5. Growth and metabolite profiles of *C. autoethanogenum* WT and the *aor2* ClosTron mutant on BOF gas.. 174
Figure 6.6. Growth and metabolite profiles of *C. autoethanogenum* WT, ClosTron *aor1* and *aor2* mutants growing on fructose..... 175
Figure 6.7. The effect of plasmid-borne *aor1* overexpression on *C. autoethanogenum* during fructose fermentation.. 177
Figure 6.8. The effects of plasmid-borne *aor1* overexpression on *C. autoethanogenum* on CO..... 178
Figure 6.9. Screening and validation of *aor* double KO mutants with restored *pyrE*.. 179
Figure 7.1. Schematic showing the involvement of chaperones in refolding nascent and misfolded proteins.. 190
Figure 7.2. Gene organization of chaperones in *C. autoethanogenum*..... 191
Figure 7.3. Gel electrophoresis showing the expected restriction digest bands from rescued plasmids of *C. autoethanogenum* transconjugants.. 194
Figure 7.4. Growth and metabolite profiles of unchallenged *C. autoethanogenum* chaperone overexpression strains on fructose.. 195
Figure 7.5. Normalized gene expression levels of chaperones during early-, mid- and late-growth phases of *C. autoethanogenum* chaperone overexpression strains growing on fructose.. 197
Figure 7.6. Growth and metabolite profile of unchallenged *C. autoethanogenum* chaperone overexpression strains on CO.. 198
Figure 7.7. Effect of chaperone overexpression on growth and cfu/mL of *C. autoethanogenum* when challenged with ethanol on CO..... 201
Figure 7.8. Chaperone overexpression enhances viable cell counts (cfu/mL) of *C. autoethanogenum* at 42^{o}C following incubation for 5 days..... 203
Figure 7.9. The effect of chaperone overexpression on growth of *C. autoethanogenum* in the presence of high salt concentrations under heterotrophic conditions..... 204

Figure 8.1. Comparison of peak ethanol and 2,3-butanediol production during growth of *C. autoethanogenum* mutants on pure CO.. 236

List of Tables

Table 1.1. Acetogens 10
Table 1.2. Genetically modified solventogenic clostridia and acetogens 31
Table 2.1. Bacterial strains used in this work. 37
Table 2.2. Plasmids used in this study 39
Table 2.3. Oligonucleotides used in this study 41
Table 2.4. Clostridial growth medium (CGM) 46
Table 2.5. Wolfe's vitamin solution 46
Table 2.6. Trace metal solution 47
Table 2.7. Reducing agent stocks 47
Table 2.8. Antibiotic and supplement used in this study 48
Table 2.9. Primers and TaqMan MGB probes used in this study 57
Table 3.1. Electroporation efficiency of *C. ljungdahlii* 71
Table 3.2. Comparison of Restriction Methylation systems between *C. autoethanogenum* and *C. ljungdahlii.* 73
Table 3.3. Conjugation efficiencies in *C. autoethanogenum* using *E. coli* CA434 as donor 74
Table 7.1. The effect of chaperone overexpression on tolerance of microorganisms. 192
Table 7.2. Putative DnaK binding sites within proteins that participate in biosynthesis of ethanol and 2,3-butanediol in *C. autoethanogenum*. 206

Table of Contents

Declaration……I

Abstract……II

Acknowledgements……III

Abbreviations……IV

List of Figures……VII

List of Tables……XI

1 Introduction 1

1.1 Introduction 1

1.2 Overview of Past and Present Biofuels 2

1.3 The Emergence of Gas Fermentation Technologies 5

1.4 The Genus *Clostridium* 7

1.5 The Wood-Ljungdahl Pathway (WLP) and Energy Conservation 11

1.5.1 Carbonyl- and Methyl- Branch of WLP 12

1.5.2 Hydrogenase 13

1.5.3 Carbon Monoxide Dehydrogenase (CODH) 15

1.5.4 Energy Conservation in WLP 15

1.5.5 Attempts at Installation of WLP into Non-Acetogens 16

1.6 Solventogenesis 17

1.6.1 From Acetyl-CoA to Butyryl-CoA 19

1.6.2 Reassimilation of Carboxylic Acids 20

1.6.3 Indirect Alcohol Production via Aldehyde:Ferredoxin Oxidoreductase (AOR) 21

1.6.4 Alcohol Dehydrogenase (Adh) 22

1.6.5 Production of 2,3-Butanediol 23
1.6.6 Production of Acylate and Propionate 24
1.6.7 Biosynthesis of Long-Chain Fatty Acids and Higher Alcohols 24
1.7 Genetic Tools for *Clostridium* 25
1.7.1 Knockdown of Target Genes via Antisense RNA (asRNA) 27
1.7.2 Intron-Based Gene Inactivation 27
1.7.3 Precise Genetic Manipulation via Allelic-Exchange 28
1.7.4 Transposon Mutagenesis 29
1.7.5 Metabolic Engineering of Solventogenic Clostridia 30
1.7.6 Recent Developments in Genetic Tools for Acetogens 32
1.8 Aims of PhD Project 34
2 Materials and Methods 37
2.1 Materials 37
2.1.1 Bacterial Strains 37
2.1.2 Plasmids 39
2.1.3 Oligonucleotide Primers 41
2.2 Bioinformatics Tools 44
2.3 Data Analysis and Presentation 45
2.4 General Microbiological Techniques 45
2.4.1 Growth Medium 45
2.5 General Molecular Techniques 48
2.5.1 Generation of Genomic DNA from Clostridial Species 48
2.5.2 Southern Blot Analysis 49
2.5.3 Preparation of Plasmid DNA from *E. coli* and Clostridial Species 50
2.5.4 Quantification, Separation and Visualization of Nucleic Acids 50
2.5.5 Polymerase Chain Reaction (PCR) 50

2.5.6 Restriction Digest, Dephosphorylation and Ligation of DNA Fragments 51
2.5.7 DNA Fragment Sequencing 51
2.5.8 Preparation and Transformation of Chemically Competent *E. coli* Cells 52
2.6 Serum Bottle Growth Experiments of *C. autoethanogenum* 52
2.7 Ethanol Tolerance Assay of *C. autoethanogenum* 53
2.8 Analytical Chemistry 54
2.8.1 High Performance Liquid Chromatography (HPLC) 54
2.8.2 Gas Chromatography 54
2.9 Quantitative Reverse Transcriptase Polymerase Chain Reaction (qRT-PCR) 54
2.9.1 Harvest of *C. autoethanogenum* Cultures for qRT-PCR Analysis 54
2.9.2 Total RNA Extraction 55
2.9.3 cDNA Synthesis 56
2.9.4 Design and Testing of TaqMan Primers and Probes 56
2.9.5 Real-Time PCR 58
2.10 Preparation of Crude Lysates 58
2.11 Sodium Dodecyl Sulphate –Poly-Acrylamide Gel Electrophoresis 59
2.12 Development of Transformation Protocols for *Clostridium spp.* 60
2.12.1 Preparation of Electro-Competent *C. autoethanogenum* and *C. ljungdahlii*, and Electroporation 60
2.12.2 Preparation of *C. acetobutylicum* Electro-Competent Cells and Electroporation 60
2.12.3 Conjugation 61
2.12.4 Verification of *Clostridium spp.* Transformants 61
2.13 Generation of *C. autoethanogenum* ClosTron Mutants 61
2.13.1 Intron Design and Synthesis of ClosTron Plasmids 61

2.13.2 Generation and Verification of *C. autoethanogenum* ClosTron Mutants 63

2.14 Allele-Coupled Exchange (ACE) 63

2.14.1 Generation of *C. autoethanogenum* Δ*pyrE* Strain 63

2.14.2 Construction of In-Frame Deletion Plasmids and *pyrE* Restoration Plasmids 65

2.14.3 Implementation of In-Frame Deletion Protocol Using *pyrE* as Selectable Marker 66

2.14.4 Restoration of *pyrE* Locus 67

3 Development of Genetic Tools for *Clostridium autoethanogenum* 69

3.1 Introduction 69

3.2 Development of Transformation Methodologies for *C. autoethanogenum* 69

3.2.1 Electroporation of *C. ljungdahlii* 70

3.2.2 Electroporation of *C. autoethanogenum* 71

3.2.3 Conjugation of *C. autoethanogenum* 73

3.2.4 Exemplification of ClosTron Mutagenesis by Targeting *fruA* 75

3.2.5 Testing of Counter-Selectable Markers 81

3.2.6 Generation of Δ*pyrE* Mutant using ACE 88

3.2.7 Restoration of *pyrE* using ACE 90

3.3 Discussion 91

3.3.1 *C. autoethanogenum* is Genetically Tractable via Conjugation (and Electroporation) 91

3.3.2 Exemplification of ClosTron Mutagenesis by the Construction of *fruA* Mutant 93

3.3.3 Exploration of *fruA* as Counter Selectable Marker 95

3.3.4 Testing of Counter-Selectable Markers *pyrE* and *codA* 95

3.3.5 Generation of Δ*pyrE* Mutant and Its Subsequent Restoration using ACE 97

3.4 Chapter Summary 98

4 Generation and Characterization of Carbon Monoxide Dehydrogenase Mutants 101

4.1 Introduction 101

4.2 Generation of ClosTron Knockout Mutants of *cooS1*, *cooS2* and *acsA* 104

4.3 Characterization of ClosTron *acsA* Knockout Mutant 105

4.3.1 Autotrophic Growth Experiments 105

4.3.2 Complementation of *acsA* ClosTron Mutants 106

4.3.3 Heterotrophic Growth Experiments 108

4.3.4 Mixotrophic Growth Experiments on Fructose and Carbon Monoxide 110

4.3.5 Mixotrophic Growth Experiments on Carbon Monoxide and Acetic Acid 112

4.4 Plasmid Overexpression of *acsA* 114

4.4.1 Construction of *acsA* Plasmid Overexpression Strain 114

4.4.2 Autotrophic Growth Experiments on Carbon Monoxide 115

4.4.3 Heterotrophic Growth Experiments 116

4.5 Investigation of *C. autoethanogenum acsA* Translational Read-Through 116

4.5.1 Construction of FLAG-Tagged *acsA* Variants 118

4.5.2 Expression of FLAG-Tagged AcsA Variants 119

4.6 Characterization of *cooS1* and *cooS2* ClosTron Mutants 124

4.6.1 Autotrophic Growth Experiments 124

4.7 Attempt at Generation of Double Knockout Mutant of *cooS1* and *cooS2* 127

4.8 Discussion 129

4.8.1 *acsA* is Empirical for Autotrophy in *C. autoethanogenum* 129

4.8.2 Plasmid Overexpression of AcsA Reduced Growth Lag Phase in CO and Increased Biomass in Fructose 131

4.8.3 KO of *acsA* Shifted Carbon and Electrons from Biomass and Acetate into the Products Ethanol and 2,3-Butanediol Under Heterotrophic Conditions 132

4.8.4 No Evidence of CO Oxidation by *cooS1* and/or *cooS2* in *acsA* KO Mutant Mixotrophic Growth Experiments 134

4.8.5 Partial Translational Read-Through in *acsA* of *C. autoethanogenum* 135

4.8.6 *cooS1* ClosTron Mutant Grows Better in H_2+CO_2 Conditions and Produces More Ethanol in the Presence of CO than WT 138

4.8.7 Autotrophy and Product Formation of *cooS2* Mutant is Not Significantly Affected 139

4.8.8 Attempt at Generation of Double KO *cooS1* and *cooS2* Mutant 139

4.9 Chapter Summary 140

5 Generation and Characterization of Bi-functional Aldehyde/Alcohol Dehydrogenase Mutants 143

5.1 Introduction 143

5.2 Generation of ClosTron Knockout Mutants *adhE1a*, *adhE1b* and *adhE2* 145

5.3 Characterization of ClosTron *adhE1a*, *adhE1b* and *adhE2* Mutants 146

5.3.1 Autotrophic Growth Experiment on CO 146

5.3.2 Heterotrophic Growth Experiment 148

5.4 Generation of Δ*adhE1* and Δ*adhE1+2* In-Frame Deletion Mutants 149

5.5 Characterization of Δ*adhE1*^{mut} Mutants 152

5.5.1 Heterotrophic Growth Experiment and Gene Expression of *adhE2* 152

5.5.2 Autotrophic Growth Experiment 154

5.6 Discussion 155

5.6.1 Unlike *C. ljungdahlii,* Inactivation of *adhE1* in *C. autoethanogenum* Does Not Affect Ethanol Production Under Heterotrophic Conditions 155

5.6.2 Inactivation of *adhE2* in *C. autoethanogenum* Reduced Fructose Utilization and Ethanol Formation Under Heterotrophic Conditions 158

5.6.3 Inactivation of Either *adhE1* or *adhE2* in *C. autoethanogenum* Increased Ethanol Production In the Presence of CO 159

5.6.4 Effects of *adhE* Inactivation on Solventogenesis and ATP Synthesis Under Autotrophic Conditions 161

5.7 Chapter Summary 163

6 Generation and Characterization of Aldehyde:Ferredoxin Oxidoreductase Mutants 167

6.1 Introduction 167

6.2 Generation of ClosTron Knockout Mutants *aor1* and *aor2* 169

6.2.1 Generation of *aor1* Complementation and Overexpression Mutants 170

6.3 Characterization of ClosTron Knockout Mutants *aor1* and *aor2* 171

6.3.1 Autotrophic Growth Experiment 171

6.3.2 Heterotrophic Growth Experiment 174

6.4 Plasmid Overexpression of *aor1* 175

6.4.1 Comparison of *aor1* mRNA during Heterotrophic Growth using qRT-PCR 175

6.4.2 Autotrophic Growth Experiment 177

6.5 Attempt at Generation of a *aor1* and *aor2* Double Knockout Mutant 179

6.6 Discussion 181

6.6.1 Inactivation of *aor1* Diminished Ethanol Production under Autotrophic and Heterotrophic Conditions 181

6.6.2 Plasmid Overexpression of *aor1* Had No Positive Impact on Ethanol Formation under Autotrophic and Heterotrophic Conditions 182

6.6.3 Inactivation of *aor2* Increased Ethanol Production under Autotrophic and Heterotrophic Conditions 183

6.6.4 Generation of *aor1+2*KO Mutant 184

6.7 Chapter Summary 185

7 Effect of Chaperone Overexpression on Product Formation and Tolerance towards Ethanol, Heat, and Saline 188

7.1 Introduction 188

7.2 Construction of Chaperone Overexpression Strains in *C. autoethanogenum* 192

7.3 Heterotrophic Growth Experiments and Chaperone Gene Expression Studies 194

7.4 Autotrophic Growth Experiments 197

7.4.1 Ethanol Challenge Assay under Autotrophic Conditions 199

7.4.2 Heat Stress Plating Assay 202

7.4.3 Salinity Stress Growth Experiment 203

7.5 Discussion 205

7.5.1 Enhanced Ethanol and 2,3-Butanediol Titres from DnaKJE Overexpression During Fructose Growth 205

7.5.2 Molecular evidence for Increased Chaperone Gene Overexpression in Recombinant Strains While Metabolizing Fructose 209

7.5.3 Co-Overexpression of DnaKJE and GroESL Chaperones Increases Ethanol Production during CO Growth 211

7.5.4 Overexpression of Chaperones under Autotrophic Conditions Enhanced Tolerance towards Ethanol in the Early-Phase of Ethanol Challenge Assay 212

7.5.5 Chaperone Overexpression Enhances Tolerance of *C. autoethanogenum* towards Thermal Stress and High Salinity 215

7.6 Chapter Summary 216

8 Summary Discussion 219

8.1 Introduction 219

8.2 Development of Genetic Tools for *C. autoethanogenum* 219

8.3 Characterization of CODHs in *C. autoethanogenum* 222

8.4 Elucidation of Ethanologenic Pathway of *C. autoethanogenum* 224

8.4.1 Characterization of *adhE* Mutants 225

8.4.2 Characterization of *aor* Mutants 227

8.5 Impact of Chaperone Overexpression on Ethanol, Heat and Saline Tolerance of *C. autoethanogenum* 230

8.6 Generation of Robust, Hyper-Ethanol Producing Strains and Future Studies 234

8.7 Conclusion 238

9 References 240

CHAPTER 1

INTRODUCTION

1 Introduction

1.1 Introduction

From a pre-2008 global financial crisis high of US$134 per barrel (July 2008), the price of Brent crude oil (per barrel) plunged to US$45 (January 2009) before recovering at the US$95-125 mark between January 2011 and September 2014 (Figure 1.1). Imbalance in supply and demand of global oil recently reduced the price to US$48 in January 2015 (www.indexmundi.com). This level of price volatility not only highlights the uncertain nature of global oil supply but also contributes significantly to instability in the global economies. The inherently finite nature of fossil fuels and an increasing global population (hence demand for fossil fuels) translates into the inevitable increase in pressure for greater oil supply. This, coupled with the deleterious environmental impacts that result from the accumulating atmospheric CO_2 generated by the burning of fossil fuels, has driven an urgent requirement for the development of affordable and environmentally sustainable fuels.

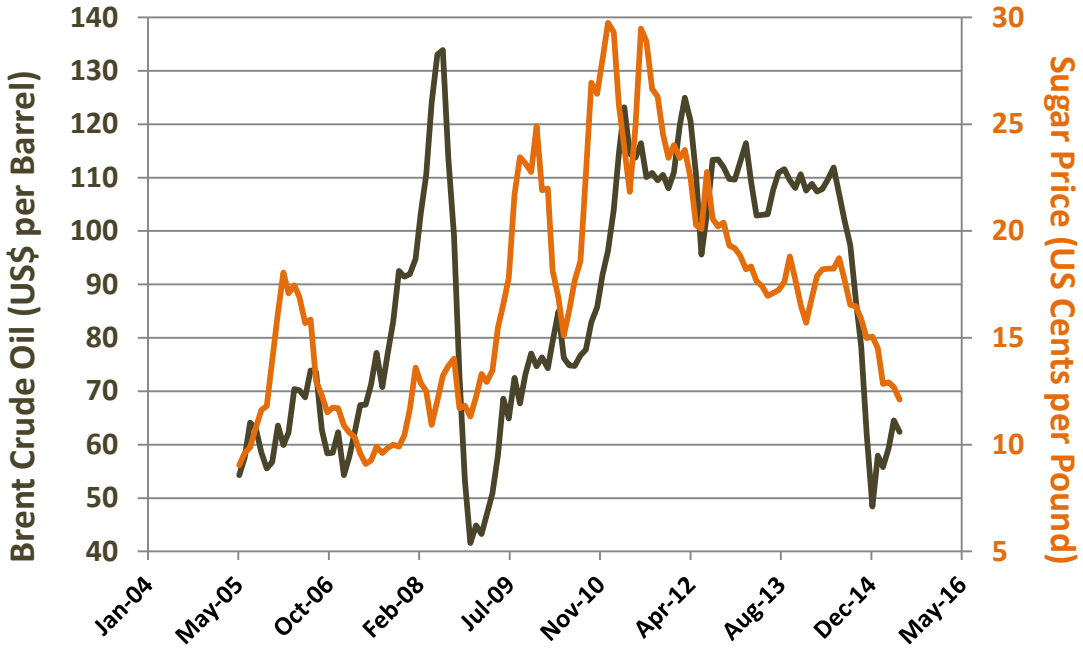


Figure 1.1. Fluctuations of Brent crude oil (grey) and sugar (orange) prices between June 2005 and June 2015. Source: www.indexmundi.com.

Amongst the plethora of renewable technologies that aim to reduce the world's dependence on fossil fuels, gas fermentation has emerged as one of the more promising technologies that could have a real impact in tackling this issue. Gas fermentation is the microbial process which converts synthesis gas (or syngas) into fuels and chemicals. Syngas consists of CO, H_2 and CO_2 and is generated via the gasification of carbonaceous materials at high temperature. Globally three major companies (INEOS Bio, Coskata, and LanzaTech) are actively engaged in the development of gas fermentation technology and are at various stages of commercialization. For instance, LanzaTech has secured investment from China Steel Corporation to build a commercial scale facility (34 M gallons ethanol per annum) in Taiwan (1), and partnered with ArcelorMittal and Primetals Technologies to build a 47000 tons ethanol per annum commercial facility in Ghent, Belgium (2).

This chapter explores the use of syngas and industrial waste gas as feedstocks to produce not only biofuels, but also other high-value added products. The advantages and disadvantages of gas fermentation over conventional sugar-based fermentation and thermochemical conversions will also be discussed. The biochemistry, genetic and energetic background of the microorganisms that perform this bioconversion process will be critically examined, together with recent advances in systems biology and synthetic biology that offer growing opportunities to improve the biocatalysts.

1.2 Overview of Past and Present Biofuels

Biofuels have been defined as solid (bio-char), liquid (bioethanol, biobutanol, and biodiesel) and gaseous (biogas, biosyngas, and biohydrogen) fuels that are mainly derived from biomass (3). Liquid biofuels provide a small but growing contribution towards worldwide fuel usage, accounting for 2.7% of global road transport fuels in 2010 (4). The world's largest producer of biofuels is the United States (U.S.), followed by Brazil and the European Union (E.U.) (4). In 2009, U.S. and Brazil accounted for approximately 85% of global bioethanol production while Europe generated about 85% of the world's biodiesel (5). The global market for liquid biofuels (bioethanol and

biodiesel) increased dramatically in recent years, reaching US$83 billion in 2011 and is projected to be US$139 billion by 2021 (6).

The advent of beer brewing in Mesopotamia in 5000 B.C. means that the fermentative production of ethanol has been used for thousands of years. In contrast the fermentative production of another potential biofuel butanol, was only discovered just over a century ago. Nevertheless, its discovery and implementation had significant impact. During the World War 1, Chaim Weizmann successfully applied a process called ABE (acetone-butanol-ethanol) fermentation using *Clostridium acetobutylicum* to generate industrial scale acetone (for cordite, the propellant of cartridges and shells) from starchy materials (5, 7, 8). His contribution was later recognised in the Balfour declaration in 1917 and he became the first president of the newly founded State of Israel (5, 7). Intriguingly, the enormous potential of butanol produced at that time was not realized and the substance was simply stored in huge containers (5). ABE fermentation became the second biggest ever biotechnological process (after the ethanol fermentation process) ever performed, but the low demand for acetone following the conclusion of the war led to closure of all the plants (7, 8). Although ABE fermentation briefly made a comeback during the Second World War, increasing substrate costs and increasing stable supply of low cost crude oil from the Middle East rendered the technology economically unviable. Recently, a resurgence of the technology is underway as some old plants are reopened and new plants are being built or planned in China, the U.S., the United Kingdom (U.K.), Brazil, France and Austria (5, 7).

Biofuel production has initially focussed on the use of feedstocks that are easily accessible. Thus, bioethanol production has been reliant on the sugar and/or starch components of food crops such as sugar beet, sugar cane, corn, wheat and cassava, whereas biodiesel has been derived from vegetable oils and animal fats. The fuels produced are generally referred to as first generation biofuels. Although years of intense R&D have made methods of bioethanol production (typically using the yeast *Saccharomyces cerevisiae*) technologically mature, there remain some serious questions regarding its sustainability. One of the main concerns is the supply and sustainability of sugar as feedstock for large scale biofuel production as the world

raw sugar prices have witnessed significant volatility over the last decade (Figure 1.1) or so, ranging from US$216/ton in year 2000 to a 30 year high of US$795/ton in February 2011 due to global sugar deficits and crop shortfall (9). The use of food crops as a source of carbohydrate feedstocks by these processes requires high-quality agricultural land. The inevitable conflict between the increasing diversion of crops or land for fuel rather than food production has been highlighted as one of the prime causes of rising global food prices. Furthermore, corn ethanol producers in the U.S., have until 2012 enjoyed a 45-cent-a-gallon federal tax credit, costing the government US$30.5 billion between 2005 and 2011, raising questions about its economic competitiveness with gasoline (10, 11).

These arguments have stimulated the search for so-called second generation biofuels, which utilize non-food lignocellulose biomass such as wood, dedicated energy crops, agricultural residues and municipal solid wastes as feedstocks. Biomass consists of cellulose, hemicellulose and lignin, the latter of which is extremely resistant to degradation. One approach to unlocking the potential in this abundant feedstock is to separate the lignin from the carbohydrate fraction of the biomass via extensive pre-treatment of the lignocellulose involving, for example, steam-explosion and/or acid hydrolysis. These pre-treatments are designed to allow the carbohydrate portion of the biomass to be broken down into simple sugars, for example by enzymatic hydrolysis using exogenously added cellulases to release fermentable sugars (12). Such approaches have been found to be expensive and rate limiting (5, 12, 13). Alternatively, processes using cellulolytic microorganisms (such as *Clostridium cellulolyticum*, *Clostridium thermocellum*, and *Clostridium phytofermentans*) to carry out both the hydrolysis of lignocelluloses and sugar fermentation in a single step, termed 'Consolidated Bioprocessing Process (CBP)'(12) have been proposed, but the development of these is still at an early stage, and again low conversion rates seem to be a major limitation that needs to be overcome.

1.3 The Emergence of Gas Fermentation Technologies

Microorganisms such as acetogens, carboxytrophs and methanogens are able to utilize the CO_2 + H_2, and/or CO available in syngas as their sole source of carbon and energy for growth as well as the production of biofuels and other valuable products. However, only acetogens are described to synthesize metabolic end products that have potential as liquid transportation fuels.

Due to the flexibility of the microbes to ferment syngas with diverse composition, virtually any carbonaceous materials can be used as feedstock for gasification. Non-food biomass that can be employed as feedstock for gasification includes agricultural wastes, dedicated energy crops, forest residues, and municipal organic wastes, or even glycerol and feathers (14-18). It has been estimated that out of a global energy potential from modern biomass of 250 exajoules (EJ) per year in 2005, only 9 EJ (3.6%) was used for energy generation (15). The use of existing waste streams such as municipal organic waste also differentiates itself from other feedstocks such as dedicated energy crops because these wastes are available today at economically attractive prices, and they are often already aggregated and require less indirect land use. Alternatively, gasification of non-biomass sources such as coal, cokes, oil shale, tar sands, sewage sludge and heavy residues from oil refining, as well as reformed natural gas are commonly applied as feedstocks for the Fischer-Tropsch' process (FTP) and can also be used for syngas fermentation (19, 20). Furthermore, some industries such as steel manufacturing, oil refining and chemical production generate large volumes of CO and/or CO_2 rich gas streams as wastes. Tapping into these sources using microbial fermentation processes essentially converts existing toxic waste gas streams into valuable commodities such as biofuels. The overall process of gas fermentation is outlined in Figure 1.2.

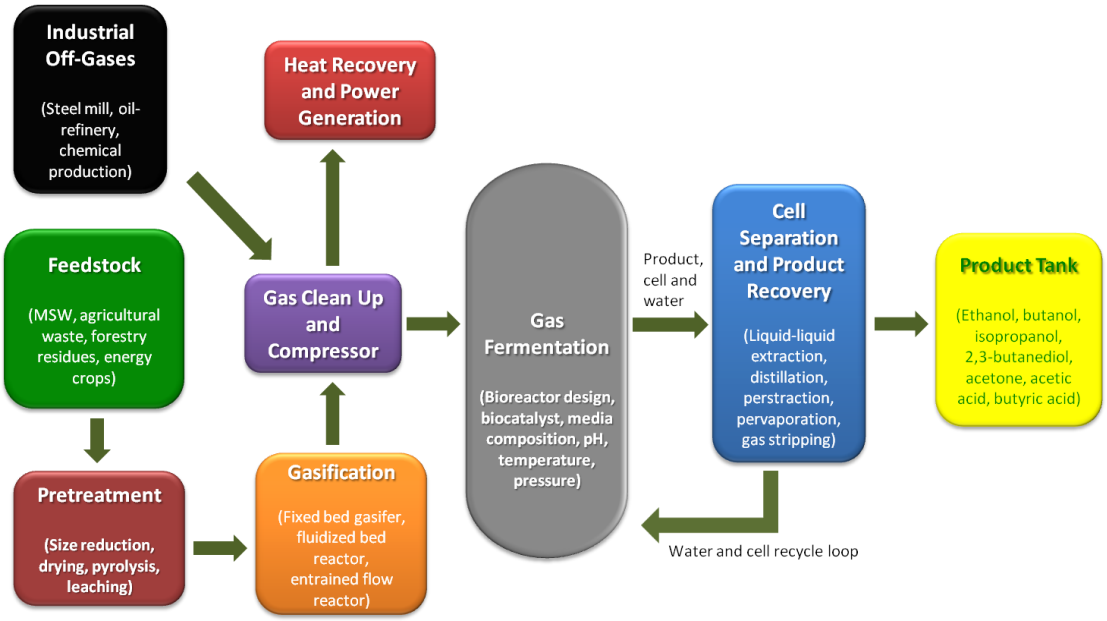


Figure 1.2. Overview of the gas fermentation process.

While biological processes are generally considered slower than chemical reactions, the use of microbes to carry out syngas fermentation offers several key advantages over alternative thermo-chemical approaches such as the FTP. First, microbial processes operate at ambient temperatures and low pressures which offer significant energy and cost savings. Second, the ambient conditions and irreversible nature of biological reactions also avoid thermodynamic equilibrium relationships and allow near complete conversion efficiencies (19, 21). Third, biological conversions are commonly more specific due to high enzymatic specificities, resulting in higher product yield with the formation of fewer by-products. Fourth, unlike traditional chemical catalysts which require a set feed gas composition to yield desired product ratios, microbial processes have freedom to operate for the production of the same suite of products across a wider range of CO:H_2 ratios in the feed gas (16). Fifth, biocatalysts exhibit a much higher tolerance to poisoning by tars, sulphur and chlorine than inorganic catalysts (5, 16).

The main challenges associated with commercialization of gas fermentation have been identified as gas-to-liquid mass transfer limitation, long retention times due to slow cell growth, sub-optimal substrate utilization efficiency, low alcohol production rates and broth concentrations, and inefficient product recovery (14, 22, 23). Further

development of the bioreactor is necessary to improve the availability of gas substrates and maintain high cell density for higher productivity. Improvement in integrated product recovery technology is also essential to lower the costs of product recovery and alleviate product inhibition. Besides substrate utilization and productivity issues, water usage and overall energy footprint of the process constitute increasingly important environmental considerations.

1.4 The Genus *Clostridium*

Most of the industrially relevant acetogens belong to the genus *Clostridium,* which is one of the largest bacterial genera. To date, more than 300 different species of genus *Clostridium* are listed in culture collections ATCC (American Type Culture Collections) and DSMZ (Deutsche Sammlung von Mikroorganismen und Zelkulturen). The old and over-simplistic phenotypic criteria for attribution to this genus are anaerobic metabolism, Gram-positive-type cell wall, endospore formation and inability to undertake dissimilatory sulfate reduction (24). Molecular markers such as 16S rRNA sequence homology, DNA/DNA hybridization and genomic DNA fingerprinting allowed a more sophisticated strain/species differentiation and have led to reclassification of many formerly described *Clostridium* species into other genera such as *Moorella*, *Eubacterium*, *Syntrophospora*, *Thermoanaerobacterium* and *Oxobacter* (24, 25).

Although clostridia are more commonly known for the potent cocktail of toxins they produce, they are also incredibly metabolically diverse and play crucial roles in regulation of global carbon cycle, production of industrially important fuels and chemicals, degradation and bioremediation of complex organic molecules, and medical applications (26, 27). The cytotoxins produced by *C. tetani* and *C. botulinum* are the most potent natural toxins known to mankind, but even these have established medical applications ranging from the removal of facial frown lines and wrinkles, to treatment of muscle spasms affecting vision, cerebral palsy and pain syndromes (25, 27). A novel antibiotic, closthiomide, was reported to be produced by *C. cellulolyticum* as a secondary metabolite (28). Recently, recombinant apathogenic

Clostridium spores have been explored as a vehicle for targeted delivery of anti-cancer drugs to anoxic tumour cells (29).

Given that clostridia are found in virtually any anaerobic habitats such as animal guts, soil, marine sediments, anaerobic digesters, and sewage sludge, it is unsurprising that they have developed an appetite to utilize an impressively broad spectrum of substrates or feedstocks (25, 26). Saccharolytic clostridia such as *C. thermocellum*, *C. cellulolyticum*, *C. cellulovorans*, *C. methylpentosum* and *C. phytofermentans* are able to degrade complex biological polymers cellulose, hemicellulose, xylan, starch and pectin into the fermentable sugars glucose, xylose, rhamnose, arabinose, galactose, and mannose (25, 26). Most cellulolytic clostridia produce a cell-wall-bound multicomponent, multienzyme complex termed the cellulosome. It comprises a cellulose binding domain, a scaffolding subunit, dockerin modules, cohesion modules, enzymatic subunits, and an anchoring protein (12, 30). Recent developments in CBP compressed cellulase production, cellulose hydrolysis and fermentation into a single process using cellulolytic microorganisms to produce biofuel and hydrogen gas (12, 30). Conventional bioprocessing of cellulose requires costly pre-treatment steps such as steam-explosion and/or acid pre-treatment, and addition of exogenously produced cellulolytic enzymes prior to fermentation (12).

Besides utilization of sugars as substrates, some clostridia are acetogens capable of growing chemolithotrophically solely on inorganic CO_2 + H_2, and CO. Figure 1.3 depicts the phylogenetic relationship of acetogens and solventogenic clostridia. It is worth mentioning that acetogens are currently estimated to fix about 20% of the earth's CO_2, and produce approximately one billion tons of acetate annually (31). This, coupled with the ability of some clostridia such as *C. pasteurianum*, *C. acetobutylicum*, and *C. beijerinckii* in nitrogen fixation (32), underlines the contribution of this diverse genus of bacteria in the earth's carbon and nitrogen cycles.

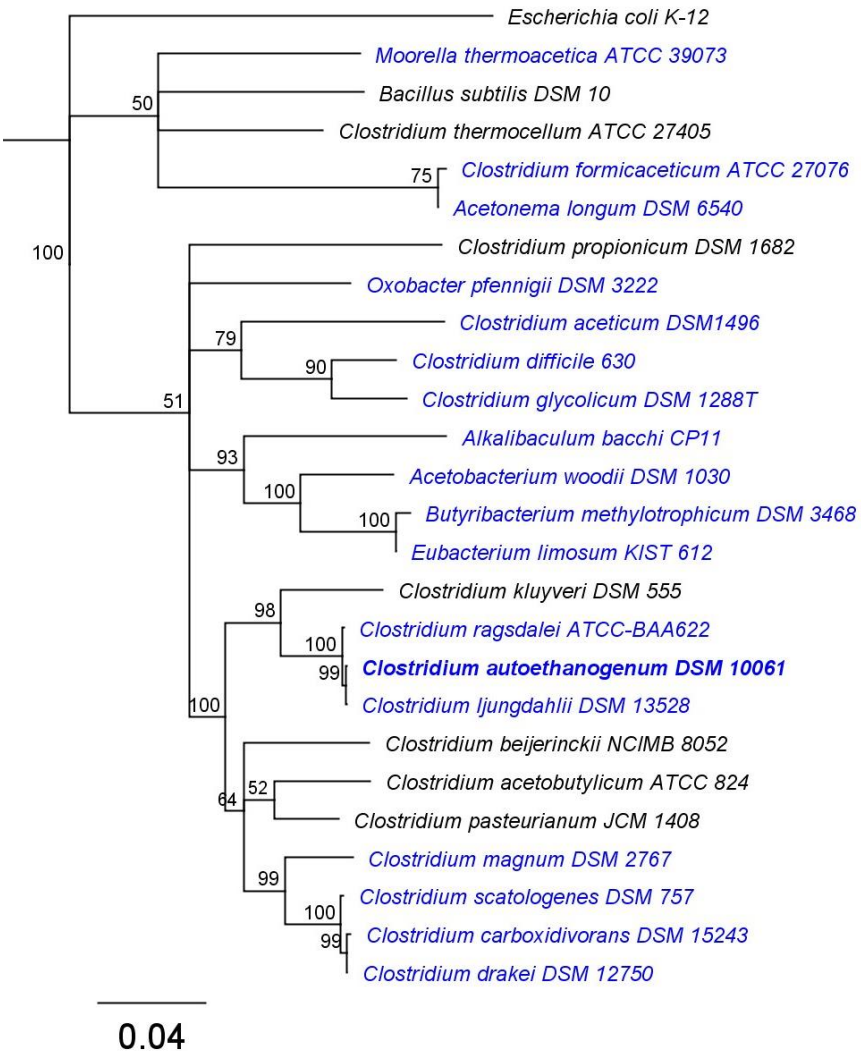


Figure 1.3. Phylogenetic tree of acetogens, solventogenic *Clostridium* species and model bacteria. The tree was constructed using the neighbour-joining method of Geneious 7.1.7 (Biomatters Ltd) and was based on complete 16S rRNA DNA sequences. Bootstrap values expressed as a percentage of 100 replications are given at the branching points. Sequence divergence is represented by horizontal bar. Acetogens are highlighted in blue.

The fixation of CO_2 by acetogens requires electron donors such as H_2 or CO. Recently *C. ljungdahlii*, *C. aceticum*, *M. thermoacetica*, *Sporomusa ovata*, and *S. sphaeroides* have also been shown to accept electrons derived from electrodes to reduce CO_2 into organic compounds such as acetate, formate, and 2-oxo-butyrate (33). Termed microbial electrosynthesis, this nascent concept offers another route for acetogens to harvest the electrons generated from renewable strategies (e.g., solar and wind) to reduce CO_2 into useful multi-carbon products such as biofuels (34).

The importance of clostridia is reflected by the increasing number of *Clostridium* genome sequencing projects. To date, 52 clostridial genome sequences are publicly available in the KEGG (Kyoto Encyclopaedia of Genes and Genomes) database. The genome of *C. acetobutylicum* ATCC 824 was the first *Clostridium* to be completely sequenced (35) and it provided invaluable insights into its metabolic potentials. Apart from revealing the whole set of solventogenic genes and pathways, it also brought surprising discovery of previously unknown cellulosome components (35, 36). Despite the demonstration of cellulosome formation *in vivo*, *C. acetobutylicum* remains unable to hydrolyze cellulose (36). The genomes of solventogenic acetogens *C. ljungdahlii* (37), *C. autoethanogenum* (38) and *C. carboxidivorans* strain P7 (39, 40) have also recently been released, allowing in-depth examination of their Wood-Ljungdahl pathway (WLP) and solventogenic capability. Similar to *C. acetobutylicum*, *C. carboxidivorans* strain P7 also harbours an extra-chromosomal 19 kb plasmid but this plasmid is much smaller in size (*C. acetobutylicum* megaplasmid pSOL1 is 192 kb) and does not encode solventogenic genes (39). A selection of mesophilic and thermophilic acetogens are presented in Table 1.1.

Table 1.1. Acetogens

Species	Substrate	Product(s)	T_{opt} (^{o}C)	pH_{opt}	Genome Status	Ref.
Mesophilic Microorganisms						
Acetobacterium woodii	H_2/CO_2, CO	Acetate	30	6.8	Yes	(41, 42)
Acetonema longum	H_2/CO_2	Acetate, butyrate	30-33	7.8		(43)
Alkalibaculum bacchi	H_2/CO_2, CO	Acetate, ethanol	37	8.0-8.5		(44, 45)
Butyribacterium methylotrophicum	H_2/CO_2, CO	Acetate, ethanol, butyrate, butanol	37	6		(46-48)
Clostridium aceticum	H_2/CO_2, CO	Acetate	30	8.3	Under construction	(49-51)
Clostridium autoethanogenum	H_2/CO_2, CO	Acetate, ethanol, 2,3-butanediol, lactate	37	5.8-6.0	Yes	(38, 52, 53)
***Clostridium carboxidivorans* or "P7"**	H_2/CO_2, CO	Acetate, ethanol, butyrate, butanol, lactate	38	6.2	Draft	(39, 54)
Clostridium difficile	H_2/CO_2, CO	Acetate, ethanol, butyrate	35-40	6.5-7.0	Yes	(55-57)
Clostridium drakei	H_2/CO_2, CO	Acetate, ethanol, butyrate	25-30	3.6-6.8		(54, 58, 59)
Clostridium formicoaceticum	CO	Acetate, formate	37	NR		(49, 60, 61)

Species	Substrate	Product(s)	T_{opt} (°C)	pH_{opt}	Genome Status	Ref.
Clostridium glycolicum	H_2/CO_2	Acetate	37-40	7.0-7.5		(62, 63)
Clostridium ljungdahlii	H_2/CO_2, CO	Acetate, ethanol, 2,3-butanediol, lactate	37	6	Yes	(37, 53, 64)
Clostridium magnum	H_2/CO_2	Acetate	30-32	7.0		(65, 66)
Clostridium mayombei	H_2/CO_2	Acetate	33	7.3		(67)
Clostridium methoxybenzovorans	H_2/CO_2	Acetate, formate	37	7.4		(68)
"Clostridium ragsdalei" or "P11"	H_2/CO_2, CO	Acetate, ethanol, 2,3-butanediol, lactate	37	6.3		(53, 69)
Clostridium scatologenes	H_2/CO_2, CO	Acetate, ethanol, butyrate	37-40	5.4-7.5		(54, 58)
Eubacterium limosum	H_2/CO_2, CO	Acetate, butyrate	38-39	7.0-7.2	Yes	(41, 70)
Oxobacter pfennigii	H_2/CO_2, CO	Acetate, butyrate	36-38	7.3		(71)
Blautia productus	H_2/CO_2, CO	Acetate	37	7		(72)
Thermophilic Microorganisms						
Moorella thermoacetica	H_2/CO_2, CO	Acetate	55	6.5-6.8	Yes	(73-75)
Moorella thermoautotrophica	H_2/CO_2, CO	Acetate	58	6.1		(76)

Notes: NR, Not reported

1.5 The Wood-Ljungdahl Pathway (WLP) and Energy Conservation

Acetogens are defined as obligate anaerobes that utilize the reductive acetyl-CoA pathway for the reduction of CO_2 to the acetyl moiety of acetyl-coenzyme A (CoA), for the conservation of energy, and for the assimilation of CO_2 into cell carbon (31). The reductive acetyl-CoA pathway is also known as the 'Wood-Ljungdahl' pathway (WLP), in recognition to the two pioneers, Lars G. Ljungdahl and Harland G. Wood, who elucidated the biochemistry and enzymology of the pathway using *Moorella thermoacetica* (formerly: *Clostridium thermoaceticum*) as a model acetogen (77). This ancient pathway is diversely distributed among at least 23 different bacterial genera: *Acetitomaculum*, *Acetoanaerobium*, *Acetobacterium*, *Acetohalobium*, *Acetonema*, *Alkalibaculum, Bryantella*, *Butyribacterium, Caloramator*, *Clostridium*, *Eubacterium*, *Holophaga*, *Moorella*, *Natroniella*, *Natronincola*, *Oxobacter*, *Ruminococcus*, *Sporomusa*, *Syntrophococcus*, *Tindallia*, *Thermoacetogenium*, *Thermoanaerobacter*, and *Treponema* (31). Acetogens are able to utilize gases CO_2 +

H_2, and/or CO to produce acetic acid and ethanol according to the following stoichiometries:

$$2\ CO_2 + 4\ H_2 \rightarrow CH_3COOH + 2\ H_2O \quad \Delta H = -75.3\ kJ/mol \quad (1)$$

$$2\ CO_2 + 6\ H_2 \rightarrow C_2H_5OH + 3\ H_2O \quad \Delta H = -97.3\ kJ/mol \quad (2)$$

$$4\ CO + 2\ H_2O \rightarrow CH_3COOH + 2\ CO_2 \quad \Delta H = -154.9\ kJ/mol \quad (3)$$

$$6\ CO + 3\ H_2O \rightarrow C_2H_5OH + 4\ CO_2 \quad \Delta H = -217.9\ kJ/mol \quad (4)$$

1.5.1 Carbonyl- and Methyl- Branch of WLP

The Acetyl-CoA pathway is essentially a terminal electron-accepting process that assimilates CO_2 into biomass (77). It constitutes an *Eastern* (or Carbonyl) branch and a *Western* (or Methyl) branch (Figure 1.4). The *Western* branch employs a series of enzymes to carry out a six-electron reduction of CO_2 to the methyl group of acetyl-CoA, starting from the conversion of CO_2 to formate by formate dehydrogenase. Formyl-THF (tetrahydrofolate) synthase then condenses formate with THF to form 10-formyl-THF, which is then converted to 5,10-methenyl-THF by a cyclohydrolase. This is followed by a dehydrogenase that reduces methenyl- to 5,10-methylene-THF, before (6S)-5-CH_3-THF is formed by methylene-THF reductase (78). A B12-depedent methyltransferase (MeTr) then transfers the methyl group of (6S)-5-CH_3-THF to corrinoid iron-sulphur protein (CoFeSP) of the bi-functional carbon monoxide dehydrogenase/acetyl-CoA synthase (CODH/ACS) complex (78).

The bi-functional CODH/ACS enzyme complex is formed by two autonomous proteins, an $\alpha_2\beta_2$ tetramer (CODH/ACS) and a γδ heterodimer (CoFeSP), and the encoding genes are often arranged in an operon, together with MeTr (78, 79). In the *Eastern* branch, the CODH component catalyzes the reduction of CO_2 to CO. The central molecule, acetyl-CoA, is finally generated when CO, methyl group (bound to CoFeSP) and CoASH are condensed by ACS. Given the pivotal role of CODH/ACS, it is unsurprising that the genes which encode this complex were found to be the most highly expressed transcripts under autotrophic conditions in *C. autoethanogenum* (53), and can represent up to 2% of the soluble cell protein of an acetogen (80). In

addition to CODH/ACS, CODH disulfide reductase and NADP or ferredoxin are also required for the addition of CoASH into acetyl-CoA (81).

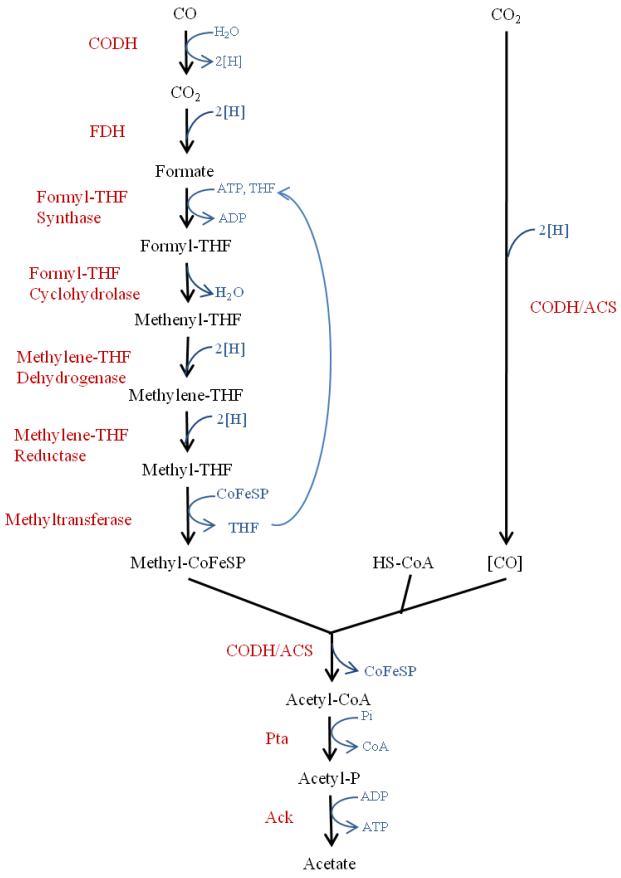


Figure 1.4. Wood-Ljungdahl Pathway. Ack, acetate kinase; ACS, acetyl-CoA synthase; CODH, carbon monoxide dehydrogenase; CoFeSP, corrinoid iron sulfur protein; FDH, formate dehydrogenase; Pta, phosphotransacetylase; THF, tetrahydrofolate.

1.5.2 Hydrogenase

The reducing equivalents required for fixation of CO_2 carbon into acetyl-CoA come from the oxidation of molecular hydrogen, NADH and/or reduced ferredoxin (82, 83). An extensive review by Calusinska *et al.* (2010) highlighted the diversity of hydrogenases that clostridia possess (84), which catalyze the reversible oxidation of hydrogen:

$$H_2 \leftrightarrows 2\,H^+ + 2\,e^- \qquad (5)$$

The direction of the reaction is directed by the redox potential of the components able to interact with the enzyme. Hydrogen evolution occurs when an electron donor is available, whereas the presence of an electron acceptor results in hydrogen oxidation (85). Hydrogenases can be classified into three phylogenetically distinct classes of metalloenzymes: [NiFe]-, [FeFe]-, and [Fe]-hydrogenases (84). In *Methanosarcina barkeri*, the Ech hydrogenase, a [NiFe]-hydrogenase, was demonstrated to oxidize H_2 to reduce ferredoxin (86). During acetoclastic methanogenesis, Ech hydrogenase oxidizes ferredoxin to generate H_2 (86). Although genome analysis revealed the presence of Ech-like hydrogenases in *C. thermocellum, C. phytofermentans*, *C. papyrosolvens*, and *C. cellulolyticum*, their physiological roles remain unknown (84).

Clostridia harbour multiple distinct [FeFe]-hydrogenases, perhaps reflecting their ability to respond swiftly to changing environmental conditions (84). The monomeric, soluble [FeFe]-hydrogenase of *C. pasteurianum* is one of the best studied. It transfers electrons from reduced ferredoxins or flavodoxins to protons, forming H_2 (87). Trimeric [FeFe]-hydrogenases found in *C. difficile*, *C. beijerinckii*, and *C. carboxidivorans* were hypothesized to couple formate oxidation to reduction of protons into H_2 (84). In *Thermotoga maritima*, an electron-bifurcating, trimeric [FeFe]-hydrogenase was identified, that was shown to simultaneously oxidize reduced ferredoxin and NADH to evolve hydrogen under low H_2 partial pressure (88). Under high H_2 partial pressure, the authors hypothesized that the NADH is oxidized to produce ethanol. *In silico* analysis revealed homologs of this bifurcating hydrogenase in a few clostridia including *C. beijerinckii* and *C. thermocellum* (88). Recently, a NADP-specific electron-bifurcating [FeFe]-hydrogenase that forms a functional complex with formate dehydrogenase was characterized in *C. autoethanogenum*. This complex was purified and demonstrated to catalyze both the reversible reduction of NADP with ferredoxin and formate or H_2, and the reversible production of H_2 and CO_2 from formate (89).

1.5.3 Carbon Monoxide Dehydrogenase (CODH)

Besides CO_2 and H_2, most acetogens are also able to utilize another gas carbon monoxide. In contrast to CO_2, CO can serve as both carbon source and electron source for acetogens so that hydrogen is not necessarily needed. With a CO_2/CO reduction potential of -524 to -558 mV, CO is about 1000-fold more potent than NADH in generating extremely low potential electrons, which then reduce cellular electron carriers such as ferredoxin and flavodoxin (79, 90). The reducing equivalents generated from CO oxidation can be coupled to reduction of sulphur species to H_2S, evolution of molecular hydrogen from protons, reduction of CO_2 to acetate, butyrate and/or methane, reduction of nitrate/nitrite to ammonium, and reduction of aldehydes to alcohols (77, 91). However, relatively few microorganisms are able to utilize CO as sole carbon and energy source, probably due to growth inhibition from sensitivity of their metalloproteins and hydrogenases towards CO (79, 91). CODH has been reported to be a very rapid and efficient CO oxidizer at rates between 4,000 and 40,000 s^{-1}, and reduces CO_2 at 11 s^{-1} (92, 93). CODH is able to split water in a biological water-gas shift reaction into hydrogen and electrons according to the stoichiometry:

$$CO + H_2O \rightarrow CO_2 + 2H^+ + 2e^- \quad (7)$$

1.5.4 Energy Conservation in WLP

Under chemolithoautotrophic conditions, acetogenesis must not only fix carbon but also conserve energy. Approximately 0.1 mol of ATP is required for generation of 1g of dry biomass in anaerobes (90). Through the combined actions of Pta (phosphotransacetylase) and Ack (acetate kinase), one ATP can be generated via substrate level phosphorylation (SLP) from central molecule acetyl-CoA. However, the activation of formate to 10-formyl-THF in the methyl-branch of the Acetyl-CoA pathway consumes one ATP so no net gain in ATP is achieved via this mechanism (77, 82). Furthermore, the reduction of CO_2 to the carbonyl group also requires energy, estimated at one third of ATP equivalent (77). Recent advances indicated that electron transport phosphorylation (ETP) or chemiosmotic processes that are

coupled to the translocation of protons or sodium ions are implicated in the energy conservation of acetogens.

Acetogens such as *M. thermoacetica* harbour a membrane-associated electron transport system containing cytochromes, menaquinones, and oxidoreductases that translocates H^+ out of the cell (31). A non-cytochrome, non-menaquinone ferredoxin:NAD^+-oxidoreductase termed Rnf complex was demonstrated to play vital roles in energy conservation in acetogens such as *A. woodii*, *C. ljungdahlii* and *C. autoethanogenum* (37, 89, 94-97). Using reduced ferredoxin generated by CODH, carbohydrate and/or hydrogenase, this membrane-bound electron transfer complex is predicted to reduce NAD^+ with concomitant translocation of Na^+/ H^+. The ion gradient generated from the above processes is harvested by H^+- or Na^+- ATP synthase to generate ATP (31, 95). Recently, an energy conservation mechanism which involves bifurcation of electrons by hydrogenases was proposed for anaerobes (98) and demonstrated for various enzymes such as hydrogenases (see above; (88, 89, 99-101)), butyryl-CoA dehydrogenase (25, 98), an NADH-dependent reduced ferredoxin:NADP oxidoreductase Nfn (89, 102), a formate dehydrogenase (103), a caffeyl-CoA reductase (104) and a dehydrogenase involved in heme biosynthesis (105). A similar mechanism has also been proposed for the methylene-THF reductase of the reductive acetyl-CoA pathway, which would enable this highly exergonic reduction step ($\Delta G^{0'}$ = −22 kJ/mol) to be coupled with the Rnf complex for additional energy conservation (37). However, no experimental proof has been found to date.

1.5.5 Attempts at Installation of WLP into Non-Acetogens

During glycolysis, the decarboxylation of pyruvate into acetyl-CoA (via PFOR) leads to the loss of carbon in the form of carbon dioxide, which reduces the theoretical maximum of substrate utilization in a fermentation process. To maximize sugar-based feedstock conversion rate, it has been proposed that the installation of WLP into non-acetogenic chassis may lead to improved productivity and yield (106).

In an attempt to generate an autotrophic *E. coli*, the genes encoding MeTr, the two subunits of CODH/ACS, and the two subunits of CoFeSP from *M. thermoacetica* were

cloned and overexpressed (107). Although the MeTr was found to be active, the other subunits misassembled hence no active enzymes were found (107). In contrast, the purified heterologously expressed CODH/ACS from *M. thermoacetica* in *E. coli* was shown to be functional in both CO oxidation and CO/acetyl-CoA exchange activities by Loke *et al.* (2000) (108). Eleftherios Papoutsakis and co-workers expressed heterologous CODH/ACS and its accessory proteins, Fdh, MeTr and CoFeSP from *C. difficile* and *C. ljungdahlii* in *C. acetobutylicum*. While heterologous gene expression was demonstrated using qRT-PCR and some enzymatic activities were shown, the resultant recombinant *C. acetobutylicum* was unable to grow autotrophically (109, 110).

The capability of autotrophic growth is clearly a very complex process that on one hand involves enzymes such as the CODH/ACS complex and THF pathway that have delicate metal centres but on the other hand also requires many parts, including compatible cofactors, electron carriers, specific chaperones and energy conservation mechanisms. For instance, more than 200 genes are predicted to be involved in methanogenesis and energy conservation from CO_2 and H_2 in methanogens (111).

1.6 Solventogenesis

Acetyl-CoA generated via the WLP, serves as key intermediate for synthesis of biomass as well as products. All acetogens are reported to produce acetate, in order to gain energy via SLP to compensate for the energy invested in activating CO_2 in the Western branch of the reductive acetyl-CoA pathway. Acetate and ATP are formed via acetyl-phosphate through the successive actions of Pta and Ack. The respective encoding genes *pta* and *ack* are arranged in the same operon and they were reported to be constitutively expressed (112). With CO_2 and H_2 as substrate, only acetate has been observed as major product (44), with minor amounts of ethanol produced in rare cases with *C. ljungdahlii* (113), *C. autoethanogenum* (52), or "*Moorella sp.*" (114, 115). Using the more reduced substrate CO, production of a whole range of other products has been reported, such as ethanol, butanol, butyrate, 2,3-butanediol (53), or lactate (116) (Figure 1.5). Ethanol producers include

C. ljungdahlii (37, 64), *C. autoethanogenum* (52, 53), *"C. ragsdalei"* ("*Clostridium* strain P11") (117, 118), "*Moorella sp.*" (114, 115), *Alkalibaculum bacchii* (44), *C. carboxidivorans* ("*Clostridium* strain P7") (39, 54), or *B. methylotrophicum* (48, 119). The latter two have also been described to produce butanol.

Among solventogenic clostridia, sugar- or starch-utilizing *C. acetobutylicum*, *C. beijerinckii*, *C. saccharobutylicum*, and *C. saccharoperbutylacetonicum* are known as the best solvent producers and have been employed in industrial ABE fermentation (25). Since *C. acetobutylicum* was the first *Clostridium* to be fully sequenced (35) and it remains the most commonly used species for industrial production of solvents to date (120), it provides a model for study of solventogenesis.

Clostridial solvent production which utilizes sugars as substrate typically undergoes biphasic fermentation. The first phase is the accumulation of carboxylic acids (acidogenic), H_2 and CO_2 during exponential growth. This is followed by the solventogenic phase in which part of the produced acids are reassimilated or reduced into solvents, which usually occurs during stationary growth phase (121). This shift from acidogenesis to solventogenesis is of industrial importance and several transcriptional analyses on *C. acetobutylicum* (112, 122), and *C. beijerinckii* (123) have been performed to shed light on this process. In both organisms, the onset of solventogenesis coincides with an increase in expression of master sporulation/solventogenesis regulator *spo0A*, solventogenic genes such as *adhE* (aldehyde/alcohol dehydrogenase), *ctfA-ctfB* (CoA transferase A and B), and *adc* (acetolactate decarboxylase), as well as down-regulation of chemotaxis/motility genes (112, 122, 123). These solventogenic genes are arranged in the so-called *sol* operon in *C. acetobutylicum* (124), *C. beijerinckii* (125) and *C. saccharoperbutylacetonicum* (126). In *C. acetobutylicum*, phosphorylated Spo0A was shown using gel retardation assays and targeted mutagenesis to bind to the promoter of *adc* and *sol* operons, thus providing a link between sporulation and solventogenesis (127, 128). Physiologically, the signals that induce solventogenesis were hypothesized to involve temperature, low pH, high concentrations of undissociated acetic and butyric acids, limiting concentrations of sulphate or phosphate, ATP/ADP ratio and/or NAD(P)H levels (129).

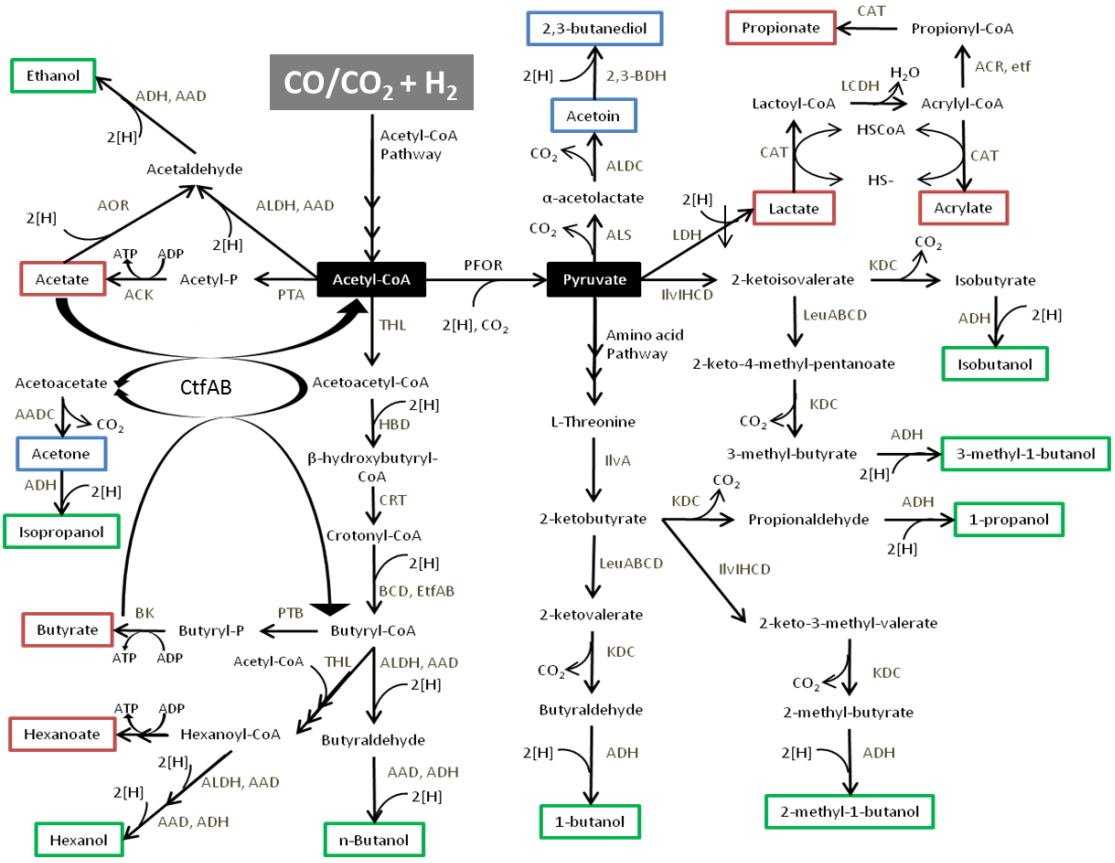


Figure 1.5. Scheme of metabolite production from gas fermentation using native and genetically engineered clostridia. Alcohols are highlighted in green boxes. Acids are highlighted in red boxes. Valuable chemical commodities are shown in blue boxes. 2,3-BDH, 2,3-butanediol dehydrogenase; AAD, aldehyde/alcohol dehydrogenase; AADC, acetoacetate decarboxylase; ACK, acetate kinase; ACR, acrylyl-CoA reductase; ADH, alcohol dehydrogenase; ALDC, acetolactate decarboxylase; ALDH, aldehyde dehydrogenase; AOR, aldehyde:ferredoxin oxidoreductase; BCD, butyryl-CoA dehydrogenase; BK, butyrate kinase; CAT, CoA transferase; CtfAB, CoA transferase A & B; CRT, crotonase; Etf, electron-transferring flavoprotein; HBD, hydroxybutyryl-CoA dehydrogenase; IlvA, threonine deaminase; IlvIHCD, enzymes involved in valine and isoleucine biosynthesis; KDC, 2-ketoacid decarboxylase; LCDH, lactoyl-CoA dehydrogenase; LDH, lactate dehydrogenase; LeuABCD, enzymes involved in leucine and norvaline biosynthesis; PFOR, pyruvate:ferredoxin oxidoreductase; PTA, phosphotransacetylase; PTB, phosphotransbutyrylase; THL, thiolase.

1.6.1 From Acetyl-CoA to Butyryl-CoA

For a clostridial acetogen such as *C. carboxidivorans* (39), which harbours the genes thiolase (*thlA*), 3-hydroxybutyryl-CoA dehydrogenase (*hbd*), crotonase (*crt*) and butyryl-CoA dehydrogenase (*bcd*), the two carbon acetyl-CoA can be converted to four carbon butyryl-CoA (25). ThlA competes with the activities of Pta, Aldh, and

pyruvate:ferredoxin oxidoreductase (PFOR) to condense two acetyl-CoA into one acetoacetyl-CoA, and plays a key role in regulating the C2:C4 acid ratio (120, 130). Since the formation of acetate yields twice as much ATP per mole of acetyl-CoA relative to butyrate formation, ThlA indirectly affects ATP yield (130). Under physiological conditions, Crt catalyzes dehydration of β-hydroxybutyryl-CoA to crotonyl-CoA (131). Bcd was shown to require a pair of electron transfer flavoproteins (EtfA and EtfB) to convert crotonyl-CoA to butyryl-CoA (132). Furthermore, the Bcd was demonstrated to form a stable complex with EtfA and EtfB, and they were hypothesized to couple the reduction of crotonyl-CoA to butyryl-CoA with concomitant generation of reduced ferredoxins, which can be used for energy conservation via Rnf complex (98, 131). Subsequent actions of phosphotransbutyrylase (*ptb*) and butyrate kinase (*buk*) then generate ATP and butyrate from butyryl-CoA (130).

1.6.2 Reassimilation of Carboxylic Acids

Under low extracellular pH of 4 - 4.5, the secreted undissociated acetic acid and/or butyric acid diffuse back into cell cytoplasm and then dissociate into salts and protons once inside the cell because of the more alkaline intracellular conditions. Without further interventions, the result of this is abolishment of the proton gradient and inevitable cell death (25). The conversion of acetate and butyrate into solvents increases the pH, thus providing some time for the organism to sporulate and secure long term survival. However, the solvents produced are toxic because they increase membrane fluidity and disrupt critical membrane-associated functions such as ATP synthesis, glucose uptake and other transport processes (121, 133). In *C. acetobutylicum*, it has been demonstrated that the addition of 7-13 g/L of butanol, or up to 40 g/L of acetone and ethanol resulted in 50% growth inhibition (8).

The reassimilation of acetate and butyrate into the respective acyl-CoA and acetoacetate is catalyzed by acetoacetyl-CoA:acetate/butyrate CoA transferase (CtfA and CtfB) (120, 129, 130). Acetoacetate is deconstructed by acetoacetate decarboxylase (Adc) into acetone and CO_2. Interestingly, this enzyme is missing in

acetogenic *C. carboxidivorans* compared to the ABE strains (39, 40). Some ABE strains such as *C. beijerinckii* NRRL B593 also possess a primary/secondary alcohol dehydrogenase that converts acetone further to isopropanol (134). Recently, a NADPH-dependent primary/secondary alcohol dehydrogenase was reported in *C. autoethanogenum*. This enzyme catalyzes not only the conversion of acetone or butanone to the respective alcohols (isopropanol and 2-butanol), but also the reduction of acetoin to 2,3-butanediol (135). The recycled acetyl-CoA and butyryl-CoA can be converted to ethanol and butanol through the actions of coenzyme A-acylating aldehyde dehydrogenase (Ald) and alcohol dehydrogenase (Adh) (120, 130). Ald converts acyl-CoA to aldehydes, and the enzyme has been purified from *C. beijerinckii* NRRL B593 and was shown to be NADH-specific, exhibit higher affinity with butyraldehyde than acetaldehyde, but possess no Adh activity (136).

1.6.3 Indirect Alcohol Production via Aldehyde:Ferredoxin Oxidoreductase (AOR)

Besides the direct reduction of acetyl-CoA or butyryl-CoA to ethanol or butanol via aldehyde intermediates, an alternative route exists for the synthesis of alcohols via carboxylic acids. Termed 'aldehyde:ferredoxin oxidoreductase' (Aor), this enzyme was shown in whole cell experiments with a number of acetogens to catalyze the reduction of carboxylic acids to the respective aldehydes (137-139), which can be further reduced to alcohols via the action of Adh (see Figure 1.5). Under ATP-limited conditions of acetogenesis, it has been hypothesized that the action of Aor is integral for ethanol production because this solventogenic route allows a valuable ATP to be generated during synthesis of acetate via SLP, in comparison to the direct reduction of acetyl-CoA (140). Supporting this hypothesis, the genomes of prominent ethanol producers *C. ljungdahlii* and *C. autoethanogenum* harbour genes that encode Aor, which are predicted to couple ferredoxin reduction to CO oxidation via the CODH to perform the reversible reduction of acetate into acetaldehyde, which can be further reduced to ethanol (37, 38). Recently, "*C. ragsdalei*" was shown to use Aor to reduce n-fatty acids to the corresponding aldehyde intermediates in a ferredoxin- and CO-

dependent manner (141). The deletion of *aor* in *Pyrococcus furiosus* resulted in a mutant that produced only trace amounts of ethanol from maltose (142).

1.6.4 Alcohol Dehydrogenase (Adh)

The final step of solventogenesis utilizes Adh to reduce acetaldehyde and butyraldehyde to ethanol and butanol, respectively. For ethanol synthesis, transposon mutagenesis and enzymatic assay in *C. acetobutylicum* showed the involvement of a specific Ald that does not interact with butyryl-CoA, and a NAD(P)H-dependent Adh (143, 144). The production of butanol in *C. acetobutylicum* is mainly due to the actions of butanol dehydrogenase A and B (BdhA and BdhB), and bi-functional butyraldehyde/butanol dehydrogenase 1 and 2 (AdhE1 and AdhE2) (25). The gene encoding AdhE1 (*adhE1*), together with those that code for CtfA (*ctfA*), and CtfB (*ctfB*), resides on the solventogenic mega plasmid pSOL1 (25, 129, 144). The observations that insertional inactivation of *adhE1* significantly diminished butanol yield (145), and butanol productivity in a solvent-negative mutant can be restored by transforming plasmid-encoded *adhE1* (146) highlighted the role of this enzyme in butanol formation. Although *bdhA* and *bdhB* are highly similar in nucleotide sequence, and they are arranged in a mono-cistronic operons directly next to each other in the *C. acetobutylicum* genome (129, 144), they exhibit very different properties. BdhB shows significantly higher affinity for butyraldehyde in comparison to BdhA (147), and reporter assays demonstrated that the *bdhB* promoter is 17-fold stronger than the *bdhA* promoter (148). A second *adhE* (*adhE2*) carried by the pSOL1 mega plasmid of *C. acetobutylicum* was found to be mono-cistronically expressed under alcohologenic culture but not solventogenic culture, and its expression successfully restored butanol production in a mutant strain without pSOL1 plasmid (149). In *C. carboxidivorans* (39) and *C. ljungdahlii* (37) both *adhE1* and *adhE2* are arranged in tandem and separated by 200 bp of non-coding DNA which contains a putative terminator (37, 150). This is likely the result of gene duplication (37). qRT-PCR analysis of *C. carboxidivorans* fed with syngas showed that the two *adhE* genes exhibited differential expression, and the more abundant *adhE2* was significantly up-

regulated over 1000-fold in a time span that coincided with the greatest rate of butanol production (150).

1.6.5 Production of 2,3-Butanediol

Pyruvate is a central molecule for anabolism and it is predominantly generated from glycolysis during heterotrophic growth. But under autotrophic conditions, this three carbon molecule can be synthesized by PFOR and potentially also the pyruvate-formate lyase (PFL). Two variants of PFOR were reported in *C. autoethanogenum*, and transcriptional analysis showed that they were differentially expressed when grown under commercial waste gases (containing CO, CO_2 and H_2) (53). Unlike PFL from most other microorganisms that only catalyze the lysis of pyruvate into formate and acetyl-CoA, clostridial PFL (*C. kluyveri, C. butylicum*, and *C. butyricum*) were reported to readily catalyze the reverse reaction (i.e., pyruvate formation) (151).

Apart from roles in anabolism, pyruvate is also a precursor to other products such as lactic acid and 2,3-butanediol. Low amount of lactic acid is produced from pyruvate in acetogens, and the reaction is catalyzed by lactate dehydrogenase (Ldh) (53, 130). Köpke and co-workers (2011) reported the production of 2mM 2,3-butanediol by acetogenic bacteria (*C. autoethanogenum*, *C. ljungdahlii*, and *C. ragsdalei*) using industrial waste gases (containing CO, CO_2 and H_2) as feedstock (53). 2,3-butanediol is a high value commodity which can be used to synthesize chemical products such as 1,3-butadiene, methyl ethyl ketone (MEK), and gamma butyrolactone, with potential market sale value of $43 billion (53). Pyruvate is first converted into α-acetolactate by the enzyme acetolactate synthase (ALS), followed by acetolactate decarboxylase (ALDC) which splits acetolactate into acetoin and CO_2, before a final reduction of acetoin to 2,3-butanediol by 2,3-butanediol dehydrogenase (2,3-BDH) (53) or the above mentioned secondary alcohol dehydrogenase (135) (Figure 1.5).

1.6.6 Production of Acrylate and Propionate

Microorganisms such as *C. propionicum* possess an acrylate pathway, which allows the production of acrylate when growing on alanine and/or fermentation of lactate (152-154). Although the microorganism itself is unsuitable for industrial scale production of acrylate due to its inability to utilize conventional carbon sources, it has been demonstrated to produce acrylate from propionate in its resting states (155). Nonetheless, Mascoma Corporation filed a prophetic patent application which described the incorporation of the acrylate pathway from *C. propionicum* into cellulolytic clostridia such as *C. saccharolyticum* or *C. thermocellum* (156). Acrylate is commonly used in paints, polymeric flocullants, dispersants, adhesives, coatings, and binders for leather, paper and textiles, with an estimated annual production capacity of 4.2 million metric tons (154). In addition to acrylate, *C. propionicum* is also capable of synthesizing propionate (157).

1.6.7 Biosynthesis of Long-Chain Fatty Acids and Higher Alcohols

In comparison to ABE fermentation, the ability of some butyric-acid producing clostridia in synthesizing longer chain carboxylic acids and alcohols (C5, C6, and C8) has attracted less attention. Caproic (C6) and caprylic (C8) acids can be used as chemicals directly, or converted into biodiesel by ketonization (158, 159). By using a mixed culture dominated by relatives of *C. kluyveri*, up to 8.17 g/L of hexanoate (caproate) and 0.32 g/L of caprylate have been reported (160). Although the biochemical pathway has not yet been experimentally verified, it is likely to involve ThlA in condensing one molecule of butyryl-CoA and one acetyl-CoA into 3-oxo-hexanoyl-CoA, which is then converted into hexanoyl-CoA by Crt, Hbd, Bcd, EtfA and EtfB (26). *C. kluyveri* is unique among clostridia in having a second set of non-clustered *crt, hbd, bcd, etfA* and *etfB* in its genome, which might play a role in the formation of hexanoyl-CoA (131). Furthermore, *C. kluyveri* has also been reported to form pentanoate (valerate) when grown on propanol and ethanol, but the biochemical pathway has not been characterized (161).

In similar fashion to the formation of butyrate and butanol from butyryl-CoA, hexanoate and hexanol can be generated from hexanoyl-CoA (26, 161). *C. carboxidivorans* P7, which is also a butanol producer, was recently shown to synthesize 0.52 g/L n-hexanol while growing in H_2 + CO_2 (162). In a continuous syngas fermentor containing mixed culture dominated by *A. bacchi* strain CP15 (56%) and *C. propionicum* (34%), 6 g/L n-propanol and 1 g/L n-butanol were generated (163).

1.7 Genetic Tools for *Clostridium*

Although the genomes of several solventogenic clostridia have been sequenced since 2001 (35, 37, 39, 40, 131, 164) and an array of transcriptomic (112, 123, 133, 165-167), proteomic (166) and systems analysis (168-170) are being made increasingly available, the generation of stable recombinant clostridia has been severely hindered by difficulty in introducing foreign DNA into cells and a lack of established genetic tools for this genus of bacteria. From a commercial biofuel production perspective, a desirable microorganism for the bioprocess might exhibit the following traits: high product yield and selectivity, low product inhibition, slow strain degeneration, asporogenous, prolonged cell viability, strong aero-tolerance, high biomass density and efficient utilization of substrates. For instance, the inherent toxicity of solvents such as butanol has been identified as a major factor limiting the productivity of ABE fermentation. Traditional chemical mutagenesis (171-173) and adaption strategies (174, 175) have been deployed to select for solvent tolerant clostridia but the outcome has been less than satisfactory. While an increase in butanol tolerance was achieved in many cases, it was not accompanied by a significant increase in solvent productivity (174, 175). By applying a targeted genetic approach, Thomas *et al.* (2003) over-expressed heat shock proteins GroES and GroEL in *C. acetobutylicum* ATCC 824, which resulted in both an 85% decrease in butanol inhibition and also a 33% increase in solvent yield relative to the control strain (176).

A major obstacle in genetic engineering of *Clostridium* species lies in the difficulty of introducing foreign DNA into the bacteria. Two methods of DNA introduction have been successfully applied to some *Clostridium* species: conjugation (*C. difficile*, *C.*

sporogenes, *C. beijerinckii* NCIMB 8052 and *C. acetobutylicum* ATCC 824*)* (177-180), and electroporation (*C. acetobutylicum* ATCC 824, *C. ljungdahlii*, *C. beijerinckii*, *C. perfringens*, *C. cellulolyticum*) (37, 181-185), and *C. acetobutylicum* NI-4081 (186)). In addition to overcoming the physical barrier of the Gram-positive cell wall, exogenous DNA also has to 'survive' the attack of the restriction and methylation systems present in most clostridia. For instance, the gene CA_C8241 of *C. acetobutylicum* encodes a type II restriction endonuclease that recognizes the 5'-GCNGC-3' or 5'-GGCC-3' site (187). Researchers typically circumvent this problem by carrying out *in vivo* methylation of the target plasmid in a strain bearing plasmid pAN1 or pAN2 containing a Φ3TI methyltransferase gene from the phage Φ3TI of *Bacillus subtilis* (188). In 2010, Dong *et al.* successfully genetically engineered *C. acetobutylicum* ATCC 824 to accept unmethylated DNA by inactivating CA_C8241 (187). In similar fashion, a putative *mspI* endonuclease in *C. cellulolyticum* was recently inactivated using ClosTron (see below), producing significantly improved transformation efficiency using unmethylated plasmids (189).

The ability to selectively inactivate gene(s) is an invaluable tool to not only eliminates competing pathway(s) which lead to the production of undesirable by-products, but also to allow researchers to assess the roles of specific gene(s) in a reverse genetic manner. Prior to 2007, only a limited number of insertional mutants were successfully created in clostridia: *C. acetobutylicum, C. beijerinckii, C. perfringens,* and *C. difficile* (190). For instance, Green and Bennett (1996) were able to independently inactivate the genes encoding aldehyde/alcohol dehydrogenase (*adhE*) and butyrate kinase (*buk)* of *C. acetobutylicum* ATCC 824 (145, 191). Another example is the inactivation of the gene coding for the master regulator of sporulation and solventogenesis, SpoOA, of *C. beijerinckii* NCIMB 8052, which abolished spore formation and solvent production (192). These earlier knockout mutants were almost exclusively generated from single crossover events via homologous recombination from a replication defective plasmid (145, 191-196). The resulting mutants are segregationally unstable and can revert back to wild type because a second crossover event might occur in the duplicated DNA sequences flanking the integrated plasmid DNA. An integrant generated via allelic exchange is stable but such a double

crossover event is rare and for a long time this has only been reported in *C. perfringens* (197, 198). A negative or counter selective marker is commonly employed to detect the rare second recombination event, but a reliable counter selective marker that is not patent restricted has yet to be established in *Clostridium*.

1.7.1 Knockdown of Target Genes via Antisense RNA (asRNA)

Due to the difficulty in generating stable inactivation mutants, knockdown of target genes via the actions of plasmid-delivered antisense RNA (asRNA) represents an alternative route for genetic manipulation. In cases where the target gene is essential to survival of the microorganism, knockdown is preferred to a complete knockout. By applying asRNA, up to 90% reduction in gene expression together with high level of specificity were reported for *Clostridium* (199-201). Nakayama *et al.* (2008) successfully used asRNA to down-regulate hydrogenase *hupCBA* in *C. saccharoperbutylacetonicum* strain N1-4 and significantly reduced the hydrogen uptake activity to 13% (202). In *C. acetobutylicum* ATCC 824, the knockdown of *ctfB* using asRNA coupled with overexpression of *adhE1* resulted in the production of 30 g/L solvents with significantly suppressed acetone yield (203, 204).

1.7.2 Intron-Based Gene Inactivation

To address the lack of reliable mutagenic tools for clostridia, two independent strategies for stable, targeted insertion into clostridial genomes have recently been developed. The first approach utilizes the specificity of mobile group II intron Ll.*ltrB* from *Lactoccocus lactis* to propagate into the specified site via a RNA-mediated, retro-homing mechanism (205). Heap *et al.* (2007) adapted such mobile elements for use in a wide spectrum of clostridia, and the technology is termed 'ClosTron'. Without a selection marker, the screening effort necessary for the isolation of the desired integrant can be immense due to the variability in integration frequency between target sites. By incorporating a clostridial retro-transposition activating marker (RAM) based on the *ermB* gene of the *Enterococcus faecalis* plasmid pAMβ1, positive selection for the desired integration can be conveniently made by the

bacteria's acquisition of erythromycin resistance (190, 206). Thanks to these properties, this technique is reproducible and has been widely applied to various clostridia, including *C. acetobutylicum* ATCC 824 and DSM 1731, *C. difficile* 630Δ*erm*, R20291 and VPI 10463, *C. sporogenes* NCIMB 10696 and DSM 795, *C. perfringens*, C. *botulinum* ATCC 3502 and Beluga E, and *C. sordellii* ATCC 9714 (190, 206, 207). This technique was further optimized to generate multiple insertional mutations in the same strain by recycling of marker through the actions of FLP recombinase, and the delivery of cargo sequence of up to 1kb was successfully demonstrated in *C. sporogenes* (206).

1.7.3 Precise Genetic Manipulation via Allelic-Exchange

In contrast to ClosTron, another method for stable genome insertion into clostridial genomes proceeds via homologous recombination using a counter-selective marker originally developed for *B. subtilis* (208) but modified for use in *C. acetobutylicum* (209). The use of UPP (uracil-phosphoribosyl-transferase) as counter selective marker allows efficient screening for the rare second recombination event, and the presence of an antibiotic resistance marker between the left- and right- homology arm facilitates the selection for the appropriate recombination event that produces the insertional mutants. The flanking of this antibiotic resistance marker by FRT sites (FLP recombinase target) enables the generation of 'markerless' insertional mutants and also the recycling of markers for creation of multiple insertional mutants in the same strain (209). This method has been successfully applied to replace the endogenous [FeFe]-hydrogenase from *C. acetobutylicum* with an algal hydrogenase for hydrogen evolution (210). A patent application reported two multiple gene knockout mutants of *C. acetobutylicum* that were successfully generated via this technique (211). With the aim of eliminating by-products, one of the generated mutants had the *buk, ctfAB, ldh,* and *pta-ack* genes deleted, while the other had the *buk, ctfAB, ldh,* and *hydA* genes knocked out. However, no details on yields and growth performance were given.

Recently, a novel genetic tool that allows stable genome insertion via homologous recombination was developed. Termed Allele-Coupled Exchange (ACE), this approach does not employ a counter selective marker to select for the rare second recombination event. Instead, it utilizes the activation or inactivation of gene(s) that result in a selectable phenotype, and asymmetrical homology arms to direct the order of recombination events (212). For example, a promoterless primary/secondary *adh* from *C. beijerinckii* NRRL B593 coupled to the *ermB* gene was introduced into the downstream region of the *thlA* gene in the genome of *C. acetobutylicum* ATCC 824. The native promoter of *thlA* drives the expression of *ermB* and *adh*, allowing selection for the second recombination event using erythromycin (or acid-stable analogue clarithromycin for organisms with low pH optimum (213)), and also creation of a recombinant that reduces acetone to the more desirable isopropanol (212). Remarkably, the whole genome of phage lambda (48.5 kb minus a 6 kb region) was successfully inserted into the genome of *C. acetobutylicum* ATCC 824 in three successive steps using this genetic tool. This technique was also demonstrated in *C. difficile* strain 630Δ*erm* and *C. sporogenes* NCIMB 10696, suggesting it is applicable to other *Clostridium* spp. (212, 214).

1.7.4 Transposon Mutagenesis

The clostridial genetic tools described so far constitute 'reverse genetics', in which a defined gene(s) is selectively inactivated or introduced to study the phenotype. In contrast, 'forward genetics' does not make any assumptions about the genes involved and aims to determine the genotype resulting in a particular phenotype. To achieve this, a random pool of mutants needs to be generated and this can be accomplished by means of transposon mutagenesis. Earlier efforts of transposon mutagenesis were demonstrated in *C. acetobutylicum* P262 (now: *C. saccharobutylicum* (215)), *C. acetobutylicum* DSM 792, *C. acetobutylicum* DSM 1732, and *C. beijerinckii* NCIM 8052, but issues with multiple transposon insertions per mutant, and non-random distribution of insertions were also reported (216, 217). Recent developments have seen the successful generation of mono-copy random

insertion of transposon *Tn1545* into *C. cellulolyticum* (218) and mariner transposon *Himar1* into *C. difficile* (219).

1.7.5 Metabolic Engineering of Solventogenic Clostridia

With established transformation protocols and great familiarity with its physiology, it is unsurprising that the majority of clostridial metabolic engineering efforts have been focused on *C. acetobutylicum* ATCC 824. The acetone that *C. acetobutylicum* naturally produces is not suitable as fuel, so a recent effort was made to convert the acetone into biofuel isopropanol by over-expressing a primary/secondary alcohol dehydrogenase from *C. beijerinckii* NRRL B593 and a synthetic *adc-ctfA-ctfB* operon. The engineered strain was able to convert almost all of the acetone into 5.1 g/L of isopropanol in flask culture (220). By inactivating *hbd* using ClosTron, production of C4 products such as butyric acid and butanol was diverted into ethanol biosynthesis, resulting in 33 g/L of ethanol (221). Transformation of *C. acetobutylicum* with a plasmid over-expressing acetoin reductase from *C. beijerinckii* NCIMB 8052 successfully converted acetoin into 22 mM of 2,3-butanediol (222). By overexpressing the native *ribGBAH* operon and mutated PRPP amidotransferase (involved in purine biosynthesis), *C. acetobutylicum* was able produce up to 190 mM butanol and 70 mg/L riboflavin, which is a valuable food/health supplement (223).

High aero-tolerance and solvent tolerance are desirable traits for industrial biofuel production. Both of these traits were improved when glutathione *gshA* and *gshB* genes from *E. coli* were overexpressed in *C. acetobutylicum* (224). In *C. cellulolyticum*, 8.9 mM isobutanol was successfully produced from cellulose when *kivD, yqhD, alsS, ilvC,* and *ilvD* were overexpressed (225). This approach is based on diverting 2-keto acid intermediates into alcohol production, and demonstrated in engineered *E. coli* to produce isobutanol, 1-butanol, 2-methyl-1-butanol, 3-methyl-1-butanol and 2-phenylethanol (226).

In cellulolytic *C. thermocellum*, inactivation of *ldh* and *pta* via homologous recombination using *hpt* (hypoxanthine phosphoribosyl transferase) as counter selective marker, followed by evolutionary adaptation increased ethanol yield by

four fold relative to WT (5.61 g/L vs. 1.3 g/L) (227). Recently, *C. tyrobutylicum* was successfully engineered to synthesize 16 g/L n-butanol from mannitol (a more reduced substrate than glucose), by overexpression of *C. acetobutylicum adhE2* in a Δ*ack* knockout mutant (228). A selection of genetically engineered solventogenic clostridia and acetogens are summarized in Table 1.2.

Table 1.2. Genetically modified solventogenic clostridia and acetogens

Organism	Genetic modification	Phenotypes/Effects	Ref
Acetogens			
C. ljungdahlii	Plasmid overexpression of butanol biosynthetic genes from *C. acetobutylicum* (*thlA, crt, hbd, bcd, adhE* and *bdhA*)	Produced 2 mM butanol from syngas	(37)
C. ljungdahlii	Chromosomal deletion of *adhE1* and/or *adhE2*	Ethanol titre of Δ*adhE1* mutant was reduced by 6 fold under heterotrophic conditions	(229)
C. ljungdahlii	Plasmid expression of acetone biosynthetic genes from *C. acetobutylicum* (*thlA, coAt,* and *adc*) under lactose inducible promoter	Produced 15 mM acetone from CO when induced	(230)
C. ljungdahlii	Chromosomal integration (single crossover recombination) of *thl-crt-bcd-etfB-etfA-hbd-ptb-buk* (from *C. acetobutylicum*) into *pta* promoter region	Produced ~10 mM butyrate under H_2 + CO_2 conditions	(231)
C. autoethanogenum	Plasmid overexpression of butanol biosynthetic genes from *C. acetobutylicum* (*thlA, crt, hbd, bcd*, *etfA, &etfB*)	Produced 26 mM butanol using steel mill gas	(232)
C. autoethanogenum	Plasmid expression of native *groES* and *groEL*	Increased alcohol tolerance	(233)
C. aceticum	Plasmid overexpression of acetone operon from *C. acetobutylicum* (*adc, ctfAB, thlA*)	Produced up to 140 µM acetone using gas	(234, 235)
A. woodii	Plasmid overexpression of formyl-THF-synthetase, methenyl-THF-cyclohydrolase, methylene-THF-dehydrogenase and methylene-THF-reductase of *C. ljungdahlii*	Increased volumetric acetate production rate by 14% under H_2 + CO_2 conditions in bioreactor	(236)
M. thermoacetica	Genome insertion of *ldh* from *Thermoanaerobacter pseudethanolicus* into *pyrF* locus	Produced 6.8 mM lactate from fructose while no lactate was detected in WT control	(237)
Acidogenesis and Solventogenesis			
C. acetobutylicum	Inactivation of *buk* and overexpression of *aad*	Produced same amount of butanol as control but relatively more ethanol, corresponding to a total alcohol tolerance of 21.2 g/L	(238)
C. acetobutylicum	Inactivation of *hbd* using ClosTron	Produced 716 mM ethanol by diverting C4 products	(221)

Organism	Genetic modification	Phenotypes/Effects	Ref
C. acetobutylicum	Inactivation of *ack* using ClosTron	Reduction in acetate kinase activity by more than 97% resulted in 80% less acetate produced but similar final solvent amount	(239)
C. tyrobutyricum	Inactivation of *ack* and plasmid overexpression of *adhE2* from *C. acetobutylicum*	Produced 216 mM butanol from mannitol	(240)
C. thermocellum	Inactivation of *ldh* and *pta* via homologous recombination	Showed 4 fold increase in ethanol yield (122 mM instead of 28 mM)	(227)
C. cellulolyticum	Inactivation of *ldh* and *mdh* (malate dehydrogenase) using ClosTron	Generated 8.5 times higher ethanol yield (56.4 mM) than wild type (6.5 mM)	(241)
C. acetobutylicum	Plasmid overexpression of a synthetic acetone operon (*adc, ctfA, ctfB*) and primary/secondary *adh* from *C. beijerinckii* NRRL B593	Produced 85 mM isopropanol	(220)
C. acetobutylicum	Genome insertion of *adh* gene from *C. beijerinckii* NRRL B593 using Allele-Coupled Exchange	Converted acetone into 28 mM isopropanol without affecting the yield of other fermentation products	(212)
Biosynthesis of New Products			
C. cellulolyticum	Plasmid overexpression of *kivD, yqhD, alsS, ilvC* and *ilvD*	Produced 8.9 mM isobutanol by diverting 2-ketoacid intermediates	(225)
C. acetobutylicum	Plasmid expression of native *ribGBAH* operon and mutated PRPP amidotransferase	Produced 70 mg/l riboflavin and 190 mM butanol	(223)
Solvent- and Aero-tolerance			
C. acetobutylicum	Plasmid overexpression of glutathione *gshA* and *gshB* from *E. coli*	Improved aero- and solvent-tolerance	(224)
C. acetobutylicum	Plasmid overexpression of chaperone *groESL*	Showed 85% decrease in butanol inhibition and 33% increase in solvent yield	(176)
Substrate Utilization			
C. acetobutylicum	Plasmid expression of *codh/acs, CoFeSP, cooC1, cooC2,* and *metr* from *C. ljungdahlii.* Genome integration of *fdh* from *C. ljungdahlii.*	Enzymatic activities of acetyl-CoA/CO exchange and CO oxidation demonstrated *in vitro*, but the recombinant organism was unable to grow autotrophically	(109, 110, 242)
C. acetobutylicum	Plasmid expression of *acsC, acsD* and *acsE* from *C. difficile*	Increased incorporation of CO_2 into extracellular products	(242)
***C. saccharoperbutylacetonicum* strain N1-4**	Knockdown hydrogenase *hupCBA* expression using siRNA delivered from plasmid	Significantly reduced hydrogen uptake activity to 13% (relative to control strain)	(202)

1.7.6 Recent Developments in Genetic Tools for Acetogens

Despite strong biotechnological interests and a long history of fundamental research, in particular the elucidation of the WLP, genetic manipulation of acetogens remains challenging. However, significant progress was made over the last 5 years as the

reports of recombinant acetogens began to emerge (Table 1.2). *A. woodii* was shown to be transformable with shuttle vectors using electroporation or conjugation as early as 1994 (243), but similar success has not been reported again until the publication by Straub *et al.* (2014) (236). In the latter study, the authors overexpressed the four THF-dependent enzymes from the WLP of *C. ljungdahlii* in *A. woodii*, resulting in 14% increase in volumetric acetate production rate (236). By delivering a plasmid that overexpresses *ctfA*, *ctfB*, *adc*, and *thlA* under the control of the *thlA* promoter, *C. aceticum* was demonstrated to produce up to 140 µM acetone using gas (80% H_2/20% CO_2 or 67% H_2/33% CO_2) as sole carbon and energy source (234, 235).

Ethanol producer *C. ljungdahlii* was first shown to be genetically amenable via electroporation by Köpke *et al.* (2010) (37). *C. ljungdahlii* does not naturally produce butanol, but by delivering a plasmid that overexpresses butanol biosynthetic genes (*thlA*, *hbd*, *crt*, *bcd*, *adhE* and *bdhA*) from *C. acetobutylicum* into this acetogen, up to 2 mM of butanol was produced (37). Although there has been no journal publication reporting recombinant *C. autoethanogenum*, a patent described the production of 25.7 mM butanol by genetically modified *C. autoethanogenum* using steel mill gas (composition 44% CO, 32% N_2, 22% CO_2, and 2% H_2) as the only source of carbon and energy (232). The acetogen was transformed with plasmid over-expressing *thlA, hbd, crt, bcd, etfA,* and *etfB*, from the promoter of the *pta-ack* operon.

The electroporation procedure for *C. ljungdahlii* was further improved by Leang *et al.* (2013) to reach transformation efficiencies of up to 1.7 x 10^4 cfu/µg DNA (229). The publication also reported the generation of chromosomal deletion of *adhE1* and/or *adhE2*, showing that *adhE1* but not *adhE2* is required for ethanol formation in *C. ljungdahlii* under heterotrophic conditions (229). By introducing a plasmid expressing *adhE1* from a lactose inducible promoter to the Δ*adhE1* mutant, ethanol production was restored to levels comparable to those in the WT strain (230). Ueki *et al.* (2014) was able to integrate (via single crossover recombination) the butyrate-biosynthetic pathway (*thlA-crt-bcd-eftB-etfA-hbd-ptb-buk*) from *C. acetobutylicum* into the promoter region of *pta*, resulting in the production of ~10 mM butyrate under H_2 + CO_2 conditions using *C. ljungdahlii* (231).

It should be mentioned that the group of Michael Tyurin from Syngas Biofuels Energy has published 12 articles during 2012-2013 regarding the genetic manipulation of acetogen *Clostridium* sp MT 351 (23). Besides the abnormally high recombinant product titres produced by the engineered strains, a number of other anomalies were detected in the reports of Tyurin and co-workers so these results should be examined with a note of caution (23).

1.8 Aims of PhD Project

Motivated by the potential of *C. autoethanogenum* to produce ethanol and 2,3-butanediol from waste gases, the overall aim of this PhD project was to develop genetic tools for this acetogen. Since no genetic manipulation has been reported for this microbe in the literature, the development of genetic tools including transformation protocols, plasmid overexpression, intron-based mutagenesis and homologous recombination were vigorously pursued. Once these tools were in place, they were deployed to investigate three industrially relevant aspects of *C. autoethanogenum*, including carbon fixation, ethanol formation and stress tolerance. The ambition was to utilize knowledge learnt from these three physiological aspects to formulate metabolic engineering efforts to construct a hyper-ethanol producing strain.

The specific aims of this PhD project were:

1. To establish an efficient method for introducing foreign DNA into *C. autoethanogenum* host cells.
2. To exemplify the feasibility of ClosTron mutagenesis to rapidly generate stable knock out mutants in *C. autoethanogenum*.
3. To demonstrate the utility of Allele-Coupled Exchange (ACE) in *C. autoethanogenum* by inactivation and subsequent activation of *pyrE* allele.

4. To generate *cooS* and *acsA* knockout mutants using ClosTron mutagenesis and examine the resulting phenotype under autotrophic and heterotrophic conditions.
5. To construct *adhE* and *aor* knockout mutants via ClosTron mutagenesis and investigate their impact on autotrophy and solventogenesis.
6. To overexpress native chaperones in *C. autoethanogenum* and determine its effects on stress tolerance and solventogenesis.
7. To create *acsA* and *aor* overexpression strains and assess outcomes in terms of autotrophy and product formation.

CHAPTER 2

MATERIALS AND METHODS

2 Materials and Methods

2.1 Materials

Unless stated otherwise, all chemicals and biochemicals were supplied by Sigma-Aldrich and Fisher Scientific. Bacterial growth media were purchased from Oxoid. New England Biolabs (NEB) and Fermentas supplied enzymes and buffers for the purpose of molecular biology. Qiagen Ltd, Life Technologies, and Zymo Research provided kits for the extraction and purification of nucleic acids. Analytic consumables were provided by Thermo Scientific. Glassware and accessories for anaerobic culturing were sourced from Glasgerätebau Ochs GmbH. For genetic manipulation and cultivation of clostridia, both MG1000 Mark II Anaerobic Work Station (Don Whitley Scientific Ltd) and anaerobic chambers (Coy Laboratory Products) were employed. Inside both anaerobic cabinets, an atmosphere containing 80% N_2, 10% CO_2 and 10% H_2 was maintained. Research grade gases (CO, CO_2, H_2, and N_2) were purchased from BOC.

2.1.1 Bacterial Strains

Table 2.1. Bacterial strains used in this work.

Strain	Description/Genotype	Source/Reference
Escherichia coli TOP10	Plasmid storage strain. F- *mcrA Δ(mrr-hsdRMS-mcrBC) φ80lacZΔM15 ΔlacX74 deoR recA1 araD139 Δ(ara-leu)7697 galU galK rpsL*(Str^R) *endA1 nupG*	Invitrogen Ltd
Escherichia coli XL1-Blue MRF` Kan	Plasmid storage strain. *Δ(mcrA)183 Δ(mcrCB-hsdSMR-mrr)173 endA1 supE44 thi-1 recA1 gyrA96 relA1 lac* [*F'proAB lacI^{q}ZΔM15* Tn*10* (Tet^R)]	Stratagene
Escherichia coli CA434 (HB101 + plasmid R702)	Conjugative transfer strain. *thi-I hsdS20* (r_B, m_B) *supE44 recAB ara-14 leuB5proA2 lacYI galKI rpsL20* (Str^R) *xyl-5 mt1-1*	M. Young, UCW, Aberystwyth, UK (178)
Clostridium acetobutylicum ATCC 824	Wild-type isolate	N.P. Minton, University of Nottingham, UK
Clostridium ljungdahlii DSM 13582	Wild-type isolate	DSMZ (German Collection of Microorganisms and Cell Cultures GmbH)
Clostridium autoethanogenum DSM 10061	Wild-type isolate	DSMZ
Clostridium autoethanogenum pyrE::CTermB-144s	Group II intron directionally inserted at *pyrE* (CAETHG_1476) gene locus	This study

Strain	Description/Genotype	Source/Reference
Clostridium autoethanogenum codA::CTermB-532s	Group II intron directionally inserted at *codA* (CAETHG_4058) gene locus	This study
Clostridium autoethanogenum fruA::CTermB-1126s	Group II intron directionally inserted at fructose phosphotransferase (*fruA*) EIIABC subunit (CAETHG_0142) gene locus	This study
Clostridium autoethanogenum cooS1::CTermB-601s	Group II intron directionally inserted at mono-functional *cooS1* (CAETHG_3005) gene locus	This study
Clostridium autoethanogenum cooS2::CTermB-529s	Group II intron directionally inserted at mono-functional *cooS2* (CAETHG_3899) gene locus	This study
Clostridium autoethanogenum acsA::CTermB-143s	Group II intron directionally inserted at *acsA* gene locus (CAETHG_1621; encodes CODH subunit of bi-functional CODH/ACS complex)	This study
Clostridium autoethanogenum adhE1a::CTermB-115s	Group II intron directionally inserted at upstream ald domain of *adhE1* (CAETHG_3747) gene locus	This study
Clostridium autoethanogenum adhE1b::CTermB-541s	Group II intron directionally inserted at downstream adh domain of *adhE1* (CAETHG_3747) gene locus	This study
Clostridium autoethanogenum adhE2::CTermB-662s	Group II intron directionally inserted at *adhE2* (CAETHG_3748) gene locus	This study
Clostridium autoethanogenum aor1::CTermB-361s	Group II intron directionally inserted at *aor1* (CAETHG_0092) gene locus	This study
Clostridium autoethanogenum aor2::CTermB-370s	Group II intron directionally inserted at *aor2* (CAETHG_0102) gene locus	This study
Clostridium autoethanogenum ΔpyrE in-frame deletion (IFD) mutant	*pyrE* IFD created via ACE	This study
Clostridium autoethanogenum pyrE complemented mutant	*pyrE* IFD complemented via ACE with concurrent insertion of *lacZ* downstream of *pyrE* locus	This study
Clostridium autoethanogenum pyrE corrected mutant	*pyrE* IFD corrected via ACE	This study
Clostridium autoethanogenum ΔadhE1 IFD mutant	*adhE1* IFD in *ΔpyrE* strain	This study
Clostridium autoethanogenum $\Delta adhE1^{mut}$ IFD mutant	*adhE1* IFD with unintended *adhE2* promoter deletion in *ΔpyrE* strain	This study
Clostridium autoethanogenum ΔadhE1+2 IFD mutant	*adhE1* and *adhE2* IFD in *ΔpyrE* strain	This study
Clostridium autoethanogenum Δaor2 IFD mutant	IFD of *aor2* in *aor1*::CTermB-361s; *pyrE* allele restored to WT	This study
Clostridium autoethanogenum ΔcooS1 IFD mutant	IFD of *cooS1* in *cooS2*::CTermB-529s; Δ*pyrE* strain	This study

2.1.2 Plasmids

Table 2.2. Plasmids used in this study

Plasmid	Description	Source/Reference
***E. coli/Clostridium* Shuttle Plasmids**		
pMTL82151	*E. coli/Clostridium* modular shuttle vector, pBP1, ColE1+tra, Cm^R/Tm^R	Heap *et al.* (2009) (244)
pMTL83151	*E. coli/Clostridium* modular shuttle vector, pCB102, ColE1+tra, Cm^R/Tm^R	Heap *et al.* (2009) (244)
pMTL84151	*E. coli/Clostridium* modular shuttle vector, pCD6, ColE1+tra, Cm^R/Tm^R	Heap *et al.* (2009) (244)
pMTL85151	*E. coli/Clostridium* modular shuttle vector, pIM13, ColE1+tra, Cm^R/Tm^R	Heap *et al.* (2009) (244)
pMTL500E	*E. coli/Clostridium* shuttle vector, pAMβ1, Em^R	Swinfield *et al.* (1990) (245)
pJIR418	*E. coli/Clostridium* shuttle vector, pIP404, pMB1, Cm^R, Em^R	N.P. Minton, University of Nottingham, UK
Methylation Plasmid		
pAN2	Methylation plasmid derived from pAN1 but with Tet^R. φ3T I methyltransferase gene of *Bacillus subtilis* phage φ3tI , p15a	S. Cartman, University of Nottingham, UK
ClosTron Retargeting Plasmids		
pMTL007C-E2	Clostridial expression vector for the ClosTron, containing a directed Group II intron with Erm RAM, flanked by FRT sites, ColE1, pCB102, Cm^R/Tm^R	Heap *et al*. (2010) (206)
pMTL007C-E2::*pyrE*-144s	ClosTron vector targeting Group II insertional knockout at the *C. autoethanogenum pyrE* locus (CAETHG_1476)	A. M. Henstra, University of Nottingham, UK
pMTL007C-E2::*codA*-532s	ClosTron vector targeting Group II insertional knockout at the *C. autoethanogenum codA* locus (CAETHG_4058)	This work
pMTL007C-E2::*fruA*-1126s	ClosTron vector targeting Group II insertional knockout at the *C. autoethanogenum fruA* EIIABC subunit locus (CAETHG_0142)	This work
pMTL007C-E2::*cooS1*-601s	ClosTron vector targeting Group II insertional knockout at the *C. autoethanogenum cooS1* locus (CAETHG_3005)	This work
pMTL007C-E2::*cooS2*-529s	ClosTron vector targeting Group II insertional knockout at the *C. autoethanogenum cooS2* locus (CAETHG_3899)	This work
pMTL007C-E2::*acsA*-143s	ClosTron vector targeting Group II insertional knockout at the *C. autoethanogenum acsA* locus (CAETHG_1621)	This work
pMTL007C-E2::*adhE1a*-115s	ClosTron vector targeting Group II insertional knockout at the *C. autoethanogenum adhE1* locus (upstream Ald domain of CAETHG_3747)	This work
pMTL007C-E2::*adhE1b*-541s	ClosTron vector targeting Group II insertional knockout at the *C. autoethanogenum adhE1* locus (downstream Adh domain of CAETHG_3747)	This work
pMTL007C-E2::*adhE2*-662s	ClosTron vector targeting Group II insertional knockout at the *C. autoethanogenum adhE2* locus (CAETHG_3748)	This work
pMTL007C-E2::*aor1*-361s	ClosTron vector targeting Group II insertional knockout at the *C. autoethanogenum aor1* locus (CAETHG_0092)	This work

Plasmid	Description	Source/Reference
pMTL007C-E2::*aor2*-370s	ClosTron vector targeting Group II insertional knockout at the *C. autoethanogenum aor2* locus (CAETHG_0102)	This work
Overexpression Plasmids		
pMTL83156	Overexpression plasmid with C. autoethanogenum *pfor* (CAETHG_3029) promoter cloned between NotI and NdeI sites	This work
pMTL83157	Overexpression plasmid with *C. autoethanogenum acsA* (CAETHG_1621) promoter cloned between NotI and NdeI sites	This work
pMTL83157-*acsA*^{trunc}	Overexpression plasmid of *C. autoethanogenum* truncated *acsA* (CAETHG_1621)	This work
pMTL83157-*acsA*^{full}	Overexpression plasmid of *C. autoethanogenum acsA* (CAETHG_1621 and CAETHG_1620)	This work
pMTL83151-P_{acsA}-*acsA*(TGA)-FLAG	Overexpression plasmid of *C. autoethanogenum acsA* (CAETHG_1621 and CAETHG_1620) with native 'TGA' codon. FLAG tag at C-terminus	This work
pMTL83151- P_{acsA}-*acsA*(TCA)-FLAG	Overexpression plasmid of *C. autoethanogenum acsA* (CAETHG_1621 and CAETHG_1620) with mutated 'TCA' codon. FLAG tag at C-terminus	This work
pMTL83151- P_{acsA}-*acsA*(TAA)-FLAG	Overexpression plasmid of *C. autoethanogenum acsA* (CAETHG_1621 and CAETHG_1620) with mutated 'TAA' codon. FLAG tag at C-terminus	This work
pMTL83151-P_{acsA}-FLAG-*acsA*	Overexpression plasmid of *C. autoethanogenum acsA* (CAETHG_1621 and CAETHG_1620) with native 'TGA' codon. FLAG tag at N-terminus	This work
pMTL83157-*aor1*	Overexpression plasmid of *C. autoethanogenum aor1*	This work
pMTL83156-*groESL*	Overexpression plasmid of *C. autoethanogenum* chaperone *groES-groEL* (CAETHG_1573-1572) operon	This work
pMTL83156-*grpE-dnaKJ*	Overexpression plasmid of *C. autoethanogenum* chaperone *grpE-dnaK-dnaJ* (CAETHG_2890-2892) operon	This work
pMTL83156-*grpE-dnaKJ*-P_{acsA}-*groESL*	Overexpression plasmid of *C. autoethanogenum* chaperone *grpE-dnaK-dnaJ* operon. The second *C. autoethanogenum* chaperone operon *groES-groEL* is driven by a second promoter, P_{acsA}	This work
In-Frame Deletion and Correction Plasmids		
pMTL84151-Δ*pyrE*	ACE plasmid for creation of the Δ*pyrE* (CAETHG_1476) IFD strain in *C. autoethanogenum.* Plasmid contains functional *C. acetobutylicum pyrE*	This work
pMTL84151-com*pyrE*	ACE plasmid for complementation of the Δ*pyrE* IFD strain in *C. autoethanogenum* with concurrent insertion of *lacZ* downstream of *pyrE* locus (CAETHG_1476)	This work
pMTL84151-fix*pyrE*	ACE plasmid for repair of the Δ*pyrE* (CAETHG_1476) IFD strain in *C. autoethanogenum*	This work
pMTL84151-*adhE1*-IFD	ACE plasmid for the creation of *adhE1* (CAETHG_3747) IFD in *C. autoethanogenum.* Plasmid contains functional *C. acetobutylicum pyrE*	This work
pMTL84151-*adhE1&2*-IFD	ACE plasmid for the creation of *adhE1* and *adhE2* (CAETHG_3747-3748) IFD in *C. autoethanogenum*. Plasmid contains functional *C. acetobutylicum pyrE*	This work
pMTL84151-*cooS1*-IFD	ACE plasmid for the creation of *cooS1* (CAETHG_3005) IFD in *C. autoethanogenum*. Plasmid contains functional *C. acetobutylicum pyr*E	This work

Plasmid	Description	Source/Reference
pMTL84151-*aor2*-IFD	ACE plasmid for the creation of *aor2* (CAETHG_0102) IFD in *C. autoethanogenum*. Plasmid contains functional *C. acetobutylicum pyrE*	This work

2.1.3 Oligonucleotide Primers

Table 2.3. Oligonucleotides used in this study

Oligonucleotides	DNA Sequence (5`-3`)	Function(s)
General		
Univ-0027-F	GCGAGAGTTTGATCCTGGCTCAG	Amplification and sequencing of 16s rRNA for Eubacteria; (Weisburg *et al.,* 1991) (246)
Univ-1492-R	CGCGGTTACCTTGTTACGACTT	
RAM-F	ACGCGTTATATTGATAAAAATAATAATAGTGGG	PCR screening for splicing of ermRAM from ClosTron vector
RAM-R	ACGCGTGCGACTCATAGAATTATTTCCTCCCG	
M13 Forward (-20)	TGTAAAACGACGGCCAGT	Sequencing of cloned insert(s) in pMTL modular plasmids
M13 Reverse	CAGGAAACAGCTATGACC	
repHf	AAGAAGGGCGTATATGAAAACTTGT	Detection of plasmids with catP resistance marker and repH replicon
catR	TTCGTTTACAAAACGGCAAATGTGA	
ClosTron Screening Oligonucleotides		
pyrE-F	TCTGTGGATTTTTCTCCGTGAGCGT	PCR screening for integration of Intron I into *pyrE*
pyrE-R	TGGCGGGAGCTTATGCAATTCAAGT	
codA-532s-F	AGATGTTACAGATCCAGAGCTTACAGCATT	PCR screening for integration of Intron I into *codA*
codA-532s-R	TTGCCGTAACCTTTTCTCCTATTCCGT	
fruA-1126s-F	ACAGGCTTTATACCTTCAAGTGAAGCAGG	PCR screening for integration of Intron I into *fruA*
fruA-1126s-R	TGGCATTAAAAGCTTTGATCCTAAAGATCCG	
cooS1-601s-F	TGGAGTGCTGGTGGCCTGTT	PCR screening for integration of Intron I into *cooS1*
cooS1-601s-R	AAAAGCTGTACTAGTAGCTGATGCCGT	
cooS2-529s-F	GAGCTGGTACATATAGCCATCATGC	PCR screening for integration of Intron I into *cooS2*
cooS2-529s-R	CTGTACCATTTCAAGTCCTATTTGTGC	
acsA-ClosTron-F	AGGCTACTTTACAATTATTGGACAAGGC	PCR screening for integration of Intron I into *acsA*
acsA-ClosTron-R	GCCCTTGGATATACACCTAATTTTCTCC	
adhE1a-115s-F	ACTGCTAAAAATTAGGAAAGAGGTGTCGCT	PCR screening for integration of Intron I into upstream Ald domain of *adhE1*
adhE1a-115s-R	CTGCATCTCTCTCTAAAACTCCACAGGT	
adhE1b-255a-F	ATGTGGACAAAGTTACAAAAGTTCTTGAGGAAC	PCR screening for integration of Intron I into downstream Adh domain of *adhE1*

Oligonucleotides	DNA Sequence (5`-3`)	Function(s)
adhE1b-255a-R	CTCATAGCTAAATCTTCAAATTTTACTTCTGGATGC	
adhE2-662s-F	GCTAAGATAGTACTTGATGCAGCAGTTAAAGC	PCR screening for integration of Intron I into *adhE2*
adhE2-662s-R	CTGACTGCTCTGAAGCACAAATCATACCA	
aor1-559s-F	GCACCGCTTACAGGAACTATAGG	PCR screening for integration of Intron I into *aor1*
aor1-559s-R	CAGCTAAAGCTATTTTTCCAGTTCC	
aor2-370s-F	GCACCTGTTCCAACAAGCGGAA	PCR screening for integration of Intron I into *aor2*
aor2-370s-R	ACTTTTCCCCAGCTGGTCCTATGC	
Oligonucleotides for Construction of Overexpression Plasmids		
acsA-NdeI-F	GGGAATTAGCCATATGGAAGAAAAAGC	Forward primer for cloning of *C. autoethanogenum acsA* (CAETHG_1621 or CAETHG_1621&1620)
acsA-SacI-R	CTTGGAGCTCTTCATTTCAATTCAGG	Reverse primer for cloning of part of *C. autoethanogenum acsA* (CAETHG_1621)
acsA-SOE-B	CAAGAACCCATGTGAAGTACAGG	SOE PCR to mutate internal *NdeI* restriction site in downstream CDS of *C. autoethanogenum acsA* (CAETHG_1620)
acsA-SOE-C	CCTGTACTTCACATGGGTTCTTG	
acsA-SacI-R2	ATTTGAGCTCTGGCATGGC	Reverse primer for cloning of complete *C. autoethanogenum acsA* (CAETHG_1621 & 1620)
P_{acsA}-SacI-F	TTCACCAGAGCTCGTCATAATAGTTCCAG	Forward primer for amplification and cloning of *C. autoethanogenum acsA* with native promoter
acsA(TCA)-SOE-B	CAAAATTGCCTTTGATTTCAATTCAGG	To mutate internal 'TGA' codon of *C. autoethanogenum acsA* into 'TCA' codon
acsA(TCA)-SOE-C	TGAATTGAAATCAAAGGCAATTTTGGG	
acsA(TAA)-SOE-B	CAAAATTGCCTTTTATTTCAATTCAGG	To mutate internal 'TGA' codon of *C. autoethanogenum acsA* into 'TAA' STOP codon
acsA(TAA)-SOE-C	TGAATTGAAATAAAAGGCAATTTTGGG	
acsA-FLAG-BamH1-R	TTGGATCCTTATTATTTGTCATCGTCATCTTTATAATCGATACCTAATTTTTTAC	Reverse primer for amplification and cloning of *C. autoethanogenum acsA* fused with FLAG tag at C-terminus
NcoI-FLAG-acsA-F	TTACCATGGATTATAAAGATGACGATGACAAAGAAGAAAAAGCAAAATC	Amplification and cloning of *C. autoethanogenum acsA* (CAETHG_1621 & 1620) with FLAG tag fused at N-terminus
acsA-HindIII-R	TTTAAGCTTTGGCATGGCAATTGC	
P_{acsA}-NcoI-R	AATCCATGGTAATAATTCCCTCCTTAAAG	Reverse primer for amplification and cloning of native promoter of *C. autoethanogenum acsA*
aor1-NdeI-F	AATTCATATGTATGGTTATGATGGTAAAGTATTAAG	SOE PCR to mutate two internal *Nde*I restriction sites and clone *aor1* from *C. autoethanogenum*
aor1-SOE-B1	CTAAATCATAAGAACCACAGTCAGATCC	
aor1-SOE-C1	CTGACTGTGGTTCTTATGATTTAGATGC	
aor1-SOE-C2B	ATTCCAGCTTATGATCCAAGGGG	
aor1-SOE-B2B	CCCCTTGGATCATAAGCTGGAAT	
aor1-KpnI-R	CTAGGTACCCGAATCAAACTAGAACTTACC	
P_{pfor}-NotI-F	AAGCGGCCGCAAAATAGTTGATAATAATGC	Amplification and cloning of *pfor* (CAETHG_3029) promoter from *C. autoethanogenum*
P_{pfor}-NdeI-R	TACGCATATGAATTCCTCTCCTTTTCAAGC	

Oligonucleotides	DNA Sequence (5`-3`)	Function(s)
SOE-groESL-a-NdeI	GGGTTCATATGAAAATTAGACCACTTGG	SOE PCR to mutate internal *Nde*I restriction site and clone chaperones *groES-groEL* from *C. autoethanogenum*
SOE-groESL-b	TCCCATGTTTTCATAAGGATCTTCTAATTC	
SOE-groESL-c	ATTAGAAGATCCTTATGAAAACATGGGAGC	
SOE-groESL-d-EcoRI	CTTAGAATTCCTTTTGAATTAGTACATTCC	
grpE-NdeI-F	GCCATATGTTAAAGGATAAAGGTGATAATG	Amplification and cloning of chaperones *grpE-dnaK-dnaJ* from *C. autoethanogenum*
dnaJ-SacI-R	CCGAGCTCTATTAGTGGTGATGTTTAAG	
P_{acsA}-KpnI-F	CAAGGTACCAGATAGTCATAATAGTTCCAG	Amplification and cloning of *acsA* promoter of *C. autoethanogenum* for overexpression of second chaperone operon
P_{acsA}-BamH1-R	TTCGGATCCAATAATTCCCTCCTTAAAG	
groESL-BamH1-F	ACTATGGATCCAAAATTAGACCACTTG	Amplification and cloning of *C. autoethanogenum groES -groEL* operon for construction of double chaperone overexpression plasmid
groESL-SalI-R	CTTAGTCGACCTTTTGAATTAGTACATTCC	
Oligonucleotides for Screening and Construction of IFD Mutants		
IFD-plasmid-F	TGAAGTACATCACCGACGAGC	Anneal to region prior to left homology arm (LHA) of IFD plasmid. To be used for screening of single crossover mutant at LHA
IFD-plasmid-R	TTCCCAAATCCTTACATCTCCCC	Anneal to region downstream of right homology arm (RHA) of IFD plasmid. To be used for screening of single crossover mutant at RHA
ACE-pyrE-SC-F1 (also known as “P1”)	ACGCTCACGGAGAAAAATCCACAGA	Detection of single crossover at the great homology arm of *pyrE*, but also amplify from ACE plasmid
ACE-pyrE-SC-R1 (also known as “P2”)	ACTCTGCTTGGTCGGCTTAGGG	
ACE-pyrE-F3 (also known as “P3”)	GTTCCTGTAGTTGGAATAGGTGGAATAGTAAGC	Detection of double crossover at the short homology arm of *pyrE*
ACE-pyrE-R3 (also known as “P4”)	TCGAGATCTCCATGGACGCGTGA	
ACE-pyrE-F	GAGCTTATGCAATTCAAGTAGGTACTGCAAAC	Detection and subsequent sequencing of restored *C. autoethanogenum pyrE*
ACE-pyrE-R	CATCAAAGCTATACTATTTTCCGTATTTACATTTGGG	
adhE1-IFD-F	CTAACATCAAGGGGTTTATTTGTCAC	Screening of double crossover and subsequent sequencing of *C. autoethanogenum adhE1*
adhE1-IFD-R	GTTACCTTAGTTACCTTCATTAATGACAC	
adhE1-seq-F	GCAAGATTTCAATAAAGGGTGTATTTTACC	Screening of double crossover and subsequent sequencing of *C. autoethanogenum adhE1 + adhE2*
adhE2-seq-R	CAATATATTATAAAATAGGGAGTGGAATGTTCC	
aor2-seq-F	CACCTTTAAGAGATAGAAAAGAAGATATCCC	Screening of double crossover and subsequent sequencing of *C. autoethanogenum aor2*
aor2-seq-R	TTTTCCTAATGCTTTTACCTCTATTAGTGG	
cooS1-seq-F	GGAATATCTGAATTGCAAGCTAAGTC	Screening of double crossover and subsequent sequencing of *C. autoethanogenum cooS1*
cooS1-seq-R	ATACATCTTGAATAAACTGCATCATCC	
adhE1-ald-LHA-SacII-F	TATCTTCCGCGGGTATTAAATTG	SOE-PCR to construct homology arms for IFD of *C.*

Oligonucleotides	DNA Sequence (5`-3`)	Function(s)
	TAAAATATCC	*autoethanogenum adhE1*
adhE1-IFD-LHA-R	ATTTAATAATTACATTAATTAGC GACACCTCTTTCC	
adhE1-IFD-RHA-F	GGTGTCGCTAATTAATGTAATTA TTAAATAAAAATGGTG	
adhE1-IFD-RHA-AscI-R	TTGGCGCGCCTAGTGATTTAAAT ATTGC	
adhE1&2-SOE-B	ATTATATATTTACATTAATTAGCG ACACCTCTTTCC	SOE-PCR to construct homology arms for IFD of *C. autoethanogenum adhE1 & 2*
adhE1&2-SOE-C	CGCTAATTAATGTAAATATATAA TAAATTGAATATAGTAAAC	
adhE1&2-RHA-AscI-R	GGTGGCGCGCCTTTATTTCC	
cooS1-LHA-SacII-F	TGTCCGCGGAAGTATATATGCC	SOE-PCR to construct homology arms for IFD of *C. autoethanogenum cooS1*
cooS1-LHA-R	CCACCTTCTAAATTTTACATAATA AAACCTCC	
cooS1-RHA-F	GGAGGTTTTATTATGTAAAATTT AGAAGGTGG	
cooS1-RHA-AscI-R	GTTGGCGCGCCATTTATTCC	
aor2-LHA-SacII-F	ACTCCGCGGCTAAAGTAAGTAA G	SOE-PCR to construct homology arms for IFD of *C. autoethanogenum aor2*
aor2-LHA-R	CTCTAATTAATCAAACTACATAA AAACCCTCC	
aor2-RHA-F	GGAGGGTTTTTATGTAGTTTGAT TAATTAGAG	
aor2-RHA-AscI-R	TTTGGCGCGCCTATAGTATCTG	
Oligonucleotides for Sanger Sequencing		
acsA-seq-F	GTTATTTCTTTAAGGAGGGAATT ATTAAAATGG	Amplification and sequencing of *acsA* in *C. autoethanogenum*
acsA-seq-R	AGCTTTTAAGGCATTTTAACTTTG GC	
acsA-seq1	CCATTGATACAGAGGCAAATCTT GG	
acsA-seq2	AAAGAGGTATATGTGGAGCTAC AGC	
acsA-seq3	GTTGATATAAGTCGTATATTAGA TTTGGTTGG	
grpE-seq1	CATCAGTAGTATCATTCCAGGC	Sequencing of cloned *grpE-dnaK-dnaJ* operon
grpE-seq2	AAATAAGATCATATTAGTTGGTG G	
grpE-seq3	GGAATTACATCTAAAATATATAG TCAG	

Notes: Restriction sites are underlined.

2.2 Bioinformatics Tools

Visualization of genomes, annotations, sequence alignment, oligonucleotide design, and gene translation were performed using Geneious (Biomatters Ltd). Prediction of bacterial promoter, operon and gene finding were undertaken with Softberry

(www.softberry.com). Basic Local Alignment Searches against a nucleotide database were performed using the BLASTn algorithm provided by NCBI.

2.3 Data Analysis and Presentation

Statistical analysis and graphically presented results were performed using GraphPad Prism. Two-tailed, unpaired, parametric student's t-tests were employed for comparison of means.

2.4 General Microbiological Techniques

2.4.1 Growth Medium

Outlined below are the compositions for all media used in this study. Solid agar medium was prepared by the addition of 1.5% (w/v) No. 1 bacteriological agar (Oxoid) to the liquid broth in question prior to autoclaving. All media were sterilised by autoclaving for 20 min at 121^{o}C unless otherwise stated.

2.4.1.1 Luria-Bertani Medium (LB)

Luria-Bertani (LB) broth contained 10 g of tryptone (Difco Laboratories), 5 g of yeast extract (Difco Laboratories) and 10 g sodium chloride in 1 L of dH_2O.

2.4.1.2 Clostridial Growth Medium (CGM)

For growth experiments of *C. autoethanogenum* and *C. ljungdahlii*, clostridial growth medium (CGM; Table 2.4) was employed. The entire ingredients listed in Table 2.4 except MES were added before microwaving until bubbles were visible (approximately 10 min in the microwave for 1 L medium). Following the addition of MES, the solution was bubbled with N_2 for 2 h before pH adjustment to 5.8 using HCl. Inside the anaerobic chamber (Coy Laboratory Products), an appropriate amount of medium was dispensed into serum bottles or Schott bottles and then transferred out the anaerobic chamber and sterilized by autoclaving. Prior to inoculation, reducing

agent stock 1 and 2 (Table 2.7) were added to 1x concentration. For heterotrophic growth experiments, 10 g/L fructose was added prior to microwaving and the medium was designated 'CGMF'. When 1 g/L of yeast extract was added the medium was termed 'CGMYF'. The medium was designated 'CGMCF' when 1 g/L of casein acid hydrolysate was added.

Table 2.4. Clostridial growth medium (CGM)

Media component	Amount per 1 L of media
NH_4Cl	0.25 g
KCl	0.1 g
$MgSO_4.7H_2O$	0.2 g
KH_2PO_4	0.2 g
$CaCl_2.2H_2O$	0.02 g
NTA (Nitriloacetic acid)	0.05 g
$Fe(SO_4)_2.7H_2O$	0.05 g
Sodium acetate.$3H_2O$	0.25 g
Resazurin	1 mg
Trace metal solution	10 mL
Wolfe's vitamin solution	10 mL
MES (2-(N-morpholino)ethanesulfonic acid)	20 g
Yeast extract or casein acid hydrolysate	1 g
Optional: D-Fructose	10 g
dH_2O	Up to 1 L, pH 5.8 (adjusted with HCl)

Table 2.5. Wolfe's vitamin solution

Wolfe's Vitamin Solution	Amount per L of Stock
Biotin	2 mg
Folic acid	2 mg
Pyridoxine hydrochloride	10 mg
Thiamine.HCl	5 mg
Riboflavin	5 mg
Nicotinic acid	5 mg
Calcium D-(+)-pantothenate	5 mg
Vitamin B_{12}	0.1 mg
p-Aminobenzoic acid	5 mg
Thioctic acid	5 mg
dH_2O	To 1 L

Table 2.6. Trace metal solution

Trace Metal Solution	Amount per L of Stock
Nitrilotriacetic Acid	2 g
$MnSO_4.H_2O$	1 g
$Fe\ (SO_4)_2(NH_4)_2.6H_2O$	0.8 g
$CoCl_2.6H_2O$	0.2 g
$ZnSO_4.7H_2O$	0.2 mg
$CuCl_2.2H_2O$	0.02 g
$NaMoO_4.2H_2O$	0.02 g
Na_2SeO_3	0.02 g
$NiCl_2.6H_2O$	0.02 g
$Na_2WO_4.2H_2O$	0.02 g
dH_2O	To 1 L

Table 2.7. Reducing agent stocks

Reducing Agent Stock 1 (100x)	Amount per 100 mL of Stock
Cysteine.HCl	4 g
dH_2O	To 100 mL
Reducing Agent Stock 2 (200x)	**Amount per 100 mL of Stock**
NTA (Nitrilotriacetic acid)	7.64 g
Na_2CO_3	5.33 g
$TiCl_3$	62.7 mM
dH_2O	To 100 mL

2.4.1.3 YTF and YTG Medium

To prepare 1 L of YT medium, 16 g of tryptone, 10 g of yeast extract, 0.2 g of sodium chloride, 10 mL of Wolfe's vitamin solution (Table 2.5), and 10 mL of trace metal solution (Table 2.6) were added. For YTF medium, 10 g of fructose was added per litre. For YTG medium, 10 g of glucose was added per litre. The pH was adjusted to 5.8 using 3 M sodium hydroxide. Following autoclave sterilization and immediately prior to use, 1% (v/v) of cysteine stock solution and 0.5% (v/v) of Ti-NTA were added to liquid medium. For solid medium, 200 µL of cysteine stock solution was spread on top of 20 mL solid medium in a plate and was allowed to dry for at least 4 h prior to use.

2.4.1.4 Supplements

All media supplements were prepared as stock solutions (Table 2.8) according to the manufacturer's instructions, and stored at the appropriate temperature for no longer than four weeks. Supplements that were dissolved in dH_2O and DMSO (Dimethylsulfoxide) were sterilised by syringe filtration through a 0.2 µm membrane prior to use (Minisart®).

Table 2.8. Antibiotics and supplements used in this study.

Antibiotic/Supplement	Stock concentration (mg/mL)	Solvent	Working concentration for *E. coli* (µg/mL)	Working concentration for clostridia (µg/mL)
Chloramphenicol (Cm)	25	Ethanol	25	
Erythromycin (Em)	50	Ethanol	500	
Trimethoprim	10	DMSO	10	
Spectinomycin	100	dH_2O	250*	
Tetracycline	5	70% Ethanol	10	
Thiamphenicol (Tm)	15	DMSO		7.5 - 15
Clarithromycin (Cla)	6	DMSO		6
5-Fluoroorotic acid (FOA)	150	DMSO		1500
5-Fluorocytosine (FC)	100	DMSO		100
Uracil	1	dH_2O		20

*100 µg/mL for *E. coli* CA434

2.5 General Molecular Techniques

2.5.1 Generation of Genomic DNA from Clostridial Species

For PCR amplifications, genomic DNA (gDNA) from clostridia was isolated using DNeasy Blood and Tissue kit (Qiagen) or Purelink Genomic DNA Mini kit (Life Technologies). For Southern blot analysis, genomic DNA from *C. autoethanogenum* was extracted according to Bertram and Dürre (216). A 100 mL overnight culture was harvested (6,000 x *g*, 15 min, 4 °C), washed with potassium phosphate buffer (10 mM, pH 7.5) and suspended in 1.9 mL STE buffer (50 mM Tris-HCl, 1 mM EDTA, 200 mM sucrose; pH 8.0). 300 µL lysozyme (~100,000 U) were added and the mixture was incubated at 37°C for 30 min, followed by addition of 280 µL of a 10% w/v SDS

solution and another incubation for 10 min. RNA was digested at room temperature for 10 min by addition of 240 µL of an EDTA solution (0.5 M, pH 8), 20 µL Tris-HCl (1 M, pH 7.5), and 10 µL RNase A (Fermentas). Then, 100 µL Proteinase K (0.5 U) were added and proteolysis took place for 1-3 h at 37 °C. Finally, 600 µL of sodium perchlorate (5 M) were added, followed by a phenol-chloroform extraction and an isopropanol precipitation.

2.5.2 Southern Blot Analysis

Each DNA sample (1 µg) was digested overnight with *Hind*III restriction enzyme according to 2.5.6 and was run on a 0.8% agarose gel as described in 2.5.4. DNA was transferred to a piece of Amersham Hybond ECL nitrocellulose membrane (GE Healthcare) by pressure-driven capillary action using filter paper (Whatman) soaked with 0.4 M NaOH. Following 2 – 3 h of transfer, the membrane was wrapped in cling film and exposed to UV light for 2 min on each side to crosslink the DNA, and then rinsed in 2x SSC (300 mM sodium chloride, 30 mM sodium citrate, pH 7) to remove excess NaOH. Blots were incubated in 10 mL DIG Easy Hyb (Roche) in Techne Hybridiser oven HB- 1D at 42^{o}C for 1 h. The Easy Hyb solution was discarded and replaced with 10 mL DIG Easy Hyb containing 1 µg DIG-labelled DNA probe which had been boiled for 10 min and chilled on ice prior to use. Probes were generated by PCR, followed by purification and labelling by incorporating DIG-labelled dUTPs using DIG High Prime (Roche). The probe solution was incubated overnight at 42^{o}C.

The membrane was subjected to two low stringency washes (2 X SSC, 0.1% w/v SDS) for 5 min at room temperature and then two high stringency washes (0.5 X washing solution) for 15 min at 68^{o}C. It was then equilibrated in washing buffer (0.1 M maleic acid, 0.15 M NaOH, pH 7, 0.3% v/v tween 20) for 1 min at room temperature and blocked in blocking buffer (part of Easy Hyb kit) for 30 min at room temperature. The membrane was incubated in blocking buffer containing 1:10,000 diluted anti-digoxigenin antibody (Roche) for 30 min at room temperature, followed by two washes in washing buffer for 15 min at room temperature. After equilibration in detection buffer (100 mM Tris HCl, pH 9.5, 100 mM NaCl) for 2 min at room

temperature, the membrane and 1 mL of chemi-luminescent substrate CSDP Star (Roche) was sandwiched between two acetate sheets and incubated for 5 min at room temperature, followed by 10 min at 37^{o}C and exposed to Amersham Hyperfilm ECL (GE Healthcare).

2.5.3 Preparation of Plasmid DNA from *E. coli* and Clostridial Species

Plasmid DNA was extracted from overnight *E. coli* or 1 – 3 day old *Clostridium* spp. Cultures using QIAprep Spin Miniprep kit (Qiagen) or Purelink Quick Plasmid Miniprep kit (Life Technologies) according to manufacturers' instructions. For clostridial samples, 20 mg/mL of chicken lysozyme was freshly added to resuspension buffer and allowed to incubate at 37^{o}C for 30 min before proceeding to downstream lysis and purification steps.

2.5.4 Quantification, Separation and Visualization of Nucleic Acids

The concentration and purity of nucleic acids were quantified using Nanodrop ND1000 (Thermo Scientific). To visualize nucleic acids, samples were electrophoresed in 0.7 – 1.2% w/v agarose gel (MP Biomedicals) in TAE buffer (40 mM Tris, 1mM EDTA, 0.1% Glacial acetic acid). SYBR Safe (Life Technologies) was added immediately prior to pouring. DNA fragments and plasmids were combined with NEB loading buffer (6X concentration) prior to loading onto the gel, and separated by electrophoresis at 90 – 120 V for 40-60 min in TAE buffer. DNA was subsequently visualized in Odyssey Fc Imager (LI-COR, Inc.) or Gel Doc EZ^{TM} System (Bio-Rad Laboratories, Inc.).

2.5.5 Polymerase Chain Reaction (PCR)

Oligonucleotides (Table 2.3) were designed using Geneious (Biomatters Ltd) and synthesized by Eurofins MWG Operon or Sigma-Aldrich. Phusion® High-Fidelity DNA Polymerase (NEB), Q5® High-Fidelity DNA Polymerase (NEB) and iProof High-Fidelity DNA Polymerase (Bio-Rad Laboratories Ltd) were employed for polymerase chain

reaction (PCR) and performed as per manufacturers' instructions. Standard PCR was carried out in T3000 Thermocycler (Biometra) while PCR with varying annealing temperature (T_a) was undertaken in SensoQuest Gradient Labcycler (Geneflow Ltd). A typical PCR reaction involved an initial denaturation step of 98^{o}C for 30 sec, followed by 35 cycles of 98^{o}C for 10 sec, 58^{o}C for 30 sec and 72^{o}C for 30 sec/kb. This was followed by an extension step of 72^{o}C for 2 minutes before holding at 15^{o}C.

All IFD clusters (and their subsequent complementations), consisting of two precise regions of homology to the host genome located adjacent to each other and flanked by incorporated restriction sites, were generated by Splicing by Overlap Extension (SOE) PCR (247). The same procedure was also applied for the mutation of internal base(s), such as alteration of codon(s) and the mutation of *Nde*I restriction site(s) which may interfere with cloning strategies.

2.5.6 Restriction Digest, Dephosphorylation and Ligation of DNA Fragments

DNA was subjected to restriction digests (NEB or Fermentas) as per manufacturers' instructions for diagnostic purposes or cloning. To minimize re-circularisation of restriction digested vectors, dephosphorylation using Antarctic Phosphatase (NEB) was carried out to remove 5`-phosphate from DNA. For the assembly of DNA fragments and plasmid constructions, T4 DNA ligase (NEB) was added to (gel) purified and linearised DNA fragments that were combined in a reaction at insert to vector ratios of 1:1, 3:1 and 5:1. Ligation reactions were incubated at 16^{o}C overnight before transformation into chemically competent *E. coli*.

2.5.7 DNA Fragment Sequencing

All Sanger sequencing of amplicons and plasmids was performed by Source Bioscience (UK) and Massey University (NZ) using supplied oligonucleotides (Table 2.3). Amplicons were purified using DNA Clean and Concentrator kit (Zymo Research) or PureLink PCR Purification Kit (Invitrogen) prior to sequencing.

2.5.8 Preparation and Transformation of Chemically Competent *E. coli* Cells

The procedures for the preparation and transformation of chemically competent *E. coli* cells were derived from Sambrook *et al.* (2001) (248). One mL of *E. coli* overnight culture was inoculated into 100 mL LB medium (in conical flask) and incubated at 37^{o}C with agitation until optical density at 600 nm (OD_{600}) reached 0.4 - 0.6. Bacterial cultures were then transferred into 50 mL Falcon tubes and chilled on ice for 10 min, followed by centrifugation at 2700 x *g* at 4^{o}C for 10 min. Supernatant was removed and the cell pellet was gently resuspended in 20 mL ice-cold calcium chloride buffer (100 mM $CaCl_2$, 20% v/v glycerol) and chilled on ice for 15 min. The cell suspension was subjected to another centrifugation under the same conditions as previously and the harvested cell pellet was gently resuspended in 4 mL ice-cold calcium chloride buffer and chilled on ice for 1 – 2 h. Finally, 100 µL aliquots of chemically competent cells were stored in -80^{o}C freezer.

For transformation, 10 µL DNA ligation mixture or 0.2 - 1 µL of intact plasmid was added to aliquots of competent cells that had been thawed on ice for 10 min. Following 60 sec of heat shock at 42^{o}C, the cells were immediately chilled on ice for 5 min before 1 mL of LB medium was added and incubated at 37^{o}C with agitation for 1 h. At the end of the recovery period, cells were centrifuged at 13,523 x *g* for 30 sec and 900 µL of supernatant was discarded. The remaining ~200 µL supernatant was used to resuspend the pellet by gently vortexing before plating onto selective LB agar.

2.6 Serum Bottle Growth Experiments of *C. autoethanogenum*

Unless otherwise stated, *C. autoethanogenum* wild-type (WT) and mutant strains were cultivated in triplicates of 250 mL serum bottles containing 50 mL CGMY (section 2.4.1.2) for strain characterisation purposes. Inocula were prepared in CGMY inside the anaerobic workstation and OD_{600} of 0.5 equivalent of active culture was inoculated into each serum bottle. For instance, a preculture with OD_{600} of 2.0 will have 0.25 mL used as inoculum. Depending on the aim of the experiments, five

different substrates were provided: (i) 10 g/L fructose, (ii) 2 bar CO, (iii) 10 g/L fructose + 2 bar CO, (iv) 0.7 bar CO_2 + 1.3 bar H_2, or (v) 2 bar blast oven furnace (BOF) gas (52.6% CO, 12.2% CO_2, 3.2% H_2 and 31.9% N_2; collected from Glenbrook Steel Mill, New Zealand).

Incubations of upright serum bottle cultures were carried out inside New Brunswick Innova 44 shakers (Eppendorf) at 37^{o}C with agitation at 225 rpm. Up to 1 mL of liquid samples were harvested at various time points for optical density measurement using Jenway 7300 Spectrophotometer (Bibby Scientific Ltd) and High-Performance Liquid Chromatography (HPLC) analysis (section 2.8.1). Headspace pressure was measured using Rugged Digital Pressure Gauge DPG120 (Omega Engineering, Inc.) and gas composition analysed using gas chromatography (section 2.8.2). The HPLC and gas data allowed the calculation of percentage carbon recovery. Percentage of carbon recovery was calculated by dividing the molar sum of production of biomass, acetate, ethanol, 2,3-butanediol, lactate, CO and CO_2 by the molar sum of consumption of fructose, CO, and CO_2. As quality control, microscope inspection and/or PCR were performed using 16S rRNA validation primers to verify the identity of the cultures.

2.7 Ethanol Tolerance Assay of *C. autoethanogenum*

To examine ethanol tolerance of *C. autoethanogenum* mutant and plasmid control strains, the bacteria were cultured in serum bottles according to section 2.6 in the presence of 7.5 µg/mL thiamphenicol and 2 bar CO. When the OD_{600} reached 0.2, anaerobic ethanol was injected to bacterial cultures to reach final ethanol challenge concentrations of 20 g/L and 40 g/L. As unchallenged controls, equal volume of media blank was added. After 12 h of incubation in shakers, 1 mL of bacterial culture was harvested inside the anaerobic workstation and serially diluted before plating onto CGMY supplemented with 10 g/L fructose and 7.5 µg/mL thiamphenicol. The colony forming units (cfu) after five days of incubation were recorded for comparison of ethanol tolerance capability between the bacterial strains. In parallel, serum bottle

liquid samples were periodically taken up to 50 days for OD_{600} measurements and metabolite analysis using HPLC (section 2.8.1).

2.8 Analytical Chemistry

2.8.1 High Performance Liquid Chromatography (HPLC)

Analysis of metabolites was performed using Varian ProStar HPLC system equipped with a RID (Refractive Index Detector) operated at 30°C and a Aminex HPX-87H column (1300 x 7.8 mm, particle size 9 µm) (Bio-Rad Laboratories) kept at 30°C. Slightly acidified water was used (0.005 M H_2SO_4) as mobile phase with a flow rate of 0.5 mL/min. To remove proteins and other cell residues, samples were centrifuged at 20,238 x *g* for 5 min and the supernatant was filtered with Spartan 13/0.2 RC filters. 10 µL of the supernatant was then injected into the HPLC for analyses.

2.8.2 Gas Chromatography

Measurements of headspace gas compositions were carried out on a Varian CP-4900 micro GC with two installed channels. Channel 1 was a 10 m Mol-sieve column running at 70°C., 200 kPa argon and a backflush time of 4.2 sec, while channel 2 was a 10 m PPQ column running at 90°C., 150 kPa helium and no backflush. The injector temperature for both channels was 70°C. Runtimes were set to 120 sec, but all peaks of interest would elute before 100 sec.

2.9 Quantitative Reverse Transcriptase Polymerase Chain Reaction (qRT-PCR)

2.9.1 Harvest of *C. autoethanogenum* Cultures for qRT-PCR Analysis

C. autoethanogenum cultures used for qRT-PCR analysis were cultivated in 500 mL Schott bottles containing 200 mL CGMF supplemented with 7.5 µg/mL thiamphenicol and incubated in 37^{o}C shakers. Approximately the equivalent of 12 OD_{600} worth of cells were harvested by centrifugation at 4^{o}C and 3,220 x *g* for 10 min. Supernatant

was removed and the cell pellet was resuspended in 1 mL RNAlater Stabilization Solution (Ambion) by pipetting. After overnight incubation at 4^{o}C, the cell suspension was centrifuged at 3,220 x *g* at 4^{o}C for 10 min and supernatant discarded before storage at -80^{o}C until RNA extraction.

2.9.2 Total RNA Extraction

Following the addition of 1.5 mL cold TRIzol (Ambion), the frozen cell pellet was allowed to thaw on ice for 5 min before being divided into two pre-chilled 2 mL microfuge tubes, each containing 1 g of dnature 0.1 mm diameter Zirconia/Silica beads (dnature Ltd). Cell disruption was performed in 3 cycles of 1 min bead beating using Mini Beadbeater-16 (dnature Ltd), with 1 min chilling on ice in between the cycles. Following 1 min of 4^{o}C centrifugation at 20,238 x *g*, the supernatant was transferred to pre-chilled 1.5 mL microfuge tubes. 100 µL of chloroform was added, vortexed for 20 sec and then incubated at room temperature for 15 min with occasional mixing. After the centrifugation at 20,238 x *g* (4^{o}C) for 15 min, the aqueous phase was transferred into a new microfuge tube and 0.7 volume of isopropanol was added and mixed using pipette actions.

The samples were incubated at room temperature for 10 min before centrifugation at 20,238 x *g* (4^{o}C) for 10 min. Supernatant was removed and the nucleic acid pellet was washed with 700 µL of ice-cold 70% (v/v) ethanol before another round of centrifugation 20,238 x *g* (4^{o}C) for 10 min. After the careful removal of supernatant, the nucleic acid pellet was dried inside a Type II biological safety cabinet (Thermo Scientific) for 15 min before resuspension in 100 µL of RNase-free water and 1 µL of RNaseOUT (Invitrogen). gDNA was removed by the addition of 2 µL TURBO DNase enzyme (Ambion) and 37^{o}C incubation for 30 min. The DNase treated RNA was purified using RNA Clean and Concentrator Kit (Zymo Research) as per manufacturer's instructions and stored at -80^{o}C. The concentration and purity of isolated RNA was analyzed spectrophotometrically using Nanodrop (Thermo Scientific).

As quality control, 1 µL of the RNA samples were subjected to PCR analysis (reaction volume 20 µL) using primer pair "adhE2-662s-F" and "adhE2-662s-R" (Table 2.3) and gel electrophoresis to detect residual gDNA. WT gDNA was used as positive control. Occasionally gDNA was detected so the RNA samples were subjected to another round of DNase treatment followed by RNA extraction and purification (as above). The quality of RNA was examined using 2100 Bioanalyzer (Agilent Technologies) and RNA samples with RNA integrity number (RIN) greater than 7 were used for cDNA synthesis.

2.9.3 cDNA Synthesis

cDNA synthesis was performed using SuperScript III Reverse Transcriptase (Invitrogen) and random hexamers according to manufacturer's instructions. Two µg of total RNA was used per 20 µL reverse transcriptase reaction and diluted 10 fold with RNase-free water prior to qRT-PCR analysis.

2.9.4 Design and Testing of TaqMan Primers and Probes

Primers and probe sets for target genes (*grpE, dnaK, dnaJ, groES, groEL, aor1* and *adhE2*) and housekeeping genes (*gyrA* and *rho*) were designed using the Custom TaqMan Assay Design Tool and purchased as Single-Tube Custom TaqMan Gene Expression Assays from Applied Biosystems. *gyrA* (CAETHG_2130; encodes DNA gyrase subunit A) and *rho* (CAETHG_2327; encodes transcriptional termination factor) were chosen as housekeeping genes because they exhibited the most stable gene expression levels in different carbon sources and stresses in the closely related acetogen *C. ljungdahlii* DSM 13528 (249). Each Custom TaqMan Gene Expression Assay consisted of a forward and reverse unlabelled PCR primer (18 µM each), and a fluorescent reporter FAM-labelled TaqMan MGB probe (5 µM) (Table 2.9). To determine the amplification efficiencies of TaqMan probes and primers, standard curves using 3.333x serially diluted cDNA (20 ng, 6 ng, 1.8 ng, 0.54 ng, 0.162 ng, 0.0486 ng, and 0.0146 ng total RNA) were constructed in technical triplicates. All the examined TaqMan probe and primers have excellent amplification efficiencies

between 94.2% and 99.7% ($R^2 \geq 0.998$) (Figure 2.1). Amplification efficiencies (E) were determined from the slope of the curve and the formula E (100%) = ($10^{(-1/slope)}$ - 1)*100%.

Table 2.9. Primers and TaqMan MGB probes used in this study.

Assay ID	Assay Name	Forward Primer Sequence	Reverse Primer Sequence	Reporter 1 Sequence
AI89K3D	*gyrA*	GAATTGATGGAAACAATAAAAC ATCTCAAGGA	AGTTTTTCTTTCATCACCATATTTAT CTCTTATCTCAATTA	TCAGCAGCAATTC TTT
AIAAZ86	*rho*	GGCATTATTGTATGTTGAAAAAG TAAATGGAGA	ACAGGAGTGAGTGTTTCAAAAGG TT	TCCCACTGCCCTT TCT
AIBJYFE	*groES*	AAGAAGCAGAAGTTGTGGCAGT A	TCCTACTTTTACTTCCATTTTAACTT CTTTTCCA	CTGTTCCACCAAT TCC
AICSWLM	*groEL*	TTAAGAGGAACATTTACTTGTGT AGCAGT	TCCTGAAGCATTTCTTTTCTTCTGT CA	AAGGCACCTGGA TTTG
AID1URU	*grpE*	GCAGAAGATTTGAAAAAAGGTA TAGAGATGAC	CCTTCGCAAGGAATTTCCTCTACAT	ATGCCCTTTCAAA ATT
AIFASX2	*dnaK*	GGGAGTTAACCCTGATGAATGT GT	GGTGTAACATCAAGGAGTAATAC GTCTT	ACTCCGGCCTGA ATTG
AIGJQ4A	*dnaJ*	GGAACAGGACAGATGAGAACTC AGA	CTCTTCCACCACATTTATCACAAGT G	CCAAGAGGCGTA TTCC
AIHSPAI	*aor1*	AACTTGCAAATCAGAAAATTTAG ATTTAGATAAAGCT	CTGGTGATAATGCATCTATTTTAG GATCTATTTCA	CCTAGTCCCCTAC AACCTA
AII1NGQ	*adhE2*	CCTGAAGAAGAGCCCTTTGCT	AGTGCTTCATCAAAATCTTTTGCTT TGT	CTGGAGACAGCT TTTC

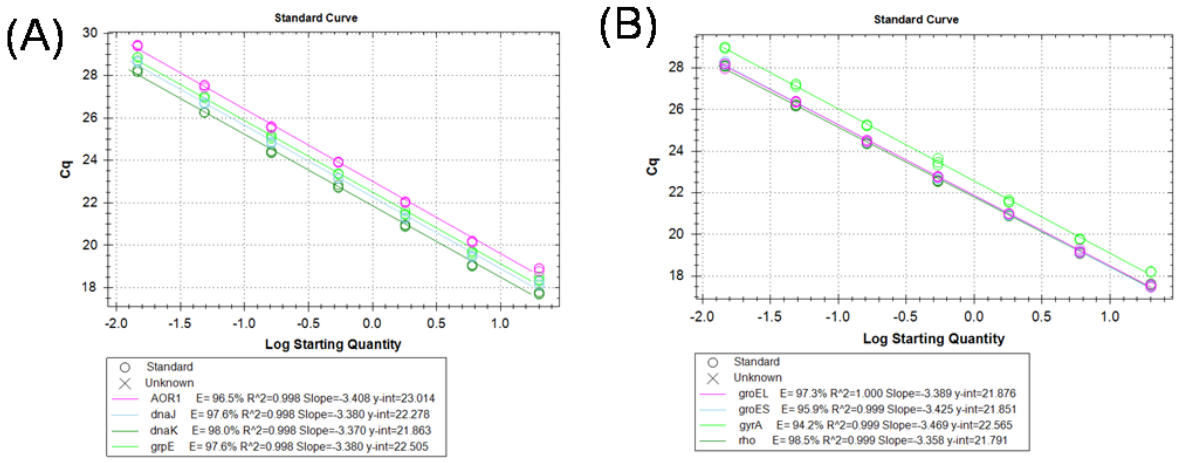


Figure 2.1. Standard curves of qRT-PCR with various amount of cDNA template for assessments of amplification efficiency of each TaqMan probe and primers. (A) Standard curves for *aor1, dnaJ, dnaK* and *grpE*; (B) Standard curves for *groEL, groES, gyrA* and *rho*. E = amplification efficiency. N = 3.

2.9.5 Real-Time PCR

All RT-PCR reactions were set up in 96-well Microseal PCR plates (Bio-Rad Laboratories) and performed in triplicates of 20 µL volume containing 1 µL diluted cDNA, 1 µL of 20x Custom TaqMan Gene Expression Assay, 10 µL of 2x TaqMan Gene Expression Master Mix (Applied Biosystems) and 8 µL nuclease-free water. For each cDNA sample, TaqMan probe and primers for two housekeeping genes (*gyrA* and *rho*) were included for normalization purposes. Non-template controls (NTC) were also included for each TaqMan probe and primer qRT-PCR master mix. Each qRT-PCR run comprised an initial denaturation and polymerase activation at 95^{o}C for 12 min, followed by 40 cycles of denaturation at 95^{o}C for 15 sec and combined annealing and extension at 60^{o}C for 60 sec. The CFX connect Real-Time PCR Detection System (Bio-Rad Laboratories) was employed to record the accumulation of signals in each well within the PCR plate, and the accompanying CFX Manager Software was used to perform normalized gene expression analysis.

2.10 Preparation of Crude Lysates

Transformed *E. coli* strain XL1-Blue MRF', *C. autoethanogenum* and *C. acetobutylicum* were cultured in 50 mL Falcon tubes inside the anaerobic cabinet. Transformed *E. coli* was cultivated in 50 mL LB medium supplemented with 20 mM glucose, 10 µM Na_2SeO_3, and 25 µg/mL chloramphenicol for 23 – 28 h. *C. autoethanogenum* transconjugants were cultivated in 10 mL YTF medium supplemented with 15 µg/mL thiamphenicol for 44 – 51 h. Electroporated *C. acetobutylicum* was cultured in 50 mL YTG medium supplemented with 15 µg/mL thiamphenicol for 28 h.

Cell pellets were harvested by centrifugation at 4^{o}C at 7197 *x g* for 10 min and then resuspended in 300 µL lysis buffer (50 mM Tris-HCl, pH 7.4, 100 mM NaCl) containing fresh 20 mg/mL chicken lysozyme. Following incubation at 37^{o}C for 45 min, the cell suspensions were sonicated using Bioruptor® Plus (Diagenode) for 60 cycles (in rounds of 30 sec sonications/30 sec rest per cycle) at 4^{o}C. Following ultracentrifugation at 20,238 x *g* for 5 min at 4^{o}C, the supernatant was harvested as the soluble fraction whereas the pellet represents the insoluble fraction and was

resuspended in 300 µL lysis buffer without chicken lysozyme. Protein contents were quantified using Bradford reagent (Sigma-Aldrich) with bovine serum albumin (BSA) as standard. Both soluble and insoluble fractions of crude lysates were stored at -20^{o}C for further analysis.

2.11 Sodium Dodecyl Sulphate –Poly-Acrylamide Gel Electrophoresis (SDS-PAGE) and Western Blot Analysis

Cell lysates and purified proteins were analysed by SDS-PAGE. NuPAGE LDS sample buffer (Invitrogen) and 83.3 mM Dithiothreitol (DTT; final concentration) were added to each sample and boiled at 100°C for 5 min to denature the proteins. The samples and Precision Plus Protein Kaleidoscope Standards (Bio-Rad Laboratories) were then loaded onto 4-12% NuPage Bis-Tris gels (Invitrogen) in XCell SureLock Mini-Cell Electrophoresis System (Life Technologies), and NuPage MES Running Buffer (Invitrogen) was added to cover the electrodes. The samples were then subjected to electrophoresis at 150 V for 140 min to separate the proteins, after which the gel was removed from the cast, laid onto Amersham Hybond ECL nitrocellulose membrane (GE Healthcare) and then fitted into XCell II Blot Module (Life Technologies). To transfer proteins to the membrane, Novex transfer buffer (10% v/v methanol) was added to the blot module and subjected to electrophoresis at 30 V for 2 h.

Following disassembly of the blot module, the membrane was blocked in 30 mL of TBS buffer (50 mM Tris-HCl, 150 mM NaCl, pH 7.5, 3% w/v skim milk) at room temperature for 1 h with mild agitation on a shaker. After removing the used TBS buffer, the membrane (covered in foil to protect from light) was subjected to overnight incubation in 30 mL of TBS buffer containing 10 µL monoclonal Anti-FLAG M2-Peroxidase (HRP) antibody (Sigma-Aldrich) at room temperature with mild agitation. Following 3 washes of 5 min in TBST (50 mM Tris-HCl, 150 mM NaCl, 0.1% v/v Tween, pH 7.5), 4 mL of 3,3`,5,5`-Tetramethylbenzidine (TMB) detection substrate (Sigma-Aldrich) was added onto the membrane, and incubated at room

temperature for 5 min before gentle rinsing with dH_2O. The membrane was air dried for 30 min before an image was captured using EOS 600D DSLR camera (Canon).

2.12 Development of Transformation Protocols for *Clostridium spp.*

2.12.1 Preparation of Electro-Competent *C. autoethanogenum* and *C. ljungdahlii*, and Electroporation

For preparation of electro-competent *C. autoethanogenum* and *C. ljungdahlii* cells, 300 mL of CGMYF was inoculated with 10% (v/v) of active culture and incubated overnight in the anaerobic workstation. Cells were harvested via centrifugation at 4226 x *g* for 5 min at room temperature inside the anaerobic workstation when the OD_{600} reached 0.3-0.5. The process of washing the cell pellet by resuspending in 30 mL anaerobic SMP buffer (7 mM phosphate, 1 mM $MgCl_2$, 270 mM sucrose, pH 5.8) followed by centrifugation at 4226 x *g* for 5 min at room temperature was repeated twice, before a final resuspension in 2 mL SMP buffer and 250 µL anaerobic DMSO. Aliquots of 400 µL electro-competent cells were made in 2 mL microfuge tubes and stored at -80^{o}C.

Inside the anaerobic workstation, 100 µL of thawed electro-competent cells were transferred into prechilled sterile electroporation cuvettes (2 mm electrode gap; Bio-Rad Laboratories) containing 1-5 µg plasmid DNA. The suspensions were subjected to 1 kv discharge from a 50 µF capacitor using the Gene Pulser Xcell electroporation system (Bio-Rad Laboratories). The cells were immediately transferred to 10 mL of CGMYF and incubated for 20 h before plating onto solid selective CGMYF.

2.12.2 Preparation of *C. acetobutylicum* Electro-Competent Cells and Electroporation

Preparation of *C. acetobutylicum* electro-competent cells and the subsequent electroporation procedures were carried out according to Mermelstein *et al.* (1992) (183). Plasmid DNA was *in vivo* methylated by a methylase encoded in plasmid pAN2 in *E. coli* Top10 prior to electroporation.

2.12.3 Conjugation

Plasmids were conjugated into *C. autoethanogenum* according to a protocol modified from Purdy *et al.* (2002) (250). Briefly, 1.5 mL of overnight *E. coli* CA434 harbouring plasmid growing on LB medium was washed in phosphate-buffered saline (PBS) and transferred to the anaerobic workstation. 200 µL of overnight *C. autoethanogenum* culture grown in YTF medium was used to gently resuspend the washed donor pellet and spotted onto YTF solid media. After 20-24 h of incubation at 37^{o}C in the anaerobic workstation, the conjugation mixture was harvested into 500 µL of anaerobic PBS and spotted onto selective YTF agar containing 10 µg/mL trimethoprim and 15 µg/mL Tm or 6 µg/mL Cla. Transconjugant colonies that emerged within the first 5 days were picked and restreaked.

2.12.4 Verification of *Clostridium spp.* Transformants

After at least one round of restreak on selective solid YTF medium, putative *Clostridium* spp. transformed colonies were transferred into 300 µL selective liquid medium (YTF or YTG) inside the anaerobic workstation at 37^{o}C. These 300 µL bacterial cultures were further up-scaled to 2 mL volume for the preparation of glycerol stocks and also plasmid DNA miniprep extractions. Because the quality of the isolated plasmid DNA from *Clostridium* spp. (section 2.5.3) was not sufficient for most molecular applications, plasmid verification was carried out by PCR or by retransformation into *E. coli* strains XL1-Blue or Top10 followed by plasmid miniprep and restriction digest analysis (“plasmid rescue”). The identity of the transformants was verified by amplification and sequencing of 16S rRNA using primer pairs Univ-0027-F and Univ-1492-R (Table 2.3).

2.13 Generation of *C. autoethanogenum* ClosTron Mutants

2.13.1 Intron Design and Synthesis of ClosTron Plasmids

Appropriate Intron targeting regions within genes of interest were generated *in silico* at www.ClosTron.com using Perutka algorithm (251). DNA 2.0 Inc. then synthesized the 344 bp intron targeting region and cloned it into ClosTron vector pMTL007C-E2

using restriction sites *Hind*III and *BsrG*I. The mechanism of ClosTron mutagenesis is described in Kuehne and Minton (2012) (252) and is summarized in Figure 2.2.

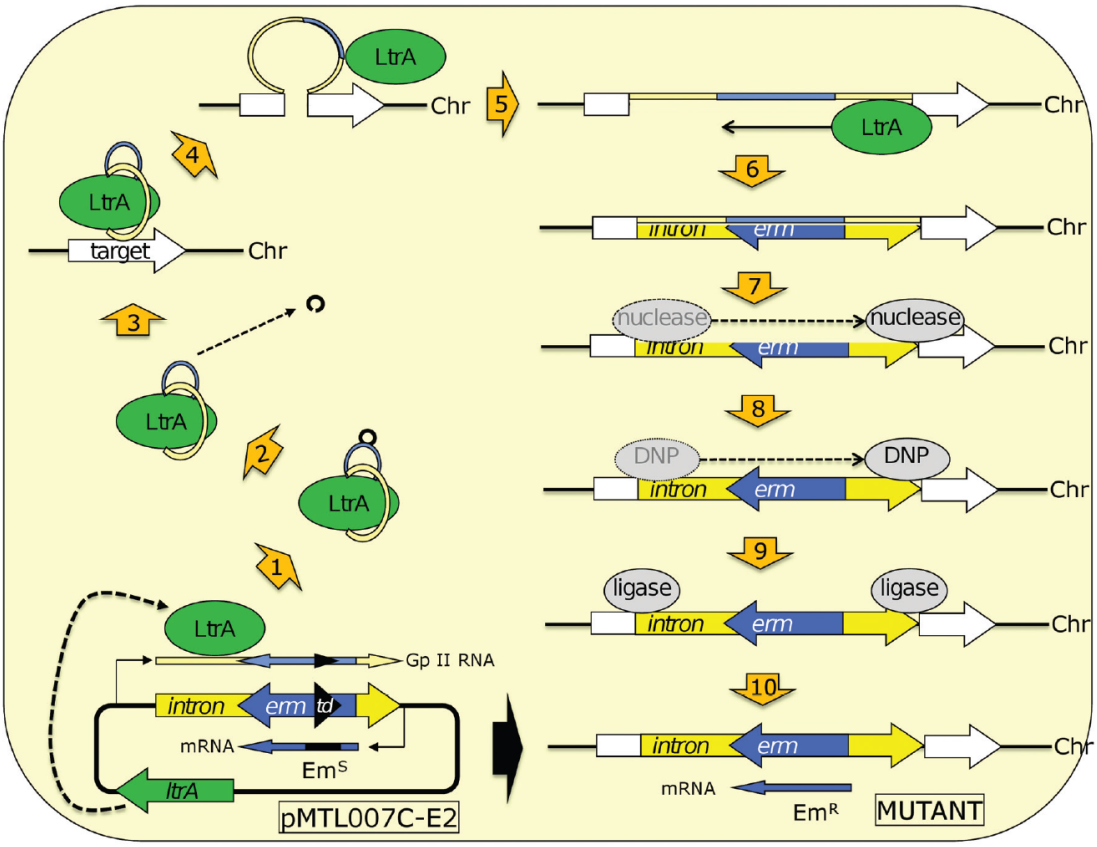


Figure 2.2. The overall steps involved in the generation of ClosTron insertional mutants using plasmid pMTL007C-E2. The group II intron (shown in yellow) encompasses an *erm* marker (shown in blue) to facilitate selection using antibiotics erythromycin or clarithromycin. A small fragment of DNA containing phage td group I intron (shown in black) is incorporated within the *erm* gene for inactivation purposes, but is spliced out (self-catalyzed) under the correct orientation during association with the LtrA protein to form a ribonuclear protein (RNP) complex. Following RNP recognition and binding to the target gene within the chromosome, the LtrA protein (shown in green) 'nicks' the DNA target, inserts the RNA, and synthesizes the complementary DNA strand via its reverse transcriptase activity. Finally, the host ligases seal the gaps which leads to functional expression of the *erm* gene. This figure was obtained from Kuehne and Minton (2012) (252).

2.13.2 Generation and Verification of *C. autoethanogenum* ClosTron Mutants

Following conjugation of ClosTron plasmids into *C. autoethanogenum* and selection with 7.5 µg/mL thiamphenicol on solid CGMF, colonies were transferred onto solid CGMF supplemented with 6 µg/mL clarithromycin to select for Intron insertion into the target locus. Cla^R colonies were inoculated into selective liquid medium for gDNA isolation (section 2.5.1) and PCR verification using locus flanking primers (Table 2.3). WT controls were included for these PCRs and successful Intron integrants produced amplicons that were 1.8 kb larger than the WT controls. Occasionally a screened colony generated both a WT band and ClosTron band so these colonies were subjected to further rounds of purification by restreaking onto selective plates until the WT band was no longer detected. Successful ClosTron amplicons were purified and sent for Sanger sequencing (section 2.5.7). Cla^R colonies were then tested for thiamphenicol sensitivity to check that the ClosTron plasmid has been lost, before a final verification by Southern Blot analysis (section 2.5.2) to ensure that only one ClosTron insertion has occurred in the mutants. Glycerol stocks (15% v/v glycerol) were made for clones that satisfied all the above verification procedures, and stored at -80^{o}C.

2.14 Allele-Coupled Exchange (ACE)

Allele-Coupled Exchange (ACE) is a genetic tool developed by Heap *et al.* (2012) (212) which allows the selection of rare second recombination events without the use of counter-selectable marker. This technique can be used for the generation of IFD mutants and integration of foreign DNA into the genome, and it is a major focus of the project. Although a counter-selectable marker is not required for ACE, the generation of a Δ*pyrE* strain using ACE is valuable because *pyrE* is both a negative and positive selectable marker for genetic manipulation work.

2.14.1 Generation of *C. autoethanogenum* Δ*pyrE* Strain

The plasmid used for deletion of *pyrE* C-terminus in *C. autoethanogenum,* pMTL84151-Δ*pyrE* (Figure 2.3), was provided by Dr. Anne M. Henstra (University of Nottingham). It comprises a 303 bp short homology arm and a 1219 bp long

homology arm with *lacZα* in between, for replacement of 227 bp at the C-terminus of *pyrE* with *lacZα*. Furthermore, a heterologous *pyrE* from *C. acetobutylicum* ATCC 824 (CAC_0027) with a ribosomal binding site (RBS) is also included 18 bp downstream of the *catP* gene to facilitate the loss of the plasmid using 5-fluoroorotic acid (FOA) as counter-selectable marker. The *pyrE* gene of *C. acetobutylicum* shares only 45% nucleotide identity with the corresponding gene in *C. autoethanogenum*, minimizing the probability of unintended homologous recombinations between the two homologs.

Following the conjugation of plasmid pMTL84151-Δ*pyrE* into *C. autoethanogenum,* colonies that emerged on solid YTF supplemented with 7.5 µg/mL thiamphenicol and 10 µg/mL trimethoprim were subjected to further rounds of streaking onto YTF supplemented with 7.5 µg/mL thiamphenicol. Clones in which the single crossover integration event had occurred at the large homology arm were identified by an increased growth rate relative to non-integrant plasmid carriers. gDNA was isolated from several of these fast-growing Tm^R colonies and subjected to PCR screening using primer pairs 'ACE-pyrE-SC-F1' and 'ACE-pyrE-SC-R1' to confirm the integration event had occurred.

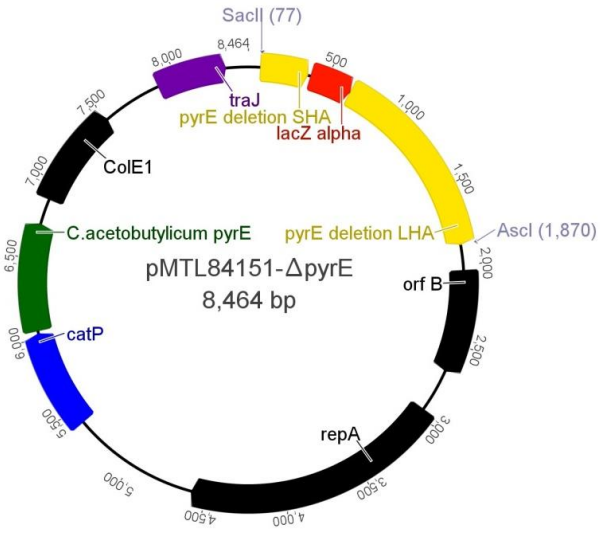


Figure 2.3. Vector map of pMTL84151-Δ*pyrE* for the deletion of *pyrE* gene in *C. autoethanogenum*.

After PCR confirmation of the single crossover event, the clones were inoculated into 3 mL liquid CGMYF supplemented with 7.5 µg/mL thiamphenicol and allowed to grow inside the anaerobic workstation for 2 days. 80 µL of undiluted, 10x diluted and 100x diluted (with anaerobic PBS) culture was spread onto solid CGMF medium that had 1 g/L yeast extract replaced with 1g/L casein acid hydrolysate (CGMCF), and supplemented with 1.5 mg/mL FOA and 5 µg/mL uracil to select for the double crossover event. The efficacy of FOA is reduced by the presence of uracil and yeast extract contains substantial amounts of uracil so a less enriched supplement such as casein acid hydrolysate was used instead. The plates were covered in foil to protect from light during incubation, and they were closely monitored to detect early emerging colonies (24 - 48 h), which were then screened by PCR for the double crossover event using primer pairs 'ACE-pyrE-F3' and 'ACE-pyrE-R3'. Sanger sequencing of the *pyrE* amplicon was carried out to confirm replacement of the 3` end of *pyrE* gene with *lacZα*. Serial passage on non-selective solid CGMYF medium was then performed until the plasmid has been lost, confirmed by replica plating onto CGMYF agar medium supplemented with 7.5 µg/mL thiamphenicol.

2.14.2 Construction of In-Frame Deletion Plasmids and *pyrE* Restoration Plasmids

All IFD plasmids and *pyrE* complementation or correction plasmids were constructed using plasmid pMTL84151-Δ*pyrE* by substitution of the homology arm cassettes using restriction sites *Sac*II and *Asc*I (Figure 2.3). The IFD cassettes for *adhE1*, *adhE1*+*adhE2*, *cooS1,* and *aor2* consisted of two homology arms of similar lengths (518 – 580 bp), and were assembled using SOE-PCR (section 2.5.5) and oligonucleotides in Table 2.3. All the IFD cassettes retained only the start and stop codons of the target loci without affecting the 5`-UTR (Un-translated region) and 3`-UTR.

For the restoration of *pyrE*, two slightly different plasmids were used: pMTL84141-fix*pyrE* and pMTL84141-com*pyrE* (both provided by Dr. Anne M. Henstra, University of Nottingham). However, these plasmids lacked the *traJ* gene for conjugation so the

colE1 module was replaced by *colE1 + traJ* module, which was obtained from a *Pme*I and *Sbf*I fragment of plasmid pMTL83151. The resultant plasmids pMTL84151-fix*pyrE* and pMTL84151-com*pyrE* have the same long homology arm as pMTL84151-Δ*pyrE* but an extended short homology arm (526 bp instead of 303 bp) to cover the deleted *pyrE* portion. Importantly, unlike pMTL84151-Δ*pyrE*, both restoration plasmids lack the heterologous *pyrE* from *C. acetobutylicum* which may interfere with selection for uracil prototrophy. Plasmid pMTL84151-fix*pyrE* is used for complete restoration of *pyrE* back to its original state in a scar-less fashion. In contrast, plasmid pMTL84151-com*pyrE* has *lacZα* incorporated between the short and long homology arms, so *lacZα* is concurrently integrated into the genome during restoration of the *pyrE* locus.

2.14.3 Implementation of In-Frame Deletion Protocol using *pyrE* as Selectable Marker

In order to exploit the use of *pyrE* as a counter-selectable marker, *C. autoethanogenum* Δ*pyrE* strain (section 2.14.1) was used to construct all IFD mutants in this project. Following conjugation of IFD plasmids (Table 2.2) into *C. autoethanogenum* Δ*pyrE* strain, single crossover mutants were identified by faster growth rate in the presence of 7.5 µg/mL thiamphenicol relative to non-integrant plasmid carrier. PCR screening using oligonucleotides in Table 2.3 was carried out to confirm that a single crossover event had occurred. These single crossover clones were then subjected to FOA selection according to section 2.14.1 to select for the double crossover event. PCR screening using locus flanking oligonucleotides specifically designed outside of the homology arm (so the primers will not anneal to the homology arms in the IFD plasmids) (Table 2.3) was performed to identify the double crossover event. Sanger sequencing of the PCR products were undertaken to confirm the IFD event. Serial passage on solid CGMCF medium supplemented with 1.5 mg/mL FOA and 5 µg/mL uracil was then performed to trigger plasmid loss, tested by replica plating onto solid YTF medium supplemented with 7.5 µg/mL thiamphenicol.

2.14.4 Restoration of *pyrE* Locus

For restoration of *pyrE* locus, plasmid pMTL84151-fix*pyrE* or pMTL84151-com*pyrE* was conjugated into *C. autoethanogenum* Δ*pyrE* strain, and transconjugants were selected on the basis of resistance to thiamphenicol. Faster growing colonies were preferentially selected and streaked onto selective solid YTF to obtain single crossover integrants at either homology arm, followed by streaking onto solid CGMF without uracil supplementation to select for uracil prototrophs. These clones were streaked onto the same medium before PCR screening using oligonucleotides 'ACE-*pyrE*-F' and 'ACE-*pyrE*-R' was performed to detect the second crossover event. Sanger sequencing of the resultant amplicons confirmed successful restoration of *pyrE* with or without concurrent integration of *lacZα* into the 3`-UTR of the *pyrE* locus.

CHAPTER 3

DEVELOPMENT OF GENETIC TOOLS FOR *CLOSTRIDIUM AUTOETHANOGENUM*

3 Development of Genetic Tools for *Clostridium autoethanogenum*

3.1 Introduction

Successful industrial application of gas fermentation technology requires a robust microbial catalyst that exhibits the following traits: high product yield and selectivity, low product inhibition, no strain degeneration, asporogenous, prolonged cell viability, strong aero-tolerance, high biomass density and efficient utilization of gas substrates. Given that microorganisms isolated from nature generally display low product yield and selectivity, significant strain improvement is often necessary to select for these traits. Traditionally this has been achieved by directed evolution (174, 175) and/or chemical mutagenesis (173, 253, 254) but these strategies are limited and often come with the expense of unwanted events. Rational genetic engineering offers not only the opportunity to enhance existing traits but also the unique opportunity to expand the product suite and substrate range.

Motivated by the demonstrated ability of *C. autoethanogenum* in producing ethanol and 2,3-butanediol at semi-commercial scale (Dr. Sean Simpson, LanzaTech Inc; personal communications), this acetogen was selected as chassis for the development of genetic tools in this work. To date, no report of genetic engineering for *C. autoethanogenum* has been published in the scientific literature despite strong biotechnological interests, suggesting that there are some obstacles that make genetic engineering of this microbe particularly challenging. This chapter reports the development of transformation methodologies, exemplification of ClosTron mutagenesis, demonstration of three counter-selectable markers for genetic manipulation, and the deletion and subsequent restoration of the *pyrE* locus using the ACE method.

3.2 Development of Transformation Methodologies for *C. autoethanogenum*

The establishment of an efficient protocol to introduce foreign DNA into a microbial host is frequently the most challenging step in any genetic engineering endeavour.

This is especially true for Gram-positive bacteria such as clostridia due to the physical barrier of thick peptidoglycan cell wall and highly active restriction-modification (RM) systems (255). Due to these reasons, the advancement of genetic tools in this important genus has been severely hindered and lagged behind model organisms such as *E. coli*, *B. subtilis*, and *S. cerevisiae*. Some of the well-studied clostridia such as the ABE model organisms *C. acetobutylicum* (183) and *C. beijerinckii* (181), and important pathogens such as *C. difficile* (256) and *C. botulinum* (257), have transformation protocols that were established as early as 1988. In contrast, methods for genetic manipulation in acetogens are only beginning to emerge since 2010, including for *C. ljungdahlii* (37, 229), *C. aceticum* (234), *M. thermoacetica* (237), and *A. woodii* (236). Notable absentees from the list of transformed acetogens are *C. carboxidivorans*, *C. ragsdalei, C. scatologenes, C. drakei, E. limosum,* and *O. pfennigii*.

3.2.1 Electroporation of *C. ljungdahlii*

At the beginning of this PhD project (November 2011) and prior to the publication of Leang *et al.* (2013) (229), a novel and reliable electroporation protocol was developed for *C. ljungdahlii* by Dr. Anne M. Henstra and Dr. Elizabeth Steiner (unpublished results) in this laboratory.

As a proof of concept, four *E. coli*-clostridia shuttle vectors (pMTL82151, pMTL83141, pMTL84141 and pMTL85141) (244) were electroporated into *C. ljungdahlii* according to section 2.12.1. In contrast to *Clostridium* strains such as *C. acetobutylicum*, electroporation of *C. ljungdahlii* appears to be achievable without methylation, so the electroporation plasmids were harvested from *E. coli* strain Top10 (Invitrogen) without a methylation plasmid such as pAN2. Following electroporation using 3 µg of plasmid and plating onto selective solid media, the number of colonies was recorded within 5 days of incubation and the electroporation efficiencies achieved are shown in Table 3.1. The electroporation efficiency appears to depend on the type of Gram-positive replicon rather than size of plasmid. Both replicons pCB102 and pBP1 produced the highest electroporation efficiencies, followed by pCD6, while no

colonies were obtained for pIM13. It was observed that the transformants with replicon pCD6 also grew slower on solid agar in comparison to those with other replicons (data not shown). These results are consistent with observations made by Dr. Anne M. Henstra and Dr. Elizabeth Steiner (unpublished results). The transformation efficiencies for replicons pCB102 (2.5 x 10^3 cfu/µg DNA) and pBP1 (2.7 x 10^3 cfu/µg DNA) in this study are comparable to the report by Leang *et al.* (2013) (229): 3.8 x 10^3 and 3.1 x 10^3 cfu/µg DNA, respectively. The same set of Gram-positive replicons (pBP1, pCB102, pCD6 and pIM13) exhibit conjugation efficiencies that vary by 30-fold in *C. tyrobutyricum* (258).

Table 3.1. Electroporation efficiency of *C. ljungdahlii*

Plasmid	Gram-positive replicon	Size of plasmid (bp)	Electroporation efficiency (Cfu/µg DNA)
pMTL82151	pBP1	5254	2488
pMTL83141	pCB102	3710	2667
pMTL84141	pCD6	5531	388
pMTL85141	pIM13	2963	0

3.2.2 Electroporation of *C. autoethanogenum*

Given the phylogeny proximity between *C. ljungdahlii* and *C. autoethanogenum* with 100% sequence identity in 16S rRNA and high similarity on a genome level (38), there was reason to expect that the electroporation protocol would be applicable to *C. autoethanogenum*. Surprisingly, the same protocol did not work as well in *C. autoethanogenum*. In 11 attempts, only 2 electroporation experiments successfully resulted in transformed colonies. In the fifth attempt, very low electroporation efficiencies were obtained for plasmids pMTL82151 (0.3 cfu/µg DNA) and pJIR418 (1 cfu/µg DNA). In the eleventh attempt, 3.8 cfu/µg DNA and 0.2 cfu/µg DNA were achieved for plasmids pMTL82151 and pMTL83141, respectively. The identity of these transformants were validated by 16s rRNA sequencing and the presence of electroporation plasmids were confirmed by plasmid rescue into *E. coli* followed by restriction digest analysis.

Various factors were investigated in these electroporation experiments but none resulted in significant improvement in electroporation efficiencies. These variables included: stage of culture for preparation of competent cells, other plasmids (pMTL500E with pAMβ1 replicon; and pJIR418 with pIP404 recplicon), *E. coli* strain (XL1-Blue MRF' Kan) for propagation of plasmids, fresh competent cells without freezing, with and without DMSO, *in vitro* plasmid methylation using methyltransferase GpC or Taq1 (NEB), recovery medium, and recovery duration.

To explain the marked differences in electroporation efficiencies between *C. autoethanogenum* and *C. ljungdahlii*, genome comparison of their RM systems was performed (Table 3.2). The genome of *C. autoethanogenum* encodes 12 putative RM systems that are absent in *C. ljungdahlii*. It is tempting to speculate that these differences contribute to difference in electroporation efficiencies between the two species. In agreement with this hypothesis, re-electroporation of plasmids (pMTL82151 and pJIR418 from the fifth experiment) isolated from transformed *C. autoethanogenum* resulted in higher electroporation efficiencies. The electroporation efficiencies for plasmids pJIR418 and pMTL82151 showed an increase of 80-fold and 20-fold, respectively, when the electroporation plasmids were propagated in *C. autoethanogenum* instead of *E. coli*. Gel electrophoresis of undigested plasmids isolated from *C. autoethanogenum* showed that the plasmid pMTL82151 was already heavily degraded by the host's RM systems while pJIR418 was rather intact prior to the electroporation experiment (data not shown), suggesting that the actual improvement in electroporation efficiency might be significantly greater.

In addition to the differences in RM systems between *C. autoethanongeum* and *C. ljungdahlii*, the former also contains CRISPR (Clustered Regularly Interspaced Short Palindromic Repeats) systems whereas the latter contains none (38). CRISPR has been demonstrated experimentally to prevent the transfer of plasmid DNA via conjugation (38).

Table 3.2. Comparison of Restriction-Methylation systems between *C. autoethanogenum* (CAETHG) and *C. ljungdahlii* (CLJU_c).

Putative Restriction-Methylation Systems	CAETHG*	CLJU_c^
Type II restriction enzyme and methyltransferase	0535	24700
Type II methyltransferase	1296	33980
Type II restriction enzyme	1649	-
Type II N4-cytosine or N6-adenine DNA methyltransferase	1650	-
Type II methyltransferase	2939	8460
Type III restriction enzyme	1021	-
Type IV methyl-directed restriction enzyme	3519	-
Type IV methyl-directed restriction enzyme	3525	-
Type IV methyl-directed restriction enzyme	3526	-
Type IV methyl-directed restriction enzyme	3527	-
Type IV methyl-directed restriction enzyme	3547	-
Type IV methyl-directed restriction enzyme	3557	-
Type IV methyl-directed restriction enzyme	3559	-
Type IV methyl-directed restriction enzyme	3560	-
Type IV methyl-directed restriction enzyme	3577	35160
Type IV methyl-directed restriction enzyme	3617	15150
Type IV methyl-directed restriction enzyme	3757	-

*CAETHG is the coding sequence number of *C. autoethanogenum*
^CLJU_c is the coding sequence number of *C. ljungdahlii*

3.2.3 Conjugation of *C. autoethanogenum*

Since attempts at improving electroporation efficiencies of *C. autoethanogenum* were not fruitful, conjugation was evaluated as an alternative method of introducing foreign DNA into the bacterium. Although conjugation requires the use of counter-selective agents for donor cells, this method can be advantageous for overcoming high extracellular nuclease activities of the recipient cells (259). Conjugation plasmids pMTL82151, pMTL83151, pMTL85151, pMTL007C-E2::*pyrE*-144s, and pMTL84151-Δ*pyrE* were first transformed into *E. coli* donor CA434, and the resulting donors were used to conjugate *C. autoethanogenum*.

After 2-4 days incubation in the presence of 7.5 µg/mL thiamphenicol and 10 µg/mL trimethoprim (counter selective agent against donor CA434), colonies emerged and they were streaked onto the same selective medium at least once before confirmation via plasmid rescue and restriction digest analysis, and 16S rRNA amplification and sequencing. With the exception of pMTL85151, all the plasmids

were successfully conjugated into *C. autoethanogenum* with conjugation efficiencies ranging from 2.8 x 10^{-9} to 5.2 x 10^{-8} mean cfu per donor (Table 3.3). These results are consistent with the electroporation results of *C. ljungdahlii* in which transformation using plasmids with Gram-positive replicons pBP1, pCB102 and pCD6 are attainable, but not pIM13 (Table 3.1). It is worthwhile to mention that two out of the five attempts of conjugating plasmid pMTL85151 into *C. autoethanogenum* did produce Tm^R and $Trim^R$ colonies (2.0–6.8 x 10^{-9} cfu per donor) on the initial selective plates, but none of the screened colonies was able to grow when streaked onto the same selective medium. This observation can be interpreted as pMTL85151 (with the pIM13 Gram-positive replicon) being segregationally unstable in *C. autoethanogenum*.

Table 3.3. Conjugation efficiencies for *C. autoethanogenum* using *E. coli* CA434 as donor

Plasmid	Gram-positive replicon	Mean cfu per donor	Standard error of mean	N
pMTL82151	pBP1	3.9 x 10^{-8}	1.1 x 10^{-8}	5
pMTL83151	pCB102	2.8 x 10^{-9}	1.3 x 10^{-9}	5
pMTL007C-E2::*pyrE*_144s	pCB102	5.2 x 10^{-8}	2.7 x 10^{-8}	4
pMTL84151-Δ*pyrE*	pCD6	8.3 x 10^{-9}	3.0 x 10^{-9}	4
pMTL85151	pIM13	0*	N/A	5

*Two of the five conjugation attempts did produce colonies on the initial selective plate but the colonies were unable to grow when streaked onto a second selective plate.

Throughout this project, conjugation was the method of choice for introduction of foreign DNA into *C. autoethanogenum.* Overexpression plasmids (based on pMTL83151), ClosTron plasmids (based on pMTL007C-E2) and IFD plasmids (based on pMTL84151) were routinely conjugated into *C. autoethanogenum* with high success rates (estimated at around 80%). The largest plasmid that was attempted and successfully conjugated into *C. autoethanogenum* in this project is pMTL83156-grpE-dnaK-dnaJ-P_{acsA}-groESL, which is 11,494 bp.

3.2.4 Exemplification of ClosTron Mutagenesis by Targeting *fruA*

Since its inception in 2007 by Dr. John Heap, ClosTron mutagenesis (190, 206) has proven to be an invaluable tool for rapid generation of stable knock-out mutants across the *Clostridium* genus. The ability to stably knock out gene(s) by insertion of a group II intron is useful for elimination of unwanted product(s), diversion of carbon and/or electron fluxes towards the desired product(s), and also fundamental research by studying the resulting phenotype from inactivation of a gene. To investigate the feasibility of ClosTron mutagenesis in *C. autoethanogenum*, the EIIABC subunit of the fructose-specific phosphotransferase system (*fruA*) was chosen as target for proof-of-principle study because the resultant knock out mutant is likely to display an easily identifiable phenotype: inability to grow using fructose as a substrate.

Similar to many anaerobic bacteria, clostridia rely heavily, but not exclusively, on a phosphoenolpyruvate (PEP)-dependent phosphotransferase system (PTS) to import specific sugars and sugar derivatives necessary for heterotrophic growth. PTS transport of monosaccharides (e.g., glucose, fructose, and galactose) and disaccharides (e.g., sucrose, lactose and maltose) have been characterized in a few clostridia, including *C. acetobutylicum* ATCC 824, *C. beijerinckii*, *C. thermocellum*, *C. saccharobutylicum*, and *C. difficile* (25). However, the prevalence of ATP- and ion-dependent transport systems in the genome of several sequenced clostridia and biochemical evidence from *C. pasteurianum* and *C. beijerinckii* also highlighted the importance of non-PTS mechanisms in the transport of sugar substrates (25). Furthermore, pentoses (e.g., xylose, arabinose and ribose) are not known to be substrates of the PTS in bacteria so a non-PTS process must exist.

The PTS is a multi-protein complex consisting of various phosphoryl transfer chains, which transfer phosphate between PEP and the sugar substrates (Figure 3.1A). The end result is the concomitant uptake and activation of sugar substrates. Genome analysis of *C. autoethanogenum* revealed the presence of 2 putative PTS: One has all three EII subunits (EIIA, EIIB, and EIIC) fused into one coding sequence (CAETHG_0142) and is located directly downstream of the phosphofructokinase catalysing the next step in the Embden-Meyerhof-Parnas pathway, and is annotated

as fructose-specific transporter PTS (Figure 3.1B); the second PTS has all EII subunits separated into three coding sequences (CAETHG_0674-0676), and the substrate specificity is predicted to be fructose/mannose-specific (Figure 3.1C). In this project, the first PTS (CAETHG_0142; fructose-specific, and termed '*fruA*') from *C. autoethanogenum* was selected for gene knockout using ClosTron mutagenesis.

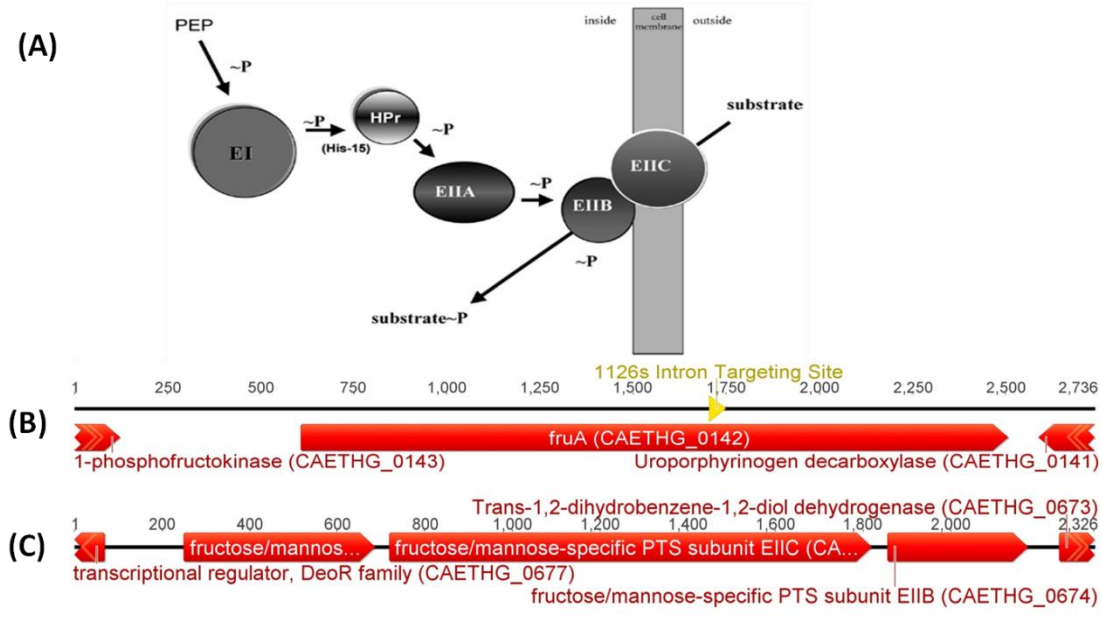


Figure 3.1. Putative phosphotransferase systems (PTS) in *C. autoethanogenum*. (A) A schematic diagram showing the roles of various PTS components in importing sugar substrate (Figure obtained from (25)); (B) Gene arrangement of a putative fructose-specific PTS transporter (*fruA*). The ClosTron intron I targeting site at position 1126s (sense orientated from start codon) is shown by a yellow triangle; (C) Gene architecture of a putative fructose/mannose-specific PTS transporter operon; Figures are not drawn to scale.

The Intron targeting region of *fruA* was *in silico* generated using Perutka algorithm (251), synthesized and cloned into a pMTL007C-E2 plasmid by DNA 2.0 Inc. (Section 2.13.1). The resultant plasmid pMTL007C-E2:fruA-1126s was transformed into *E. coli* CA434 donor and conjugated into *C. autoethanogenum* as described before. The transformed colonies were re-streaked once on solid media containing 7.5 µg/mL Tm and 10 µg/mL trimethoprim, and then three times on solid YTF media containing 6 µg/mL clarithromycin before screening. Usually this re-streaking regime is sufficient

to isolate pure mutants that have also lost the ClosTron plasmid, but occasionally more re-streaking is necessary. For screening of intron II insertion into the specified locus, genomic DNA was extracted from overnight culture and two combinations of PCR were carried out. The first set of primers binds to genomic regions outside the intron II insertion site (termed 'gene specific exon-spanning'), so successful integrants can be differentiated from wild-type (WT) by a PCR product that is ~1800 bp larger than a ~300 bp WT amplicon (Figure 3.2A). The second set of primers targets the RAM (retrotransposition activated marker) cassette of the ClosTron plasmid: the excision of Td group I intron from the RAM will generate a 900 bp amplicon whereas the retention of the group I intron will produce a 1200 bp PCR product (Figure 3.2A). The presence of Td intron within the RAM prevents functional expression of *ermB* prior to intron II insertion (as shown in Figure. 2.2). In some cases, a mixture of WT and integrant bands of the same PCR reaction were detected in gel electrophoresis (data not shown), indicating the PCR conditions were able to amplify both short and long fragments in the same PCR reaction.

All the screened *fruA*::CTermB-1126s colonies showed the expected ClosTron insertion and splicing event from PCR analyses using both *fruA*-specific primers ('fruA-1126s-F' and 'fruA-1126s-R') and RAM primers ('RAM-F' and 'RAM-R') (Figure 3.2B). The PCR product from *fruA*-specific primers was subjected to Sanger sequencing to confirm the identity of the disrupted locus. ClosTron plasmid loss is essential for the stability of sense-strand targeted mutants because the continued presence of LtrA in the plasmid may lead to splicing of the intron encoding region from the RNA. Plasmid loss was demonstrated by the inability of the mutants in forming colonies on solid YTF medium containing 7.5 µg/mL thiamphenicol after several re-streaking steps (data not shown). Finally, to ensure that only one copy of intron II had inserted into the genome, Southern Blot analysis using probes that target the RAM (Section 2.5.2) was carried out and all the screened clones showed a single band of the expected size (Figure 3.2C).

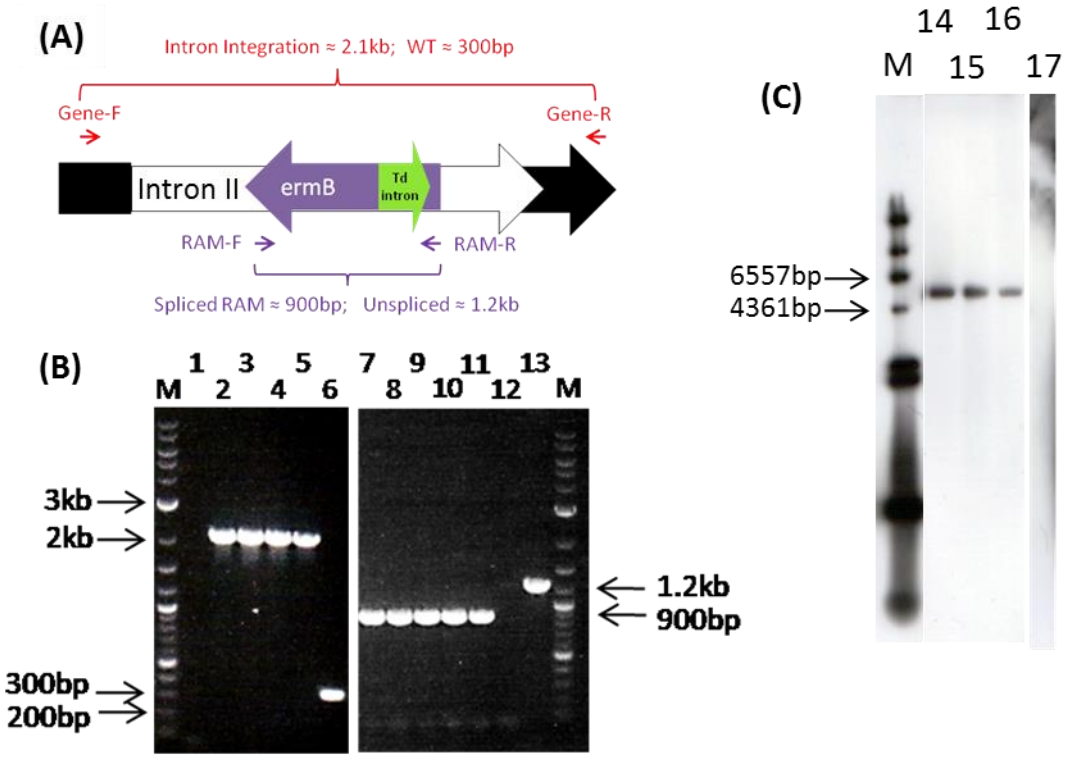


Figure 3.2. Screening for *C. autoethanogenum fruA*::CTermB-1126s mutants. (A) The genomic context of a ClosTron mutant is schematically presented, showing annealing sites for exon-spanning PCR primers (Red arrows) and RAM PCR primers (Short purple arrows), including the possible PCR product sizes; (B) Gel electrophoresis showing PCR products of screened colonies using *fruA*-specific exon-spanning primers (Lanes 1-6) and RAM primers (Lanes 7-13). (C) Southern Blot analysis of *Hind*III digested genomic DNA of *fruA*::CTermB-1126s mutants. Lanes: M, molecular marker; 1, non-template control; 6, 12 & 17, wild-type; 13, unspliced ClosTron plasmid control; 2-5, 7-11, 14-16, clones of *fruA*::CTermB-1126s mutants.

Following generation and validation of pure *fruA* mutants, growth experiments in both solid and liquid media were carried out to determine whether the mutants suffer from any deficiency in fructose utilization. A 10 µL aliquot of active culture from three independent *fruA* mutants and one WT were spotted onto solid media CGMC with 40 mM of fructose. Following 12 days of incubation inside an anaerobic cabinet, the WT was found to grow normally but all three *fruA* mutants were unable to form colonies (Figure 3.3A). In parallel, the same group of biological samples were also spotted onto solid media CGMC supplemented with 80 mM pyruvate (instead of fructose) and incubated for the same duration as positive controls. All three *fruA*

mutants and the WT were able to show some growth with pyruvate as substrate, indicating they were all viable (Figure 3.3A).

In similar fashion, these biological samples were also cultivated in technical duplicates of 3 mL liquid medium, CGMC supplemented with either 40 mM fructose or 80 mM pyruvate (Figure 3.3B). After five days of incubation, all three mutants showed little or no growth in liquid media CGMC containing fructose, while the WT achieved mean OD_{600} of 1.4 (Figure 3.3B). Despite great variability between the three *fruA* mutants, they appear to grow better than the WT when using pyruvate as substrate (Figure 3.3B). This observation indicates inactivation of *fruA* might have a compensatory effect on pyruvate uptake and utilization in *C. autoethanogenum*, but more experiments need to be conducted to test this hypothesis. Given the (near) complete deficiency in fructose uptake and utilization phenotypes of these mutants, *fruA* is very likely the main transporter for fructose in *C. autoethanogenum*.

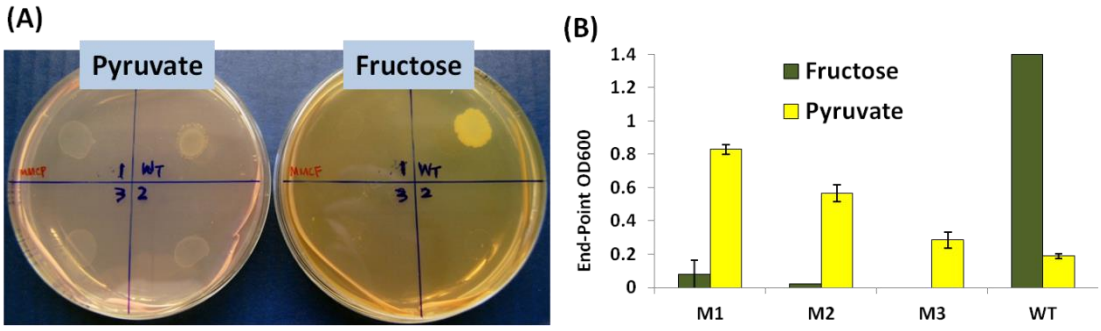


Figure 3.3. *C. autoethanogenum fruA* mutants are unable to utilize fructose as substrate. (A) Spotting of three *fruA* mutants (labelled 1, 2, & 3) and one wild-type (WT) onto solid media CGMC supplemented with either 80 mM pyruvate or 40 mM fructose; Incubation duration = 12 days; (B) Comparison of end-point OD_{600} in CGMC liquid medium supplemented with either 80 mM pyruvate (yellow) or 40 mM fructose (green) between three *fruA* mutants (labelled M1, M2 and M3) and one WT; Incubation duration = 5 days; Error bars = standard deviations derived from two technical repeats.

3.2.4.1 Exploration of *fruA* as Counter-Selectable Marker

It has been reported in the literature that certain bacterial strains, but not PTS^- strains, are sensitive to xylitol or D-arabitol (260-263). In *Salmonella typhimurium*,

mutants lacking mannitol-phosphate dehydrogenase activity are inhibited by D-mannitol concentration as low as 10^{-6} M (264). In many cases, carbohydrate toxicity in bacteria is due to lethal synthesis of phosphorylated intermediates (264, 265). Utilization of xylitol or D-mannitol has not been examined in either *C. autoethanogenum* (52) or *C. ljungdahlii* (64), but genome sequencing revealed the absence of xylitol-phosphate dehydrogenase or mannitol-phosphate dehydrogenase in these acetogens (37, 38).

The gene *fruA* has the potential to be utilized as a valuable counter-selectable marker for *C. autoethanogenum* if WT cells display sensitivity towards xylitol or D-mannitol whereas a *fruA* knockout mutant conferred resistance. To investigate this, *C. autoethanogenum* WT and *fruA*::CTermB-1126s mutants were cultivated in 3 mL CGMY supplemented with 80 mM pyruvate containing varying concentrations of xylitol or D-mannitol (0, 0.5, 10 & 100mM) inside the anaerobic workstation and incubated statically for 3.2 days. Pyruvate was chosen as the growth substrate because fructose has been shown to have a protective effect against xylitol toxicity (260), and also because the *fruA* mutants are unable to utilize fructose. The end-point OD_{600} of the WT decreased by 55% from 0.696 (no xylitol) to 0.314 (100 mM xylitol) (Figure 3.4A). In contrast, the *fruA* mutant showed only a 5% decrease in end-point OD_{600} from 0.64 (no xylitol) to 0.607 (100 mM xylitol) (Figure 3.4A). No significant difference in end-point OD_{600} was detected for either WT or *fruA* mutant due to the supplementation of D-mannitol (Figure 3.4B).

To test the sensitivity of *C. autoethanogenum* and *fruA* mutant towards xylitol on solid medium, 20 µL of active cultures (normalized to the same OD_{600}) were plated onto solid CGMC medium (with 80 mM sodium pyruvate) containing 0 mM, 100 mM, 200 mM or 300 mM xylitol. Incubation was carried out at 37^{o}C inside the anaerobic workstation for up to 10 days. In the presence of 100 mM xylitol, small colonies of *C. autoethanogenum* WT were detected whereas the *fruA* mutant was able to form large colonies after 7 days of incubation (Figure 3.4C). At 200 mM and 300 mM xylitol levels, WT colonies were not detected after 7 days and 10 days of incubation, respectively (Figure 3.4D & E). In contrast, the *fruA* mutant was able to form large colonies in the presence of these xylitol concentrations (Figure 3.4D & E). In the

absence of xylitol, WT formed colonies within 5 days of incubation but the size of the colonies was smaller than for the *fruA* mutant (data not shown), which is consistent with previous findings that *fruA* mutants grow better than WT on pyruvate (Figure 3.3B).

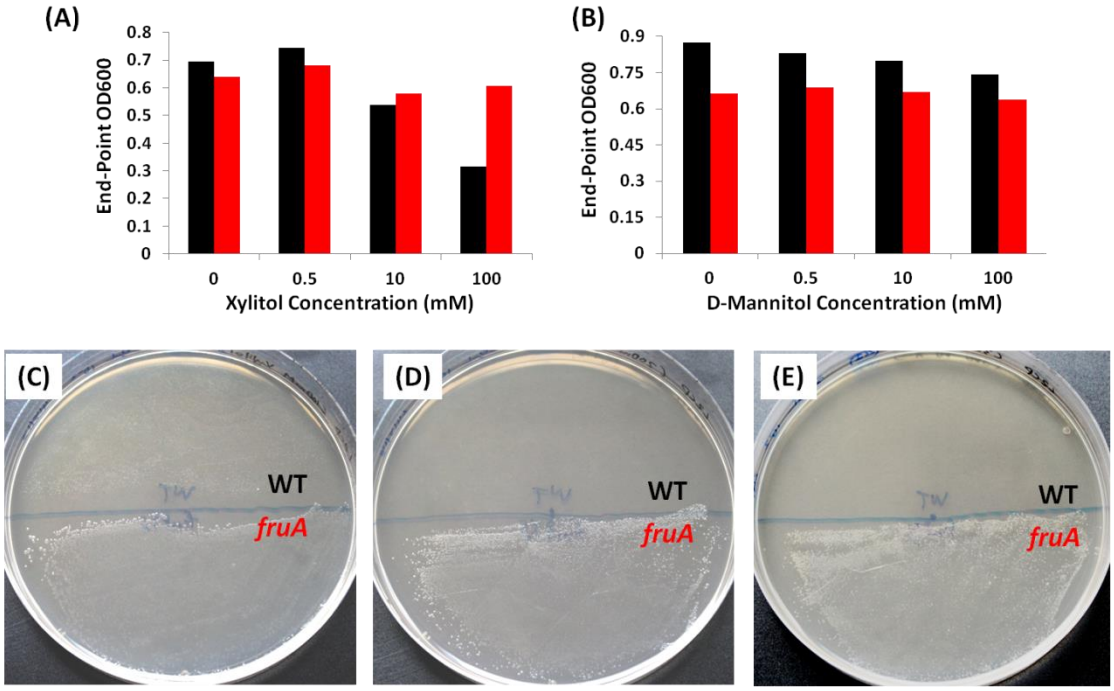


Figure 3.4. Testing of xylitol and D-mannitol toxicity in *C. autoethanogenum* WT and *fruA* mutant. (A) Effect of xylitol supplementation on end-point OD_{600} of WT (black) and *fruA* mutant (red) after 3.2 days of incubation; (B) Effect of D-mannitol supplementation on end-point OD_{600} of WT (black) and *fruA* mutant (red) after 3.2 days of incubation; (C) Plating assay with 100 mM xylitol and incubation duration of 7 days; (D) Plating assay with 200 mM xylitol and incubation duration of 7 days; (E) Plating assay with 300 mM xylitol and incubation duration of 10 days; N = 1.

3.2.5 Testing of Counter-Selectable Markers

Precise, unmarked genetic manipulation often involves the replacement of a locus by an *in vitro* modified allele. This fundamental approach is easy to perform in many bacteria, but it remains practically very challenging for some due to low transformation efficiency and low recombination frequency (212, 266). In genetically more intractable microorganisms such as clostridia, counter (negative) selectable marker is instrumental for allelic exchange by facilitating the identification of rare

recombination events. Under certain growth conditions and/or the presence of counter-selective agent, a counter-selectable gene causes death in microorganisms harbouring it. Commonly used counter-selectable markers in microorganisms are *pheS* (267), *ura3* (268), *upp* (208), *sacB* (269), *codA* (270, 271), *mazF* (109, 272, 273), *hpt* (274), *tetAR* (275), *ccdB* (276), *trpI* (277), *rpsL* (278), *lacY* (279) and *pyrE*/*pyrF* (212, 214, 280). The mechanism of negative selection can occur via sensitivity to otherwise tolerable compounds, incorporation of toxic analogs into cell components, toxin-antitoxin systems and sensitivity towards antibiotics. In this PhD project, *pyrE* was chosen for investigation due to its suitability as both positive and negative selectable marker and inhouse expertise whereas *codA* was investigated as an alternative marker in case *pyrE* did not produce the expected phenotypes in *C. autoethanogenum*.

3.2.5.1 *pyrE*

The gene *pyrE* encodes pyrimidine synthesis enzyme orotate phosphoribosyltransferase and inactivation of this gene should render the microorganism uracil auxotrophic, so its presence can be used as a positive selectable marker. In addition to pyrimidine biosynthesis, *pyrE* and *pyrF* (orotidine 5-phosphate decarboxylase) in several *Clostridium* species are also able to convert an innocuous pro-drug '5-fluoroorotic acid' (FOA) into the highly cytotoxic compound '5-fluorouracil' (FU) (212). The ability of *pyrE* or *pyrF* to confer cytotoxicity has been exploited as a counter-selectable marker in a number of clostridia including *C. acetobutylicum* ATCC 824, *C. difficile*, *C. sporogenes*, and *C. thermocellum* (212, 280).

To investigate the suitability of *pyrE* as a positive and negative selectable marker in *C. autoethanogenum*, *pyrE* (CAETHG_1476) was disrupted using ClosTron plasmid pMTL007C-E2::pyrE-144s. PCR screening using exon-spanning primers 'pyrE-F' and 'pyrE-R' successfully produced the expected 2612 bp ClosTron band while WT control produced an 812 bp product (Figure 3.5A). The PCR products were verified by Sanger sequencing and plasmid loss was demonstrated by inability of streaked mutants to grow on YTF solid medium containing 7.5 µg/mL thiamphenicol (data not shown).

Finally, genomic DNA of four *pyrE* mutants was subjected to Southern Blot analysis using probes that target RAM (Section 2.5.2) and single bands of the expected size were detected (Figure 3.5B).

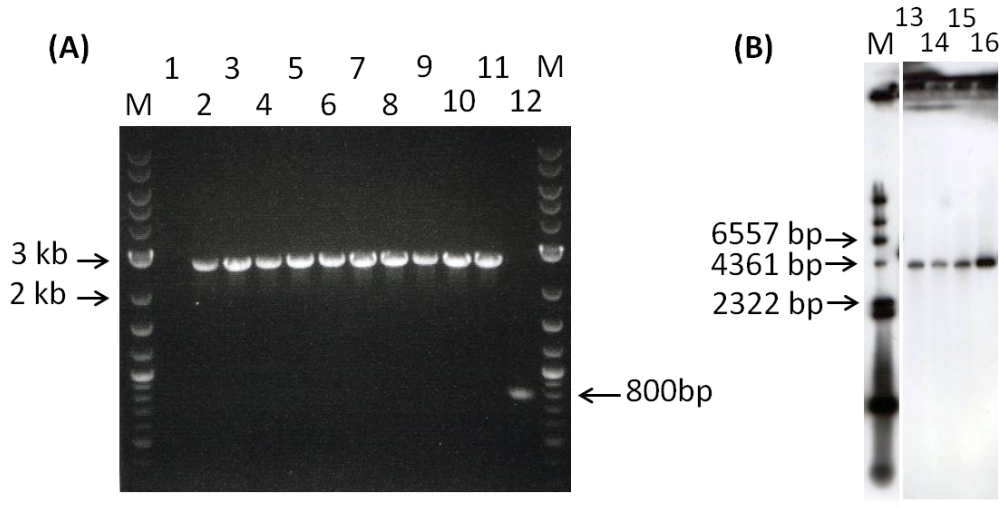


Figure 3.5. Screening and validation of *C. autoethanogenum pyrE*::CTermB-144s mutants. (A) Gel electrophoresis showing PCR of *pyrE* mutants using exon-spanning primers 'pyrE-F' and 'pyrE-R'. ClosTron insertion = 2612bp; WT = 812bp; Lane 1 = NTC; Lanes 2-11 = *pyrE* mutants; Lane 12 = WT control. (B) Southern Blot analysis of *Hind*III digested genomic DNA of *pyrE* mutants (lanes 13-16).

To investigate uracil prototrophy, 7 µl of active culture from one WT and four independent *pyrE* mutants were spotted onto solid medium CGMCF with five different concentrations of uracil (0, 10, 20, 50 & 100 µg/mL). Following four days of incubation inside the anaerobic cabinet, the WT was able to grow with and without uracil supplementation. In contrast, all four independent *pyrE* mutants were unable to grow without uracil supplementation, but able to grow when uracil was supplemented (Figure 3.6). Some variations in the level of growth were observed between the four mutants, which could be explained by differences in the state of inoculum. These results showed that *pyrE* can be used as a positively selectable genetic marker in a *pyrE* mutant background.

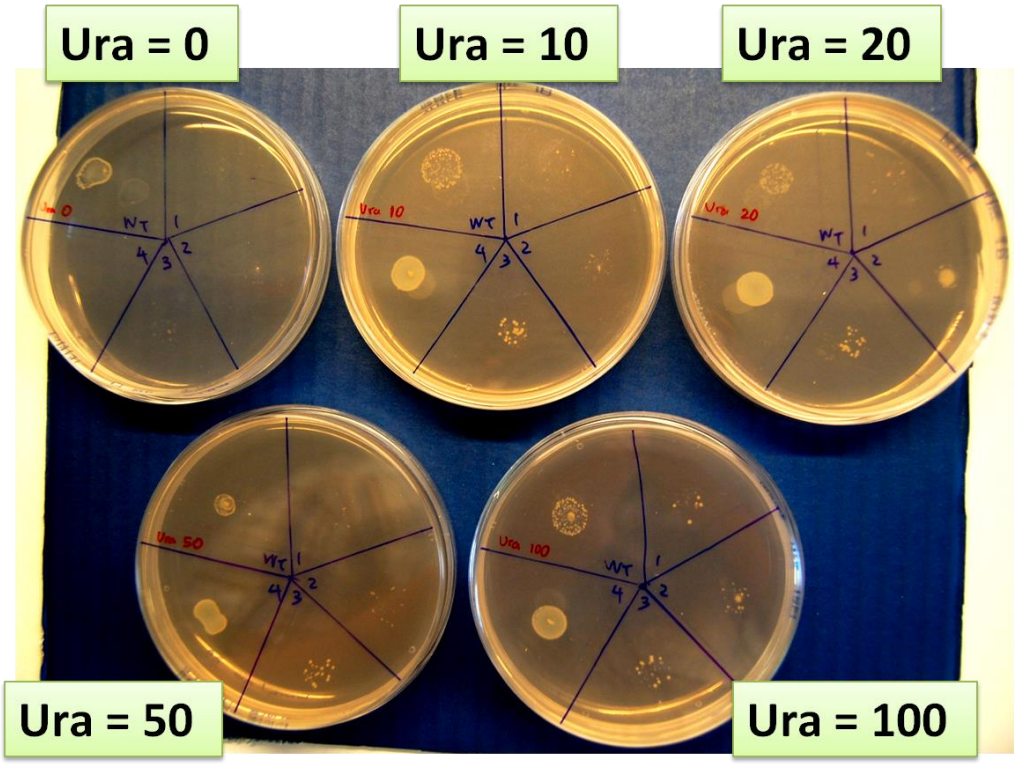


Figure 3.6. *C. autoethanogenum pyrE*::CTermB-144s mutants exhibit uracil auxotrophy. Uracil concentrations (µg/mL) clockwise from top left: 0, 10, 20, 100 and 50. Within each plate, WT = wild-type; 1-4 are four independent *pyrE* mutants. Incubation time = 4 days.

To determine whether *C. autoethanogenum pyrE* mutants are resistant to FOA, 7 µl of active culture from the same four independent *pyrE* mutants (as above) and one WT were spotted onto solid medium CGMCF and 20 µg/mL of uracil, with eight different concentrations of FOA (0, 10, 100, 500, 1000, 2000, 3000, and 4000 µg/ml). Following five days of incubation inside the anaerobic cabinet, the WT struggled to grow in the presence of 100 µg/ml of FOA and there was no growth for FOA concentrations ≥500 µg/ml (Figure 3.7). The spot of WT at 500 µg/mL FOA appears to show some growth, but this is an artefact due to accidental stabbing of pipette tip onto solid media while spotting the inoculum (Figure 3.7). In contrast to the WT, all four *pyrE* mutants were able to grow normally up to 1000 µg/mL of FOA (Figure 3.7). No growth was detected at 2000, 3000, and 4000 µg/mL FOA (data not shown). These results indicated that *pyrE* is a suitable positively and negatively selectable genetic marker for *C. autoethanogenum*, and it can be employed for ACE (section

3.2.6) to integrate foreign DNA into the genome by sequential activating and inactivating the marker (212).

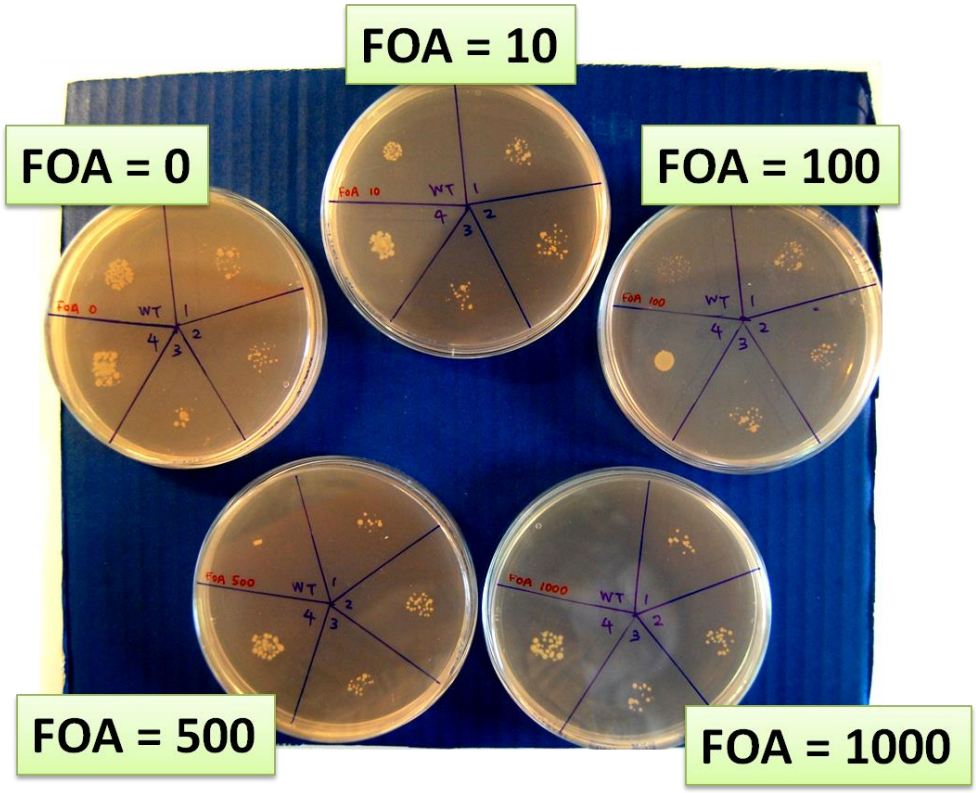


Figure 3.7. *C. autoethanogenum pyrE*::CTermB-144s mutants are resistant to FOA. The FOA concentrations (µg/mL) clockwise from top left: 0, 10, 100, 1000 and 500. Within each plate, WT = wild-type; 1-4 are four independent *pyrE* mutants. Incubation time = 5 days.

3.2.5.2 *codA*

The gene *codA* encodes cytosine deaminase which catalyzes the conversion of cytosine to uracil and ammonia. Besides its physiological role, CodA also converts the harmless pro-drug 5-fluorocytosine (FC) into highly cytotoxic FU. In many prokaryotes, *codA* is absent from the genome so it has the potential to be employed as a heterologous/exogenous counter-selectable marker without the need to first generate a mutant strain (e.g., *pyrE*). The feasibility of *codA* as exogenous counter-selectable marker has been demonstrated in *C. difficile* (270). Like *C. ljungdahlii, C.*

sporogenes, and *C. botulinum,* the genome of *C. autoethanogenum* encodes a putative *codA* (CAETHG_4058).

To investigate the possibility of using *codA* as a counter-selectable marker in *C. autoethanogenum*, *codA* knockout mutants were generated using ClosTron mutagenesis with plasmid pMTL007C-E2::*codA*-532s. PCR screening using exon-spanning primers 'codA-532-F' and 'codA-532-R' successfully produced the expected 2165 bp ClosTron band while the WT control produced 365 bp product (Figure 3.8A). The PCR products were verified by Sanger sequencing and plasmid loss was demonstrated by inability of streaked mutants to grow on YTF solid medium containing 7.5 µg/mL thiamphenicol (data not shown). Finally, genomic DNA of four *codA* mutants was subjected to Southern Blot analysis using probes that target RAM (Section 2.5.2) and single bands of the expected size were detected (Figure 3.8B).

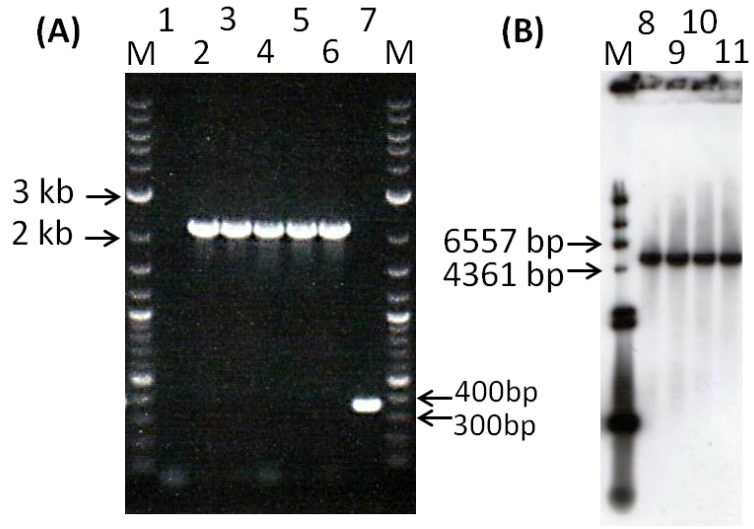


Figure 3.8. Screening and validation of *C. autoethanogenum codA*::CTermB-532s mutants. (A) Gel electrophoresis showing PCR of *codA* mutants using exon-spanning primers 'codA-532-F' and 'codA-532-R'. ClosTron insertion = 2165bp; WT = 365bp; Lane 1 = NTC; Lanes 2-6 = *codA* mutants; Lane 7 = WT control. (B) Southern Blot analysis of *Hind*III digested genomic DNA of *codA* mutants (lanes 8-11).

For assessment of FC sensitivity, 10 µL of active culture from three independent *codA* mutants and one WT were spotted onto solid medium CGMCF with different

concentrations of FC (0, 1, 10, 50, 100, and 1000 µg/mL). Following 12 days of incubation inside the anaerobic workstation, the WT struggled to grow at 10 µg/mL of FC, and exhibited no growth at 50, 100 and 1000 µg/mL FC (Figure 3.9). In contrast, *codA* mutants 1 and 3 were able to grow normally at 1000 µg/mL FC (Figure 3.9). *codA* mutant 2 was able to grow up to 100 µg/mL FC but not 1000 µg/mL FC, suggesting 100 µg/mL might be the upper threshold at which the *codA* mutants are able to tolerate FC. These results showed that *C. autoethanogenum* WT and *codA* mutant exhibited different sensitivities towards FC, raising the possibilities that *codA* can be employed as a counter-selectable marker.

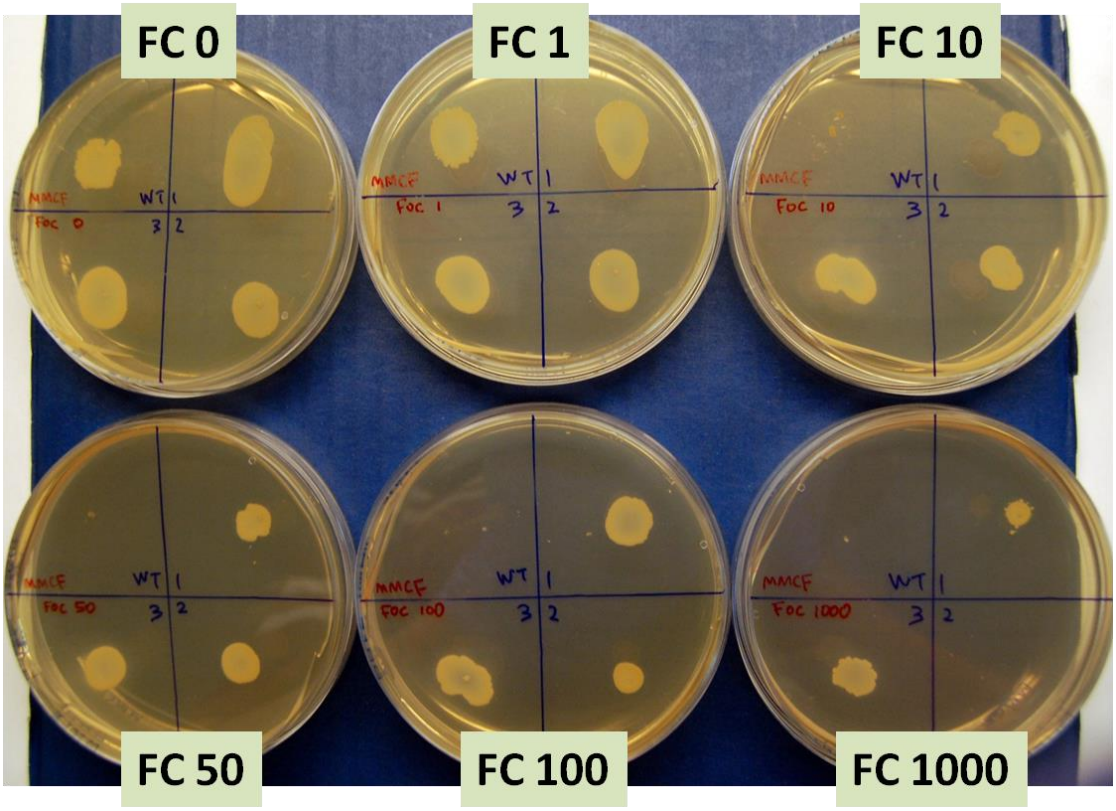


Figure 3.9. *C. autoethanogenum codA*::CTermB-532s mutants are resistant to FC. FC concentrations (µg/mL) clockwise from top left: 0, 1, 10, 1000, 100 and 50. Within each plate, WT = wild-type; 1-3 are three independent *codA* mutants. Incubation time = 12 days.

3.2.6 Generation of Δ*pyrE* Mutant using ACE

Recently, a new genetic tool which allows multi-step integration of foreign DNA fragments into *Clostridum spp.* was developed in this laboratory. Termed "Allele-Coupled Exchange (ACE)", this technology does not rely on counter-selectable marker but exploits the activation and inactivation of genes leading to a selectable phenotype (212). Allelic-exchange allows a range of genome modifications, including insertion, (in-frame) deletion, and alteration of specific codons. ACE has been exemplified in *C. acetobutylicum*, *C. sporogenes*, *C. difficile* (212) and *C. ljungdahlii* (Dr. Anne M. Henstra, University of Nottingham; unpublished results) but not yet in *C. autoethanogenum*. Although the generation of a *pyrE* deletion mutant via allelic exchange is not an absolute prerequisite for this technique, construction of this mutant allows the use of *pyrE* as a positively and negatively selectable marker in downstream allelic exchange(s).

In this project, the 3` end of *pyrE* (227 bp) of *C. autoethanogenum* was replaced by *lacZα* using plasmid pMTL84151-Δ*pyrE* (Figure 3.10A). This plasmid was constructed by Dr. Anne M. Henstra and consists of a heterologous *pyrE* from *C. acetobutylicum* (whose *pyrE* only shares 335/732 or 45% nucleotide identity with *C. autoethanogenum*) to facilitate plasmid loss via FOA selection, in addition to the asymmetric homology arms targeting the *pyrE* region (Section 2.14.1). The process involved in generating the double crossover Δ*pyrE* mutant can be found in Section 2.14.1. Figure 3.10B shows the detection of "single crossover" mutants by PCR using primer pairs 'P1' and 'P2', resulting in a PCR product of 1946 bp. However, due to an error in designing the forward primer 'P1', PCR using primers 'P1' and 'P2' was also capable of generating the same product if any pMTL84151-Δ*pyrE* plasmids were retained after genomic DNA extraction using the DNeasey Blood and Tissue kit (Qiagen), resulting in potentially false positive results. Primer 'P1' should have been designed to anneal to the 5`-UTR of *pyrE* to avoid this cross reaction. Nonetheless, these putative "single-crossover" mutants were subjected to FOA selection and double crossover Δ*pyrE* mutants were detected by PCR using primer pairs 'P3' and 'P4' (Figure 3.10C).

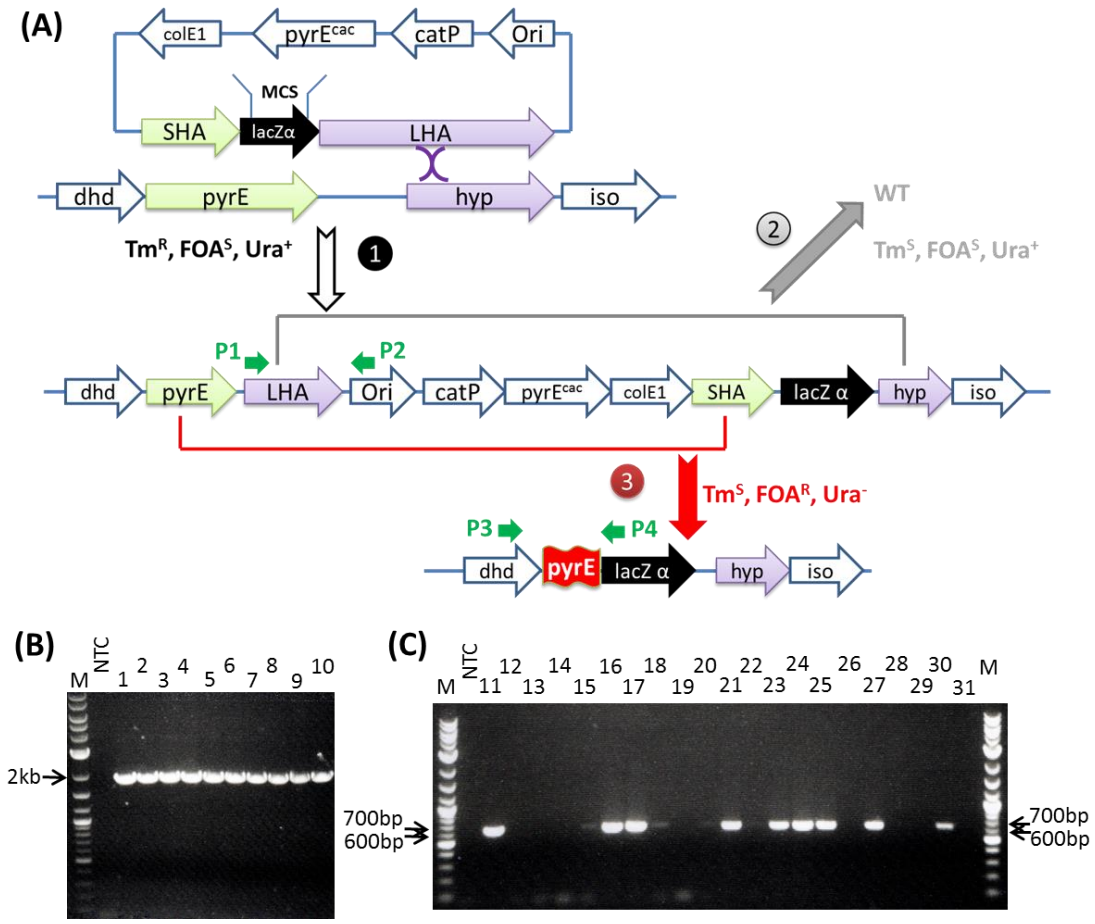


Figure 3.10. Deletion of *pyrE* using ACE in *C. autoethanogenum*. (A) Schematics showing the replacement of 3` end of *pyrE* with *lacZ* using ACE. Event one illustrates the first crossover at the great homology arm and was screened by PCR using primers 'P1' and 'P2'. Event 2 describes the reversion back to wild-type. Event 3 explains the second crossover at the short homology arm and was screened by PCR using primers 'P3' and 'P4'. FOA = 5-fluoroorotic acid; GHA = great homology arm; $pyrE^{cac}$ = *pyrE* from *C. acetobutylicum* ATCC 824; SHA = short homology arm; Tm = thiamphenicol; ura = uracil; (B) PCR screening of first crossover using primers 'P1' and 'P2'. Lanes 1-10 are fast-growing thiamphenicol resistant colonies; (C) PCR screening of second crossover using primers 'P3' and 'P4'; Lanes 11-30 are FOA resistant colonies; Lane 31 = WT control; NTC = non-template control; M = NEB 2-log DNA ladder.

Surprisingly, a large proportion (8/20) of the FOA-resistant colonies failed to produce the double-crossover PCR bands of 647 bp during gel electrophoresis analysis. In previous failed attempts at detecting double crossover events during this PhD study, DNA sequencing of the *pyrE* region from FOA-resistant colonies showed random single point mutation(s) within the *pyrE* coding region or completely intact *pyrE* gene and its promoter, indicating random mutation(s) elsewhere conferred FOA

resistance. Since FOA is known in this laboratory to have a limited efficacy period of around 3 days on solid medium at 37^{o}C, it is possible that some of the screened colonies emerged after the effect of FOA had worn off. The eventual double-crossover Δ*pyrE* mutants were verified by DNA sequencing to confirm the replacement of the 3` end of *pyrE* with *lacZα*, and thiamphenicol sensitivity was demonstrated to verify the loss of ACE plasmid (data not shown). Furthermore, these mutants were also unable to grow without uracil supplementation (data not shown).

3.2.7 Restoration of *pyrE* using ACE

In comparison to plasmid-based complementation strategies, the repair of knock out mutants back to their original state via allelic exchange eliminates gene dosage mismatch and avoids the need to include a plasmid control and antibiotic for plasmid maintenance. In the case of a Δ*pyrE* mutant, restoration can be achieved by transformation of a plasmid with an allele containing the missing 3`-end of *pyrE* followed by selection for uracil prototrophs.

In this study, two slightly different versions of *pyrE* restoration plasmids were constructed (Section 2.14.2). The first plasmid, pMTL84151-fix*pyrE*, was designed to completely 'fix' *pyrE* back to its original state without introduction of foreign DNA into the genome of *C. autoethanogenum*. The second plasmid, pMTL84151-com*pyrE*, has *lacZα* incorporated between the short and great homology arms, so *lacZα* is concurrently integrated into the genome during 'complementation' of the *pyrE* locus.

Following conjugation of *pyrE* restoration plasmids into a Δ*pyrE* mutant, fast-growing Tm^{R} colonies were preferentially streaked onto solid CGMCF medium without uracil supplementation to select for uracil prototrophs according to Section 2.14.4. Uracil prototrophs were subjected to PCR screening using primer pairs 'ACE-pyrE-F' and 'ACE-pyrE-R'. Figure 3.11A shows that all the screened 'fixed' colonies have been fully restored back to the original *pyrE* locus, evident in the presence of a 2059 bp band. Similarly, all the screened 'complemented' colonies produced a 2338 bp amplicon, which is 279 bp larger than the WT band, indicative of *lacZα* insertion

(Figure 3.11B). The resultant PCR products were also sequenced to verify the restoration of the *pyrE* genotype (data not shown).

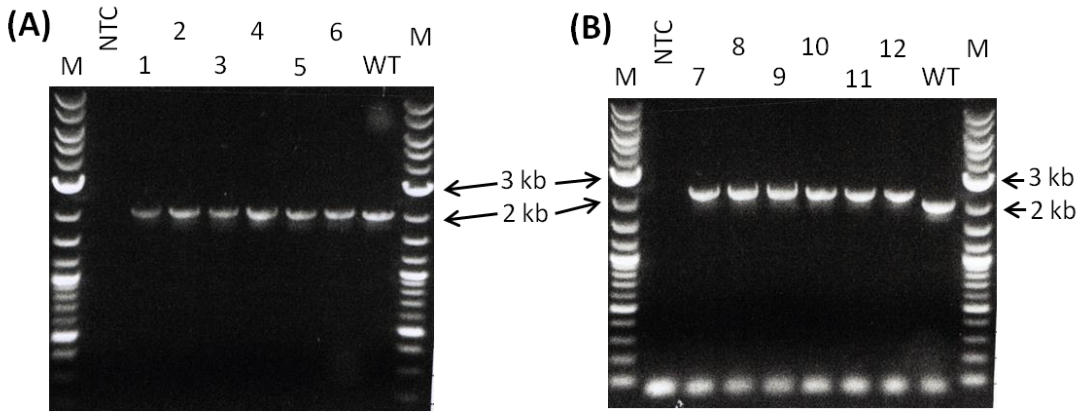


Figure 3.11. Restoration of *C. autoethanogenum pyrE* mutants. (A) PCR screening of fully restored *pyrE* mutants (lanes 1-6); (B) PCR screening of complemented *pyrE* mutants with concomitant integration of *lacZα* (lanes 7-12); For (A) & (B), forward primer = 'ACE-pyrE-F', reverse primer = 'ACE-pyrE-R'; WT= Wild-type; NTC = non-template control; M = NEB 2-log DNA ladder.

3.3 Discussion

3.3.1 *C. autoethanogenum* is Genetically Tractable via Conjugation (and Electroporation)

Pivotal to any genetic engineering effort is a reliable method of introducing foreign DNA into the host cells. Despite strong biotechnological interests and their discovery and characterization more than two decades ago, acetogens such as *C. ljungdahlii* (37, 229), *M. thermoacetica* (237), *A. woodii* (236), and *C. aceticum* (234) have only very recently been demonstrated to be genetically tractable. The formulation of a reliable transformation protocol is often one of the most challenging tasks in genetic tools development. For the microorganism of interest in this study, *C. autoethanogenum*, two transformation strategies were explored: electroporation and conjugation.

Due to its technical simplicity, higher reproducibility, greater transformation efficiency and independence from donor species, electroporation is the most

commonly explored method of transformation in clostridia. Transformation efficiencies of $10^4 – 10^6$ have been reported for *C. acetobutylicum* ATCC 824 (183), *C. saccharoperbutylacetonicum* NI-4 (281), *C. ljungdahlii* DSM 13528 (229) and *C. pasteurianum* ATCC 6013 (282). In this laboratory, an efficient electroporation protocol for *C. ljungdahlii* was developed by Dr. Anne M. Henstra and Dr. Elizabeth Steiner (unpublished results) prior to the report by Leang *et al*. (2013) (229). The transformation efficiencies for modular plasmid pMTL83151 (2.5 x 10^3 cfu/μg DNA) and pMTL82151 (2.7 x 10^3 cfu/μg DNA) in this study are comparable to the report by Leang and co-workers (229): 3.8 x 10^3 and 3.1 x 10^3 cfu/μg DNA, respectively.

Given the phylogenetic relatedness between *C. ljungdahlii* and *C. autoethanogenum*, it was surprising that the same electroporation protocol only resulted in very low transformation efficiencies (up to 3.8 cfu/μg DNA) and also low reproducibility (2/11 attempts yielded transformants). Various electroporation parameters were investigated but none ameliorated the poor transformation efficiencies. These factors included growth stage of competent cells, *in vitro* plasmid methylation, recovery medium and duration, *E. coli* host for propagation of plasmids and testing of other plasmids. Comparison of RM systems between the two acetogens revealed the presence of 12 putative RM systems that are unique to *C. autoethanogenum*. It is likely that the difference in RM systems contributed to the contrasting electroporation efficiencies. To test this hypothesis, the unique RM systems in *C. autoethanogenum* can be systematically inactivated and their impacts on electroporation efficiencies can be evaluated. For instance, a type II restriction endonuclease in *C. acetobutylicum* DSM 1731 was inactivated using ClosTron, resulting in a mutant that can be transformed with unmethylated DNA as efficiently as methylated DNA (187). Furthermore, next generation sequencing (NGS) technologies such as Single Molecule Real-Time (SMRT) sequencing can be employed to reliably detect certain methylation signatures (283, 284), which can be used to formulate *in vitro* or *in vivo* methylation strategies to protect foreign DNA from the host's restriction barrier.

The transfer of foreign DNA into host cells via conjugation represents an alternative transformation strategy. This method requires direct cell-to-cell contact during the

transfer of DNA from donor to recipient so this approach is limited by the host range of the donor. However, transfer of DNA via conjugation has been reported to occur in single strand, from which means the incoming DNA can evade the recipient's restriction endonucleases (185, 250).

In this study, a range of modular plasmids with different Gram-positive replicons (pBP1, pCB102 and pCD6) were successfully conjugated into *C. autoethanogenum* using *E. coli* CA434 donor (250) with conjugation efficiencies ranging from 2.8 x 10^{-9} to 5.2 x 10^{-8} cfu per donor. These conjugation efficiencies are similar to the DNA transfer frequencies obtained for *C. acetobutylicum* (10^{-6} to 10^{-10} cfu per donor) (178) but lower than *C. difficile* (10^{-5} to 10^{-7} cfu per donor) (250). Nonetheless, they represent a significant improvement for *C. autoethanogenum* in terms of transformation efficiency and reproducibility over electroporation. In *Neisseria gonorrhoeae*, the transfer of DNA via conjugation was also found to be more efficient than electroporation (285).

For plasmid pMTL85151 (with pIM13 Gram-positive replicon), some transconjugants were detected occasionally on the initial selective plate, but they failed to grow when streaked onto a second selective plate. This result indicates that this plasmid may be segregationally unstable in *C. autoethanogenum*, and is consistent with the inability to obtain electrotransformants in *C. ljungdahlii* using this plasmid on a regular basis by others in this laboratory. However, pIM13-based plasmids have been successfully transformed into *C. ljungdahlii* by two independent research groups (37, 229). Throughout this project, the Gram-positive replicon pCB102 was utilized for the construction of ClosTron mutants and also over-expression plasmids. Plasmids based on pCD6 Gram-positive replicon were used for the construction of deletion mutants using ACE.

3.3.2 Exemplification of ClosTron Mutagenesis by the Construction of a *fruA* Mutant

ClosTron mutagenesis offers a quick, stable and reproducible way of inactivating a gene to study its functions. To exemplify this technique in *C. autoethanogenum*, one

EIIABC subunit of fructose-specific PTS (*fruA*) was selected for disruption because of the anticipated clear-cut phenotype: inability to grow using fructose as substrate. According to the literature, *C. autoethanogenum* is able to utilize fructose, pyruvate, xylose, arabinose, rhamnose and L-glutamate as substrate, in addition to its ability to grow autotrophically (52).

The intron targeting region for *fruA* was designed using the Perutka algorithm (251) (freely available from www.clostron.com), and then synthesized and cloned into ClosTron plasmid pMTL007C-E2 by DNA2.0, Inc. This process takes 1-2 weeks, and costs US$150 per target to synthesize and clone the intron targeting region without involving any cloning work from the end user. Following conjugation of ClosTron plasmid into host cells, Tm^R colonies were streaked onto plates containing clarithromycin to select for intron integrants. PCR screening and subsequent Sanger sequencing showed that all the screened Cla^R clones had the intron successfully inserted into the target region of *fruA*. Southern Blot analysis confirmed there was only one intron insertion event per mutant. As expected the *fruA* mutants were unable to grow using fructose as substrate in both liquid and solid medium. In parallel, the same set of biological samples was capable of growing on medium supplemented with pyruvate as carbon source, indicating that the mutants were viable. Although the genome of *C. autoethanogenum* encodes one other putative PTS of unknown substrate specificities, the knocked out *fruA* (CAETHG_0142) is likely to be the main, if not the only, fructose transporter in *C. autoethanogenum* based on the clear-cut phenotype this mutant exhibited.

In this PhD project, a total of 11 Southern Blot verified ClosTron mutants were generated and most of the screened Cla^R colonies were shown to contain ClosTron insertion at the targeted locus. These results highlighted the credentials of ClosTron as a routine genetic tool for generation of KO mutant in *C. autoethanogenum*. However, it has its limitations including undesirable polar effects and the apparent inability to recycle the ermRAM marker in this acetogen using flippase (see section 4.7) prevented its use for construction of multiple KO mutants.

3.3.3 Exploration of *fruA* as Counter-Selectable Marker

In some bacteria, the accumulation of phosphorylated sugar alcohol intermediates following the import of sugar alcohol via the PTS, exerts toxicity on the cells. For instance, *S. typhimurium* mutants that lack functional mannitol-phosphate dehydrogenase are inhibited by D-mannitol (264). It has been hypothesized that *fruA* can be employed as a counter-selectable marker if WT displays toxicity towards a sugar alcohol, while the *fruA* mutant confers resistance. Growth experiments in pyruvate-based liquid medium showed that *C. autoethanogenum* WT displayed some sensitivity towards xylitol at 100 mM concentration (55% reduction in optical density) while the *fruA* mutant were not growth inhibited. Consistent with this finding, plating assays also showed that the WT was able to form tiny colonies at 100 mM xylitol. At 200 mM and 300 mM xylitol concentrations, the WT was completely growth inhibited but the *fruA* mutant was able to form colonies.

These results showed that *fruA*, in combination with xylitol, is a potential counter-selectable marker for *C. autoethanogenum*. Since the toxic effect of xylitol is more stable than FOA (which begins to lose activity after 3 days at 37^{o}C), *fruA* is potentially a better negative selectable marker than *pyrE*. Moreover, *pyrE* is involved in pyrimidine biosynthesis so it has to be restored back to WT allele if the mutant is to be utilized in industrial gas fermentation without costly uracil supplementation whereas *fruA* is not expected to be required for autotrophic growth so *fruA* may not have to be corrected back to WT allele. However, the drawback and challenges of *fruA* as a selectable marker are that many clostridia possess several PTS genes (56, 286-288) so multiple KO may be required to completely disrupt the ability to consume a sugar substrate or import sugar alcohols. Furthermore, the toxicity of sugar alcohols such as xylitol and D-mannitol is unknown for other clostridia so its applicability across the genus *Clostridium* remains to be tested.

3.3.4 Testing of Counter-Selectable Markers *pyrE* and *codA*

In genetically more intractable microorganisms like clostridia, counter-selectable markers are invaluable during the construction of allelic exchange mutants by

facilitating the identification of rare recombination events. The gene *pyrE* has been employed as a counter-selectable marker in a number of microorganisms including *C. acetobutylicum* ATCC 824, *C. difficile*, *C. sporogenes*, and *C. thermocellum* (212, 280), due to its ability to catalyze the conversion of pro-drug FOA into the highly cytotoxic compound FU. Furthermore, because of its role in pyrimidine biosynthesis, *pyrE* can also be utilized as a positive selectable marker by selecting for uracil prototrophs.

To evaluate the suitability of *pyrE* as both a positive and negative selectable marker in *C. autoethanogenum*, a *pyrE* mutant was constructed using ClosTron. As expected, the *pyrE* mutant was unable to form colonies when plated onto solid medium devoid of uracil. Importantly, the ability of *C. autoethanogenum* WT to form colonies was found to be inhibited by FOA at 500 μg/mL while the *pyrE* mutant was able to form colonies up to 1000 μg/mL FOA. Collectively, these results show that *pyrE* can be utilized as both a positive and negative selectable genetic marker for *C. autoethanogenum*.

Similar to *pyrE*, cytosine deaminase *codA* has also been employed as a counter-selectable marker in *C. difficile* (270) due to its ability to convert an innocuous pro-drug FC into cytotoxic FU. However, unlike its *pyrE* counterpart, *codA* is relatively rare in prokaryotes so *codA* can be utilized as an exogenous negative selectable genetic marker. This means there is no native *codA* to be inactivated before a heterologous *codA* is used as a counter-selectable marker. Unfortunately the genome of *C. autoethanogenum*, like *C. ljungdahlii*, *C. sporogenes* and *C. botulinum*, encodes a *codA* (CAETHG_4058). Nonetheless, a ClosTron mutant of *codA* in *C. autoethanogenum* was generated. During FC cytotoxic assay, *C. autoethanogenum* WT was found to be sensitive to FC at 50 μg/mL, while *codA* mutants were able to grow at 100 μg/mL FC (some up to 1000 μg/mL). This leads to the conclusion that *codA* can also be applied as a counter-selectable marker in *C. autoethanogenum*.

3.3.5 Generation of Δ*pyrE* Mutant and Its Subsequent Restoration using ACE

While ClosTron mutagenesis is rapid, stable, not labour intensive and has been demonstrated in a wide selection of clostridia, it has major limitations such as unintended polar effect from intron insertion and the generation of double mutant by recycling of the *ermB* RAM marker has only been demonstrated in *C. acetobutylicum* ATCC 824 (206). For precise genetic manipulations such as base substitutions, IFD, and integration of large DNA fragments, allelic-exchange approaches are often employed. The use of a counter-selectable marker is often necessary to detect and select for the rare second recombination event during allelic-exchange. A recently developed allelic-exchange tool, termed 'ACE', does not rely on a counter-selectable marker. Instead it utilizes asymmetric homology arms to direct the sequence of recombination events and also the activation and inactivation of gene(s) that result in a selectable phenotype (212).

For this project, the creation of a Δ*pyrE* mutant in *C. autoethanogenum* using the ACE technique was desirable as the state of *pyrE* can be subsequently activated and inactivated to drive precise genetic manipulations such as the integration of novel biosynthetic pathways, IFD and specific base substitutions. After conjugation of pMTL84151-Δ*pyrE* into *C. autoethanogenum*, putative single-crossover mutants at the GHA were selected based on faster growth rate on thiamphenicol plates. PCR screening showed the single-crossover event had occurred but due to an error in primer design, the primer pairs could also amplify any carryover plasmid from the genomic DNA extraction process, resulting in false positives. Nonetheless, these putative single-crossover mutants were subjected to FOA negative selection, in conjunction with the heterologous *pyrE* from *C. acetobutylicum* in the plasmid backbone, to select for the second recombination event at the SHA.

When PCR screening was carried out, slightly more than half (12/20) of the FOA^R colonies produced the expected double-crossover PCR product during gel electrophoresis analysis. This low frequency can be explained by the potential false positive single-crossover mutants (as mentioned above) and random mutations that occurred in the promoter or coding region of *pyrE*. Sanger sequencing of positive

amplicons verified the successful replacement of the 3` end of *pyrE* with *lacZα*. Importantly, the loss of the plasmid was also demonstrated by replica plating onto thiamphenicol solid medium.

The inactivated *pyrE* in the chromosome of *C. autoethanogenum* enabled the use of a heterologous *pyrE* as a counter-selectable marker to construct allelic exchange mutants in other loci. Subsequently, these mutants can be complemented via allelic exchange concomitant with correction of *pyrE* allele to WT. As a proof-of-principle study, two slightly different restoration approaches were applied to the Δ*pyrE* mutant in *C. autoethanogenum*. The first approach aimed to fully 'fix' *pyrE* back to its original state, using plasmid pMTL84151-fix*pyrE*. The second approach intended to not only complement the missing 227 bp at the 3` end of *pyrE*, but also integrate *lacZα* at the 3-`UTR of *pyrE*, using plasmid pMTL84151-com*pyrE*. Novel biosynthetic pathways can be cloned into the *lacZα* using the multiple cloning site and be stably integrated and expressed in *C. autoethanogenum*.

After conjugation of restoration plasmids into the Δ*pyrE* mutant, single-crossover integrants were selected over plasmid carriers by preferentially streaking faster-growing colonies on thiamphenicol plates. In this study, the first crossover event was not confirmed by PCR but these faster-growing Tm^R colonies were immediately streaked onto medium without uracil supplementation to select for uracil prototrophs. As shown in the PCR screening results (Figure 3.11), all the examined clones produced the expected double-crossover PCR product. Sanger sequencing of these amplicons confirmed that the missing 3` end of *pyrE* had been successfully restored, with and without the concomitant integration of *lacZα*.

3.4 Chapter Summary

In summary, *C. autoethanogenum* was shown to be genetically tractable, overcoming one major obstacle of genetic tools development. Although both electroporation and conjugation were demonstrated to introduce foreign DNA into *C. autoethanogenum*, the latter method was found to be more efficient and reproducible. Twelve unique putative RM systems were found in the genome of *C. autoethanogenum* but not *C.*

ljungdahlii, suggesting that they may contribute to the big differences in electroporation efficiencies (or deficiencies) between the two closely related acetogens. ClosTron mutagenesis was exemplified in *C. autoethanogenum*, as demonstrated in the creation of *fruA* mutants, *pyrE* mutants, and *codA* mutants. In addition to the abolishment of ability to grow on fructose, the *fruA* mutant was also shown to be resistant to xylitol whereas the WT strain was demonstrated to be sensitive to xylitol at a concentration of 200 mM. Further studies are warranted to explore the use of *fruA* as a counter-selectable marker.

The *pyrE* allele was demonstrated to be a suitable positive- and negative-selectable genetic marker in *C. autoethanogenum*, due to its role in pyrimidine biosynthesis and conversion of pro-drug FOA into cytotoxic FU. Similarly, *codA* was also shown to be an applicable counter-selectable marker because of its ability to convert pro-drug FC into cytotoxic FU. Lastly, ACE technology was exemplified during the creation and subsequent restoration of the Δ*pyrE* mutant. Collectively, these results provided the necessary genetic tools to carry out the remainder of this PhD project, including the creation and characterization of knock-out, IFD, and overexpression mutants in this acetogen.

CHAPTER 4

GENERATION AND CHARACTERIZATION OF CARBON MONOXIDE DEHYDROGENASE MUTANTS

4 Generation and Characterization of Carbon Monoxide Dehydrogenase Mutants

4.1 Introduction

Carbon monoxide dehydrogenase (CODH) catalyzes the interconversion between CO and CO_2. CODH enzymes are present in physiologically and phylogenetically diverse microorganisms from Archaea and Bacteria domains (289). CODH can be broadly categorized into two classes (78, 289): (i) the aerobic Cox-type Mo-Cu-Se CODH from aerobic carboxydotrophic bacteria, which comprises a highly conserved molybdenum active site and uses oxygen (sometimes nitrate) as terminal electron acceptor (290-293); and, (ii) the anaerobic-type Ni-CODH, which catalyzes the transfer of the electrons liberated from CO oxidation to a range of physiological electron acceptors including ferredoxin, cytochromes, flavodoxin, rubredoxin, and NAD(P)+ or it's reverse reaction (78-80, 294-298). Carbon monoxide is a potent electron donor (CO_2/CO reduction potential of −558 mV (pH 7.0)) (299). The reducing equivalents derived by CO oxidation can then be harnessed in several pathways including acetogenesis, methanogenesis, sulphate reduction, hydrogenogenesis, and metal reduction (78, 289, 300, 301).

The O_2-sensitive Ni-CODH can be further divided into two groups: (i) mono-functional CODH which functions physiologically in CO oxidation; and (ii) CODH as part of a bi-functional CODH/ACS (acetyl-CoA synthase) complex that couples the reduction of CO_2 to a [CO] moiety used by the ACS for acetyl-CoA biosynthesis. Genome sequencing has revealed that many anaerobes encode multiple Ni-CODH whose functions are associated with neighbouring gene clusters (300). For instance, *Carboxydothermus hydrogenoformans* encodes 5 CODHs (297), *Methanosarcina acetivorans* possesses 3 CODHs (302) and *M. thermoacetica* has two CODHs (73). The sequences and functions of CODH have been shown to be diverse (303) and horizontal gene transfer has been implicated in the dispersion of CODHs (300). Besides the interconversion of CO and CO_2, Ni-CODH have been reported to produce formate during CO_2 reduction (304), to convert nitrous oxide to dinitrogen (305), to

undertake the reduction of 2,4,6-trinitrotoluene (a pollutant) (306) and to catalyse the oxidation of *n*-butyl isocyanide to *n*-butyl isocyanate (307).

X-ray crystallography has revealed that the crystal structures of mono-functional Ni-CODH and Ni-CODH of bi-functional CODH/ACS complexes are very similar, despite their sequence and functional diversity (308-313). Both Ni-CODHs exist as homodimers that comprise five metal clusters per homodimeric enzyme: 2 C-clusters, 2 B-clusters and 1 bridging D-cluster (Figure 4.1). The C-cluster contains Ni-Fe-S and is the site of CO oxidation (78, 309). The [4Fe-4S] B- and D-clusters form the internal redox chain within the homodimeric enzyme (312). The bi-functional CODH/ACS complex is encoded by *acsA* and *acsB.* The assembly of CoA, [CO] moiety and methyl-group of the methylated CoFeSP into the central molecule acetyl-CoA occurs at the A-cluster of ACS (308-310) (Figure 4.1).

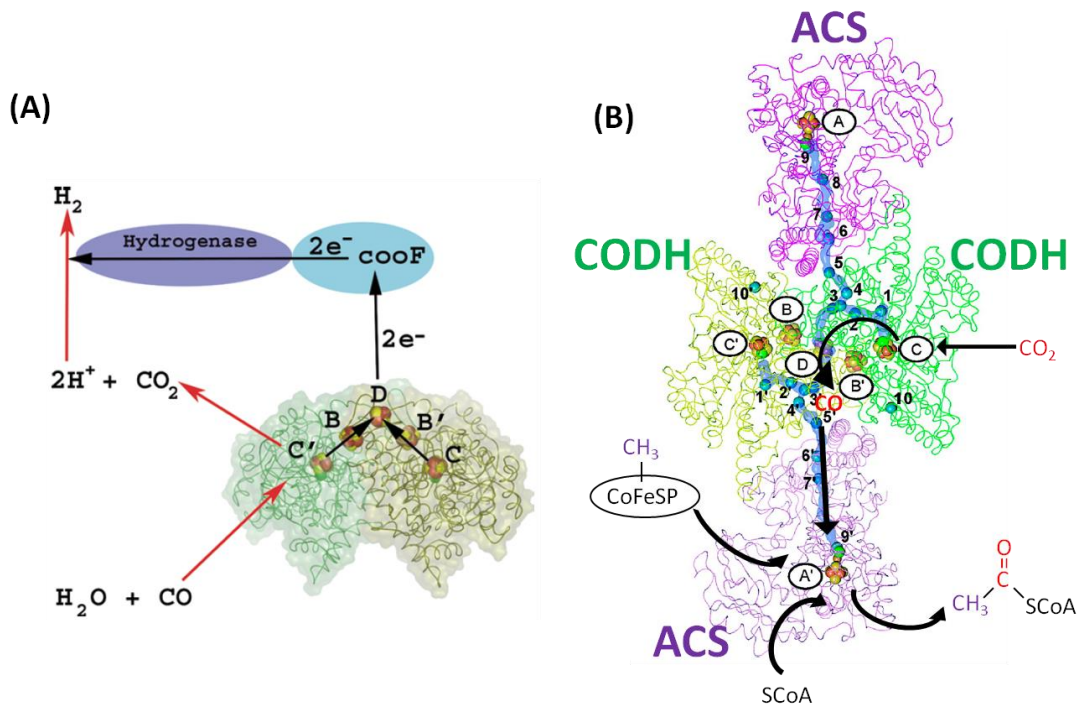


Figure 4.1. Structures of (A) mono-functional CODH; and (B) bi-functional CODH/ACS complex. (A) Coupling of *Rhodospirillum rubrum* CODH activity with hydrogen evolution via hydrogenase and Fe-S protein CooF. Figure was adapted from Ensign and Ludden (1991) (314). (B) Structure of bi-functional CODH/ACS complex from *Moorella thermoacetica* and its role in acetyl-CoA synthesis. Figure was modified from Doukov *et al.* (2008) (315). ACS, acetyl-CoA synthase; CODH, carbon monoxide dehydrogenase; CoFeSP, corrinoid iron sulphur protein. The numbers 1 to 10 in (B) represent the path of internal CO_2/CO channel within the CODH/ACS complex.

Ni-CODH has been reported to catalyze rapid CO oxidation at rates between 4,000 and 40,000 (mol CO) (mol enzyme)$^{-1}$ s^{-1} (295, 314, 316), and CO_2 reduction at 11 (mol CO_2) (mol enzyme)$^{-1}$ s^{-1} (317). However, relatively few anaerobes are able to grow on CO alone due to growth inhibition resulting from sensitivity of metal-containing enzymes towards CO (91).

C. autoethanogenum is able to grow autotrophically using CO as the sole source of carbon and energy (52). Genome sequencing uncovered three putative Ni-CODH in this acetogen: CAETHG_3005 (*cooS1*), CAETHG_3899 (*cooS2*) and CAETHG_1620-1621 (*acsA,* which encodes the CODH component of the bi-functional CODH/ACS complex) (38). The neighbouring gene clusters of these CODH are depicted in Figure 4.2. *cooS1* is genetically localized upstream of a gene encoding a putative 4Fe-4S ferredoxin Fe-S binding protein and ferredoxin-NAD(+) reductase, while *cooS2* appears to be an orphan (Figure 4.2A & B). The *acsA* gene is the first of the Wood-Ljungdahl cluster in *C. autoethanogenum* and when compared to other organisms that carry this pathway, such as *C. ljungdahlii*, uniquely contains an in-frame 'TGA' stop codon at nucleotide position 1201. The encoded enzyme is, therefore, truncated by some 231 amino acids, and the gene effectively split into two, CAETHG_1621 and CAETHG_1620 (Figure 4.2C and Figure 4.12B).

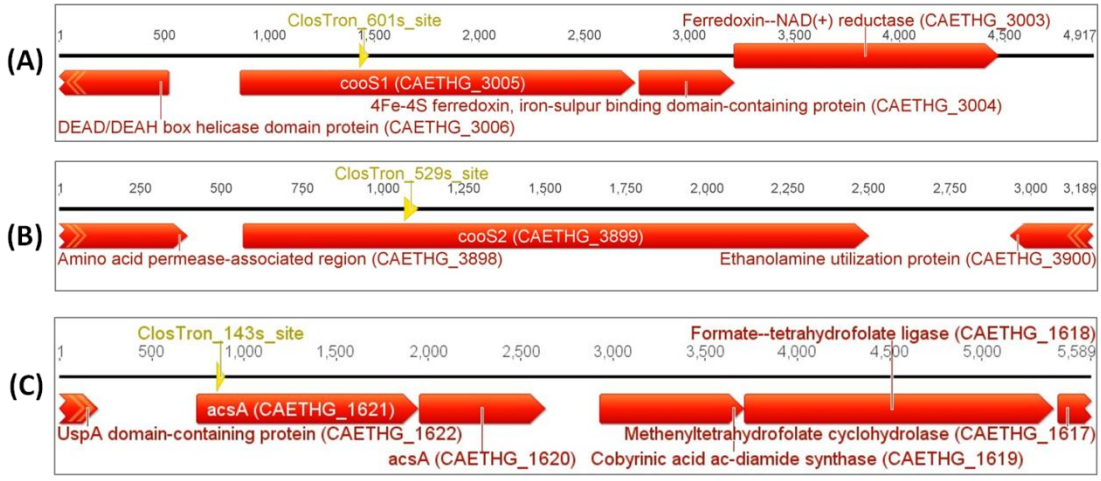


Figure 4.2. Gene arrangement of (A) *cooS1*; (B) *cooS2*; and (C) *acsA* in *C. autoethanogenum.* ClosTron insertion sites are highlighted by yellow arrows. Lengths of DNA fragments (in bp) are shown in grey. Figure is not drawn to scale and is generated using Geneious 6.1.7 (Biomatters Ltd).

To gain a better understanding of the roles of CODH in *C. autoethanogenum*, all three CODHs were independently inactivated using ClosTron mutagenesis. The resultant knockout mutants and WT were characterized under autotrophic and heterotrophic conditions to assess the impact of CODH inactivation on autotrophy, biomass formation and metabolite profile. The apparent truncation event of *acsA* was also investigated by examining translation of FLAG-tagged *acsA* variants. In an attempt to improve autotrophic capability, *acsA* was also overexpressed.

4.2 Generation of ClosTron Knockout Mutants of *cooS1*, *cooS2* and *acsA*

To generate independent knockout mutants of *cooS1*, *cooS2* and *acsA*, ClosTron plasmids pMTL007C-E2::cooS1-601s, pMTL007C-E2::cooS2-529s, and pMTL007C-E2::acsA-143s, respectively, were conjugated into *C. autoethanogenum* according to section 2.12.3. The ClosTron insertion sites are highlighted in Figure 4.2. Clarithromycin resistant colonies were subjected to PCR screening using primer pairs 'cooS1-601s-F' and 'cooS1-601s-R' for *cooS1* mutants, 'cooS2-529s-F' and 'cooS2-529s-R' for *cooS2* mutants, and 'acsA-ClosTron-F' and 'acsA-ClosTron-R' for *acsA* mutants. The screened clones showed the expected 2.2-2.3 kb bands (Figure 4.3A) and these PCR products were verified by Sanger sequencing. These ClosTron mutants were streaked onto the same selective medium until the ClosTron plasmids had been cured (shown by patch plating). As a final validation, Southern Blot analysis was performed to determine if ClosTron insertion had only occurred once per mutant. As shown in Figure 4.3B, double ClosTron insertions were detected in *cooS1* and *acsA* mutants. These double Intron insertion mutants were omitted from subsequent experiments.

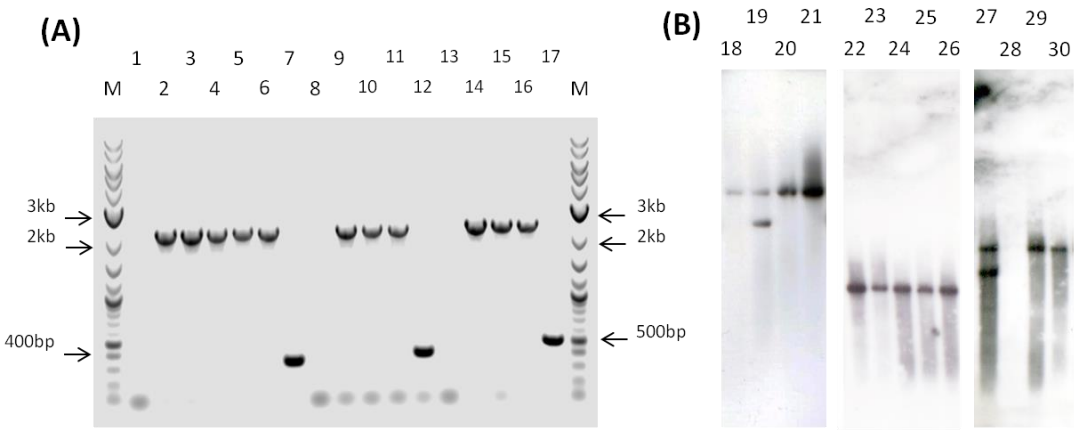


Figure 4.3. Screening and validation of ClosTron *cooS1*, *cooS2* and *acsA* mutants. (A) Gel electrophoresis of PCR using exon-spanning primers. M = NEB 2-Log DNA ladder; Lanes 2-6 = *cooS*1::CTermB-601s clones; Lanes 9-11 = *cooS*2::CTermB-529s clones; Lanes 14-16 = *acsA*::CTermB-143s clones; Lanes 1, 8 & 13 = non-template controls for *cooS1*, *cooS2* and *acsA* exon-spanning primer pairs, respectively; Lanes 7, 12 & 17 = wild-type control of *cooS1*, *cooS2* and *acsA* exon-spanning primer pairs, respectively. (B) Southern Blot analysis of *Hind*III digested genomic DNA of *cooS*1::CTermB-601s clones (lanes 18 - 21), *cooS*2::CTermB-529s (lanes 22 – 26) and *acsA*::CTermB-143s clones (lanes 27 - 30).

4.3 Characterization of ClosTron *acsA* Knockout Mutant

4.3.1 Autotrophic Growth Experiments

To examine the impact of *acsA* inactivation on autotrophic capability of *C. autoethanogenum*, both mutants (N = 3) and WT (N = 3-4) were grown in 250 mL serum bottles containing 50 mL CGMY medium (Section 2.4.1.2) with exchanged headspace of 2 bar CO or 1.3 bar H_2 and 0.7 bar CO_2. As shown in Figure 4.4A, the *acsA* mutant displayed no signs of growth in CO following 48 days of incubation whereas the WT reached an OD_{600} of 1.98 after day 7.7. Under H_2 + CO_2 conditions, the *acsA* mutant was unable to grow within 27 days whereas the WT achieved stationary phase (OD_{600} = 0.17) on ~day 15 (Figure 4.4B). These results demonstrated that *acsA* is unequivocally required for autotrophic growth in *C. autoethanogenum*.

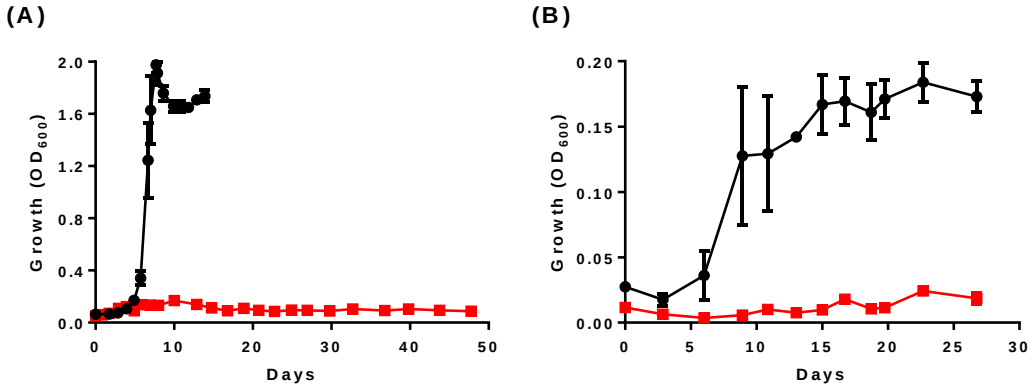


Figure 4.4. *acsA* ClosTron mutant is unable to grow autotrophically on (A) 2 bar CO; and (B) 1.3 bar H_2 + 0.7 bar CO_2. Black circles = wild-type (N = 4 for CO; N = 3 for H_2+CO_2); Red squares = *acsA* mutant (N = 3). Error bars = standard error of mean.

4.3.2 Complementation of *acsA* ClosTron Mutants

In order to unequivocally demonstrate that the loss of autotrophy was due to the inactivation of *acsA*, complementation assays were undertaken by expressing a plasmid-borne copy of the *acsA* gene in the *acsA* knockout mutant. Two versions of the gene were generated by PCR using primers (listed in Table 2.3) that incorporated the restriction recognition sites for *Nde*I and *Sac*I. In the one version (*acsA*^{full}), the entire *acsA* coding region was amplified (CAETHG_1621 and CAETHG_1620), complete with the TGA stop codon (Figure 4.2C). In the other (*acsA*^{trunc}), only the region corresponding to CAETHG_1621, and lacking the region (CAETHG_1620) downstream of the TGA stop codon was generated (Figure 4.2C). The DNA fragment encompassing *acsA*^{full} was generated using SOE-PCR in order to remove an internal *Nde*I site at nucleotide position 342 of CAETHG_1620. The primers employed (Table 2.3) replaced 'CAT' with 'CAC', a change that maintained the same encoded amino acid sequence. Both the truncated (*acsA*^{trunc}) and full version (*acsA*^{full}) of *acsA* were cloned, following cleavage with *Nde*I and *Sac*I, into a derivative of plasmid pMTL83157 into which the putative promoter region of *acsA* from *C. autoethanogenum* had been inserted as a *Not*I and *Nde*I fragment. Sanger sequencing was carried out to fully sequence the cloned promoter and cloned *acsA* genes.

The plasmids with truncated *acsA* (herein called pMTL83157-acsA^{trunc}) and full version of *acsA* (herein termed pMTL83157-acsA^{full}) were conjugated into the *acsA* KO mutant, generating complementation strains 'acsAKO+acsA^{trunc}' and 'acsAKO+acsA^{full}', respectively. A plasmid-only control was also created by the introduction of the 'empty' pMTL83157 vector into the WT strain. The presence of complementation plasmids in the resulting Tm^{R} transconjugants were verified by plasmid rescue and restriction digest analysis (data not shown).

Strains were assessed in serum bottles with 2 bar CO according to conditions described in section 2.6 except the media were supplemented with 7.5 µg/mL thiamphenicol (final concentration) to prevent plasmid loss. The plasmid-only control strain was eventually able to achieve an OD_{600} of 1.89 (similar to WT) but it experienced a 5 day longer lag phase than the WT (Figure 4.4A and Figure 4.5A). The expression of *acsA*^{trunc} in the *acsA* ClosTron mutant partially restored autotrophic growth in CO with the culture OD_{600} peaking at 1.05, but only after a significantly extended lag phase of ~43 days (Figure 4.5A). The culture of the *acsA* ClosTron mutant carrying *acsA*^{full} achieved a peak OD_{600} of 1.10 after a shorter lag phase of ~21 days (Figure 4.5A). Furthermore, complementation strain *acsA*KO+*acsA*^{full} also produced acetate (66 mM) closer to plasmid control level (78 mM) than complementation strain *acsA*KO+*acsA*^{trunc} (44 mM) (Figure 4.5B). Both complementation strains generated between 85% (*acsA*KO+*acsA*^{full}) and 120% (*acsA*KO+*acsA*^{trunc}) more ethanol than plasmid control strain (p-value = 0.056 and 0.010, respectively) (Figure 4.5C). Similar amounts of 2,3-butanediol were detected in all three strains (Figure 4.5D).

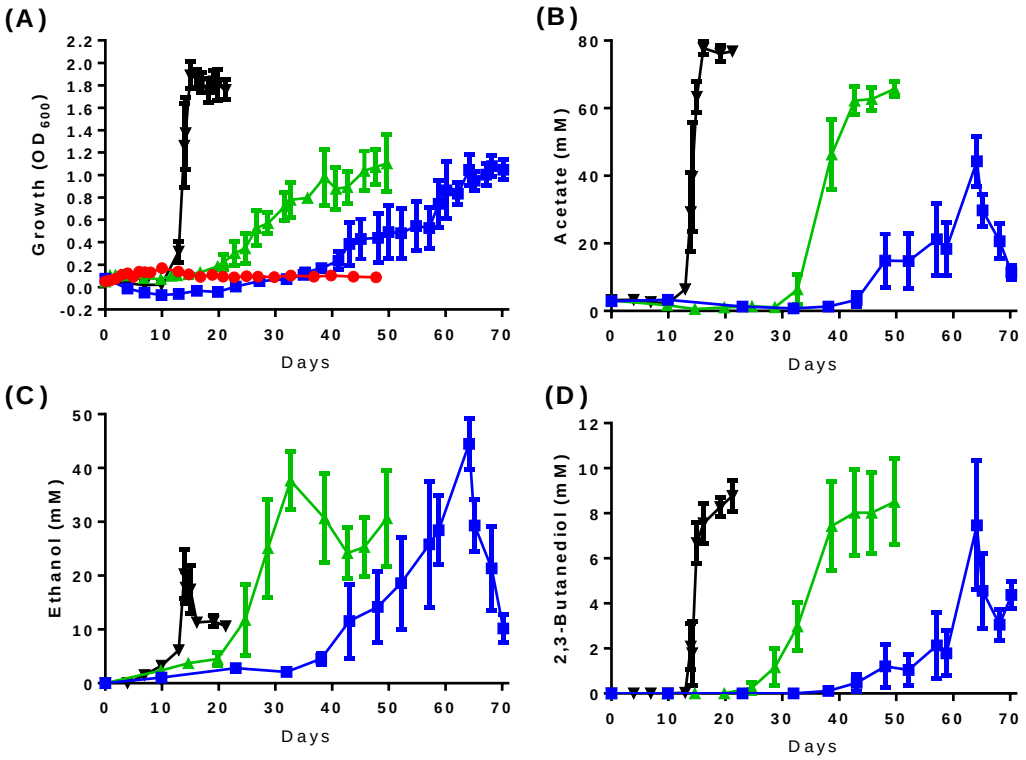


Figure 4.5. Growth and metabolite profiles of the complemented *acsA* ClosTron mutant and plasmid control strains on 2 bar CO. (A) Growth profile; (B) Acetate profile; (C) Ethanol profile; (D) 2,3-Butanediol profile. Black inverted triangles = plasmid control (N = 4); Red circles = *acsA* ClosTron mutant (N = 3); Blue squares = Complemented strain *acsA*KO+*acsA*^{trunc} (N = 4); Green triangles = Complemented strain *acsA*KO+*acsA*^{full} (N = 3). Error bars = standard error of mean.

4.3.3 Heterotrophic Growth Experiments

During heterotrophic growth, acetogens such as *C. autoethanogenum* DSM10061 are able to fix CO_2 (produced during sugar metabolism), using electrons generated from glycolysis, into biomass and products via the actions of CODH/ACS and other enzymes from the WLP. Hence, the inactivation of *acsA* is expected to have an effect on the growth and metabolite profiles while metabolizing sugars. To investigate this, the *acsA* ClosTron mutant, the complemented strains and WT strain of *C. autoethanogenum* were grown in triplicates of 250 mL serum bottles containing 50 mL of CGMY medium supplemented with 10 g/L fructose (final concentration).

As shown in Figure 4.6A, the inactivation of *acsA* significantly reduced the maximum OD_{600} reached compared to the WT from 4.53 to 1.77, equivalent to a 61% reduction.

This was also accompanied by an increase in growth lag phase to ~1.8 days in the *acsA* mutant while the WT only experienced a lag phase of ~0.9 day (Figure 4.6A). Plasmid expression of pMTL83157-*acsA*^{trunc} in the *acsA* ClosTron mutant did not shorten the growth lag phase but did allow the culture to reach a higher cell density peaking at an OD_{600} of 2.83 (Figure 4.6A). In comparison, the expression of pMTL83157-*acsA*^{full} in the knockout mutant substantially reduced the growth lag phase to WT levels (~0.9 day) and a cell density at its peak of OD_{600} to 3.11 (Figure 4.6A).

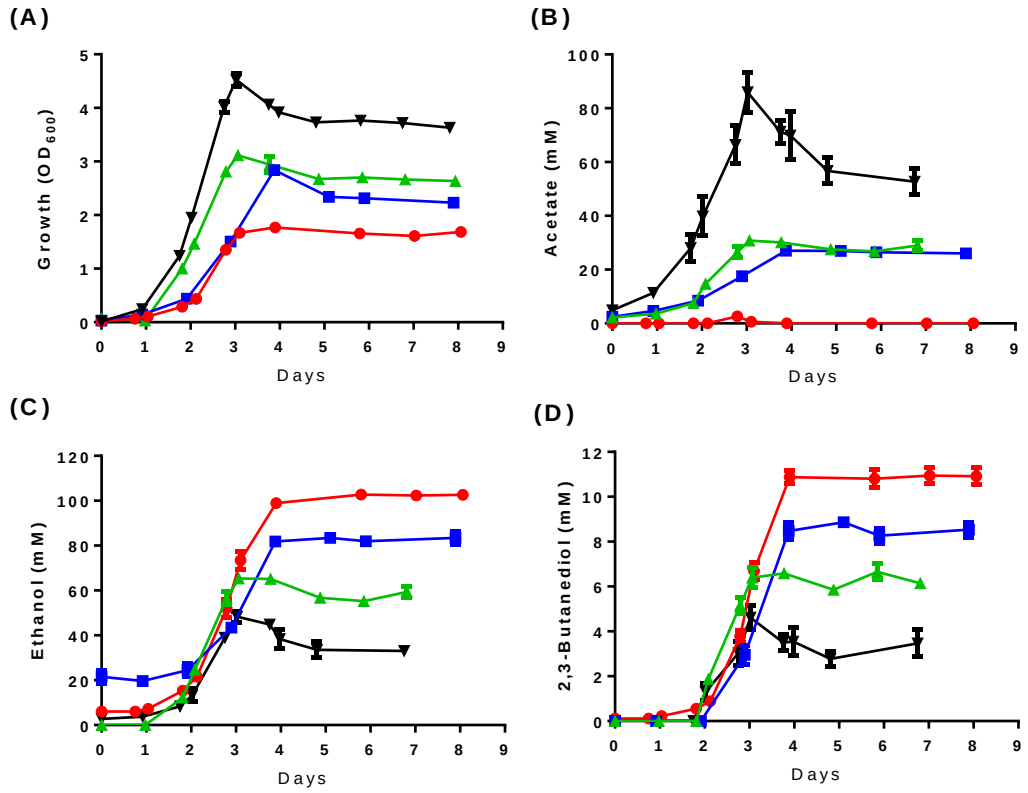


Figure 4.6. Growth and metabolite profiles of *C. autoethanogenum* wild-type (WT) and the *acsA* ClosTron mutant on 10 g/L fructose as the carbon source. (A) Growth profile; (B) Acetate profile; (C) Ethanol profile; (D) 2,3-butanediol profile. Black inverted triangles = WT; Red circles = *acsA* KO mutant; Blue squares = Complementation strain *acsA*KO+*acsA*^{trunc}; Green triangles = Complementation strain *acsA* KO+*acsA*^{full}; N = 3; Error bars = standard error of mean.

One striking feature of the *acsA* KO mutant is the lack of acetate production, with only 2.61 mM acetate being momentarily detected after day 2.8 (Figure 4.6B). In contrast, the WT had synthesized 85.96 mM acetate by day 3.0 (Figure 4.6B). In addition, the *acsA* KO mutant exhibited a 113% increase in ethanol production (102.7 mM) relative to the WT (48.3 mM), and a 138% rise in 2,3-butanediol synthesis (10.95 mM mutant vs 4.61 mM WT) (Figure 4.6C & D). Expression of $acsA^{trunc}$ and $acsA^{full}$ on a plasmid in the *acsA* KO mutant partially restored production of acetate with the two cultures respectively achieving final acetate levels of 27.0 mM and 30.8 mM (Figure 4.6B). In terms of ethanol and 2,3-butanediol levels, the expression of $acsA^{full}$ in the *acsA* ClosTron mutant resulted in more complete restoration to WT levels, in comparison to complementation by expression of $acsA^{trunc}$ (Figure 4.6C & D). For instance, the *acsA*KO+$acsA^{full}$ complementation strain produced ethanol at the reduced level of 65.4 mM compared to 102.7 mM for the non-complemented *acsA* KO mutant, whereas the ethanol titre of the *acsA*KO+$acsA^{trunc}$ complementation mutant was reduced to 83.4 mM (Figure 4.6C).

4.3.4 Mixotrophic Growth Experiments in Fructose and Carbon Monoxide

In addition to *acsA*, the genome of *C. autoethanogenum* encodes two additional CODHs: *cooS1* and *cooS2*. To investigate whether CODH1 and/or CODH2 is able to catalyze CO oxidation, the *acsA* KO mutant and the WT were subjected to mixotrophic growth. Growth experiments were conducted in triplicates in serum bottles containing 50 mL CGMY medium containing 10 g/L fructose, a headspace pressure of 2 bar CO and incubation with agitation for 268 hours (11.2 days). Liquid samples were harvested at t = 0 and t = 268 hours (end-point) for OD_{600} measurements and metabolite analysis using HPLC. The start- and end-point headspace pressures were measured using a digital pressure gauge DPG120 (Omega) and headspace gas composition was measured using gas chromatography according to section 2.8.2. The headspace pressure and composition at t = 0 were measured from an uninoculated serum bottle control containing 50 mL CGMY medium with 10 g/L fructose and 2 bar CO.

After 268 hours of growth, the headspace pressure of the *acsA* KO mutant culture increased by 0.73 bar due to the production of 2.03 mmol CO and 3.87 mmol CO_2 (Figure 4.7A & B). In contrast, the headspace of the WT culture decreased by 0.03 bar due to the consumption of 8.52 mmol CO and production of 8.32 mmol CO_2 (Figure 4.7A & B). Both strains completely exhausted fructose but neither strain exhibited H_2 production at the end of the growth experiment (data not shown). As the production of additional CO by the *acsA* KO mutant at the end of the growth experiment was unexpected, a carbon balance analysis was carried out according to Section 2.6 to assess the accuracy of metabolite, headspace and biomass readings. The % carbon recovery for all serum bottle cultures from this experiment ranged between 104% and 112%, which is in the typical error range. One explanation for the additional CO is the potent inhibitory effect of CO on hydrogenase (90, 318) at the beginning of the growth experiment, which prevented excess electrons from being evolved into H_2. While growing on fructose alone (Figure 4.6), no CO but 0.6 mmol H_2 was produced in the *acsA* ClosTron mutant.

Although the *acsA* KO mutant and the WT cultures reached very similar OD_{600} at t = 268 h (Figure 4.7C) in fructose + CO, it was observed that growth of the *acsA* KO mutant initiated noticeably earlier than the WT (data not shown). This indicates the presence of carbon catabolite repression (CCR) when both CO and fructose were provided, and the inactivation of *acsA* (hence a disconnected WLP) overcame this inhibitory effect. CCR has been reported when *C. aceticum* is grown on CO_2 + H_2 in the presence of sugars (319), and when *E. limosum* grows on glucose and methanol (utilized through the WLP like other one carbon substrates) (320). As observed previously in fructose only growth experiments (Figure 4.6B & C), the *acsA* KO mutant did not produce acetate but synthesized more ethanol under fructose + CO conditions (Figure 4.7D). However, under mixotrophic conditions the *acsA* KO mutant produced less 2,3-butanediol and lactate than the WT (Figure 4.7D).

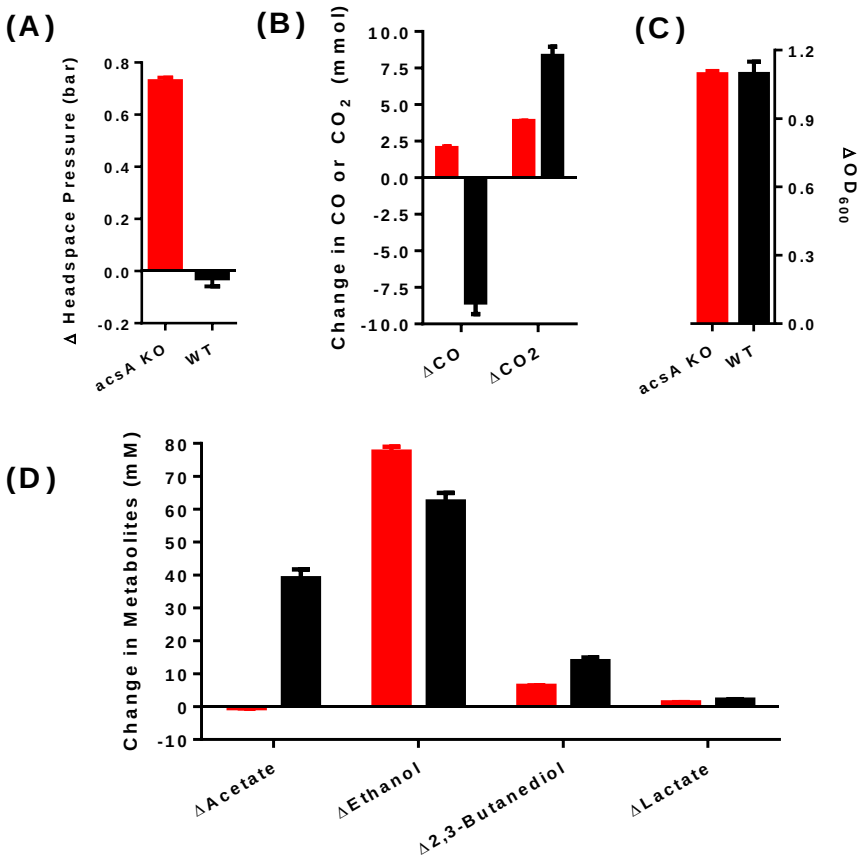


Figure 4.7. The change in biomass, headspace and metabolite levels between start and finish of mixotrophic growth experiment of *acsA* ClosTron mutant and WT on 10 g/L fructose and 2 bar CO. (A) Change in headspace pressure; (B) Change in headspace CO or CO_2; (C) Change in growth based on OD_{600}; and (D) Change in metabolites. Red columns = *acsA* KO mutant; Black columns = WT. N = 3. Error bars = standard error of mean.

4.3.5 Mixotrophic Growth Experiments in Carbon Monoxide and Acetic Acid

Some chemotrophic anaerobes are able to oxidize acetate into CO_2 by essentially running the WLP in reverse (Figure 4.8A) (78, 321, 322). For instance, cell extracts of *Desulfotomaculum acetoxidans* displayed high enzymatic activities of Ack, Pta, CODH, FDH, methylene-THF reductase, methylene-THF dehydrogenase, methenyl-THF cyclohydrolase and formyl-THF synthetase in the oxidative direction of WLP (323). In this project, a mixotrophic growth experiments using acetate and CO as substrate were conducted to determine if *C. autoethanogenum* can carry out reverse WLP and also to investigate the roles of CODH1 and CODH2 in the context of an *acsA* KO

background. Each serum bottle was pressurized with 2 bar CO and contained 50 mL CGMY medium with and without 10 g/L (166.5 mM) acetate (final concentration) supplementation. Three or four technical repeats were included for each group and the serum bottle cultures were incubated at 37°C with agitation for as long as 52 days.

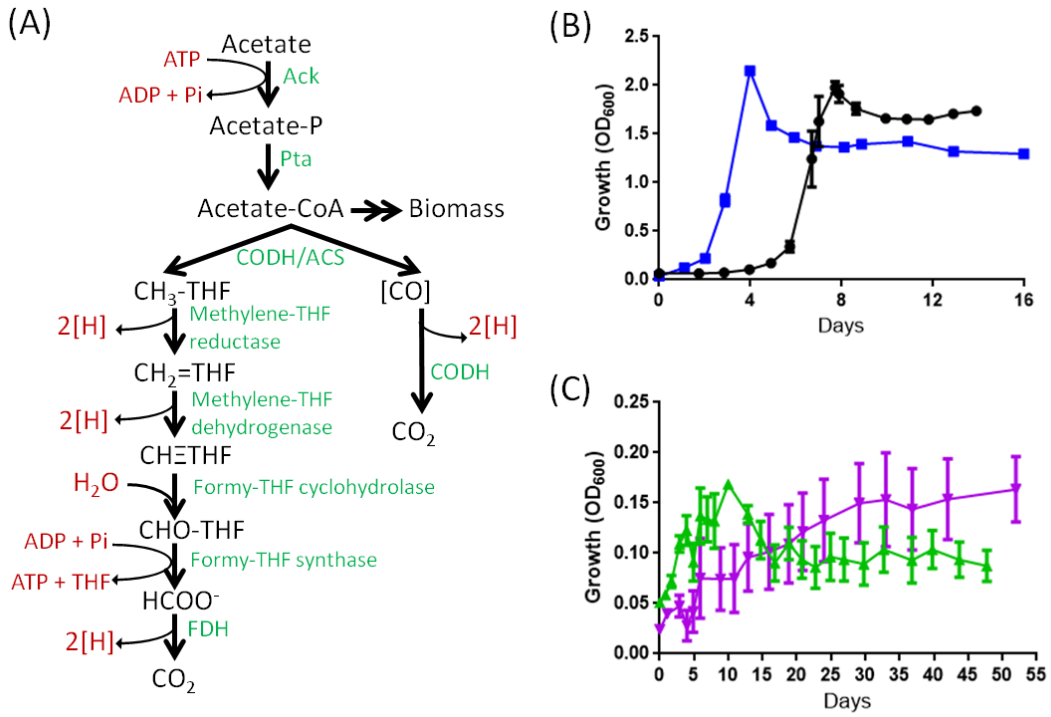


Figure 4.8. Reverse Wood-Ljungdahl Pathway (WLP) and mixotrophic growth of *acsA* ClosTron mutant. (A) Schematics for acetate oxidation via reverse WLP; (B) Mixotrophic growth profiles of the WT on CO + acetate; and (C) Mixotrophic growth profiles of the *acsA* ClosTron mutant on CO + acetate. Ack, acetate kinase; ACS, acetyl-CoA synthase; CODH, carbon monoxide dehydrogenase; FDH, formate dehydrogenase; THF = tetrahydrofolate; Black circles = WT in CO alone (N = 4); Blue squares = WT in CO + acetate (N = 3); Green triangles = *acsA* mutant in CO alone (N = 3); Purple inverted triangles = *acsA* mutant in CO + acetate (N = 3). Error bars = standard error of mean.

There was concern that 166.5 mM of acetate combined with the low pH may be inhibitory or toxic to *C. autoethanogenum*, but Figure 4.8B shows that acetate exerts a positive effect on WT autotrophic growth by reducing the growth lag phase by 3

days when compared to growth on CO alone. Instead of consuming acetate, *C. autoethanogenum* produced an additional 104 mM of acetate on day 6 (data not shown). After 48 days of incubation, the *acsA* KO mutant displayed negligible growth in either CO or CO + acetate condition (Figure 4.8C). Collectively these data showed that acetate oxidation via reverse WLP was not observed in either *C. autoethanogenum* WT cells or the *acsA* KO mutant under these conditions.

4.4 Plasmid Overexpression of *acsA*

4.4.1 Construction of *acsA* Plasmid Overexpression Strain

Plasmid control pMTL83157 and overexpression plasmid pMTL83157-*acsA*^{full} were constructed as described in section 4.3.2. Following conjugation into *C. autoethanogenum*, plasmids were rescued from Tm^{R} transconjugants followed by restriction digest analysis to check the identity of the strains. As shown in Figure 4.9A & B, both pMTL83157 transconjugants and pMTL83157-*acsA*^{full} transconjugants produced the expected fragments from *Pme*I + *Fse*I and *Nde*I + *Sac*I restriction digest, respectively.

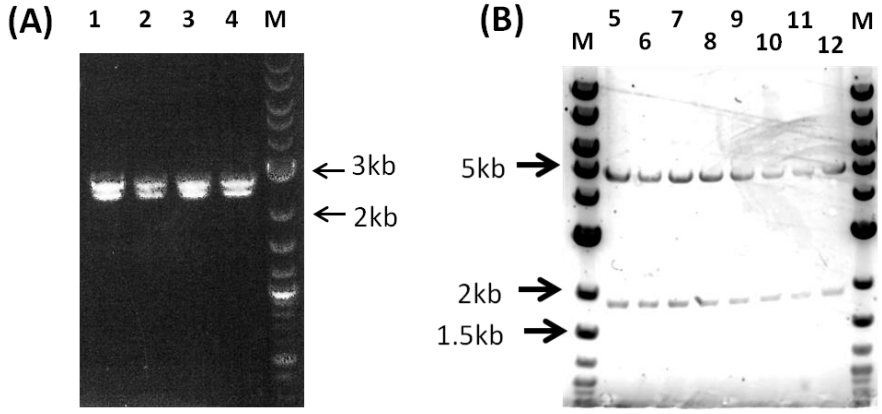


Figure 4.9. Restriction digest analysis of rescued plasmids pMTL83157 and pMTL83157-*acsA*^{full} from *C. autoethanogenum*. (A) Gel electrophoresis of *Pme*I and *Fse*I restriction digested plasmids rescued from *C. autoethanogenum* pMTL83157 transconjugants (lanes 1 – 4). The expected bands are 2600 bp and 2424 bp in length. (B) Gel electrophoresis of *Nde*I and *Sac*I restriction digested plasmids rescued from *C. autoethanogenum* pMTL83157-*acsA*^{full} transconjugants (lanes 5 – 12). The expected bands are 4995 bp and 1932 bp long. M = NEB 2-log DNA ladder.

4.4.2 Autotrophic Growth Experiments in Carbon Monoxide

To test whether overexpression of *acsA* has any positive impact on autotrophic growth of *C. autoethanogenum*, both plasmid control strain pMTL83157 (N = 4) and *acsA* overexpression strain pMTL83157-*acsA*^{full} (N = 3) were subjected to serum bottle growth experiments in the presence of 2 bar CO. Each 250 mL serum bottle contained 50 mL CGMY medium supplemented with 7.5 µg/mL thiamphenicol. As shown in Figure 4.10A, the overexpression of *acsA* did not promote higher cell densities but reduced the lag phase of growth by 4.2 days when compared to the plasmid-only control strain. In terms of metabolite production, very similar titres were achieved for acetate (Figure 4.10B) but the *acsA* overexpression strain appeared to produce 21% more ethanol than the plasmid-only control strain (24.5 mM vs 20.3 mM; not statistically significant) (Figure 4.10C). The *acsA* overexpression strain generated 29% less 2,3-butanediol than the plasmid-only control strain (p-value = 0.067) (Figure 4.10D).

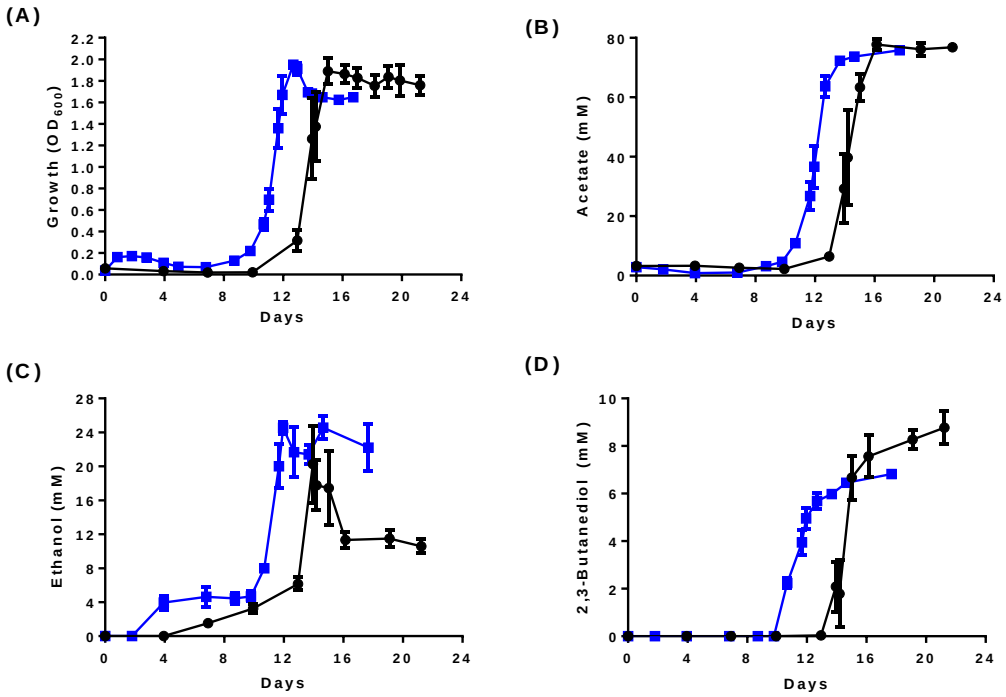


Figure 4.10. The effect of *acsA* overexpression on growth and metabolite profiles of *C. autoethanogenum* on 2 bar CO. (A) Growth profile; (B) Acetate profile; (C) Ethanol profile; (D) 2,3-Butanediol profile. Blue squares = pMTL83157-*acsA*^{full} (N = 3); Black circles = plasmid control pMTL83157 (N = 4). Error bars = standard error of mean.

4.4.3 Heterotrophic Growth Experiments

Both the *acsA* overexpression strain and the control strain carrying the empty pMTL83157 vector were subjected to heterotrophic growth experiments to assess the impact of *acsA* overexpression during fructose metabolism. The experiment was conducted in 250 mL serum bottles containing 50 mL CGMY medium supplemented with 10 g/L fructose and incubated at 37°C for up to 8.1 days. A maximum OD_{600} achieved by the *acsA* overexpression strain was increased by 24% when compared to the control strain carrying the pMTL83157 vector alone (p-value = 0.011) (Figure 4.11A). However, there was little difference in the production of acetate or ethanol between the two strains (Figure 4.11B & C).

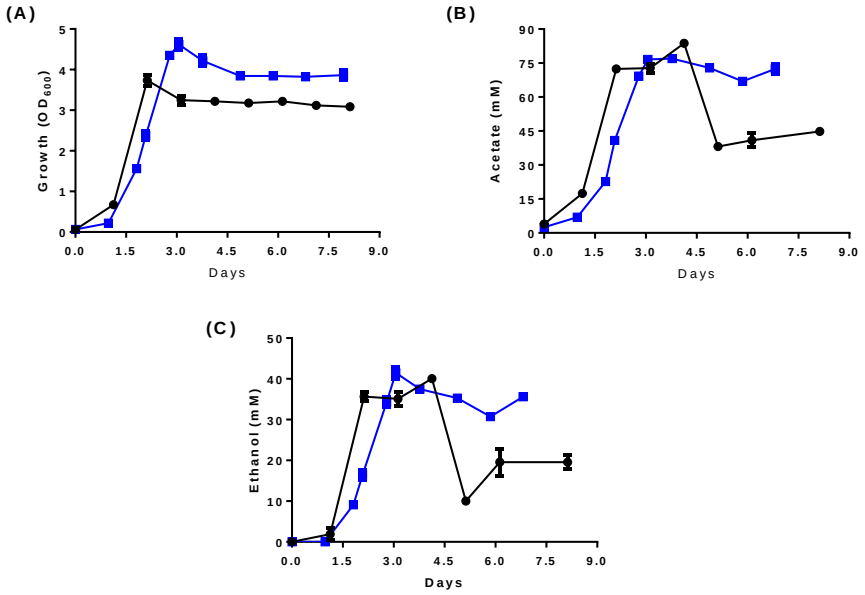


Figure 4.11. The effect of *acsA* overexpression on growth and metabolite profiles of *C. autoethanogenum* on 10 g/L fructose. (A) Growth profile; (B) Acetate profile; (C) Ethanol profile. Blue squares = pMTL83157-*acsA*^{full} (N = 3); Black circles = plasmid control pMTL83157 (N = 3). Error bars = standard error of mean.

4.5 Investigation of *C. autoethanogenum acsA* Translational Read-Through

Genome sequencing of *C. autoethanogenum* using NGS and Single-Cell sequencing (38) revealed the presence of an internal 'TGA' stop codon within the *acsA* gene of *C. autoethanogenum*, splitting the gene into two CDS: CAETHG_1621 (1203 bp) and CAETHG_1620 (684 bp) (Figure 4.12A & B). To be certain this is not an error/artefact, the gene was amplified using oligonucleotides 'acsA-seq-F' and 'acsA-seq-R' followed

by Sanger sequencing using these two primers and oligonucleotide 'acsA-seq1'. Three independent amplifications and Sanger sequencings confirmed the presence of a 'TGA' stop codon, but otherwise agreed with the genome sequence reported by Brown *et al.* (2014) (38) (data not shown).

Interestingly, the *acsA* of three other clostridial acetogens, *C. ljungdahlii*, *C. ragsdalei*, *C. carboxidivorans* P7, and of *C. difficile* 630 showed no such gene splitting event (Figure 4.12A). Instead, a 'TCA' serine codon is present at the same locus in these acetogens. The *acsA* (CAETHG_1621-1620) of *C. autoethanogenum* shared 95% nucleotide identity with *C. ljungdahlii*, 90% nucleotide identity with *C. ragsdalei*, 78% nucleotide identity with *C. carboxidivorans* and 67% nucleotide identity with *C. difficile* 630. Beyond clostridial acetogens, the nucleotide sequences of *acsA* in *M. thermoacetica*, *A. woodii* and *E. limosum* share 49%, 64% and 62% sequence identity to that of *C. autoethanogenum*, respectively. Again, no internal stop codon is detected in *acsA* of these acetogens despite being similar in length (1896 – 2025 bp) to *C. autoethanogenum* (1896 bp).

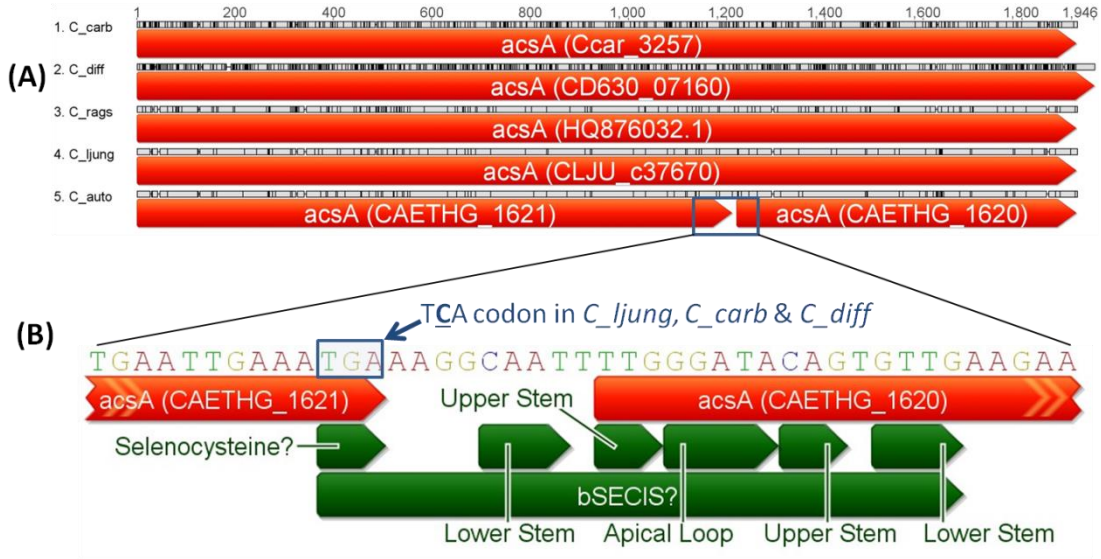


Figure 4.12. Nucleotide alignment of *acsA* and internal stop codon in *C. autoethanogenum.* (A) Nucleotide alignment of the *acsA* CDS between *C. autoethanogenum* (C_auto), *C. ljungdahlii* (C_ljung), *C. carboxidivorans* P7 (C_carb) and *C. difficile* 630 (C_diff). Variations are marked in black or as gaps in the gray sequence bar above the red annotations. (B) Inset of (A) highlighting internal 'TGA' stop codon and putative bacterial selenocysteine insertion sequence (bSECIS) in *acsA* of *C. autoethanogenum*. Figure is generated using Geneious 6.1.7 (Biomatters Ltd).

Given the empirical role of *acsA* in acetogenesis, the truncation of this gene is hypothesized to affect the WLP of *C. autoethanogenum*. It was, therefore, of interest to determine whether the gene is translated into two peptides, or whether there may be some post-transcriptional mechanisms that allow translational read-through beyond the internal stop codon. One such mechanism is the incorporation of selenocysteine at the 'TGA' codon which is generally reliant on a characteristic bacterial selenocysteine insertion sequence (bSECIS) immediately downstream of the stop codon. An algorithm developed by Zhang and Gladyshev (2005) (324), which is reported to have a 96.5% success rate in calling such a motif, failed to detect a bSECIS candidate in the *C. autoethanogenum acsA* gene. However, manual examination of the region immediately following the 'TGA' codon uncovered a putative bSECIS motif, including lower stem, apical loop and upper stem for the formation of a stem loop structure (Figure 4.12B).

4.5.1 Construction of FLAG-tagged *acsA* Variants

To examine the translation pattern of *C. autoethanogenum acsA*, the gene was fused to a FLAG tag sequence (encoding the amino acid DYKDDDDK) at either the N- or C-terminus, and then cloned to generate four *acsA* plasmids. The first plasmid 'pMTL83151-P_{acsA}-FLAG-acsA(TGA)' has an N-terminal FLAG-tagged *acsA* gene. It was constructed by the initial PCR amplification of the native *acsA* using oligonucleotides ''NcoI-acsA-F' and 'acsA-HindIII-R' and the cloning of the fragment into plasmid pMTL83151 using the restriction sites *Nco*I and *Hind*III. This was followed by the PCR amplification of a DNA fragment encompassing the native P_{acsA} promoter using primers 'P_{acsA}-SacI-F' and 'P_{acsA}-NcoI-R' and its cloning between the *Sac*I and *Nco*I sites of plasmid pMTL83151. The second plasmid, 'pMTL83151-P_{acsA}-acsA(TGA)-FLAG', was generated by amplification of native *acsA* and its promoter using oligonucleotides 'P_{acsA}-SacI-F' and 'acsA-FLAG-BamHI-R' and cloned into plasmid pMTL83151 using restriction sites *Sac*I and *Bam*HI.

The third plasmid 'pMTL83151-P_{acsA}-acsA(TCA)-FLAG' has the internal 'TGA' stop codon of *C. autoethanogenum acsA* mutated to a 'TCA' serine codon, to mimic the

acsA genes found in other clostridial acetogens. To assemble this plasmid, SOE-PCR was performed using oligonucleotides 'P_{acsA}-SacI-F', 'acsA(TCA)-SOE-B', 'acsA(TCA)-SOE-C' and 'acsA-FLAG-BamHI-R' and then cloned into plasmid pMTL83151 using restriction sites *Sac*I and *Bam*HI. Similarly, the fourth plasmid 'pMTL83151-P_{acsA}-acsA(TAA)-FLAG' consists of an *acsA* variant that has the internal 'TGA' codon mutated to another stop codon, 'TAA'. This plasmid was constructed by first SOE-PCR using primers 'P_{acsA}-SacI-F', 'acsA(TAA)-SOE-B', 'acsA(TAA)-SOE-C' and 'acsA-FLAG-BamHI-R' and then cloned into plasmid pMTL83151 using restriction sites *Sac*I and *Bam*HI. The cloned promoter and *acsA* CDS in all the above plasmids were verified by Sanger sequencing (data not shown).

4.5.2 Expression of FLAG-Tagged AcsA Variants

The FLAG-tagged *acsA* plasmids and plasmid control pMTL83157 were conjugated into *C. autoethanogenum* to investigate the sizes of the proteins produced from the different *acsA* variants. In addition, these plasmids were also transformed into *C. acetobutylicum* ATCC 824 and *E. coli* strain XL1-Blue according to sections 2.12.2 and 2.5.8, respectively, to determine if there is any organism-specific effect on the translation of *C. autoethanogenum acsA*. Restriction digest analysis (*Sac*I and *Bam*HI) of rescued plasmids from both the *C. autoethanogenum* transconjugants and *C. acetobutylicum* transformants showed the predicted restriction patterns (Figure 4.13A & B) indicating that no gross rearrangements of the plasmids had occurred.

C. acetobutylicum was selected as a host to investigate the expression of *acsA* because this *Clostridium* is not known to harbour selenoproteins and its genome is devoid of genes for selenocysteine synthesis and insertion, such as *selA* (encodes selenocysteine synthase) and *selB* (encodes selenocysteine-specific elongation factor) (287, 324). In contrast, *E. coli* has been one of the model organisms for the elucidation of selenocysteine biosynthesis and incorporation (325-327), and should, therefore, be able to incorporate selenocysteine at the TGA codon of *C. autoethanogenum acsA* if it is able to recognize the putative bSECIS signal.

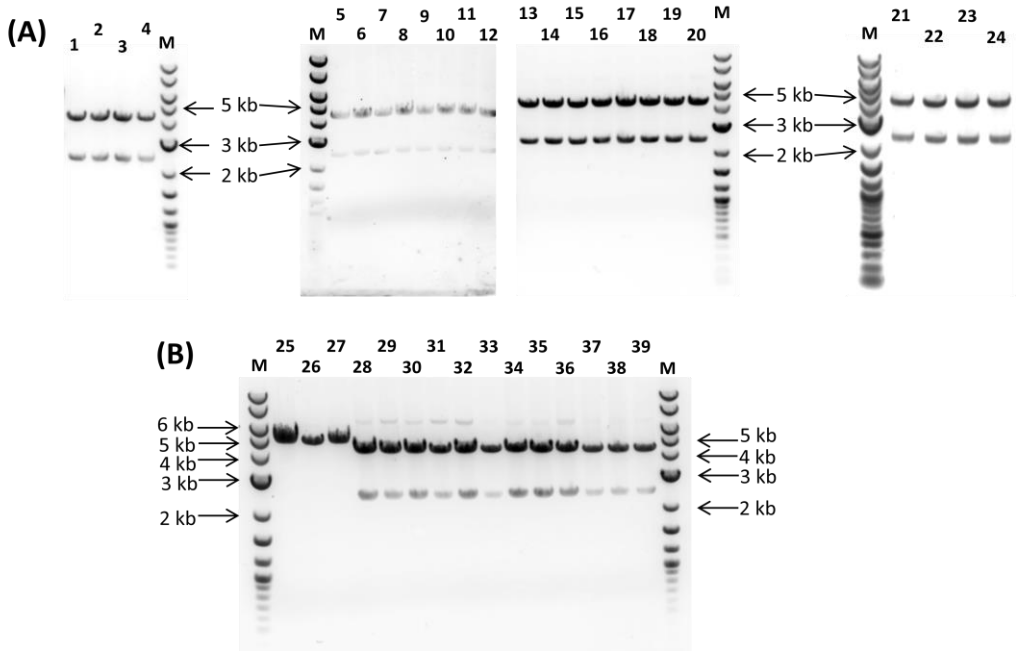


Figure 4.13. Restriction digest (*Sac*I and *Bam*HI) analysis of rescued *acsA* plasmids from (A) *C. autoethanogenum* transconjugants; 1 – 4 = pMTL83151-P_{acsA}-FLAG-acsA(TGA) clones (expect 2.5 kb + 4.4 kb fragments); 5 – 12 = pMTL83151-P_{acsA}-acsA(TGA)-FLAG clones (expect 2.5 kb + 4.4 kb fragments); 13 – 20 = pMTL83151-P_{acsA}-FLAG-acsA(TCA) clones (expect 2.5 kb + 4.4 kb fragments); 21 – 24 = pMTL83151-P_{acsA}-FLAG-acsA(TAA) clones (expect 2.5 kb + 4.4 kb fragments). (B) *C. acetobutylicum* transformants. 25 – 27 = pMTL83157 clones (expect 5.0 kb); 28 – 35 = pMTL83151-P_{acsA}-acsA(TGA)-FLAG clones (expect 2.5 kb + 4.4 kb fragments); 36 – 39 = pMTL83151-P_{acsA}-acsA(TCA)-FLAG clones (expect 2.5 kb + 4.4 kb fragments); M = NEB 2-log DNA ladder.

Verified *C. autoethanogenum*, *C. acetobutylicum* and *E. coli* transformants were cultivated in 50 mL Falcon tubes kept inside the anaerobic workstation and crude lysates were prepared according to section 2.10. It is noteworthy that *E. coli* was cultivated under conditions that were conducive to selenoprotein expression, including supplementation of 10 µM Na_2SeO_3 and a strict anoxic environment (326). Crude lysates were loaded onto a SDS-PAGE gel and Western Blot analysis was performed using anti-FLAG antibody according to section 2.11.

If a translational read-through mechanism exists in *acsA*, the gene is expected to produce a 69 kDa protein (Figure 4.14B). Depending on the orientation of the FLAG-tag, a truncation event in *acsA* should generate a 44 kDa peptide and/or 25 kDa peptide (Figure 4.14B). In Figure 4.14A lanes 1 to 4, equal amounts (13 µg) of soluble

crude lysates of *C. autoethanogenum* were loaded into each well of the SDS-PAGE gel. A ~70 kDa band was detected in all soluble and insoluble crude lysates of *C. autoethanogenum*, which is likely to be non-specific binding of the anti-FLAG antibody to a native protein of *C. autoethanogenum*. This phenomenon was previously observed by other members of our research group and one prime candidate for this native protein is DnaK (encoded by CAETHG_2891), which shares 7/8 amino acid identity with FLAG and its size is consistent with the observed 70 kDa band (Dr. Chris Humphrey and Dr. Samantha Mclean, University of Nottingham). In addition, another non-specific band of ~37 kDa was also detected in all *C. autoethanogenum* crude lysates (Figure 4.14A) but the identity of this protein is unknown.

Below the 70 kDa non-specific band is the expected protein size of the mature translational read-through AcsA product (~69 kDa), which was detected in the crude lysates of *C. autoethanogenum* cells carrying plasmids pMTL83151-P_{acsA}-acsA(TGA)-FLAG, pMTL83151-P_{acsA}-acsA(TCA)-FLAG and pMTL83151-P_{acsA}-FLAG-acsA(TGA) (Figure 4.14A, lanes 2, 3 and 6, respectively). In contrast, such a 69 kDa band was absent in the lysates of cells carrying the plasmid control pMTL83157 and plasmid pMTL83151-P_{acsA}-acsA(TAA)-FLAG in which the internal TGA stop has been changed to a TAA stop codon (Figure 4.14A, lanes 1 and 4, respectively). Furthermore, the ~69 kDa band intensity in lysates of cells carrying pMTL83151-P_{acsA}-acsA(TCA)-FLAG is substantially stronger than cells carrying pMTL83151-P_{acsA}-acsA(TGA)-FLAG (Figure 4.14A, lanes 2 and 3, respectively) when the loaded amounts of both samples were normalized. This suggests that that the translational read-through of AcsA in the internal 'TGA' stop codon is not as efficient as the 'TCA' serine codon, based on the considerable difference in the signal intensity of the ~69 kDa band.

In *C. autoethanogenum* crude lysates carrying a plasmid encoding a C-terminal FLAG-tagged *acsA* gene containing the native 'TGA' stop codon (Figure 4.14A, lane 2), no 25 kDa sized protein was detected, indicating that there is no independent translation of the downstream CDS of *acsA* (CAETHG_1620). This is supported by the apparent lack of a ribosomal binding site (RBS) for CAETHG_1620 translation (Figure 4.12B). When the native *acsA* gene is N-terminally FLAG-tagged, two products are

possible (Figure 4.14A, lane 6): a truncated ~44 kDa product and/or a full sized ~69 kDa product. Indeed, both a ~44 kDa band and a ~69 kDa band were detected in the insoluble fraction, but the intensity of the former band is noticeably stronger than the latter band (Figure 4.14A, lane 6). Both the ~44 kDa and ~69 kDa bands were absent in the plasmid control insoluble fraction. These results suggest that while there is some translational read-through of *acsA* of *C. autoethanogenum*, the predominant product is the truncated ~44 kDa fragment, which may have huge implications on acetogenesis of the acetogen.

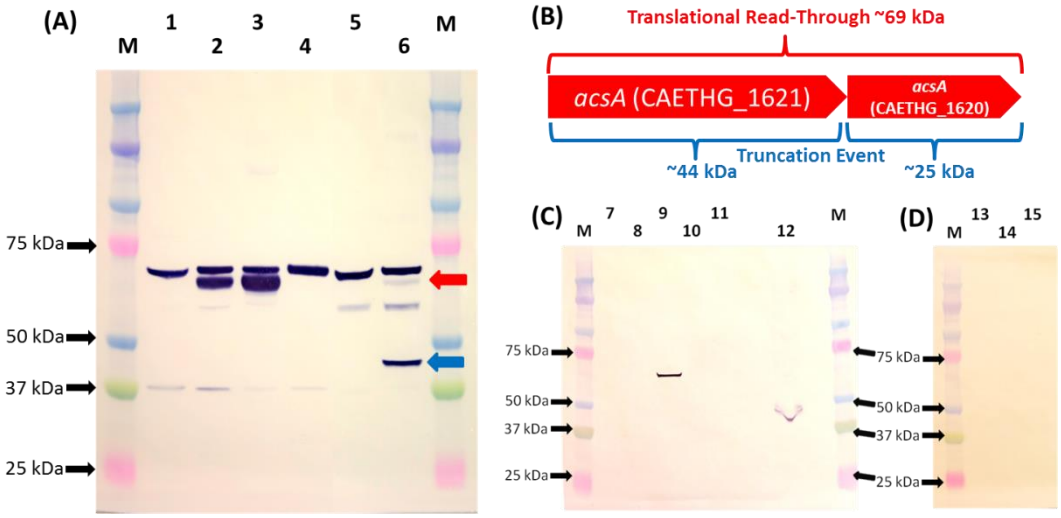


Figure 4.14. Examination of AcsA translation pattern using FLAG-tagged protein in *C. autoethanogenum*, *C. acetobutylicum*, and *E. coli*. (A) Western Blot analysis of *C. autoethanogenum* transconjugant crude lysates. 1 = 13 µg soluble lysate of pMTL83157 plasmid control; 2 = 13 µg soluble lysate of pMTL83151-P_{acsA}-acsA(TGA)-FLAG; 3 = 13 µg soluble lysate of pMTL83151-P_{acsA}-acsA(TCA)-FLAG; 4 = 13 µg soluble lysate of pMTL83151-P_{acsA}-acsA(TAA)-FLAG; 5 = 6.7 µg insoluble lysate of pMTL83157 plasmid control; 6 = 6.7 µg insoluble lysate of pMTL83151-P_{acsA}-FLAG-acsA(TGA); Red arrow indicates the position of a mature 69 kDa protein; Blue arrow indicates the position of the larger 44 kDa truncated protein; (B) Schematic showing the expected protein sizes of *C. autoethanogenum* AcsA in the event of translational read-through or truncation; (C) Western Blot analysis of *E. coli* transformant crude lysates. 7 = 15 µg soluble lysate of pMTL83157 plasmid control; 8 = 15 µg soluble lysate of pMTL83151-P_{acsA}-acsA(TGA)-FLAG; 9 = 15 µg soluble lysate of pMTL83151-P_{acsA}-acsA(TCA)-FLAG; 10 = 15 µg soluble lysate of pMTL83151-P_{acsA}-acsA(TAA)-FLAG; 11 = 39 µg soluble lysate of pMTL83151-P_{acsA}-FLAG-acsA(TGA); 12 = 38 µg insoluble lysate of pMTL83151-P_{acsA}-FLAG-acsA(TGA); (D) Western Blot analysis of *C. acetobutylicum* transformant crude lysate; 13 = 21 µg soluble lysate of pMTL83157; 14 = 21 µg soluble lysate of pMTL83151-P_{acsA}-acsA(TGA)-FLAG; 15 = 21 µg soluble lysate of pMTL83151-P_{acsA}-acsA(TCA)-FLAG. M = BioRad Kaleidoscope Precision Plus protein ladder.

In *E. coli* crude lysates of cells carrying plasmid pMTL83151-P_{acsA}-acsA(TGA)-FLAG, no ~69 kDa mature protein or ~25 kDa truncated protein was detected (Figure 4.14C, lane 8). However, a band corresponding to the ~69 kDa protein was detected in lysates of cells carrying the positive control plasmid pMTL83151-P_{acsA}-acsA(TCA)-FLAG (Figure 4.14C, lane 9), which contains the serine 'TCA' codon and a C-terminal FLAG-tag. These results showed that the *acsA* promoter of *C. autoethanogenum* is active in *E. coli* under the conditions tested, and unlike *C. autoethanogenum*, *E. coli* is unable to overcome the internal 'TGA' stop codon and synthesize the full length ~69 kDa AcsA product. As expected, the introduction of an alternative 'TAA' stop codon in place of the 'TGA' triplet successfully prevented the formation of the ~69 kDa protein (Figure 4.14C, lane 10). In *E. coli* expressing N-terminal FLAG-tagged *acsA* with the native 'TGA' stop codon, only the truncated acsA ~44 kDa band was detected (Figure 4.14C, lane 12), which again shows that *E. coli* is capable of synthesizing the truncated ~44 kDa band but unable to overcome the internal 'TGA' stop codon.

Given the ability of *E. coli* to recognize the *acsA* promoter P_{acsA} from *C. autoethanogenum* and produce AcsA protein, it is surprising that no signal was detected in all of the crude extracts of *C. acetobutylicum* (Figure 4.14D). In the *C. acetobutylicum* positive control crude extract that supposedly expressed C-terminal FLAG-tag *acsA* with 'TCA' serine codon, no ~69 kDa product was detected (Figure 4.14D, lane 15). This absence of signal is not due to an error in the Western Blot procedure because protein signals were detected in other lanes of the same SDS-PAGE (data not shown). Furthermore, the preparation of *C. acetobutylicum* crude extracts was carried out in the same batch as other bacterial hosts that generated signals. All these observations indicate that the P_{acsA} promoter of *C. autoethanogenum* is not functional in *C. acetobutylicum*.

4.6 Characterization of *cooS1* and *cooS2* ClosTron Mutants

4.6.1 Autotrophic Growth Experiments

To determine whether inactivation of either mono-functional CODH1 or CODH2 negatively affect autotrophy, *C. autoethanogenum* ClosTron mutants of *cooS1* and *cooS2* were cultivated in either 2 bar CO or 1.3 bar H_2 + 0.7 bar CO_2. Growth was conducted in 250 mL serum bottles containing 50 mL CGMY medium with 3-4 technical repeats.

When growing on CO alone, the *cooS1* mutant displayed some growth deficiencies, including ~2.9 day longer lag phase and achieved a 42% lower OD_{600} (p-value = 0.0002) than the WT (Figure 4.15A). It produced 25% less acetate (p-value = 0.0004), a similar amount of 2,3-butanediol but 64% more ethanol (not statistically significant) than the WT (Figure 4.15B - D). Unlike the *cooS1* mutant, the *cooS2* mutant started growing ~1.9 days earlier but achieved an OD_{600} that was 31% lower than the WT (p-value = 0.009) under pure CO conditions (Figure 4.15A). The *cooS2* mutant generated 13% less acetate (p-value = 0.002) but a similar amount of ethanol and 2,3-butanediol as the WT (Figure 4.15B - D).

A similar pattern was also observed when the *cooS1* mutant and the WT were grown in BOF gas (composition: 51.24% CO, 31.22% N_2, 11.98% CO_2, and 3.05% H_2) harvested from Glenbrook steel mill, New Zealand. These growth experiments were conducted in triplicate 250 mL serum bottles containing 100 mL CGMY medium and pressurized to 2 bar with BOF gas. In terms of growth in mill gas, the *cooS1* mutant did not experience longer growth lag phase but achieved 17% less OD_{600} than WT (Figure 4.16A). Furthermore, the *cooS1* mutant also produced 113% more ethanol (p-value = 0.0005) but 18% less acetate than the WT (p-value = 0.005) (Figure 4.16B & C).

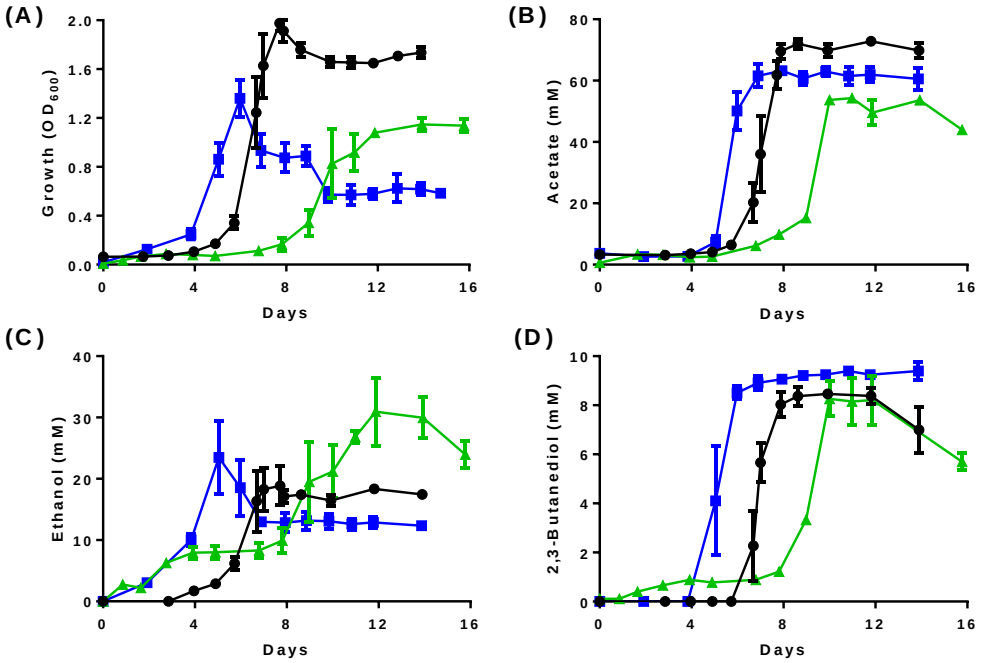


Figure 4.15. Growth and metabolite profiles of *C. autoethanogenum* WT, and ClosTron *cooS1* and *cooS2* mutants on 2 bar CO. (A) Growth profile; (B) Acetate profile; (C) Ethanol profile; and (D) 2,3-butanediol profile. Black squares = WT (N = 4); Green triangles = *cooS1* mutants (N = 3); Blue squares = *cooS2* mutants (N = 3). Error bars = standard error of mean.

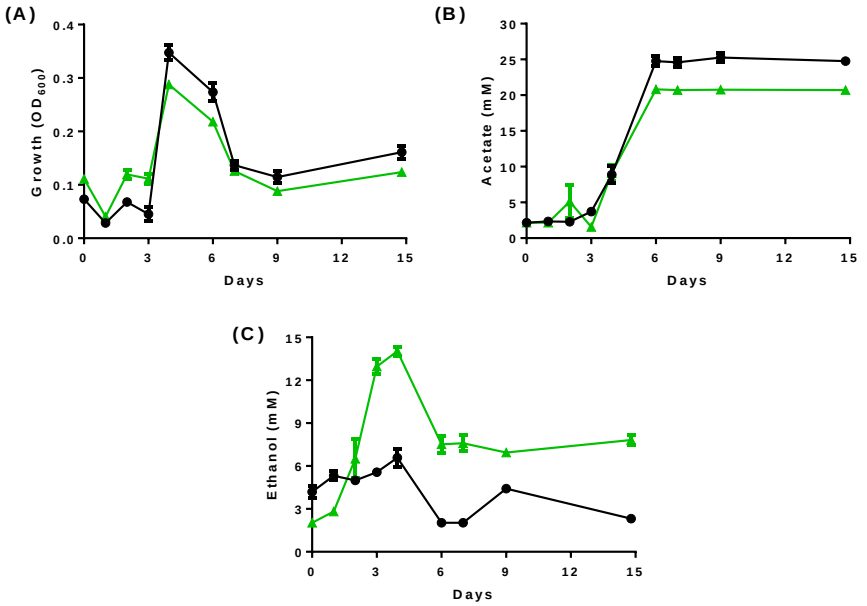


Figure 4.16. Growth and metabolite profiles of *C. autoethanogenum* WT and *cooS1* ClosTron mutant on BOF gas. (A) Growth profile; (B) Acetate profile; (C) Ethanol profile. Black circles = WT; Green triangles = *cooS1* mutant; N = 3. Error bars = standard error of mean.

Under H_2 + CO_2 conditions, the *cooS1* mutant displayed markedly improved growth compared to the WT. Growth of the latter was characterised by a ~6 day lag phase before reaching a peak OD_{600} of 0.184 after day 22.7. In contrast, the *cooS1* mutant was able to grow without an apparent lag phase and reached a peak OD_{600} of 0.40 after day 1.6 (Figure 4.17A, green triangles). To obtain more confidence that this was not an artefact, the growth experiment was repeated. On this occasion the *cooS1* mutant still showed a marked reduction in growth lag phase and grew to a peak OD_{600} of 0.324, which was 76% higher than the WT (p-value = 0.003). In the first experiment, no significant difference in metabolite production was detected between the *cooS1* mutant and the WT (Figure 4.17B & C). In the second experiment, the *cooS1* mutant generated 37% higher titre of acetate (p-value = 0.005) but 44% less ethanol (p-value = 0.037) than the WT (Figure 4.17B & C). The inactivation of *cooS2* resulted in a mutant that displayed slightly faster growth than the WT and reached a peak OD_{600} of 0.20 after day 2.9 under H_2 + CO_2 conditions (Figure 4.17A). This mutant produced similar amounts of acetate and ethanol as the WT (Figure 4.17B & C).

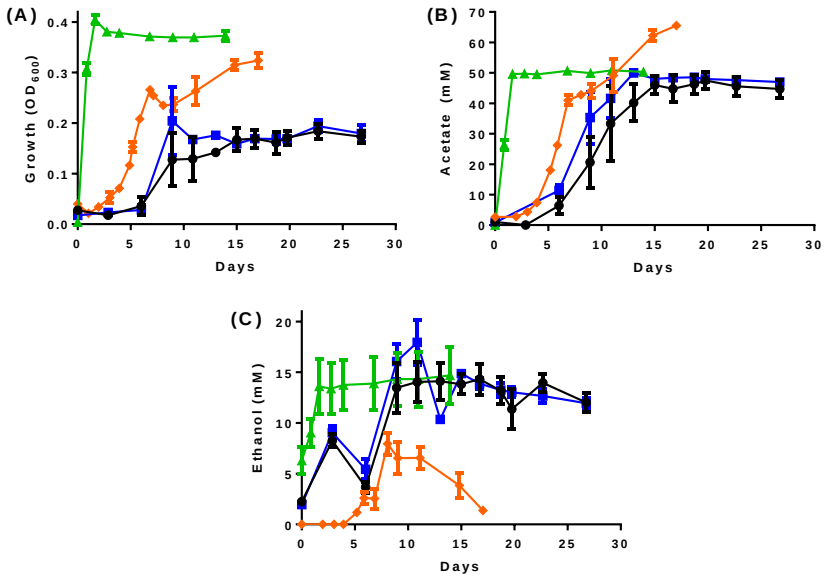


Figure 4.17. Growth and metabolite profiles of *C. autoethanogenum* WT and ClosTron *cooS1* and *cooS2* mutants under H_2 + CO_2 conditions. (A) Growth profile; (B) Acetate profile; (C) Ethanol profile. Black Circles = WT; Green triangles = *cooS1* mutant (experiment 1); Orange diamonds = *cooS1* mutant (experiment 2); Blue squares = *cooS2* mutant. N = 3. Error bars = standard error of mean.

4.7 Attempt at Generation of Double Knockout Mutant of *cooS1* and *cooS2*

Since the independent inactivation of *cooS1* and *cooS2* appeared to improve growth under H_2 + CO_2 conditions (Figure 4.17A) and enhance ethanol formation when growing in the presence of CO (Figure 4.15C & Figure 4.16C), an attempt was made to create a *cooS1* and *cooS2* double knockout mutant in *C. autoethanogenum*. The creation of such a double KO mutant would in addition help determine whether *C. autoethanogenum* can grow unhindered autotrophically using AcsA alone and hence gain insight into whether AcsA is the main/only functional CODH in this acetogen.

A quick and straightforward approach to generate a double KO mutant would be to recycle the ermRAM antibiotic marker from ClosTron insertion using FLP recombinase. To date, this approach has only been demonstrated in *C. acetobutylicum* ATCC 824 (206). In this project, the same approach was employed in *C. autoethanogenum* ClosTron mutant using plasmid pCLF1 (328) but no loss of clarithromycin resistance was detected after a few attempts of replica plating. Hence, a strategy that involves both ClosTron and ACE was utilized to create a *cooS1* and *cooS2* double KO mutant. First, a ClosTron KO of *cooS2* was generated in the *C. autoethanogenum* Δ*pyrE* strain (section 3.3.5) using the plasmid pMTL007C-E2::cooS2-529s. Screening of clarithromycin resistant colonies using primers 'cooS2-529s-F' and 'cooS2-529s-R' generated the expected 2.2 kb intron-specific bands (Figure 4.18A), and the resultant amplicons were verified by Sanger sequencing. Southern Blot analysis also showed that only a single ClosTron insertion had occurred per mutant (Figure 4.18C) and the absence of the ClosTron plasmid was demonstrated by the loss of Tm^R (data not shown).

The second step of constructing the double KO mutant of *cooS1* and *cooS2* involved IFD of *cooS1* in the above CTermB::*cooS2*-529s Δ*pyrE* strain of *C. autoethanogenum*. The *cooS1* IFD plasmid 'pMTL84151-cooS1-IFD' was constructed by first SOE PCR of the homology arms using oligonucleotides 'cooS1-LHA-SacII-F', 'cooS1-LHA-R', 'cooS1-RHA-F' and 'cooS1-RHA-AscI-R', followed by cloning into plasmid pMTL84151-Δ*pyrE* (section 2.14.1) using restriction sites *Sac*II and *Asc*I. The cloned homology arms, verified by Sanger sequencing, were designed to completely delete *cooS1* while retaining only the start and stop codons. Following conjugation of this *cooS1*

IFD plasmid into the CTermB::*cooS2*-529s Δ*pyrE* mutant, faster growing colonies on thiamphenicol solid medium were preferentially streaked onto the same selective medium to identify single crossover mutants.

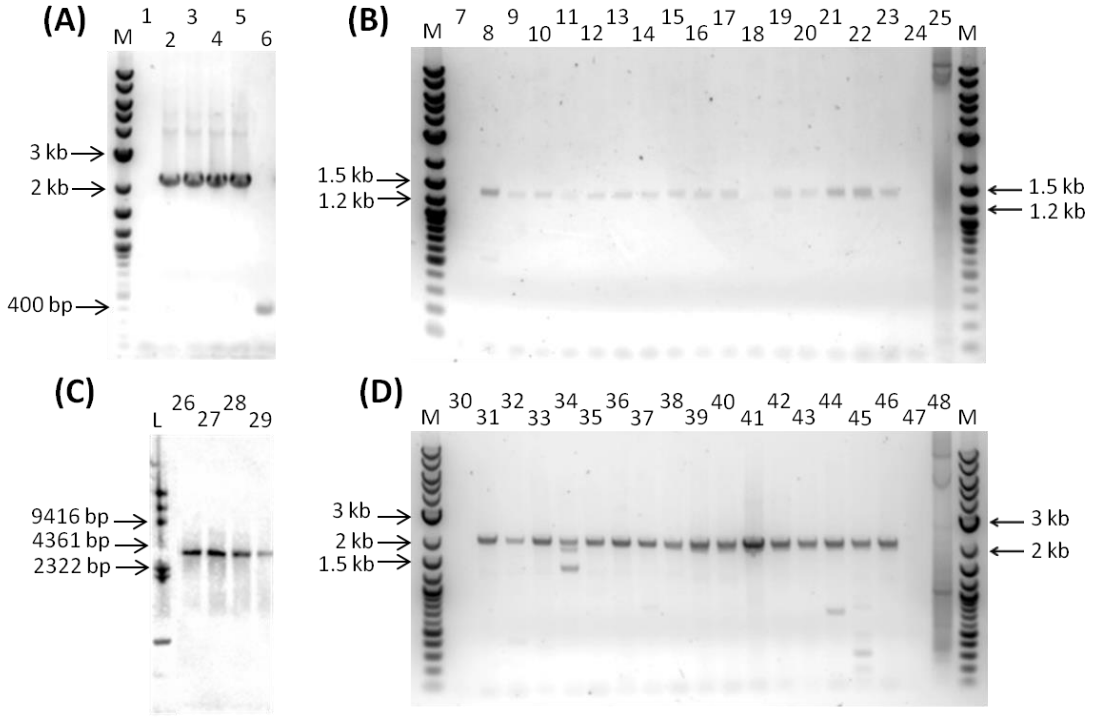


Figure 4.18. Screening of *cooS2* ClosTron mutants and *cooS1* single crossover in-frame deletion (IFD) mutants. (A) PCR screening of *cooS2* ClosTron mutants using exon-spanning primers; (B) PCR screening of *cooS1* single crossover IFD mutants at the left homology arm (LHA); (C) Southern Blot analysis of *cooS2* ClosTron mutants; and (D) PCR screening of *cooS1* single crossover IFD mutants at the right homology arm (RHA). M = NEB 2-log DNA ladder; L = Promega Lambda DNA/*Hind*III marker; 2 – 5 = *cooS2* ClosTron mutants; 8 – 23 = *cooS1* IFD single crossover mutant at LHA; 26 – 29 = *Hind*III digested genomic DNA of *cooS2* ClosTron mutants; 31 – 46 = *cooS1* IFD single crossover mutants at RHA; 1, 7 & 30 = Non-template controls; 6, 24 & 47 = *C. autoethanogenum* WT genomic DNA control; 25 & 48 = pMTL84151-cooS1-IFD plasmid control.

Since the LHA and RHA are similar in lengths (580 bp and 557 bp, respectively), single crossover should occur at either homology arm with similar frequencies. Oligonucleotides 'IFD-plasmid-F' and 'cooS1-601s-R' were used to detect single crossover at LHA while primers 'cooS1-601s-F' and 'IFD-plasmid-R' were employed for the detection of single crossover at RHA. Figure 4.18B and D showed the

expected bands of 1128 bp and 2084 bp were detected for LHA and RHA, respectively, in the screened Tm^R colonies, indicating the single crossover event had occurred at both homology arms. These bands were not detected in the NTC, WT controls and plasmid controls (Figure 4.18 B & D). Despite the lack of amplification in the controls, the presence of single crossover bands at both LHA and RHA suggests that the clones were mixed populations or non-specific amplifications that coincided with the expected amplicon sizes. Nonetheless, these putative single crossover mutants from both types of integrant were subjected to FOA selection according to section 2.14.1 to select for the second crossover event. FOA^R colonies emerged within 3 days of incubation and they were screened using oligonucleotides 'cooS1-Seq-F' and 'cooS1-Seq-R' to detect successful IFD of *cooS1*. In two independent FOA selection rounds and PCR screening of 60 colonies, none showed successful IFD of *cooS1* because the second crossover occurred at the same homology arms in 57/60 (95%) of the screened colonies (data not shown), resulting in reversion back to the WT allele of *cooS1*. No PCR product was detected in the remaining 3 screened colonies. The screening primers were carefully designed to anneal outside of the homology arms to prevent amplification of homology arms in the IFD plasmid.

4.8 Discussion

4.8.1 *acsA* is Empirical for Autotrophy in *C. autoethanogenum*

The CODH/ACS complex is encoded by five genes: *acsA* (CODH), *acsB* (ACS), *acsC* (encoding corrinoid iron-sulfur protein large subunit), *acsD* (coding for corrinoid iron-sulfur protein small subunit) and *acsE* (encoding methyltransferase subunit). These genes are often arranged in close chromosome proximity and form the Wood-Ljungdahl gene cluster as is the case in *C. autoethanogenum* (53, 73, 308). The genome of *C. autoethanogenum* encodes one *acsA*, which is uniquely split into two CDS (CAETHG_1621 and 1620) due to an internal 'TGA' stop codon. In one attempt *acsA* was knocked out using ClosTron mutagenesis so a *C. autoethanogenum* devoid of functional AcsA is viable when cultivated heterotrophically.

When the *acsA* mutant was tested autotrophically, no growth was detected in serum bottles containing 2 bar CO (48 day incubation) or 1.3 bar H_2 + 0.7 bar CO_2 (27 day incubation). In contrast, *C. autoethanogenum* WT controls were able to grow up to an OD_{600} of 1.98 in CO and an OD_{600} of 0.17 in H_2+ CO_2. While this loss of autotrophy as a result of *acsA* inactivation is not surprising, some microorganisms are able to continue to grow autotrophically when CODH/ACS is disrupted. For instance, the CODH subunit of CODH/ACS in *Methanococcus maripaludis* was inactivated via random transposon mutagenesis but the mutant was still able to grow in H_2 + CO_2 in the presence of acetate (329). Genome sequencing of this bacterium revealed only one CODH/ACS cluster (330). In *Methanosarcina acetivorans* which has two CODH/ACS isoforms, deletion studies showed that the microorganism can grow autotrophically in CO when one (but not both) of the two CODH/ACS isoforms present in this organism was deleted (302).

To provide further evidence that the loss of autotrophy in *C. autoethanogenum* is due to inactivation of *acsA*, complementation assays by plasmid expression of CAETHG_1621 (strain 'acsAKO+acsA^{trunc}') or CAETHG_1621+1620 (strain 'acsAKO+acsA^{full}') were undertaken to restore autotrophy. In CO growth experiments, both complementation strains were able to grow up to an OD_{600} 1.05 - 1.10, but the strain expressing *acsA*^{full} displayed a relatively shorter growth lag phase of ~29 days while the strain acsAKO+acsA^{trunc} exhibited an extended lag phase of ~43 days. It should be emphasized that these were only partial restorations because the plasmid control strain was able to reach an OD_{600} of 1.89 with a growth lag phase of only ~9.9 days under the same conditions. Although the complementation plasmids employ the native P_{acsA} promoter, differences in *acsA* gene dosage would have arisen due to the discrepancy between plasmid copy number and chromosomal gene number.

Besides the marked difference in growth lag phase under CO conditions between the two *acsA* complementation strains, the expression of *acsA*^{full} also restored acetate titre closer to plasmid control level than the complementation strain expressing *acsA*^{trunc}. Interestingly, both complementation strains generated 85 - 120% more ethanol than a strain carrying the plasmid only control. One possible explanation for

this phenomenon is the slow generation of biomass in complementation strains resulting in excess reducing equivalents, which were consumed in ethanol formation pathways.

The observation that expression of the upstream *acsA*^{trunc} alone is sufficient to at least partially restore autotrophy in a *acsA* KO mutant is significant because it raises questions about the role of the downstream *acsA* CDS. Although the insertional nature of ClosTron mutagenesis at the upstream *acsA* CDS means it is possible for the downstream *acsA* to still be expressed, Western Blot of *C. autoethanogenum* expressing C-terminus FLAG-tagged *acsA* provided no evidence of independent expression of the downstream *acsA* CDS (Figure 4.14A, lane 2). However, the difference in growth lag phase and product formation between the two complementation strains in CO growth experiments indicates that the downstream *acsA* CDS of *C. autoethanogenum* has a role to play in autotrophy and product synthesis.

4.8.2 Plasmid Overexpression of AcsA Reduced Growth Lag Phase in CO and Increased Biomass on Fructose

By employing qRT-PCR, *acsA* and other subunits of CODH/ACS of *C. autoethanogenum* were shown to be the most abundantly transcribed genes under autotrophic conditions (53). Furthermore, CODH/ACS was also reported to be highly expressed in *M. thermoacetica* and accounted for 2% of soluble cell protein (80). Hence, it is likely that CODH/ACS of *C. autoethanogenum* is already very highly expressed and it is not the bottleneck of the WLP. Nonetheless, given the potential benefits of enhanced carbon fixation, this project examined the effect of plasmid overexpression of *acsA*^{full} under autotrophic and heterotrophic conditions.

In the presence of 2 bar CO, the overexpression of *acsA*^{full} reduced growth lag phase by 4.2 days without affecting peak OD_{600} when compared to the plasmid control strain. Compared to the plasmid-only control, the overexpression strain generated 21% higher titres of ethanol, 29% less 2,3-butanediol but similar amounts of acetate. Under heterotrophic growth conditions, the overexpression of *acsA*^{full} allowed the

cells to achieve a 24% higher OD_{600} without significantly affecting acetate or ethanol production. While these results are not spectacular, the reduction of growth lag phase and enhancement of ethanol production by *acsA* overexpression in *C. autoethanogenum* may result in significant improvement in the economics of industrial gas fermentation.

4.8.3 KO of *acsA* Shifted Carbon and Electrons from Biomass and Acetate into the Products Ethanol and 2,3-Butanediol Under Heterotrophic Conditions

During Embden–Meyerhof–Parnas (EMP) glycolysis, one mole of hexose sugar is metabolized to 2 mol acetyl-CoA, 2 mol CO_2 (generated from PFOR reaction) and 8 electrons (Figure 4.19). Acetogens such as *C. autoethanogenum* are able to utilize the 8 electrons to reassimilate the released 2 mol CO_2 into an additional acetyl-CoA, resulting in complete carbon conversion. Recently, the ability of acetogens to perform acetogenic mixotrophy was highlighted as a novel route to improve biofuel and biochemical yields (106). Transcriptomic studies in *C. ljungdahlii* showed that gene expression of the CODH/ACS complex in the presence of fructose is down-regulated by 1.55 to 1.79-fold when compared to 80 CO: 20 CO_2 (167), and not significantly affected when compared to H_2 + CO_2 conditions (170).

In this study, the creation of a *C. autoethanogenum acsA* KO mutant provided a unique opportunity to examine the effect of a disabled WLP on a microbe that normally performs acetogenic mixotrophy. With 10 g/L fructose, the *acsA* KO mutant reached 61% lower OD_{600} and exhibited prolonged growth lag phase, while producing little or no acetate. The lack of acetate production is surprising because this pathway provides a valuable ATP via SLP from acetyl-CoA to acetate, and acetate production is one of the hallmarks of acetogens. Acetate is often viewed as an undesirable by-product during biofuel or commodity chemical production so attempts have been made in the literature to engineer strains that do not produce acetate. For instance, phosphotransacetylase and/or acetate kinase was inactivated in *C. acetobutylicum*

(239), *C. tyrobutyricum* (331), and *E. coli* (332) but acetate production was not abolished.

Without significant acetate production, most of the carbon from fructose was diverted towards reduced products ethanol and 2,3-butanediol in the *acsA* KO mutant. The inactivation of *acsA* increased peak ethanol levels by 113%, and boosted 2,3-butanediol titres by 138% when compared to the WT. This phenomenon most likely arose from the accumulation of excess reducing equivalents as a result of a disabled WLP, which generated the driving force for the electron-consuming ethanol and 2,3-butanediol biosynthetic reactions (Figure 4.19).

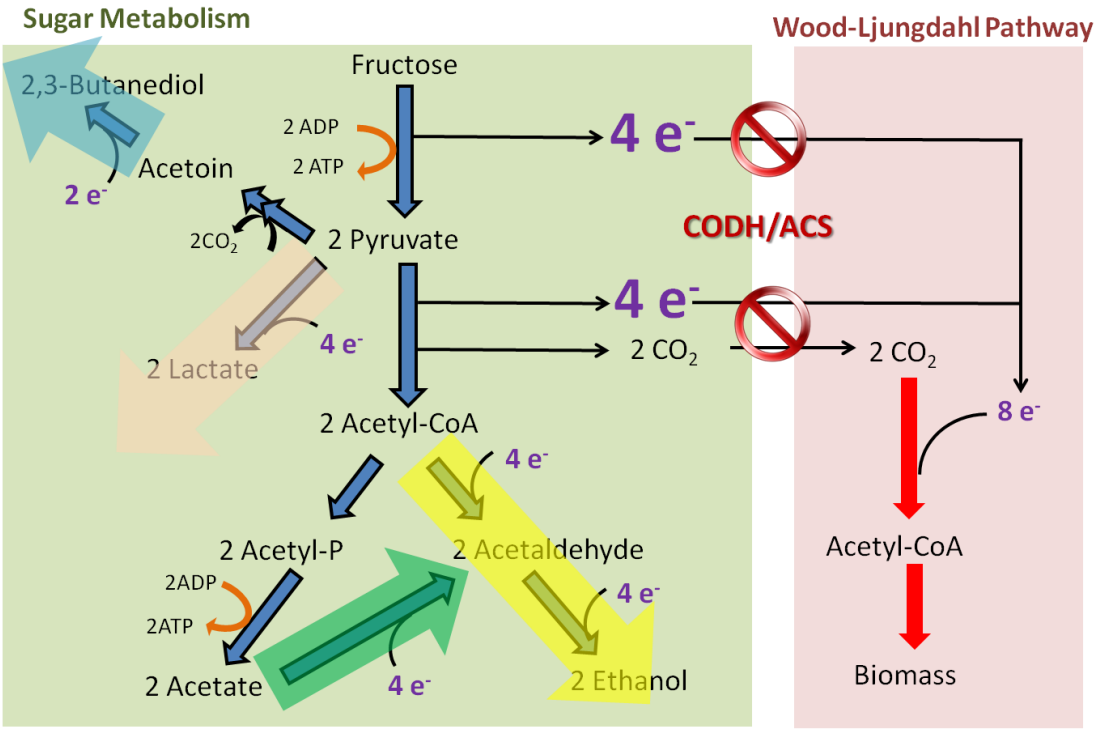


Figure 4.19. The inactivation of CODH/ACS in *C. autoethanogenum* generates excess reducing equivalents which get consumed in biochemical reactions that lead to ethanol, 2,3-butanediol and lactate formation.

During complementation assays, the plasmid expression of either *acsA*^{trunc} or *acsA*^{full} in the *acsA* KO mutant resulted in some restoration of phenotypes in the presence of 10 g/L fructose. However, the expression of *acsA*^{full} restored biomass and

metabolites to levels that better resembled the WT phenotype than the complementation strain expressing only *acsA*^{trunc}. This difference in phenotypic restoration is consistent with the autotrophic growth experiments described earlier, providing further evidence that the downstream CDS of *acsA* of *C. autoethanogenum* is not functionally redundant.

4.8.4 No Evidence of CO Oxidation by CODH1 and/or CODH2 in *acsA* KO Mutant Mixotrophic Growth Experiments

RNAseq experiments compared the transcript levels of these CODHs in *C. ljungdahlii* during early exponential growth phase and found that *cooS1* and *cooS2* were significantly down-regulated in 80 CO: 20 CO_2 conditions in comparison to growth on fructose (167). The authors predicted that the mono-functional CODHs did not significantly contribute to the oxidation of CO, but it was the CODH/ACS complex that was mostly responsible for this process. In order to gain insights into the roles of the remaining CODHs (*cooS1* and *cooS2*) in the *C. autoethanogenum acsA* KO mutant, mixotrophic growth experiments were conducted. By providing both 10 g/L of fructose and 2 bar of CO, the *acsA* KO mutant was hypothesized to grow using fructose while oxidizing CO into CO_2 if the remaining CODHs were active. Surprisingly, not only did the *acsA* mutant not consume CO it actually generated an additional 2.03 mmol CO while the WT control was able to consume 8.52 mmol CO. Based on the 2.15-fold higher amount of CO_2 produced by WT compared to *acsA* KO mutant while both strains exhausted the same amount of fructose substrate, it is deduced that the WT was able to oxidize CO to CO_2 instead of directly using CO in the carbonyl branch of the WLP. These results indicate that while the WT strain is able to oxidize CO, neither CODH1 nor CODH2 in the *acsA* mutant are able to catalyze CO oxidation. Instead, the physiological roles of these mono-functional CODHs may lie in the direction of CO_2 reduction since additional CO was produced by the *acsA* KO mutant during mixotrophic growth experiments.

To further investigate the roles of *cooS1* and/or *cooS2* in the *acsA* KO mutant, the bacterial strain was cultivated in the presence of both 10 g/L acetate and 2 bar CO.

Some sulphate-reducing bacteria (e.g., *Desulfotomaculum acetoxidans*, *Desulfobacterium autotrophic* and *Archaeoglobus fulgidus*) are able to oxidize acetate to CO_2 and H_2 via reverse WLP (321). In this study, 10 g/L acetate was found to be stimulatory rather than inhibitory to *C. autoethanogenum* in the presence of CO. Based on the lack of acetate consumption in the WT, and the absence of growth of the *acsA* KO mutant in acetate + CO growth experiments, there is no evidence that *C. autoethanogenum* is able to carry out reverse WLP. Consequently, the role of *cooS1* and *cooS2* in the *acsA* KO mutant under such experimental conditions remains unknown.

4.8.5 Partial Translational Read-Through in *acsA* of *C. autoethanogenum*

Despite the presence of an internal 'TGA' stop codon in the *acsA* gene of *C. autoethanogenum*, it was hypothesized that there may be some translational read-through mechanisms that allow the generation of a full AcsA peptide. The basis for this hypothesis was the apparent lack of a RBS to drive downstream *acsA* CDS translation, and complementation studies of *acsA* KO mutant under autotrophic and heterotrophic conditions indicated a role for the downstream CDS.

By fusing FLAG-tag to either the N-terminus or C-terminus of AcsA, the translation pattern of *acsA* was investigated in *C. autoethanogenum*, *C. acetobutylicum* and *E. coli* using Western Blots and anti-FLAG antibody. Depending on the position of the FLAG-tag, the truncation of the 69 kDa full AcsA protein can result in tagged proteins of 44 kDa or 25 kDa. In *C. autoethanogenum* crude lysates carrying an *acsA* gene encoding an AcsA protein with a C-terminal FLAG-tag, a ~69 kDa protein rather than a ~25 kDa band was detected in Western Blot. This indicates that a translational read-through of *acsA* occurs in *C. autoethanogenum* and there is no independent translation of the downstream CDS. Analysis of the abundance of the ~69 kDa protein in the lysates of cells carrying the native *acsA* gene and a variant in which the TGA codon was replaced with TCA clearly showed higher levels of protein were produced in the latter case. This indicates that the formation of the full AcsA protein

by overcoming the 'TGA' stop codon is less efficient than the synthesis of the full length AcsA product containing a 'TCA' serine codon.

To gain a better understanding of the *acsA* translation pattern, an N-terminal FLAG-tagged *acsA* plasmid was constructed so translation of the upstream *acsA* CDS (~44 kDa) could be detected. Indeed, comparison of band intensities in crude extracts of *C. autoethanogenum* showed that the ~44 kDa truncated AcsA protein is the dominant product, rather than the ~69 kDa full sized AcsA protein. This result provided further evidence that the translational read-through event that occurs for the native *acsA* gene of *C. autoethanogenum* is partial and inefficient. It is unknown whether the ability of *C. autoethanogenum* to generate mature and truncated AcsA is a novel regulatory mechanism that serves some physiological purposes, or poses as a handicap that hinders acetogenesis. It is interesting to note that under CO conditions *C. autoethanogenum* has a slightly longer doubling time of 4 h than *C. ljungdahlii's* doubling time of 3.8 h (333), and one may speculate that the different *acsA* translation patterns (TGA vs TCA) may contribute to this phenotype.

One of the mechanisms that allow translational read-through is through the incorporation of selenocysteine at the 'TGA' stop codon although to date there has been no report of selenocysteine CODH. The catalytic activities of many selenoproteins are often superior to their cysteine-containing counterparts (334). For instance, the maximal turnover number (K_{cat}) of formate dehydrogenase H in *E. coli* was reduced by 300-fold when its selenocysteine was replaced with cysteine (335). While a bSECIS was not detected in the *acsA* gene of *C. autoethanogenum* using the algorithm developed by Zhang and Gladyshev (2005) (324), manual examination of the sequence immediately downstream of the 'TGA' codon uncovered a stem-loop structure that resembles bSECIS. To investigate the possibility of selenocysteine incorporation in *acsA*, FLAG-tagged *acsA* variants were expressed in *C. acetobutylicum* ATCC 824 and *E. coli*.

C. acetobutylicum was included as a host to study the translation pattern of *acsA* because this microbe is not known to encode selenoproteins and lacks the genes to synthesize and incorporate selenocysteine. Surprisingly, none of the crude extracts

from *C. acetobutylicum* generated signals during Western Blots analysis. Given the absence of a protein band in the positive control strain that contains the FLAG-tagged *acsA* variant containing a 'TCA's serine codon, it is concluded that the P_{acsA} promoter of *C. autoethanogenum* is not functional in *C. acetobutylicum*. Further investigations that involve the use of a *C. acetobutylicum* promoter such as thiolase promoter or ferredoxin promoter may be required to determine the translation pattern of *acsA* in this microorganism.

E. coli is one of the model microorganisms for selenocysteine synthesis and incorporation. Under growth conditions that were conducive to selenocysteine formation and incorporation, *E. coli* crude extracts that expressed either N-terminal or C-terminal FLAG-tagged *acsA* failed to produce the ~69 kDa full sized AcsA product. Instead, the ~44 kDa truncated protein was detected. As a positive control with equal sample loading, the *acsA* variant with 'TCA' serine codon successfully generated the full ~69 kDa protein in the *E. coli* host. The recognition of *C. autoethanogenum* P_{acsA} in *E. coli* is not unprecedented, as the *M. thermoacetica* CODH/ACS gene cluster was efficiently expressed in *E. coli* using the native clostridial transcriptional and translational signals (107). Collectively these results showed that the post-translational read-through event in *acsA* is host-specific to *C. autoethanogenum* and it is unlikely to involve selenocysteine incorporation.

It is well established that 'TGA', 'TAG' and 'TAA' are commonly employed but not universal codes for stop signals during protein translation (336). The 'TGA' stop codon is particularly prone to failure and it has been used as a code for tryptophan in mitochondria (337), *E. coli* (338), *Mycoplasma* species (339), *Saccharomyces cerevisiae* (340) and *Spiroplasma citri* (341). In addition to the amino acid tryptophan, cysteine and arginine have also been reported to be incorporated at 'TGA' stop codons in *S. cerevisiae* (340) and Moloney murine leukemia virus (342). The genome of *C. autoethanogenum* encodes only one tRNA with anticodon 5'-CCA-3' (CAETHG_R0046) and it codes for tryptophan. As demonstrated by Blanchet *et al.* (2014), a suppressor tRNA with this anticodon is able to recognize 'TGA' stop codon due to a non-Watson Crick base pair in the wobble position, resulting in translational read-through (340). Hence, it is possible that the internal 'TGA' stop codon within the

acsA gene of *C. autoethanogenum* is used to incorporate tryptophan and allow translation to continue until the ribosome encounters the next stop codon. Peptide sequencing using mass-spectroscopy can be performed to identify the unknown amino acid corresponding to the 'TGA' stop codon.

In contrast to the leaky 'TGA' stop codon, reporter assays in *E. coli* showed that the 'TAA' stop codon is a more efficient translational stop signal (336). In agreement with this observation, alteration of the internal 'TGA' stop codon of *acsA* to a 'TAA' stop codon completely blocked the translation of the full AcsA peptide in both *C. autoethanogenum* and *E. coli* hosts, as evident by the absence of protein bands in the C-terminus FLAG-tagged acsA(TAA) crude lysates.

4.8.6 *cooS1* ClosTron Mutant Grows Better in H_2+CO_2 Conditions and Produces More Ethanol in the Presence of CO than WT

The mono-functional *cooS1* of *C. autoethanogenum* is chromosomally colocalized with genes encoding a putative 4Fe-4S ferredoxin Fe-S binding protein and ferredoxin-NAD(+) reductase but its function is not clear. It has been reported that the physiological functions of mono-functional CODH lay in the direction of CO oxidation to allow microbes to oxidize CO at low levels in the environment, whereas the CODH component of CODH/ACS complex reduces CO_2 into [CO] moiety for acetyl-CoA synthesis (78, 308). Consistent with this notion, the *cooS1* KO mutant displayed some growth deficiencies in the form of increased growth lag phase and reduced OD_{600} while metabolizing CO. However, this mutant also generated 64% more ethanol on pure CO, and 113% increased ethanol compared to the WT on BOF gas. The reduced growth of *cooS1* mutant in the presence of CO may result in accumulation of excess reducing equivalents that get consumed in ethanologenic pathways.

Under H_2 + CO_2 conditions, the mutant is able to grow without an apparent lag phase and also reaches twice the OD_{600} of the WT. Since during acetyl-CoA synthesis the reduced [CO] moiety is enclosed within the CODH/ACS complex to reduce internal thermodynamic barriers (343-345), the presence of another CODH may act as a

competitor for CO_2. This provides a possible explanation of how inactivation of mono-functional CODH may increase the efficiency of the CODH/ACS enzyme complex, which leads to enhanced growth on $H_2 + CO_2$.

4.8.7 Autotrophy and Product Formation of *cooS2* Mutant is Not Significantly Affected

Unlike the *cooS1* mutant, autotrophic growth of the *cooS2* mutant in CO is not significantly affected. The *cooS2* mutant even showed a mild decrease in growth lag phase but reduced OD_{600} in the presence of CO when compared to the WT. This result, combined with a lack of impact on $H_2 + CO_2$ autotrophic growth, suggests that *cooS2* is not heavily involved in autotrophy of *C. autoethanogenum*. The role of this protein remains unclear as it is not genetically colocalized with other relevant genes.

4.8.8 Attempt at Generation of Double KO *cooS1* and *cooS2* Mutant

The presence of multiple CODHs complicates the interpretations of phenotypes from single CODH KO mutants. One solution to this problem is the creation of multiple CODHs KO in the same cell. In this project, an attempt was made to inactivate both *cooS1* and *cooS2* in *C. autoethanogenum* to gain a better understanding of *acsA*. Given the favourable phenotypes of *cooS1* and *cooS2* under certain autotrophic conditions, the elimination of both mono-functional CODHs may reduce competition for AcsA to access CO/CO_2, resulting in a strain that is superior in carbon fixation.

Theoretically the introduction of FLP recombinase should allow the ermRAM marker of a ClosTron insertion to be recycled for generation of multiple KO mutants. However, clarithromycin sensitive colonies from *C. autoethanogenum* ClosTron mutants proved to be unattainable. Hence, an alternative approach that involved both ClosTron mutagenesis and ACE was pursued. First, a ClosTron *cooS2* mutant was constructed in a *C. autoethanogenum* Δ*pyrE* strain. Following that, an IFD plasmid that aimed to delete *cooS1* was introduced and putative single-crossover mutants were detected at both homology arms during PCR screening, indicating mixed clonal populations. These putative single-crossover mutants were then subjected to FOA

selection to select for the second crossover event. PCR screening of the FOA^R clones showed that the clones had reverted back to WT allele. For future work, clones with single crossover at either homology arms should first be isolated before FOA counter-selection.

4.9 Chapter Summary

As expected, ClosTron KO of the *acsA* abolished autotrophic growth and significantly hindered heterotrophic growth of *C. autoethanogenum*, confirming the acetogenic role of CODH/ACS under both growth conditions. The lack of acetate production, and enhanced formation of reduced products ethanol and 2,3-butanediol during heterotrophic growth of the *acsA* mutant, suggests such a mutant may be useful for the study of acetogenic mixotrophy as a novel route to improve biofuels and biochemicals production (106). Although CODH/ACS is already very highly expressed in *C. autoethanogenum* (53), this study demonstrated that plasmid overexpression of $acsA^{full}$ can reduce growth lag phase and increase ethanol yield under CO conditions. For future work, synthetic operon(s) with modified promoters that drive the expression of all five subunits of CODH/ACS could be integrated into the genome of *C. autoethanogenum* to create a potentially superior biocatalyst.

Examination of the translation pattern of *acsA* in *C. autoethanogenum,* which uniquely has an internal 'TGA' stop codon, revealed that while there is clearly a translational read-through event in *acsA*, the full length protein is only a secondary product compared to the truncated AcsA protein based on protein band intensities. Due to the empirical roles of *acsA* in acetogenesis, the 'TGA' stop codon of *C. autoethanogenum* can be 'repaired' to 'TCA' serine codon using allelic-exchange techniques such as ACE to assess its impact on autotrophic growth. The lack of translational read-through AcsA product in *E. coli* crude lysates suggests the translational read-through mechanism is unique to *C. autoethanogenum.* Peptide sequencing using mass spectroscopy should identify the mysterious amino acid corresponding to the internal 'TGA' codon of *acsA* and elucidate the precise mechanism for the translational read-through event.

While some growth deficiencies were observed with the *cooS1* inactivation mutant during CO growth, the mutant surprisingly grew significantly better than WT under H_2 + CO_2 conditions. These results indicate that *cooS1* is involved in CO oxidation but its presence somehow negatively affected the CO_2 reduction process, possibly by competing with the CODH/ACS complex. Since the inactivation of *cooS2* did not significantly affect autotrophic growth in either CO or H_2 + CO_2, it is concluded that *cooS2* is not a major player for CO oxidation and acetogenesis in *C. autoethanogenum*. To provide a more definitive insight into the roles of *cooS1* and *cooS2*, the genes can be independently cloned, expressed and purified in *C. autoethanogenum* to study their functions via enzymatic assays.

CHAPTER 5

GENERATION AND CHARACTERIZATION OF BI-FUNCTIONAL ALDEHYDE/ALCOHOL DEHYDROGENASE MUTANTS

5 Generation and Characterization of Bi-functional Aldehyde/Alcohol Dehydrogenase Mutants

5.1 Introduction

As part of the solventogenic pathway, the bi-functional aldehyde/alcohol dehydrogenase (AdhE) is prevalent in many fermentative microorganisms. The enzyme complex catalyzes the sequential conversion of acyl-CoA into alcohol via an aldehyde intermediate, with concomitant regeneration of NAD(P)+ from NAD(P)H (149, 346-348). AdhE typically consists of an N-terminal acetylating aldehyde dehydrogenase domain (Ald) followed by a C-terminal alcohol dehydrogenase domain (Adh), which is commonly of the Fe-type Adh superfamily (347, 349). The key role of AdhE in alcohol formation has been demonstrated in *C. ljungdahlii* (229, 230), *C. acetobutylicum* (149), *C. thermocellum* (350), *E. coli* (347), *Lactococcus lactis* (348), *Geobacillus thermoglucosidasius* (349) and *Thermoanaerobacter ethanolicus* (346). The purified AdhE2 from *C. acetobutylicum* and AdhE from *T. ethanolicus* exhibited high Ald activity but low Adh activity (149, 346), which may explain why many fermentative microorganisms possess multiple *adh* genes.

Deletion studies and the characterization of the separate AdhE domains indicate that the Ald domains and Adh domains are functionally autonomous (348, 351, 352). It has been hypothesized that the fusion of ALDH and ADH activities into the same peptide may enhance the successive reduction of an acyl-CoA to an alcohol by bringing the two catalytic sites into close proximity, and helps lower the steady state level of aldehydes, which are generally very toxic intermediates (346, 347, 351). Recently, the structure of the Adh domain of AdhE from *G. thermoglucosidasius* was solved using X-ray crystallography, and combined with *in silico* prediction of the Ald domain to generate an AdhE protein complex structure that resembles spirosomes (multimeric high molecular weight helical structures) (349). Furthermore, Western Blot of cell lysates containing AdhE from *E. coli* and *Entamoeba histolytica* also showed the presence of high molecular weight structures indicative of spirosomes (351, 353). The prospect of AdhE spirosomes may provide a mechanism for how the

formation of substrate channelling may insulate the cell from the reactive acetaldehyde intermediate and improve enzyme kinetics for Adh (349).

The importance of AdhE is highlighted by fermentative microbes that harbour multiple *adhE* genes, for instance *C. autoethanogenum* (38), *C. ljungdahlii* (37), *C. carboxidivorans* P7 (39, 40), and *C. acetobutylicum* (35). These *adhE* genes appear in tandem in the mentioned acetogens, while the two *adhE* genes in saccharolytic *C. acetobutylicum* are encoded at separate loci on the pSOL megaplasmid. During syngas (60 N_2:20 CO:15 CO_2:5 H_2) bioreactor fermentation, the two *C. carboxidivorans adhE* genes (CcarbDRAFT_4321 and CcarbDRAFT_4322) showed differential gene expression, with the mRNA level of *adhE2* higher than *adhE1*, indicating separate roles for each during solventogenesis (150). Deletion mutants of *C. ljungdahlii* showed that *adhE1* (CLJU_c16510), rather than *adhE2* (CLJU_c16520), is the homolog responsible for ethanol formation under heterotrophic conditions (229, 230).

The putative *adhE* operon (including 650 bp promoter region of *adhE1*) of *C. autoethanogenum* (Figure 5.1) shares the highest nucleotide identity with *C. ljungdahlii* at 98%, but only 78% with *C. carboxidivorans* P7. At the amino acid (AA) level, the sequence identities are 99% (867/870) in AdhE1 and 99% (869/877) in AdhE2 between *C. autoethanogenum* and *C. ljungdahlii*. The corresponding AA identities of AdhE1 and AdhE2 are 80% (705/876) and 87% (768/877) between *C. autoethanogenum* and *C. carboxidivorans*. Similar to *C. carboxidivorans*, the intergenic region between *adhE1* and *adhE2* of *C. autoethanogenum* is predicted to encode a terminator and a promoter region for *adhE2* (38, 150), which supports the potential for differential expression. In *C. autoethanogenum*, AdhE2 is 7 residues larger than AdhE1 and they share 86% AA identity.

To investigate the roles of AdhE on solventogenesis in *C. autoethanogenum*, ClosTron mutants of *adhE1* and *adhE2* were independently constructed. Furthermore, the generation of *adhE* IFD mutants was also attempted. Characterization of these mutants under autotrophic and heterotrophic conditions revealed interesting insights into the solventogenic pathway of this acetogen.

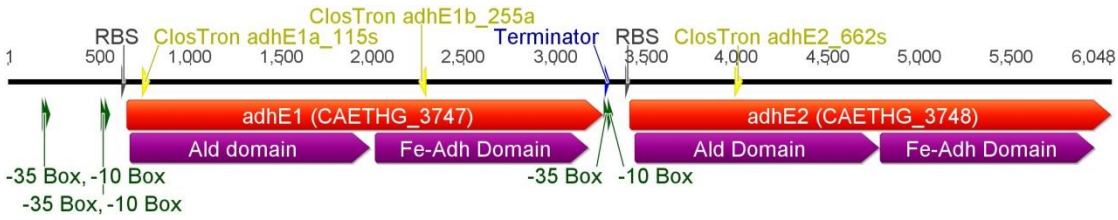


Figure 5.1. Gene arrangement of *adhE1* and *adhE2* in *C. autoethanogenum* with predicted catalytic domains (purple blocks), promoter elements (green triangles), transcriptional terminator (blue triangles), ribosomal binding sites (RBS; grey triangles) and ClosTron insertion sites (yellow triangles).

5.2 Generation of ClosTron Knockout Mutants *adhE1a*, *adhE1b* and *adhE2*

To generate independent knockout mutants of *adhE1* and *adhE2*, ClosTron plasmids pMTL007C-E2::adhE1a-115s, pMTL007C-E2::adhE1b-255a and pMTL007C-E2::adhE2-662s, respectively, were conjugated into *C. autoethanogenum* according to section 2.12.3. The first two ClosTron plasmids were constructed to separately inactivate the Ald and Adh domains of *adhE1*, generating mutants '*adhE1a*' and '*adhE1b*', respectively. The ClosTron insertion sites are highlighted in Figure 5.1. Clarithromycin resistant colonies were subjected to PCR screening using primer pairs 'adhE1-115s-F' and 'adhE1-115s-R' for *adhE1a* mutant, 'adhE1b-255a-F' and 'adhE1b-255a-R' for the *adhE1b* mutant, and 'adhE2-662s-F' and 'adhE2-662s-R' for the *adhE2* mutant. The screened clones showed the expected 2.0-2.1 kb bands (Figure 5.2A) and these PCR products were verified by Sanger sequencing. These ClosTron mutants were streaked onto the same selective medium until the ClosTron plasmids had been cured (shown by patch plating). As final validation, Southern Blot analysis was performed to ensure that a ClosTron insertion event had occurred only once per mutant (Figure 5.2B).

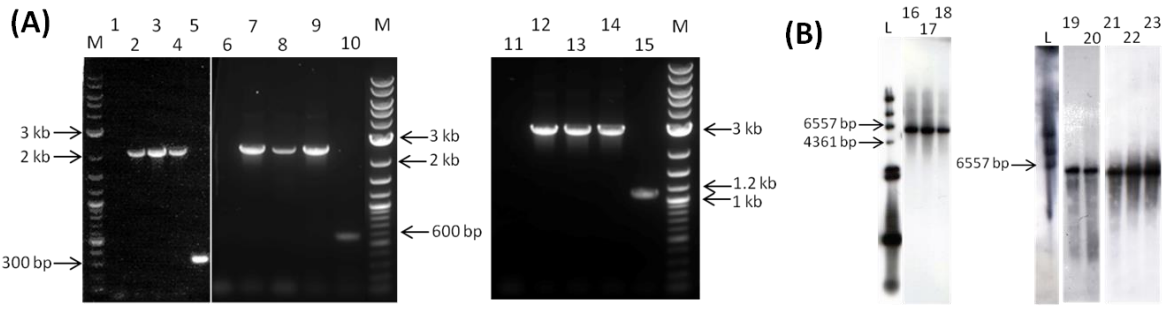


Figure 5.2. Screening and validation of *adhE1a*, *adhE1b*, and *adhE2* ClosTron mutants. (A) Gel electrophoresis of PCR using exon-spanning primers; Lanes 2 – 4 = *adhE1a* mutants; Lanes 7 – 9 = *adhE1b* mutants; Lanes 12 – 14 = *adhE2* mutants; Lanes 1, 6, & 11 = Non-template controls; Lanes 5, 10 & 15 = WT controls; M = NEB 2-log DNA ladder; (B) Southern Blot analysis of *Hind*III digested genomic DNA of *adhE1a* mutants (lanes 16 – 18), *adhE1b* mutants (lanes 19 & 20), and *adhE2* mutants (lanes 21 – 23). L = Promega Lambda DNA/HindIII marker.

5.3 Characterization of ClosTron *adhE1a*, *adhE1b* and *adhE2* Mutants

5.3.1 Autotrophic Growth Experiment in CO

Serum bottle growth experiments in the presence of CO were carried out to assess the impact of *adhE* inactivation in *C. autoethanogenum*. Each 250 mL serum bottle was filled with 50 mL CGMY medium and 2 bar CO headspace, or 100 mL CGMY medium with 2 bar BOF gas (composition: 51.24% CO, 31.22% N_2, 11.98% CO_2, and 3.05% H_2) harvested from a steel mill in Glenbrook, New Zealand. Incubation was carried out at 37^{o}C with agitation for up to 34 days for pure CO cultures and 13 days for BOF gas cultures.

In 2 bar CO, growth of all three *adhE* mutants underwent a significantly longer lag phase compared to the WT and achieved much reduced final culture densities with the OD_{600} only 45-53% of the WT (p-values <0.01) (Figure 5.3A). When the two *adhE1* mutants were compared, the strain with the upstream domain inactivated (*adhE1a*) displayed a longer growth lag phase of ~18 days, relative to the ~11 day growth lag phase observed for the mutant with the downstream domain inactivated (*adhE1b*) (Figure 5.3A). In terms of acetate production, the *adhE1a* mutant showed the larger reduction at 34% (p-value <0.0001) , followed by the *adhE1b* mutant which displayed a 13% decrease when compared to WT (p-value = 0.034) (Figure 5.3B). In contrast, the *adhE2* mutant produced 13% higher acetate titres than the WT (p-value = 0.003)

(Figure 5.3B). Remarkably, all three *adhE* mutants synthesized higher amounts of ethanol than the WT despite achieving a relatively lower biomass. When compared to WT, the *adhE1a* mutant generated 183% more ethanol (p-value = 0.0005), the *adhE1b* mutant produced 171% higher ethanol (not statistically significant) and the *adhE2* mutant synthesized 154% elevated ethanol (p-value = 0.021) (Figure 5.3C). This increase in ethanol titre in *adhE* mutants was partially compensated by a decrease in the levels of 2,3-butanediol, which were reduced by 48 - 68% relative to the WT (p-values <0.004) (Figure 5.3D).

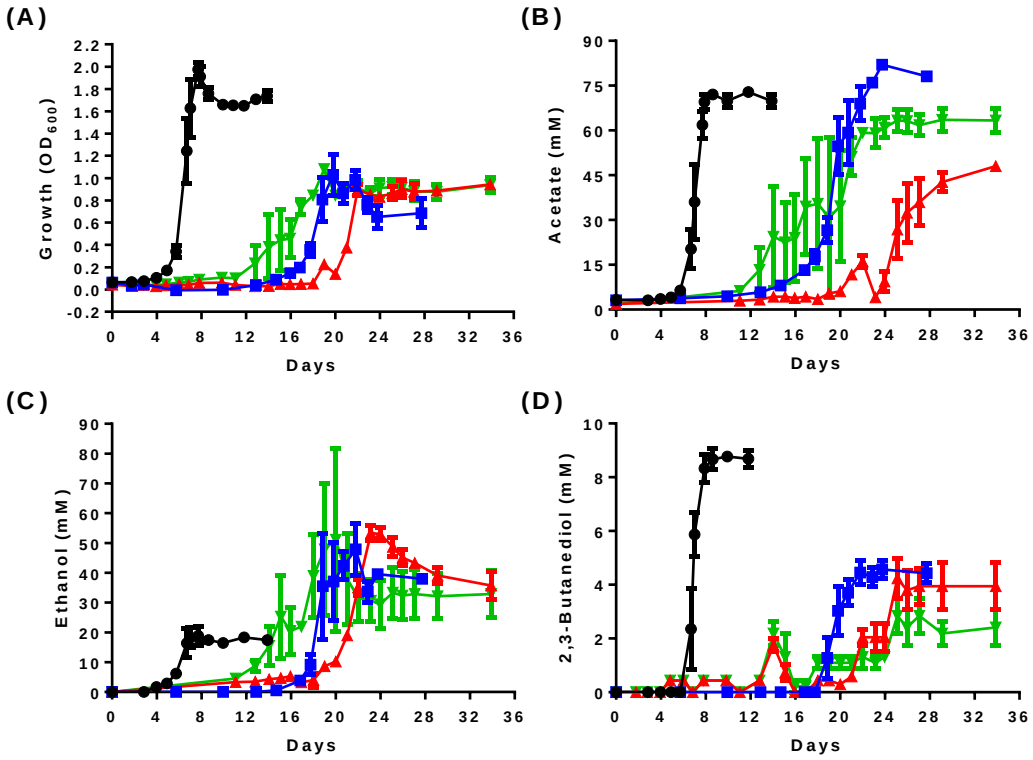


Figure 5.3. Growth and metabolite profiles of *adhE1a, adhE1b* and *adhE2* ClosTron mutants on CO. (A) Growth profile; (B) Acetate profile; (C) Ethanol profile; and (D) 2,3-Butanediol profile. Black circles = WT (N = 4); Red triangles = *adhE1a* mutant (N = 3); Green inverted triangles = *adhE1b* mutant (N = 2); Blue squares = *adhE2* mutant (N = 3); Error bars = standard error of mean.

The behaviour of the ClosTron *adhE1a* mutant and the WT when grown in serum bottles with BOF gas was also examined. Similar to growth in pure CO, the *adhE1a*

mutant underwent a longer growth lag phase than the WT and achieved a 30% lower cell density (p-value = 0.001) (Figure 5.4A). Despite the reduced biomass, the mutant produced 54% higher levels of ethanol than the WT (p-value = 0.001), but 39% less acetate (p-value <0.0001)(Figure 5.4B & C).

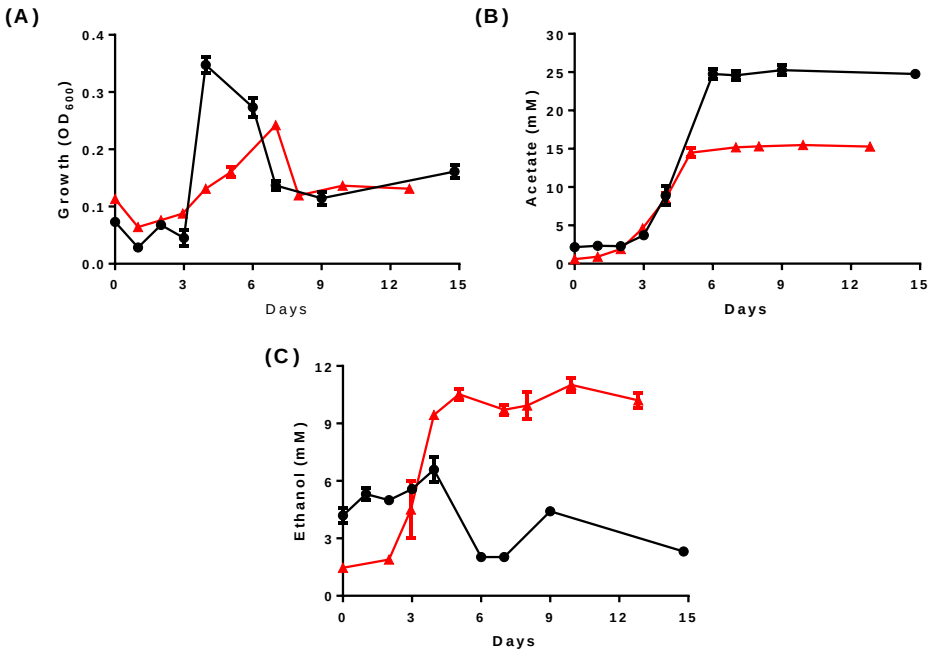


Figure 5.4. Growth and metabolite profiles of *C. autoethanogenum* WT and *adhE1a* mutant on BOF gas. (A) Growth profile; (B) Acetate profile; and (C) Ethanol profile. Black circles = WT (N = 3); Red triangles = *adhE1a* mutant (N = 4). Error bars = standard error of mean.

5.3.2 Heterotrophic Growth Experiment

For evaluation of the impact of *adhE* inactivation on heterotrophic growth, the three (*adhE1a, adhE1b* and *adhE2*) ClosTron mutants were grown in 250 mL serum bottles containing 50 mL CGMY medium supplemented with 10 g/L fructose (final concentration). As shown in Figure 5.5A, both the *adhE1a* and *adhE1b* mutants showed a slightly longer lag phase but grew to a similar OD_{600} as the WT. In contrast, the peak OD_{600} of the *adhE2* mutant was 28% lower than the WT (p-value <0.0001) (Figure 5.5A). Even after 13 days of growth, 0.92 g/L of fructose was detected in the *adhE2* mutant culture, whereas all the other strains completely exhausted the

substrate prior to day 3 (data not shown). All three *adhE* mutants reached peak acetate levels of 72.15 – 76.53 mM, which are 31 – 43% higher than the WT (55.12 mM) (p-values <0.05) (Figure 5.5B). When compared to the WT, both *adhE1* mutants synthesized similar amounts of ethanol but the *adhE2* mutant only generated 37% of the WT ethanol titres (p-value = 0.0035) (Figure 5.5C). All three *adhE* mutants produced less than half of the 2,3-butanediol recorded in the WT culture (p-values <0.05) (Figure 5.5D).

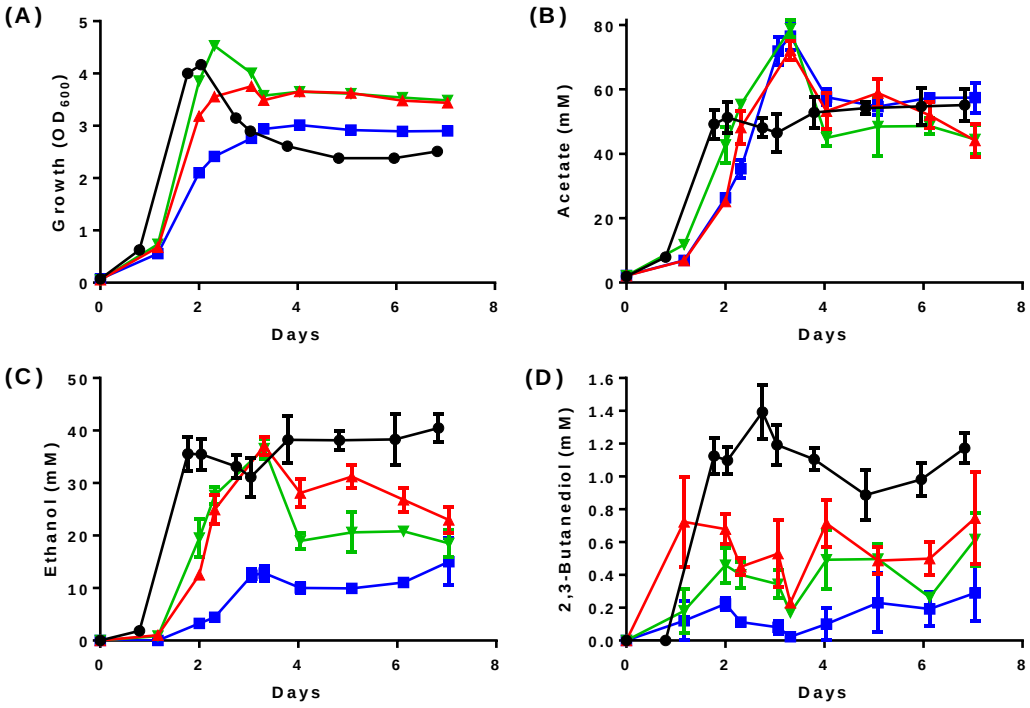


Figure 5.5. Growth and metabolite profiles of *C. autoethanogenum* WT and *adhE* ClosTron mutants growing on fructose. (A) Growth profile; (B) Acetate profile; (C) Ethanol profile; and (D) 2,3-butanediol profile. Black circles = WT (N = 4); Red triangles = *adhE1a* mutant (N = 3); Green inverted triangles = *adhE1b* mutant (N = 3); Blue squares = *adhE2* mutant (N = 3); Error bars = standard error of mean.

5.4 Generation of Δ*adhE1* and Δ*adhE1+2* In-Frame Deletion Mutants

For long genes that have functionally autonomous domains, intron-based mutagenesis may only disrupt one of the domains and may not be sufficient to prevent the production of a polypeptide encoded by the non-disrupted coding

region. Hence, IFD was attempted to entirely delete both domains of *adhE1*, as well as *adhE1* + *adhE2* in *C. autoethanogenum*. For the deletion of *adhE1*, homology arms were constructed using SOE-PCR with oligonucleotides 'adhE1-ald-LHA-SacII-F', 'adhE1-IFD-LHA-R', 'adhE1-IFD-RHA-F' and 'adhE1-IFD-RHA-AscI-R'. Restriction sites *Sac*II and *Asc*I were used to clone the homology arm cassette into plasmid 'pMTL84151-ΔpyrE' (section 2.14.1) to generate plasmid 'pMTL84151-adhE1-IFD'.

For the construction of *adhE1* + *adhE2* IFD homology arm cassette, SOE-PCR was performed using primers 'adhE1-ald-LHA-SacII-F', 'adhE1&2-SOE-B', 'adhE1&2-SOE-C' and 'adhE1&2-RHA-AscI-R'. This cassette was then cloned into plasmid 'pMTL84151-ΔpyrE' using restriction sites *Sac*II and *Asc*I, resulting in plasmid 'pMTL84151-adhE1&2-IFD'. The cloned homology arms were verified by Sanger sequencing and they were designed to completely delete *adhE1* or *adhE1* + *adhE2* while retaining only the start and stop codons. Following conjugation of these IFD plasmids into the Δ*pyrE* mutant, faster growing colonies on thiamphenicol solid medium were preferentially streaked onto the same selective medium to identify single-crossover mutants.

Since the LHA and RHA are similar in length (less than 21 bp difference) for both IFD plasmids, single crossover should theoretically occur at either arm with similar frequencies. PCR screening using oligonucleotides 'IFD-plasmid-F' and 'adhE2-662s-R' detected a single crossover event at the RHA (generating a 1892 bp amplicon) for *adhE1* IFD in 11 of the 16 fast growing Tm^R colonies (data not shown). These single crossover clones were then subjected to FOA selection to trigger the second recombination event and PCR using oligonucleotides 'adhE1-IFD-F' and 'adhE1-IFD-R' were performed to detect the 347 bp double crossover amplicon. Of the 16 screened FOA^R colonies, 6 showed a ~250 bp amplicon, 9 showed the WT 2954 bp band, while 1 produced no PCR product (Figure 5.6A). These ~250 bp amplicons were visibly smaller than the expected 347 bp IFD product, and Sanger sequencing revealed that the *adhE1* of *C. autoethanogenum* was deleted but there was also an unintended deletion of 84 bp in the promoter region of *adhE2* (Figure 5.6D). Examination of this promoter region revealed the presence of two 9 bp repeats, and it was evident that homologous recombination between these elements would result in the observed 84

bp deletion (Figure 5.6D). Herein termed '$\Delta adhE1^{mut}$' mutant, it lacks the putative *adhE1* terminator and the -10 and -35 box of the *adhE2* promoter. A second attempt at generating a 'clean' IFD mutant of *adhE1* successfully produced the expected 347 bp amplicon 6 months later (Figure 5.6B), herein termed '$\Delta adhE1$' mutant. Sanger sequencing revealed *adhE1* was successfully deleted as intended without the unintended 84 bp deletion in the *adhE2* promoter region. Patch plating showed that Tm^S clones were isolated in the first attempt for $\Delta adhE1^{mut}$ mutant (data not shown), indicating that the plasmid used to generate the IFD mutant had been lost. However, repeated attempts to isolate Tm^S colonies for Δ*adhE1* mutant were unsuccessful.

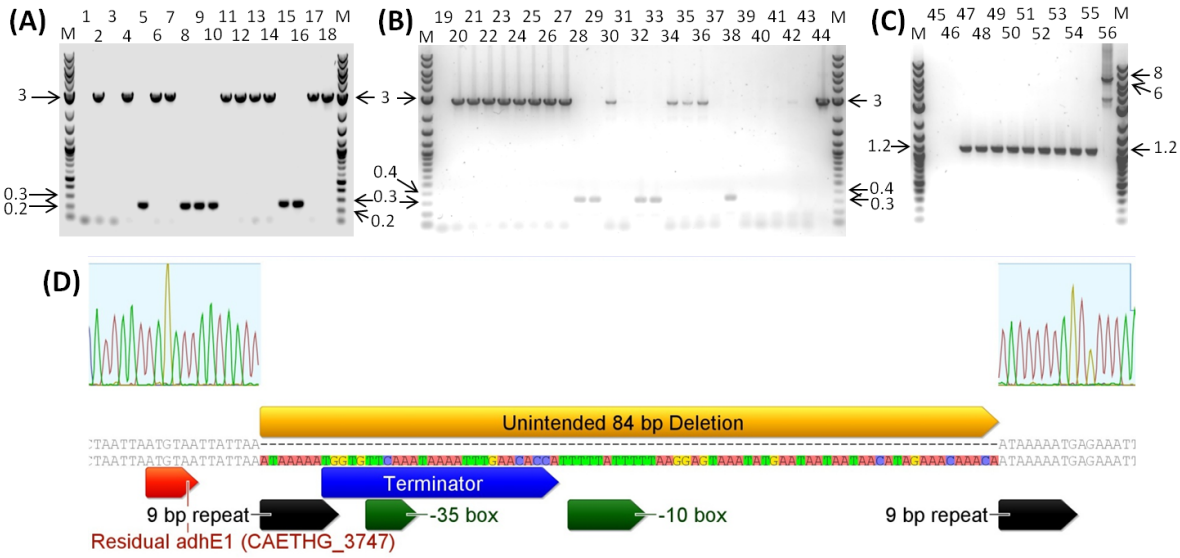


Figure 5.6. Screening of *C. autoethanogenum* $\Delta adhE1^{mut}$, Δ*adhE1* and Δ*adhE1+2* mutants. (A) PCR screening of $\Delta adhE1^{mut}$ mutants; (B) PCR screening of Δ*adhE1* mutants; (C) PCR screening of Δ*adhE1+2* mutants; and (D) Nucleotide alignment of Sanger sequencing read from $\Delta adhE1^{mut}$ mutant highlighting the unintended 84 bp deletion in the inter-genic region of *adhE1* and *adhE2*. Green peak = thymine; Red peak = adenine; Brown peak = guanine; Blue peak = cytosine; Lanes 5, 8, 9, 10, 15 & 16 = $\Delta adhE1^{mut}$ mutants; Lanes 28, 29, 32, 33 & 38 = Δ*adhE1* mutants; Lanes 47 – 55 = Δ*adhE1+2* mutants; Lanes 1, 19 & 45 = non-template controls; Lanes 18, 44 & 56 = WT genomic DNA control; M = NEB 2-log DNA ladder in kb.

For the *adhE1* + *adhE2* IFD mutant, oligonucleotides 'IFD-plasmid-F' and 'adhE1-115s-R' were used to detect single-crossover integrants that had arisen through homologous recombination with the LHA, while primers 'adhE2-662s-F' and 'IFD-

plasmid-R' were employed to detect those clones in which integration was mediated by the RHA. Of 8 screened colonies, 3 were single crossover integrants reliant on the LHA while plasmid integration in another had been mediated by the RHA (data not shown). Cells from all four clones were plated on medium containing FOA to select for cells in which the plasmid had excised through a recombination event involving homologous recombination between either the duplicated LHA or the RHA. A total of 10 FOA resistant colonies were screened in PCR using the oligonucleotide primers 'adhE1-seq-F' and 'adhE2-seq-R'. From the size of DNA fragment generated it was concluded that 9 of the 10 clones were doubled cross over mutants (Figure 5.6C). Sanger sequencing of the generated DNA fragments confirmed this conclusion, and the mutants therefore represented clones in which *adhE1* and *adhE2* had been deleted (herein called '*ΔadhE1+2*' mutants), leaving only the start codon of the former and stop codon of the latter (data not shown). Plasmid loss was attempted by repeatedly streaking onto solid medium containing FOA without thiamphenicol but no Tm^S colony was detected for these *adhE* IFD mutants.

5.5 Characterization of Δ*adhE1*^{mut} Mutants

5.5.1 Heterotrophic Growth Experiment and Gene Expression of *adhE2*

The unintended deletion of 84 bp in the inter-genic region between *adhE1* and *adhE2* in *C. autoethanogenum* Δ*adhE1*^{mut} may affect *adhE2* expression. To test this hypothesis, *adhE2* mRNA levels in the Δ*pyrE* strain and the Δ*adhE1*^{mut} mutant were compared. Strains were cultivated in 500 mL Schott bottles containing 200 mL CGMY medium supplemented with 10 g/L fructose and 10 µg/mL uracil. In addition to routine sampling of liquid cultures for HPLC analysis and OD_{600} measurements, cells were harvested at early exponential phase, late exponential phase, and stationary phase for gene expression analysis according to section 2.9.1. Total RNA was extracted as described in section 2.9.2 and reverse transcribed into cDNA according to section 2.9.3. For qRT-PCR analysis, TaqMan® primers and probes were employed for the two housekeeping genes (*gyrA* and *rho*) and gene of interest (*adhE2*). Given the high nucleotide identity (87%) between *adhE1* and *adhE2* in *C.*

autoethanogenum, the TaqMan® primer pairs and probes for *adhE2* were carefully designed to ensure high specificity. Standard curves using serially diluted cDNA were generated and the TaqMan® primers and probes demonstrated excellent amplification efficiencies (section 2.9.4).

In comparison to the Δ*pyrE* strain, growth of the Δ*adhE1*^{mut} mutant had a longer lag phase but both strains achieved a similar final cell density in the presence of fructose (Figure 5.7A). Both strains produced equivalent amounts of acetate (Figure 5.7B), ethanol (Figure 5.7C) and 2,3-butanediol (data not shown). As a consequence of the longer lag phase of the Δ*adhE1*^{mut} mutant, the sampling time-points for gene expression analysis were delayed by ~one day in comparison to the Δ*pyrE* strain to match the growth stage. qRT-PCR analysis showed that *adhE2* normalized transcript level of the Δ*pyrE* strain was stable across all three time points (less than 3.2-fold difference) (Figure 5.7D). In contrast, *adhE2* mRNA levels in the Δ*adhE1*^{mut} mutant exhibited large fluctuations with an initial decrease of 114-fold from early exponential growth phase to late exponential growth phase, followed by a 16-fold increase at the stationary growth phase (Figure 5.7D). Moreover, *adhE2* transcript levels in the Δ*adhE*1^{mut} mutant were also significantly higher than in cells of the Δ*pyrE* mutant at all three sample time points (p-value <0.05) (Figure 5.7D).

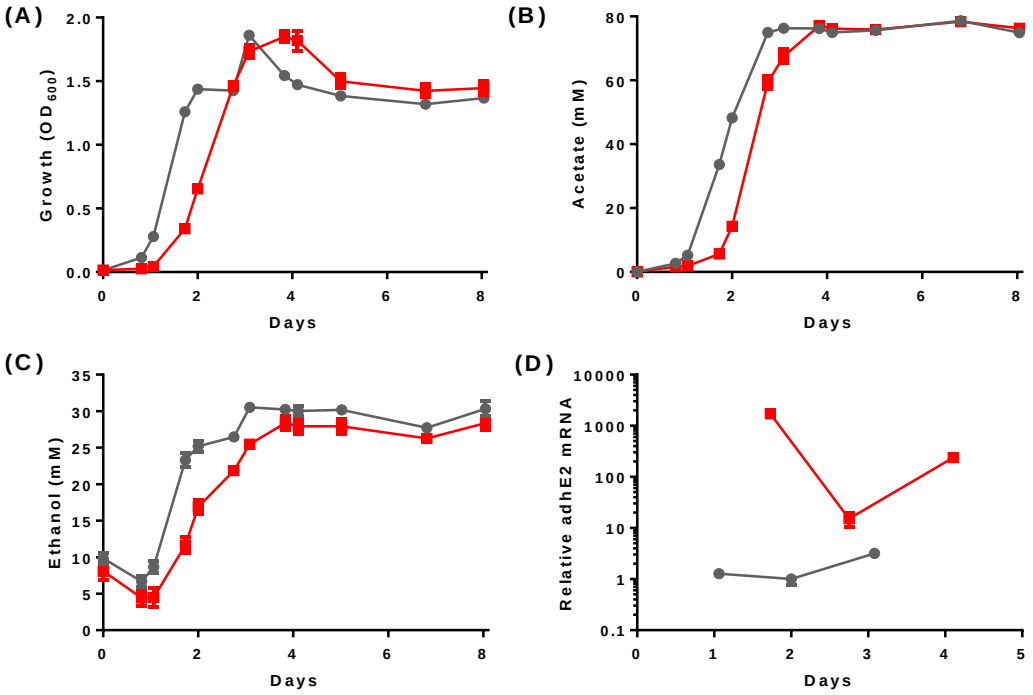


Figure 5.7. Growth, metabolite and *adhE2* transcript profiles of *C. autoethanogenum* Δ*pyrE* and Δ*adhE1*^{mut} strains growing on fructose. (A) Growth profile; (B) Acetate profile; (C) Ethanol profile; and (D) Relative *adhE2* mRNA profile. Grey circles = Δ*pyrE* (N = 3); Red squares = Δ*adhE1*^{mut} (N = 3). Error bars = standard error of mean.

5.5.2 Autotrophic Growth Experiment

Both the Δ*pyrE* and Δa*dhE1*^{mut} mutant strains were cultured in 250 mL serum bottles containing 2 bar CO to examine the effect of deletion in *adhE1* and part of the *adhE2* promoter region on autotrophy and alcohologenesis. The serum bottle growth experiment was conducted in technical triplicates containing 50 mL CGMY medium supplemented with 10 µg/mL uracil. Incubation was undertaken at 37^{o}C with agitation over a period of 34 days. In the presence of CO, growth of the Δ*adhE1*^{mut} mutant exhibited a longer lag phase of ~14 days compared to the ~11 days observed with the Δ*pyrE* control strain (Figure 5.8A). Very similar amounts of acetate (Figure 5.8B) and 2,3-butanediol (Figure 5.8D) were synthesized by both strains but the Δ*adhE1*^{mut} mutant appeared to produce 27% more ethanol than the Δ*pyrE* strain (not statistically significant) (Figure 5.8C).

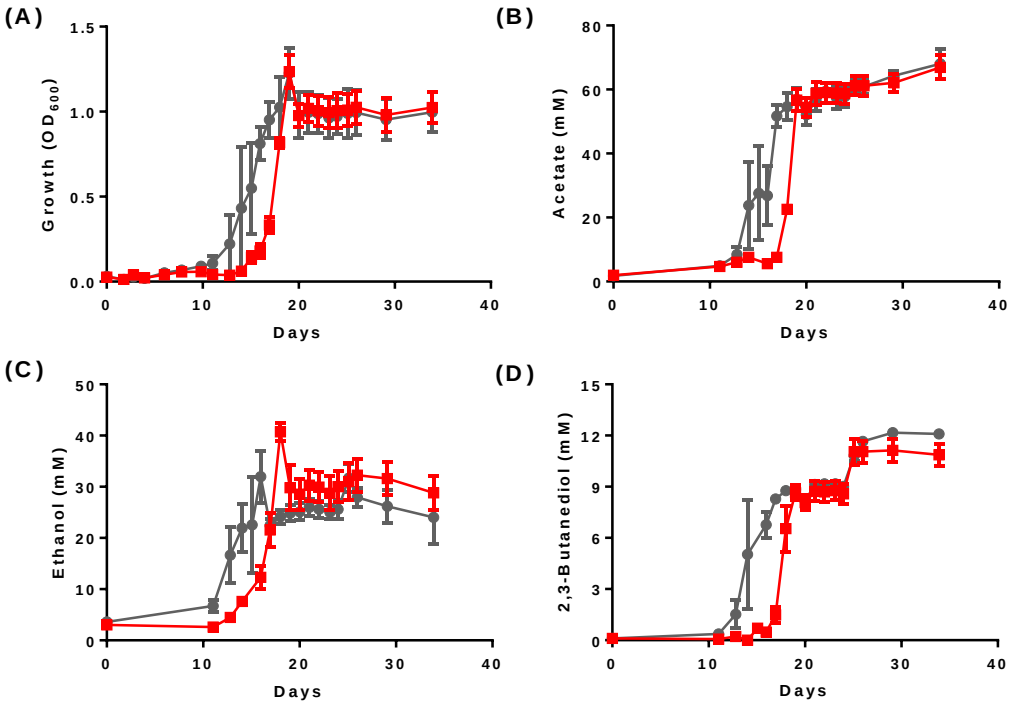


Figure 5.8. Growth and metabolite profiles of *C. autoethanogenum* Δ*pyrE* and Δ*adhE1*^{mut} strains on CO. (A) Growth profile; (B) Acetate profile; (C) Ethanol profile; and (D) 2,3-butanediol profile. Grey circles = Δ*pyrE* (N = 3); Red squares = Δ*adhE1*^{mut} (N = 3). Error bars = standard error of mean.

5.6 Discussion

5.6.1 Unlike *C. ljungdahlii,* Inactivation of *adhE1* in *C. autoethanogenum* Does Not Affect Ethanol Production Under Heterotrophic Conditions

At the beginning of the study, only an *adhE1a* ClosTron mutant had been generated. This mutant, which had the upstream Ald domain of *adhE1* inactivated via ClosTron mutagenesis, displayed no defect in ethanol formation when grown in fructose. This was in contradiction to the findings of Leang and co-workers (2013), who showed that the deletion of *C. ljungdahlii adhE1* resulted in a mutant that produced 6-fold less ethanol than the WT control when grown on fructose as the carbon source (229). One difference in methodology is the use of 10 g/L fructose in this PhD work but 5 g/L fructose in the report of Leang *et al.* (2013). In a follow up study the authors were able to demonstrate restoration of ethanol production in this *adhE1* deletion mutant by expressing functional *adhE1* under the control of a lactose-inducible promoter (230). RNA-seq experiments showed that in *C. ljungdahlii, adhE1* is transcribed at

2.99-fold higher level when growing on fructose compared to a CO:CO_2 gas mixture (80:20) (167), and 10.52-fold higher when compared to H_2 + CO_2 (170). These data suggest an important role for this gene under heterotrophic conditions.

To investigate the major discrepancy in the *adhE1* mutant phenotype between *C. autoethanogenum* and *C. ljungdahlii*, the nucleotide and deduced amino acid sequences of *adhE1* between the two species were compared (Figure 5.9A and B). At the nucleotide level, there are 15 mismatches within *adhE1* and 9 mismatches in its promoter region (650 bp upstream of *adhE1* start codon). Of these mismatches, only 3 result in a change in amino acid sequence: 2 within the Ald domain and 1 within the Adh domain. The mismatch within the Adh domain is a non-positive substitution (meaning the residues substitute rarely according to BLOSUM62 (354)) from alanine in *C. autoethanogenum* to valine in *C. ljungdahlii*, and it occurs 15 AA away from a conserved Fe-Adh signature (Prosite PS00060). The *C. ljungdahlii* Δ*adhE1* mutant created by Leang *et al.* (2013) had part of the upstream Ald and part of the downstream Fe-Adh domain deleted and replaced with an *ermC* marker gene (229) (Figure 5.9A) using homologous recombination. Accordingly, the upstream Ald domain may still be functional. In this study, the ClosTron insertion at the Ald domain of *C. autoethanogenum* should at least have inactivated this domain but it is possible that the downstream Fe-Adh domain remains functional and translated because a putative RBS and start codon could be identified prior to the Fe-Adh domain (Figure 5.9A). This is supported by literature findings that *adhE1* (part of *sol* operon) in *C. acetobutylicum* is translated into two peptides: one full-length peptide and one truncated peptide containing only the Adh domain (355).

In order to determine whether the difference in the *adhE1* mutant phenotype between *C. autoethanogenum* and *C. ljungdahlii* was due to a difference in catalytic domain inactivation, the Fe-Adh domain of *adhE1* in *C. autoethanogenum* was independently inactivated using ClosTron, resulting in mutant '*adhE1b*' (Figure 5.1). When this mutant was grown heterotrophically, the peak level of ethanol produced was equivalent to that seen with the *C. autoethanogenum* WT and *adhE1a* mutant. This suggests that the difference in domain inactivation did not result in significant variation in mutant phenotypes.

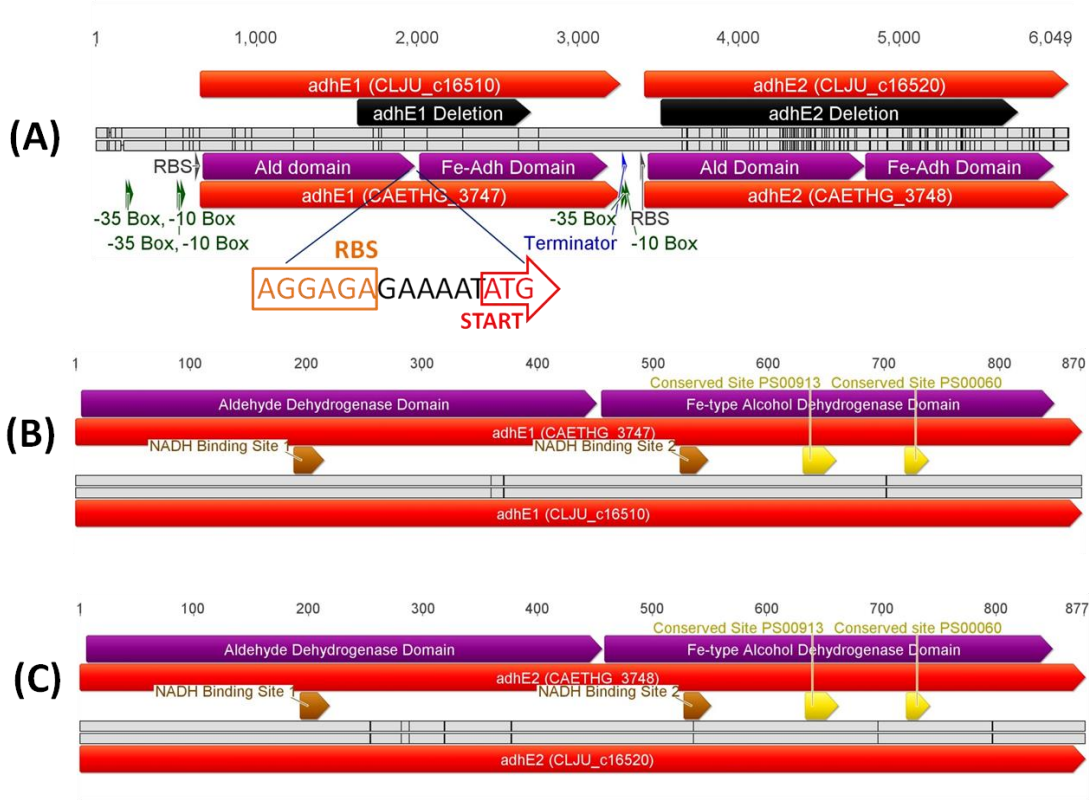


Figure 5.9. Nucleotide and deduced amino acid alignment of *adhE* between *C. autoethanogenum* (CAETHG) and *C. ljungdahlii* (CLJU_c). (A) Nucleotide alignment of *adhE1* and *adhE2* between *C. ljungdahlii* and *C. autoethanogenum* highlighting the regions of deletion (black blocks) in *C. ljungdahlii* created by Leang *et al.* (2013) (229) and a putative ribosomal binding site (RBS) and start codon prior to Fe-Adh domain of *adhE1* in *C. autoethanogenum*; (B) Amino acid alignment of AdhE1; and (C) Amino acid alignment of AdhE2. Variations are marked in black or as gaps in the gray sequence bar between the red annotations. Predicted catalytic domains (purple blocks), promoter elements (green triangles), transcriptional terminator (blue triangles), RBS (grey triangles), NADH binding sites (brown blocks) and conserved sites (yellow blocks) are shown. Figure is generated using Geneious 6.1.7 (Biomatters Ltd).

Besides domain-specific inactivation via ClosTron mutagenesis, this study also embarked on the creation of a Δ*adhE1* mutant. Sanger sequencing confirmed the successful deletion of both the Ald and Adh domains of *adhE1*, but an unwanted 84 bp deletion in the promoter region of *adhE2* was also detected. Termed '$\Delta adhE1^{mut}$' mutant, the unintended deletion likely occurred via homologous recombination between two 9 bp repeats, resulting in the removal of a putative transcriptional terminator and the -10 and -35 boxes of the *adhE2* promoter (Figure 5.6D). Although

the putative promoter of *adhE2* was accidentally deleted, *adhE2* transcription may still proceed from the promoter of the deleted *adhE1* (Figure 5.1).

The gene expression study using qRT-PCR of cDNA generated from fructose-grown cells showed that not only is *adhE2* transcribed from early exponential phase to stationary phase, its levels are also significantly higher in the Δ*adhE1*^{mut} mutant compared to the Δ*pyrE* strain. More specifically, *adhE2* mRNA level is 1360x, 15x and 75x higher in Δ*adhE1*^{mut} mutant at early exponential phase, late exponential phase and stationary phase, respectively. Indirectly these results showed that the promoter of *adhE1* is stronger than the native promoter of *adhE2*, and *adhE1* is transcribed at higher level than *adhE2* in *C. autoethanogenum*. In support of results obtained from the ClosTron mutants *adhE1a* and *adhE1b*, the Δ*adhE1*^{mut} mutant also synthesized similar amount of ethanol when growing on fructose as the Δ*pyrE* control strain. These results provided further evidence that, irrespective of which domain is inactivated, AdhE1 is not required in *C. autoethanogenum* for ethanol formation under heterotrophic conditions.

5.6.2 Inactivation of *adhE2* in *C. autoethanogenum* Reduced Fructose Utilization and Ethanol Formation Under Heterotrophic Conditions

In *C. autoethanogenum*, AdhE1 and AdhE2 share 86% (762/877) AA sequence identity and 93% (818/877) similarity. The presence of a transcriptional terminator, -10 box, -35 box and RBS in the promoter region of *adhE2* in *C autoethanogenum* (Figure 5.9A) raised the possibilities that the *adhE1* and *adhE2* may be differentially expressed. In this study, a mutant which has a ClosTron inserted into the Ald domain of *adhE2* was generated in *C. autoethanogenum*. While growing on fructose, this *adhE2* mutant reached an OD_{600} 28% lower than the WT and was unable to consume all the available substrate - even after prolonged incubation for 13 days. Despite the lower OD_{600} and incomplete fructose utilization, the mutant synthesized 39% more acetate but generated 63% less ethanol than the WT. Furthermore, 79% less 2,3-butanediol was detected in the *adhE2* mutant culture relative to the WT.

The dramatic decrease in ethanol production exhibited by the *adhE2* mutant was partially due to incomplete fructose utilization (0.92 g/L fructose remained). However, the mutant was able to generate more acetate than the WT, which suggests fundamental changes in product profile. In *C. ljungdahlii*, an *adhE2* deletion mutant was generated by replacing most of the Ald and Adh domains with *ermC* using homologous recombination (Figure 5.9A) (229). Unlike the *C. autoethanogenum adhE2* ClosTron mutant, the *C. ljungdahlii adhE2* deletion mutant showed no defect in ethanol formation when compared to the WT under heterotrophic conditions (229).

AA sequence alignment of AdhE2 between *C. autoethanogenum* and *C. ljungdahlii* revealed 8 mismatches (Figure 5.9C). One of the AA changes, serine at residue 536 of *C. autoethanogenum* vs alanine in *C. ljungdahlii,* occurs in the predicted NADH binding site 2 of the Adh domain (prediction made based on (356)). In addition, another residue change at position 697 occurs near one of the conserved sites (Prosite PS00060). It is possible that one of these AA alterations resulted in a change in substrate and/or cofactor specificity. For instance, one of the two non-synonymous AA substitutions in the Fe-Adh domain of *C. thermocellum* AdhE (Cthe_0423) was predicted to alter cofactor specificity from NADH to NADPH (357). The change in cofactor specificity is expected to have significant impact on electron and carbon flows because NADH is commonly used in catabolic reactions whereas NADPH is usually employed as reductant in anabolic processes (358). In crude extracts of fructose-grown *C. autoethanogenum*, Ald and Adh activities are mainly NADH-linked (96). In CO-grown cells, both NADH and NADPH were used as a cofactor for Ald and Adh activities (89).

5.6.3 Inactivation of Either *adhE1* or *adhE2* in *C. autoethanogenum* Increased Ethanol Production In the Presence of CO

During autotrophic growth ATP is considered to be limited (140) so disruption of the recycling of reducing equivalents due to *adhE* inactivation is likely to affect acetogenesis and biomass accumulation. In support of this notion, all three *adhE*

ClosTron (*adhE1a*, *adhE1b* and *adhE2*) mutants of *C. autoethanogenum* showed significant growth retardation while growing on pure CO. These mutants experienced prolonged growth lag phases and reached a much reduced cell density equivalent to only 45-53% of the level attained by the WT. In comparison to the *adhE1a* mutant (which has ClosTron insertion within the Ald domain), the *adhE1b* mutant displayed a milder growth lag phase and was less affected in acetate synthesis. This result is consistent with the hypothesis that the function of the upstream Ald domain of the *adhE1b* mutant is at least partially retained.

Surprisingly, all three *adhE* mutants were able to generate 154 – 183% more ethanol while growing on CO, despite only reaching approximately half of the WT OD_{600}. This increase in ethanol was partially offset by a 48 – 68% decrease in 2,3-butanediol production when compared to the WT. In addition to growth on pure CO, the *adhE1a* mutant was also subjected to growth using BOF gas (composition: 51.24% CO, 31.22% N_2, 11.98% CO_2, and 3.05% H_2). The mutant generated 51% more ethanol and 39% less acetate than the WT under these conditions, providing further evidence that inactivation of *adhE1* favours ethanol production in the presence of CO.

The Δ*adhE1*^{mut} mutant is an interesting strain to study because it has both domains of *adhE1* completely deleted but also an up-regulated *adhE2* expression due to unintended deletion of a putative transcriptional terminator in the 3`-UTR of *adhE1*. Although the elevated *adhE2* expression was determined under heterotrophic conditions, it is possible that the use of the *adhE1* promoter to drive *adhE2* transcription and translation could lead to higher *adhE2* expression under autotrophic conditions. This enhanced *adhE2* expression may compensate for the loss of AdhE1 activity in the Δ*adhE1*^{mut} mutant. In agreement with this hypothesis, when compared to either *adhE1a* or *adhE1b* mutants, the Δ*adhE1*^{mut} mutant displayed a milder growth defect and generated similar amounts of acetate and 2,3-butanediol to the Δ*pyrE* control strain while growing on pure CO. Consistent with the enhanced ethanol production phenotype under CO conditions, the Δ*adhE1*^{mut} mutant generated 27% more ethanol than the Δ*pyrE* control strain, which is less significant than the 171 - 183% increase recorded by both *adhE1a* and *adhE1b* mutants. Since none of the *C. ljungdahlii adhE* deletion mutants constructed by

Leang and co-workers (229) were subjected to autotrophic growth experiments, no comparison could be made to the phenotypes observed in this study.

5.6.4 Effects of *adhE* Inactivation on Solventogenesis and ATP Synthesis Under Autotrophic Conditions

Given the consistent enhanced ethanol production exhibited by all the mutants (*adhE1a, adhE1b, adhE2*, and Δ*adhE1*^{mut}) generated in this study when grown on pure CO and BOF gas, it is worthwhile to investigate possible mechanisms that may lead to this phenotype. In ethanol-producing acetogens, such as *C. autoethanogenum*, *C. ljungdahlii* and *C. carboxidivorans*, there are two biochemical pathways that lead to ethanol formation. One involves the two-step sequential reduction of acetyl-CoA into ethanol via acetaldehyde through the actions of bi-functional AdhE, and an indirect route that proceeds via acetate synthesis and employs Aor to catalyze the reduction of acetic acid to acetaldehyde followed by ethanol synthesis via Adh (Figure 5.10).

Although AdhE is a bi-functional enzyme with both Ald and Adh activities, there is growing biochemical evidence that it functions predominantly in reduction of acetyl-CoA to acetaldehyde. For instance, the Δ*adhE* mutant in *Thermoanaerobacter mathranii* is defective in Ald activity while retaining Adh activity (359). Furthermore, enzymatic assays of AdhE purified from *C. acetobutylicum* and *T. ethanolicus* demonstrated high Ald activity but low Adh activity (149, 346). It is noteworthy that the genomes of *C. autoethanogenum* (38) and *C. ljungdahlii* (37) contain at least 15 Adh isozymes, one of which was shown to reduce acetaldehyde to ethanol (135).

Assuming the AdhE of *C. autoethanogenum* functions predominantly as an aldehyde dehydrogenase, the inactivation of *adhE* may result in the utilization of the indirect ethanol formation pathway by increasing the availability of acetyl-CoA for acetate synthesis and ethanol formation via Aor and Adh (Figure 5.10). The generation of ATP via SLP during acetate production is crucial under ATP-limiting autotrophic growth conditions. Stoichiometric and energetic analysis of the acetogenic pathway showed that very little ethanol can be generated autotrophically without first the ATP-

generating step of acetate formation and then conversion to acetaldehyde via the action of Aor (140). In the presence of CO, the reduced ferredoxins required for Aor can be generated via the actions of CODH (Figure 5.10).

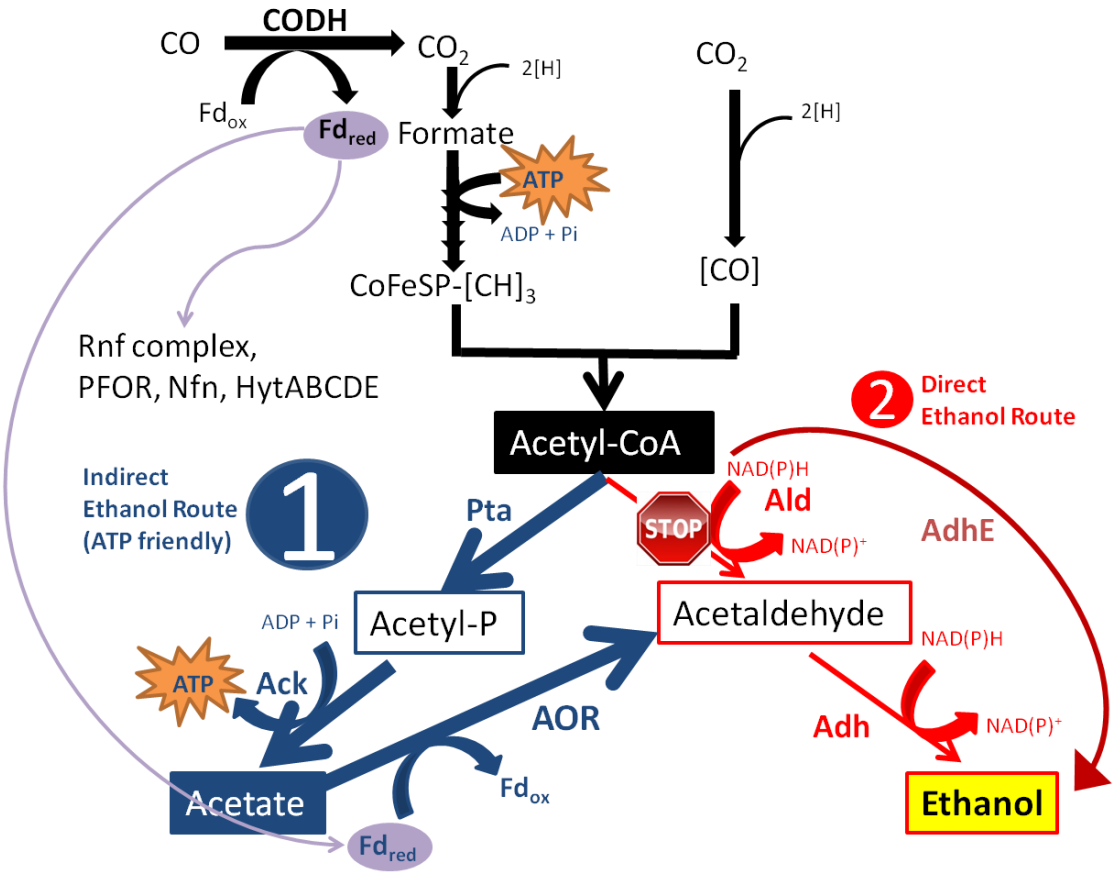


Figure 5.10. Proposed change in metabolic route to ethanol formation in *C. autoethanogenum adhE* mutants under autotrophic conditions. The inactivation of AdhE may decrease carbon and electron flow towards direct ethanol route 2 (coloured in red) by diminishing aldehyde dehydrogenase (Ald) activity (shown as 'STOP' sign). In turn, the indirect ethanol route 1 (coloured in blue) is favoured for ethanol synthesis via the combined actions of phosphotransacetylase (Pta), acetate kinase (Ack) and aldehyde:ferredoxin oxidoreductase (Aor). Adh = alcohol dehydrogenase; CODH = carbon monoxide dehydrogenase; CoFeSP = corrinoid iron sulphur protein; Fd_{ox} = oxidized ferredoxin; Fd_{red} = reduced ferredoxin; HytABCDE = electron bifurcating hydrogenase; PFOR = pyruvate:ferredoxin oxidoreductase.

It should be emphasized that in addition to *adhE1* and *adhE2*, there are three more putative *ald* genes encoded in the genome of *C. autoethanogenum*: CAETHG_1819 (*ald1*), CAETHG_1830 (*ald2*) and CAETHG_3287 (*ald3*). ClosTron mutants for *ald1* and

ald3 were generated (data not shown) but not characterized due to time constraints. ClosTron mutagenesis was attempted once for *ald2* but was not successful. Interestingly, all three *ald* genes in *C. autoethanogenum* are located in the vicinity of microcompartment genes. Microcompartments are protein-based organelles in bacteria that encapsulate functionally related enzymes and leads to sequestration of volatile and toxic intermediates (360-362). Currently the functional relevance of the genetic co-localization of *ald* and microcompartment genes is unclear, but it may enhance the reversible reduction of acetyl-CoA to acetaldehyde by trapping and insulating the cells from the volatile and toxic acetaldehyde intermediates. In contrast, none of the two *aor* genes in *C. autoethanogenum* is genetically located near microcompartment genes, which suggests fundamental differences between direct and indirect ethanol formation pathways.

In crude extracts of CO-grown *C. autoethanogenum*, the enzymatic activity of Ald was reported as 0.06 – 0.08 U/mg using either NAD^+ or $NADP^+$, whereas the enzymatic activity of Adh was recorded as 0.15 – 0.2 U/mg using either NADH or NADPH (89). The ~2-fold lower Ald activity indicates inactivation of *adhE1* and/or *adhE2* may significantly divert carbon and electron flow from the direct ethanol metabolic route to the ATP-friendly, indirect ethanol metabolic route. Conversely, the high Adh activities from CO-grown crude extracts of *C. autoethanogenum* implied that any loss in Adh activity due to *adhE* inactivation can be compensated by the presence of 15 other *adh* genes predicted in the genome.

5.7 Chapter Summary

The construction and characterization of *C. autoethanogenum adhE* mutants represents a first step in helping to understand the metabolic pathways involved in ethanol biosynthesis. The role of AdhE in ethanol formation under heterotrophic conditions has been well documented in several microbes, including *C. ljungdahlii* (229, 230), *C. acetobutylicum* (149), *C. thermocellum* (350), *G. thermoglucosidasius* (349), *T. ethanolicus* (346), *E. coli* (347), and *L. lactis* (348). However, the role of AdhE under autotrophic conditions is largely unknown.

In the presence of CO, both *adhE1* and *adhE2* mutants constructed in this study showed some growth deficiencies but they were able to generate substantially more ethanol than the WT control. The autotrophic growth deficiencies of these mutants may reflect difficulties in recycling reducing equivalents. Since literature findings showed that AdhE functions mainly as aldehyde dehydrogenase, it is possible that the inactivation of *adhE* in *C. autoethanogenum* predominantly affected the Ald activity of the direct ethanol route. As a result of this metabolic blockage, it is hypothesized that the indirect ethanol route involving ATP-generating acetate production and Aor was deployed. In addition to the two *adhE*, there are 3 other *ald* genes in the genome of *C. autoethanogenum* so generation of a triple *ald* KO mutant may provide a more appropriate background to assess the impact of *adhE* inactivation.

While growing on fructose, ethanol production by the *C. autoethanogenum adhE1* ClosTron and IFD mutants was not affected. In contrast, the *adhE2* ClosTron mutant displayed incomplete fructose utilization and diminished ethanol synthesis. Surprisingly, the *adhE1* but not the *adhE2* of *C. ljungdahlii* was found to be the homolog responsible for ethanol formation under heterotrophic conditions (229, 230). AA sequence comparison of AdhE1 and AdhE2 between *C. autoethanogenum* and *C. ljungdahlii* revealed only three substitutions in AdhE1 and eight mismatches in AdhE2. However, it is possible one of these substitutions results in modification of substrate and cofactor specificities, as demonstrated by the change of cofactor from NADH to NADPH in the AdhE of *C. thermocellum* due to one of the two non-synonymous substitutions in the Fe-Adh domain (357). An alternative explanation is that *C. autoethanogenum* may possess other enzymes that compensate for the loss of AdhE activities while growing on fructose.

To provide unambiguous evidence for the role of AdhE under autotrophic conditions, future studies may involve the cloning, purification and enzymatic assays of AdhE in the presence of CO. The expression and characterization of mono-domain AdhE may also provide valuable information regarding the contribution of the individual domains towards Ald and Adh activities. In addition, comparative transcriptomics can be deployed to determine if the *adhE* gene in *C. autoethanogenum* exhibits different

expression profiles to *C. ljungdahlii* during heterotrophic growth. It may also be informative to compare the transcriptomes between *C. autoethanogenum* WT and *adhE* mutants under autotrophic conditions to identify the genes/pathways that are responsible for the elevated ethanol production.

The vastly improved ethanol production displayed by the *adhE* mutants while growing autotrophically may represent a novel metabolic engineering strategy to deliberately manipulate the flux of acetyl-CoA towards the ATP-friendly, indirect ethanol route. Further inactivation of *ald* genes in *C. autoethanogenum* may generate a hyper-ethanol producing strain for industrial gas fermentation. In *C. acetobutylicum*, the direct butanol-forming route was reinforced by disruption of *pta* and *buk*, coupled with overexpression of a mutated *adhE* to result in a mutant that produced 160% more butanol than the WT when grown on glucose (363). Although the *C. autoethanogenum adhE* mutants displayed growth defects while growing in CO, adaptive evolution strategies may be applied to reduce the growth lag phase and raise biomass levels.

CHAPTER 6

GENERATION AND CHARACTERIZATION OF ALDEHYDE:FERREDOXIN OXIDOREDUCTASE MUTANTS

6 Generation and Characterization of Aldehyde:Ferredoxin Oxidoreductase Mutants

6.1 Introduction

Through the actions of Pta and Ack, the production of acetate with concomitant ATP synthesis via SLP from the central molecule acetyl-CoA is one of the hallmarks of acetogens (25, 31). However, the overproduction of acetate during non-pH controlled, batch fermentation can lead to the so-called 'Acid crash' (364). Undissociated acetic acid (pKa = 4.7) can diffuse through cell membranes whereas anionic acetate cannot. As a result, accumulation of acetate inside the cell occurs when the extracellular pH is lower than the intracellular pH, producing osmotic swelling. Moreover, the deprotonation of acetic acid inside cell can trigger a collapse of transmembrane proton gradient and impairment of nutrient transport (365).

In solventogenic clostridia such as *C. acetobutylicum* and *C. beijerinckii*, the produced acetic acid and butyric acid can be reassimilated via the actions of CtfA and CtfB to defend against over-acidification. Acetogens such as *C. autoethanogenum* and *C. ljungdahlii* do not possess such a defence mechanism, instead their genomes encode aldehyde:ferredoxin oxidoreductase (Aor) (37, 38). This enzyme catalyzes the reversible reduction of carboxylic acid to aldehydes using reduced ferredoxin (366-369). The resultant aldehydes can subsequently be reduced to alcohols via Adh. Stoichiometric and energetic analysis of this pathway indicated that Aor may be responsible for ethanol production in acetogens during autotrophic growth (140). This is because Aor allows the synthesis of ethanol via acetate, which generates a valuable ATP via SLP in an otherwise ATP-limiting system. Unsurprisingly, prominent acetogenic alcohol producers such as *C. ljungdahlii*, *C. autoethanogenum*, *C. carboxidivorans*, and *C. ragsdalei* all harbour *aor* gene(s) in their genomes (37-39, 141).

Thermodynamically the reduction of carboxylic acid to aldehyde is very unfavourable (ΔG^{o} ~ 8 kJ/mol) (90) because of the extremely low potential reaction (E'_{o} = -580 mV) (370). Purified Aor enzymes of *M. thermoacetica*, *C. formicoaceticum* and

Thermococcus strain ES-1 perform carboxylic acid reduction using reduced viologen at 5 - 20% the rate of aldehyde oxidation (366, 371-373). Nonetheless, whole cell experiments and enzymatic assays of purified Aor proteins demonstrated the reduction of carboxylic acids to aldehydes/alcohols in a range of acetogens, including *M. thermoacetica*, *C. formicoaceticum*, *B. methylotrophicum*, *E. limosum*, *C. ragsdalei*, *C. ljungdahlii, C. carboxidivorans* and *Alkalibaculum bacchii* (137-139, 374). The crystal structure of Aor from *Pyrococcus furiosus* identified a channel that is sufficiently spacious to accommodate a range of substrates including aliphatic and aromatic aldehydes (369). This is consistent with the reports that Aor-harbouring acetogens such as *C. ljungdahlii* and *C. ragsdalei* are able to reduce a range of carboxylic acids such as acetic, propionic, n-butyric, isobutyric, n-valeric, and n-caproic acids to their respective alcohols in the presence of CO (141, 374).

Two *aor* genes were identified in the genome of *C. autoethanogenum*: CAETHG_0092 (*aor1*) and CAETHG_0102 (*aor2*). At the AA level, both Aors are of the same length and share 78% (478/607) AA sequence identity and 88% (537/607) similarity (Figure 6.1C). Neither are located in the genome within the immediate vicinity of microcompartment genes but both are associated with σ_{54} transcriptional regulators (Figure 6.1A & B). Both Aor1 and Aor2 in *C. autoethanogenum* share 100% AA identity with the corresponding Aor in *C. ljungdahlii* (CLJU_c20110 and CLJU_c20210, respectively). In comparison, the Aor1 of *C. autoethanogenum* only shares 79% AA identity with Aor of *C. carboxidivorans* (CcarbDRAFT_RS16365) and 36% AA identity with Aor of *M. thermoacetica* (Moth_0154).

In this study, ClosTron mutagenesis was employed to independently inactivate both Aors in *C. autoethanogenum*. Subsequent characterization of the KO mutants under autotrophic and heterotrophic conditions shed some light on the functions of these proteins during solventogenesis. Furthermore, plasmid overexpression of *aor1* and the construction of double KO of *aor1* and *aor2* were also undertaken.

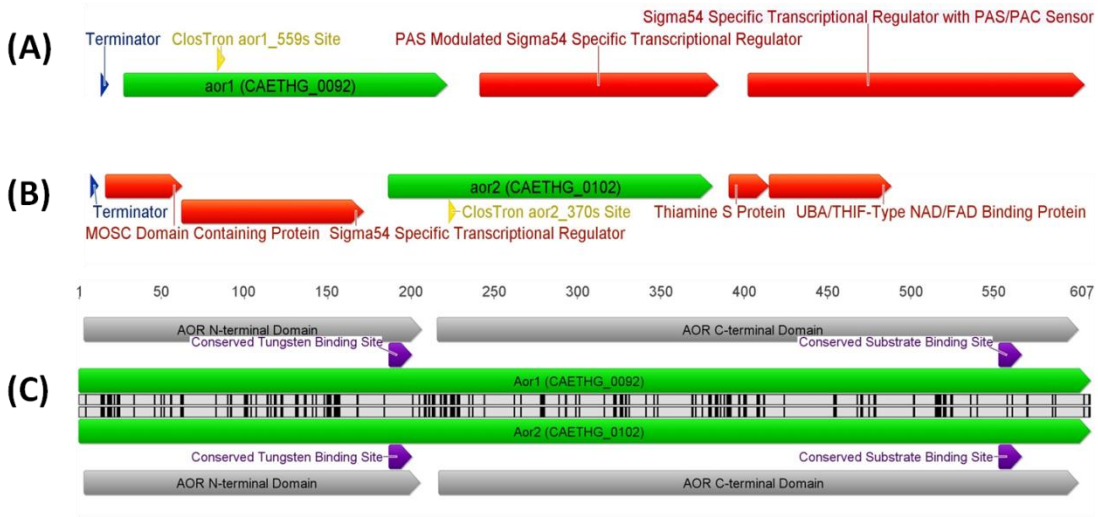


Figure 6.1. Gene arrangement and alignment of *C. autoethanogenum aor1* (CAETHG_0092) and *aor2* (CAETHG_0102). (A) Gene arrangement of *aor1*; (B) Gene arrangement of *aor2*; and (C) Amino acid alignment of Aor1 and Aor2. Variations are marked in black or as gaps in the grey sequence bar between the green annotations in (C). ClosTron insertion sites are shown as yellow triangles. Figure is drawn to scale between (A) and (B), and generated using Geneious 6.1.7 (Biomatters Ltd).

6.2 Generation of ClosTron Knockout Mutants *aor1* and *aor2*

To generate independent knockout mutants of *aor1* and *aor2*, ClosTron plasmids pMTL007C-E2::aor1-559s, and pMTL007C-E2::aor2-370s, respectively, were conjugated into *C. autoethanogenum* according to section 2.12.3. The ClosTron insertion sites are highlighted in Figure 6.1A & B. Clarithromycin resistant colonies were subjected to PCR screening using primer pairs 'aor1-559s-F' and 'aor1-559s-R' for *aor1* mutant, and 'aor2-370s-F' and 'aor2-370s-R' for *aor2* mutant. The screened clones showed the expected 2.1-2.2 kb bands (Figure 6.2A) and these PCR products were verified by Sanger sequencing. The ClosTron mutants were streaked onto the same selective medium until the ClosTron plasmids had been cured (shown by patch plating). As final validation, Southern Blot analysis was performed to confirm that a ClosTron insertion event had occurred only once per mutant (Figure 6.2B).

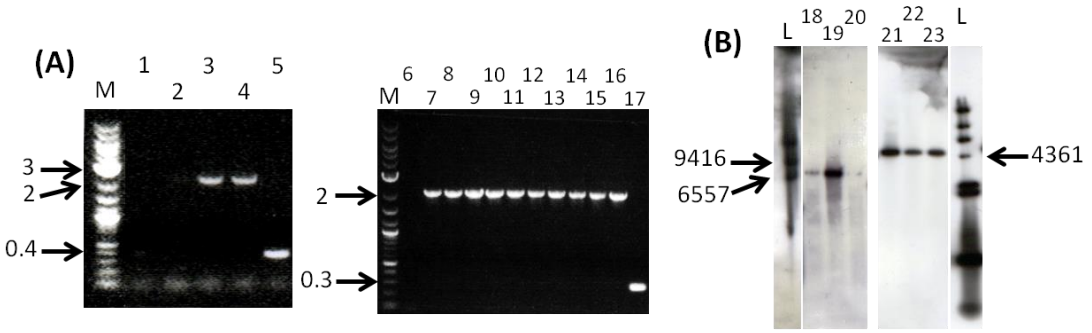


Figure 6.2. Screening and validation of *aor1* and *aor2* ClosTron Mutants. (A) Gel electrophoresis of PCR using exon-spanning primers; Lanes 3 & 4 = *aor1* mutants; Lanes 7 – 16 = *aor2* mutants; Lanes 1 & 6= Non-template controls; Lanes 5 & 17 = WT controls; M = NEB 2-log DNA ladder in kb; (B) Southern Blot analysis of *Hind*III digested genomic DNA of *aor1* mutants (lanes 18 – 20), and *aor2* mutants (lanes 21 – 23); L = Promega Lambda DNA/*Hind*III marker in bp.

6.2.1 Generation of *aor1* Complementation and Overexpression Mutants

For complementation of the *aor1* ClosTron mutant and plasmid overexpression of *aor1* in a WT *C. autoethanogenum* background, the native *aor1* gene was cloned into plasmid pMTL83157 (section 4.3.2). Due to the presence of two interfering *Nde*I restriction sites, two rounds of SOE PCR were performed to alter the nucleotides while retaining the same amino acids. In both cases, nucleotides 'CATATG' were mutated to 'CTTATG' and the altered codons are only 2.5 - 10% less frequent than the original codons within *aor1*. The first round of SOE-PCR utilized oligonucleotides 'aor1-NdeI-F', 'aor1-SOE-B1', 'aor1-SOE-C1' and 'aor1-KpnI-R' to mutate the first *Nde*I site at nucleotide number 975. The resultant PCR product was used as template for the second SOE-PCR using primers 'aor1-NdeI-F', 'aor1-SOE-B2', 'aor1-SOE-C2' and 'aor1-KpnI-R' to mutate the second *Nde*I site at nucleotide number 1284. This codon-altered *aor1* was then cloned into plasmid pMTL83157 using restriction sites *Nde*I and *Kpn*I, resulting in plasmid 'pMTL83157-aor1'. The cloned promoter and *aor1* were verified by Sanger sequencing.

With the aim of restoring Aor1 function, plasmid 'pMTL83157-aor1' was conjugated into the *aor1* ClosTron mutant. In addition, this plasmid was also conjugated into *C. autoethanogenum* WT to create an *aor1* overexpression strain. Figure 6.3A shows that PCR of *aor1* using exon-spanning primers produced the expected 388 bp for the WT and 2188 bp for *aor1* ClosTron mutants. The presence of 388 bp WT band in *aor1*

ClosTron mutants was due to carryover of complementation plasmid from genomic DNA extraction. Plasmid rescue followed by restriction digest analysis using *Asc*I and *Pme*I restriction enzymes also generated the expected 4408 bp and 2424 bp products (Figure 6.3B). The plasmid control pMTL83157 strain was constructed as described in section 4.3.2.

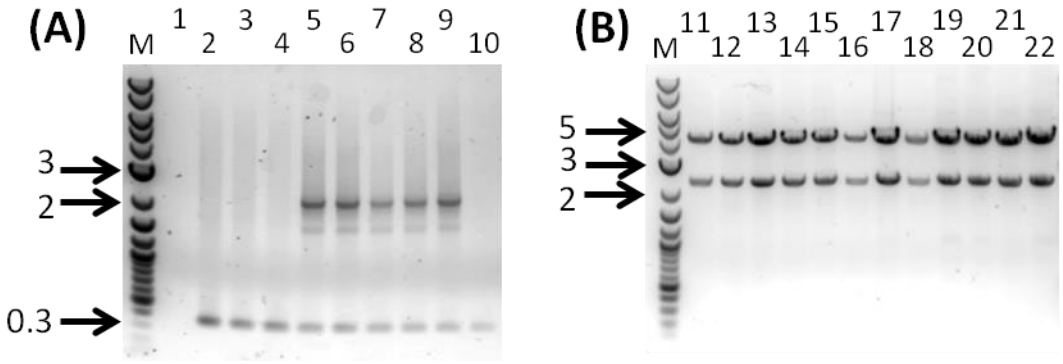


Figure 6.3. Verification of complemented and overexpressed *aor1* mutants. (A) PCR of genomic DNA from overexpressed *aor1* mutants (lanes 2-4) and complemented *aor1* mutants (lanes 5-9) using exon spanning *aor1* primers; M = NEB 2-Log DNA ladder; 1 = non-template control; 10 = WT genomic DNA control; (B) AscI and PmeI restriction digests of rescued plasmids pMTL83157-AOR1 from overexpression mutants (lanes 11-16) and complemented mutants (lanes 17-22).

6.3 Characterization of ClosTron Knockout Mutants *aor1* and *aor2*

6.3.1 Autotrophic Growth Experiment

Serum bottle growth experiments in the presence of CO were carried out to assess the impact of *aor* inactivation in *C. autoethanogenum*. Each 250 mL serum bottle contained 50 mL CGMY medium with 2 bar CO headspace, or 100 mL CGMY medium with 2 bar BOF gas (composition: 51.24% CO, 31.22% N_2, 11.98% CO_2, and 3.05% H_2) harvested from Glenbrook, New Zealand. Incubation was carried out at 37^{o}C with agitation for up to 43 days for pure CO cultures and 12 days for BOF gas cultures.

On pure CO, the growth of the *aor1* KO mutant experienced a 10 day lag phase and grew to a cell density that was only half that achieved by the WT (p-value <0.0001) (Figure 6.4A). In comparison to the WT, the *aor1* KO mutant was able to generate

similar amounts of acetate, but only 43% of the ethanol (p-value = 0.019) and 23% of 2,3-butanediol (p-value <0.0001) (Figure 6.4B-D). In contrast, the *aor1* KO mutant synthesized 2.6 mM lactate, which was 11-fold higher than that of the WT level (p-value = 0.001) (Figure 6.4E). The plasmid-based expression of *aor1* in the *aor1* KO mutant did not reduce the growth lag phase but slightly increased the final cell density achieved (not statistically significant), reaching an OD_{600} of 1.11 compared to the 0.85 achieved by the WT (Figure 6.4A). The complementation of the *aor1* mutant restored ethanol and lactate back to the WT level, and elevated 2,3-butanediol titres to 4.2 mM compared to the 1.96 mM titres obtained in the *aor1* mutant (p-value = 0.003) (Figure 6.4C-E).

Similar to *aor1* KO mutant, growth of the *aor2* KO mutant on pure CO was characterised by an extended 25 day lag phase and achieved a cell density equivalent to 50% of the WT (p-value = 0.002) (Figure 6.4A). However, relative to the WT, the *aor2* mutant generated 36% less acetate (p-value = 0.0001), 170% more ethanol (p-value = 0.009) and similar levels of 2,3-butanediol and lactate (Figure 6.4B - D). When subjected to growth on BOF gas, the *aor2* KO mutant was able to grow to a similar cell density to the WT (Figure 6.5A). Similar to growth on pure CO, the *aor2* mutant generated 16% less acetate (not statistically significant) than the WT but 93% more ethanol (not statistically significant) (Figure 6.5B & C).

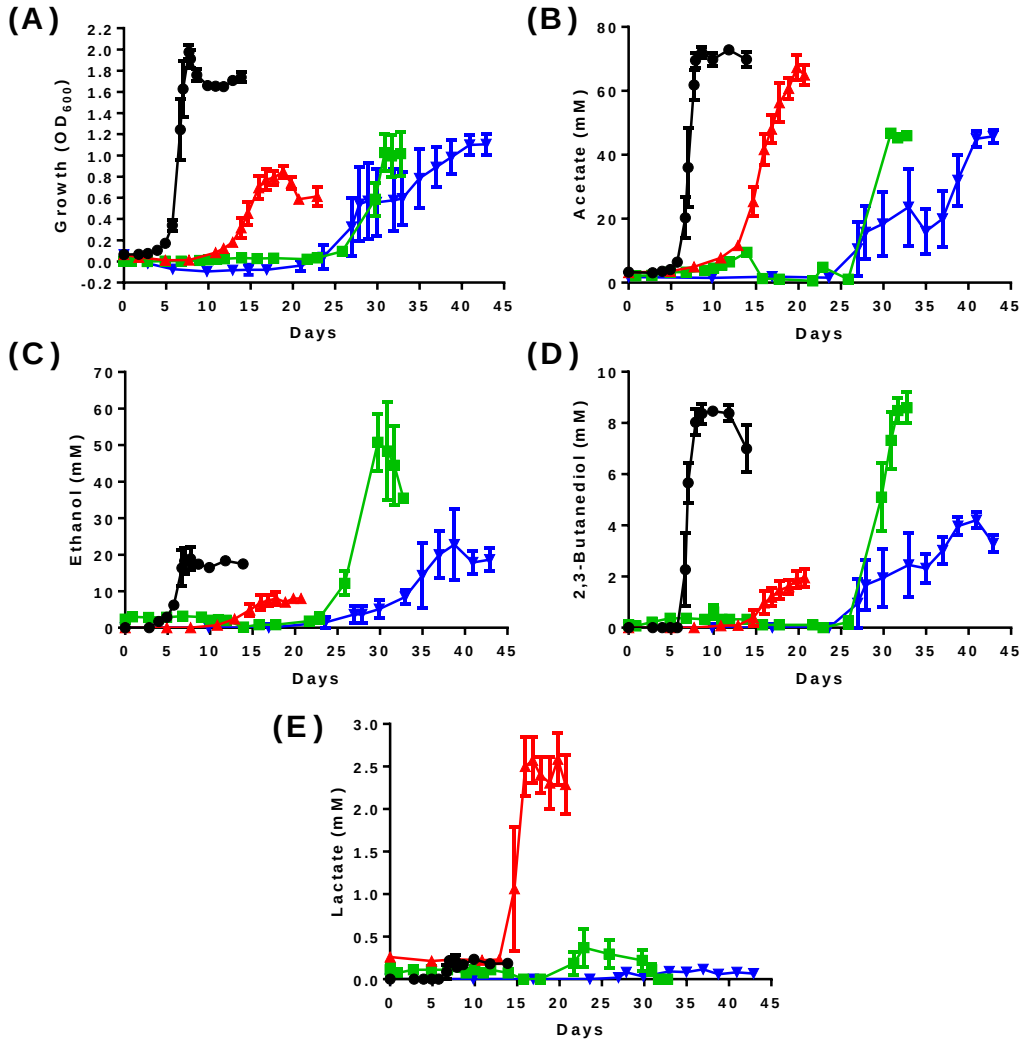


Figure 6.4. Growth and metabolite profiles of *C.* autoethanogenum WT, *aor1* and *aor2* ClosTron mutants on CO. (A) Growth profile; (B) Acetate profile; (C) Ethanol profile; (D) 2,3-Butanediol profile; and (E) Lactate profile. Black circles = WT (N = 4); Red triangles = *aor1* mutants (N = 4); Blue inverted triangles = Complemented *aor1* mutants (N = 4); Green squares = *aor2* mutants (N = 3); Error bars = standard error of mean.

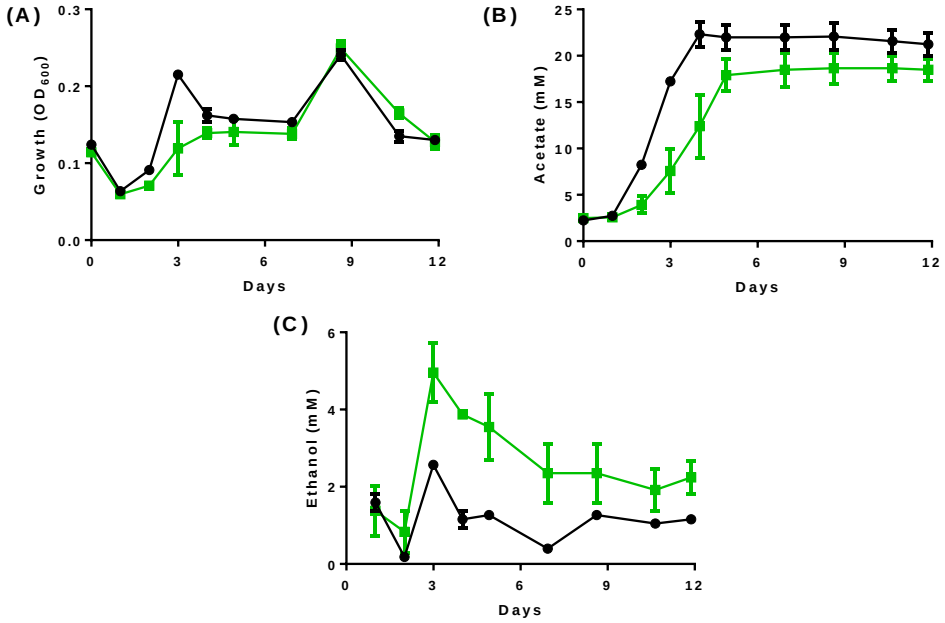


Figure 6.5. Growth and metabolite profiles of *C. autoethanogenum* WT and the *aor2* ClosTron mutant on BOF gas. (A) Growth profile; (B) Acetate profile; and (C) Ethanol profile. Black circles = WT (N = 2); Green squares = *aor2* mutant (N = 2). Error bars = standard error of mean.

6.3.2 Heterotrophic Growth Experiment

For evaluation of the impact of *aor* inactivation on heterotrophic growth, *C. autoethanogenum* and the ClosTron mutants of *aor1* and *aor2* were grown in 250 mL serum bottles containing 50 mL CGMY medium supplemented with 10 g/L fructose (final concentration) with 3 - 4 technical repeats. As shown in Figure 6.6A, both *aor* KO mutants reached similar cell densities, equivalent to the WT. The heterotrophic growth of both experienced a lag phase that was more pronounced with the *aor1* mutant. Compared to the WT, the *aor1* KO mutant generated 21% more acetate (not statistically significant), 33% less ethanol (p-value = 0.014) and 61% less 2,3-butanediol (p-value = 0.018) (Figure 6.6B-D). In contrast, the *aor2* KO mutant synthesized similar amounts of acetate and 2,3-butanediol to the WT, but 47% more ethanol (p-value = 0.003). HPLC results showed that all three strains completely exhausted the provided fructose substrate and little or no lactate was produced (data not shown).

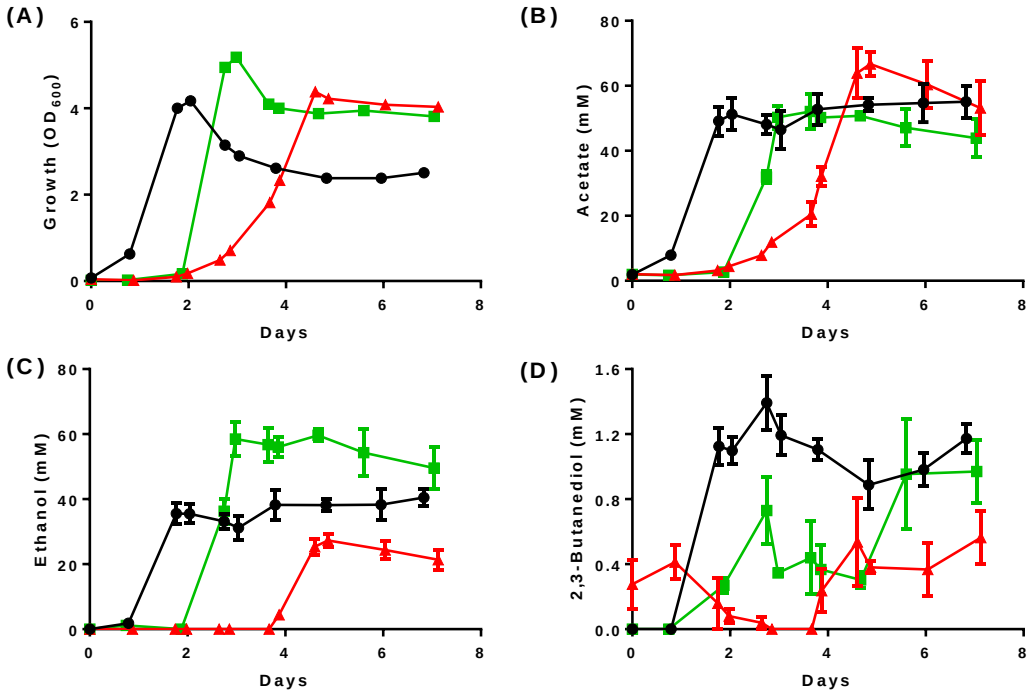


Figure 6.6. Growth and metabolite profiles of *C. autoethanogenum* WT, ClosTron *aor1* and *aor2* mutants growing on fructose. (A) Growth profile; (B) Acetate profile; (C) Ethanol profile; and (D) 2,3-Butanediol profile. Black circles = WT (N = 4); Red triangles = *aor1* mutants (N = 3); Green squares = *aor2* mutants (N = 3); Error bars = standard error of mean.

6.4 Plasmid Overexpression of *aor1*

6.4.1 Comparison of *aor1* mRNA during Heterotrophic Growth using qRT-PCR

The impact of overexpressing *aor1* from a multicopy plasmid on heterotrophic growth was investigated. For comparative purposes, a plasmid-only control (the WT containing plasmid pMTL83157) was also included in the experiment. Both strains were cultured in 500 mL Schott bottles containing 200 mL CGMY medium supplemented with 10 g/L fructose and 7.5 µg/mL thiamphenicol. In addition to routine sampling of liquid cultures for HPLC analysis and OD_{600} measurements, cells were harvested at early exponential phase, late exponential phase, stationary phase and death phase for gene expression analysis according to section 2.9.1. Total RNA was extracted as described in section 2.9.2 and reverse transcribed into cDNA according to section 2.9.3. For qRT-PCR analysis, TaqMan primers and probes were

employed for the two housekeeping genes (*gyrA* and *rho*) and the gene of interest (*aor1*). Given the high nucleotide identity (77%) between *aor1* and *aor2* in *C. autoethanogenum*, the TaqMan primer pairs and probes for *aor1* were carefully designed to ensure high specificity. Standard curves using serially diluted cDNA were generated and the TaqMan primers and probes demonstrated excellent amplification efficiencies (section 2.9.4).

While growing on fructose, the *aor1* overexpression strain showed a slight decrease in growth rate in comparison to the plasmid only control (Figure 6.7A). Furthermore, the overexpression strain produced slightly more acetate but marginally less ethanol, while retaining the same level of 2,3-butanediol production as the control strain (Figure 6.7B - D). As expected, qRT-PCR revealed that the transcript levels of *aor1* in the overexpression strain were higher than in the plasmid only control strain at all examined time-points. In particular, *aor1* mRNA level of the overexpression strain was 3.5-fold and 4.5-fold higher at early exponential phase and death phase (p-values <0.0001), respectively, when compared to the control (Figure 6.7E).

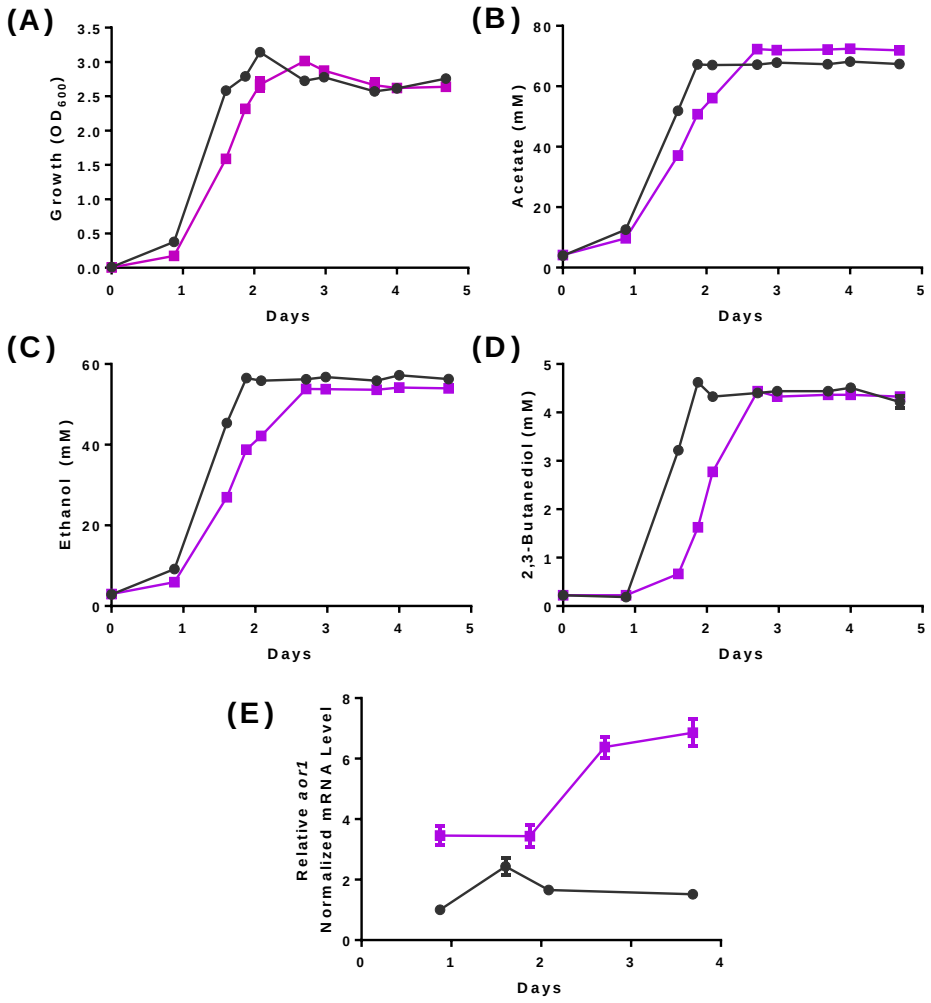


Figure 6.7. The effect of plasmid-borne *aor1* overexpression on *C. autoethanogenum* during fructose fermentation. (A) Growth profile; (B) Acetate profile; (C) Ethanol profile; (D) 2,3-Butanediol profile; and (E) Relative normalized *aor1* mRNA levels. Grey Circles = Plasmid control; Purple squares = *aor1* overexpression strain. Error bars = standard error of mean. N = 3.

6.4.2 Autotrophic Growth Experiment

Both the *aor1* overexpression strain and the plasmid only control strain were cultured in 250 mL serum bottles containing 2 bar CO to examine the effect of *aor1* overexpression on autotrophy and ethanol formation. The serum bottle growth experiment was conducted in technical triplicates or quadruplicates containing 50 mL CGMY medium supplemented with 7.5 µg/mL thiamphenicol. Incubation was undertaken at 37^{o}C with agitation for up to 43 days. In the presence of CO, the growth of the overexpression strain was characterised by an extended lag phase, and

a slower growth rate, but nevertheless achieved a similar cell density to the plasmid-only control strain (Figure 6.8A). The peak ethanol titre was similar for the two strains but the *aor1* overexpression strain produced 31% less acetate (not statistically significant) and 65% less 2,3-butanediol (p-value = 0.001) (Figure 6.8B - D). Moreover, no lactate was detected for the *aor1* overexpression strain, whereas the plasmid only control strain was able to synthesize 0.25 mM lactate (Figure 6.8E).

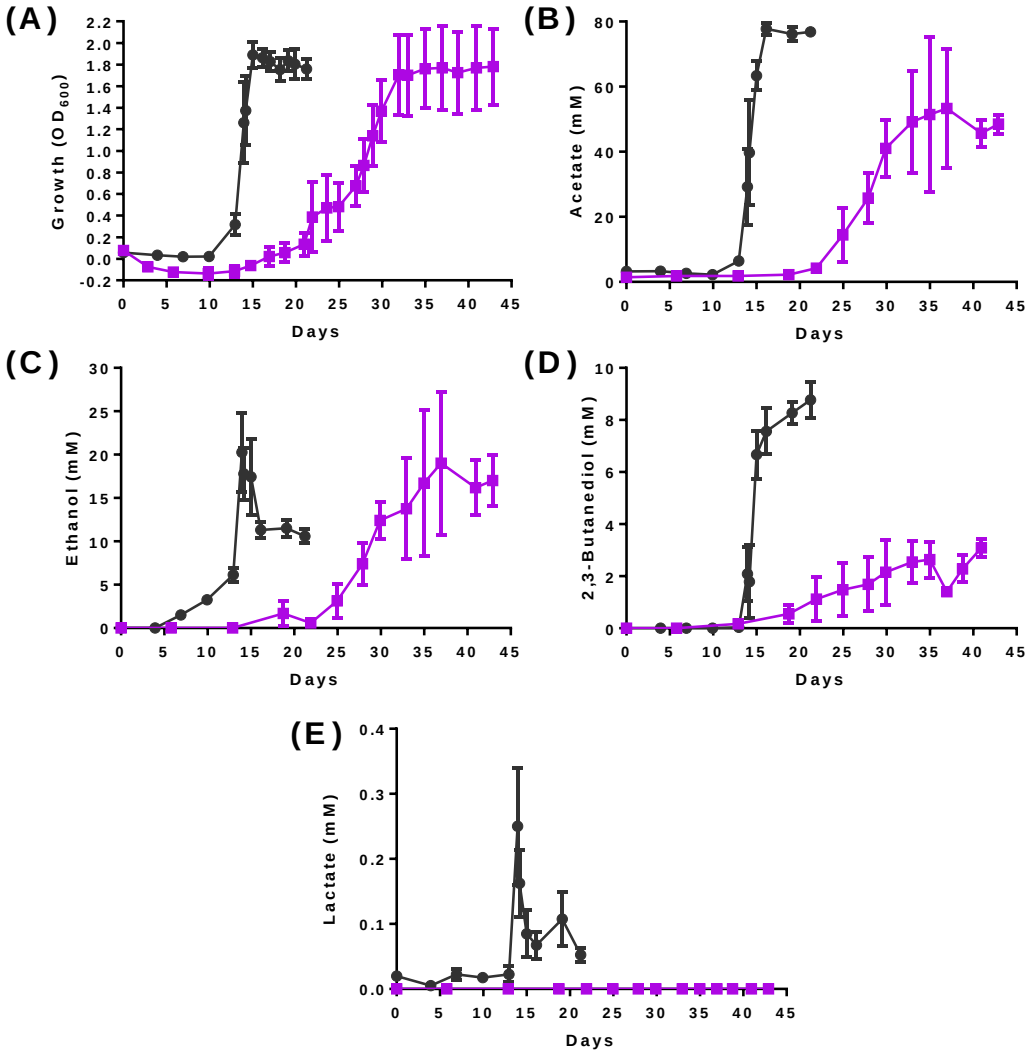


Figure 6.8. The effects of plasmid-borne *aor1* overexpression on *C. autoethanogenum* on CO. (A) Growth profile; (B) Acetate profile; (C) Ethanol profile; (D) 2,3-butanediol profile; and (E) Lactate profile. Grey circles = plasmid control strain (N = 4); Purple squares = *aor1* overexpression strain (N = 3). Error bars = standard error of mean.

6.5 Attempt at Generation of a *aor1*and *aor2* Double Knockout Mutant

The presence of multiple copies of *aor* genes in *C. autoethanogenum* complicates the assessment of mutant phenotype when only one of the two *aor* genes was inactivated, since the unperturbed *aor* may compensate for the loss of activity. The construction of a double KO mutant with both *aor1* and *aor2* inactivated would provide a more useful starting point to study the two routes of ethanol biosynthesis. Due to the inability to recycle the *ermB* marker from ClosTron insertion in *C. autoethanogenum*, a strategy that employs both ClosTron and ACE mutagenesis was attempted to generate a double *aor1* and *aor2* KO mutant.

First, a ClosTron KO of *aor1* was created in the *C. autoethanogenum* Δ*pyrE* strain (section 3.3.5) using ClosTron plasmid pMTL007C-E2::aor1-559s. Screening of clarithromycin resistant colonies using primers 'aor1-559s-F' and 'aor1-559s-R' successfully generated the expected 2.2 kb ClosTron bands (Figure 6.9A, lanes 8 – 11), and the resulting amplicons were verified by Sanger sequencing. Southern Blot analysis also showed that only a single ClosTron insertion had occurred per mutant (Figure 6.9C) and the loss of ClosTron plasmid was demonstrated by the loss of Tm^R (data not shown).

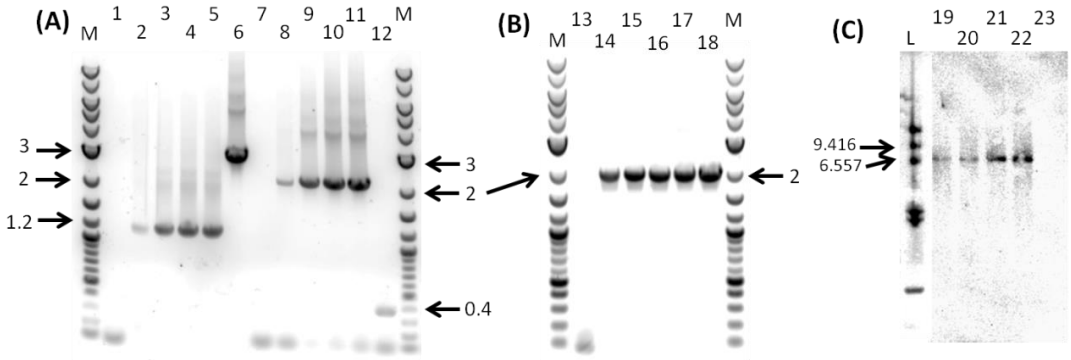


Figure 6.9. Screening and validation of *aor* double KO mutants with restored *pyrE*. (A) PCR screening of Δ*aor2 and aor1* ClosTron mutants; (B) PCR screening of uracil prototrophic *aor* double KO mutants for restored *pyrE* allele; (C) Southern Blot analysis of *aor1* ClosTron mutants. M = NEB 2-log DNA ladder; L = Promega Lambda DNA/*Hin*dIII marker; 1 – 6 = aor2-seq-F and aor2-seq-R primer pair; 7 – 12 = aor1-559s-F and aor1-559s-R primer pair; 13 – 18 = ACE-pyrE-F and ACE-pyrE-R primer pair; 1, 7 and 13 = Non-template controls; 6, 12, 18 and 23 = *C. autoethanogenum* WT genomic DNA control; 2 – 5, 8 – 11, 14 – 17 = clones of *aor* double KO mutants with restored *pyrE*; 19 – 22 = *Hin*dIII digested genomic DNA of *aor1* ClosTron mutants.

The second step of constructing the double KO mutant of *aor1* and *aor2* involved IFD of *aor2* in the above CTermB::aor1-559s Δ*pyrE* strain of *C. autoethanogenum*. The *aor2* IFD plasmid 'pMTL84151-aor2-IFD' was constructed by first undertaking a SOE PCR of the homology arms using oligonucleotides 'aor2-LHA-SacII-F', 'aor2-LHA-R', 'aor2-RHA-F' and 'aor2-RHA-AscI-R', followed by cloning into plasmid pMTL84151-ΔpyrE (Section 2.14.1) using restriction sites *Sac*II and *Asc*I. The cloned homology arms were verified by Sanger sequencing and they were designed to completely delete *aor2* while retaining only the start and stop codons. Following conjugation of this *aor2* IFD plasmid into the CTermB::aor1-559s Δ*pyrE* mutant, faster growing colonies on thiamphenicol solid medium were preferentially streaked onto the same selective medium to identify single crossover mutants.

Since the LHA and RHA are similar in lengths (530 bp and 549 bp, respectively), single crossover should occur at either arm with similar frequency. Oligonucleotides 'IFD-plasmid-F' and 'aor2-370-R' were used to detect integrants in which single-crossover had occurred at the LHA while primers 'aor2-370s-F' and 'IFD-plasmid-R' were employed for the detection of single crossover events mediated by the RHA. PCR screening showed that single-crossover event had occurred at LHA but not RHA (data now shown). The single-crossover mutants were subjected to FOA selection according to section 2.14.1 to select for the second crossover event. FOA^R colonies emerged within 3 days of incubation and they were screened using oligonucleotides 'aor2-Seq-F' and 'aor2-Seq-R' to detect successful IFD of *aor2*. PCR screening of more than 90 FOA^R colonies showed that most of the mutants had reverted back to WT allele of *aor2* because the second crossover event had occurred at the same homology arm as the first. However, four colonies exhibited the expected PCR products (1191 bp) from a successful IFD of *aor2* (Figure 6.9A, lanes 2 – 5) and the amplicons were subsequently verified by Sanger sequencing. Without extensive restreakings, patch plating onto solid medium containing thiamphenicol demonstrated that the IFD plasmid has been lost. To restore *ΔpyrE* back to WT allele, plasmid 'pMTL84151-fix*pyrE*' was conjugated into the *aor* double KO mutant and the procedures described in section 2.14.4 were followed to obtain uracil prototrophic clones. PCR and the subsequent Sanger sequencing using oligonucleotides 'ACE-pyrE-

F' and 'ACE-pyrE-R' showed that the *ΔpyrE* gene had been restored to WT allele. The resultant mutant is termed '*aor1+2*KO' in this report.

6.6 Discussion

6.6.1 Inactivation of *aor1* Diminished Ethanol Production under Autotrophic and Heterotrophic Conditions

Due to potentially limited ATP availability during acetogenesis, the autotrophic synthesis of ethanol is hypothesized to proceed via acetate assisted by Aor (106, 140). Although whole cell experiments with *C. ljungdahlii* demonstrated the reduction of a range of carboxylic acids to their corresponding alcohols using syngas as substrate (374), questions remained regarding the significance of Aor reactions in this process because of the very low redox potential required to catalyse the direct reduction of carboxylic acids. The creation of independent *aor1* and *aor2* KO mutants in this study provides a unique opportunity to assess their roles in solventogenesis under autotrophic and heterotrophic settings.

While growing on pure CO, the *aor1* KO mutant clearly showed growth deficiencies characterized by both lower final cell densities and extended growth lag phases. Despite reaching only half the OD_{600} of WT, the *aor1* mutant was able to generate similar amounts of acetate but only 43% of ethanol produced by the WT. These results indicate not only that Aor1 is involved in ethanol formation, but that the growth defects observed also suggest difficulty in recycling reduced ferredoxin under CO conditions. One potential route for the recycling of excess reduced ferredoxin is the conversion of acetyl-CoA and CO_2 to pyruvate via PFOR, which can lead to the products 2,3-butanediol and lactate. Interestingly, when growing on pure CO, the *aor1* KO mutant showed preferential production of lactate (11x higher than WT) whereas the generation of 2,3-butanediol was reduced by 77%. In order to restore the phenotype of the *aor1* KO mutant, plasmid pMTL83157-aor1 was conjugated into the mutant to create a complementation strain. On pure CO, the presence of the complementation plasmid allowed the *aor1* KO mutant to reach higher cell densities

(up 31%), but did not shorten the lag phase. Ethanol and lactate levels were restored to WT, while 2,3-butanediol synthesis was enhanced – up by 114%.

Under heterotrophic conditions, the inactivation of *aor1* is hypothesized to have lesser impact on growth and solventogenesis in comparison to growth on pure CO, because of lower reduced ferredoxin imbalance and the system is not ATP-limited. Supporting this notion, the *aor1* KO mutant was able to reach similar cell densities to the WT but experienced growth delay when the carbon source was fructose. In comparison to WT, the mutant overproduced acetate by 21%, while ethanol and 2,3-butanediol levels were reduced by 33% and 61%, respectively. Unlike growth in pure CO, the *aor1* KO mutant produced only trace amounts of lactate when growing heterotrophically.

The reduced ethanol production by the *aor1* KO mutant under both autotrophic and heterotrophic conditions strongly suggests that Aor1 is implicated in ethanol synthesis in *C. autoethanogenum*. This result is consistent with a recent publication by Basen *et al*. (2014), who showed that an *aor* deletion mutant (ΔPF0346) of the hyperthermophilic archaeon *P. furiosus* generated 45-fold less ethanol when growing on maltose (142).

6.6.2 Plasmid Overexpression of Aor1 Had No Positive Impact on Ethanol Formation under Autotrophic and Heterotrophic Conditions

Since inactivation of *aor1* resulted in reduced ethanol production, it was hypothesized that the overexpression of *aor1* may increase ethanol synthesis. A plasmid control pMTL83157 strain and overexpression pMTL83157-aor1 strain of *C. autoethanogenum* were constructed to test this hypothesis. qRT-PCR study showed that *aor1* mRNA level of the overexpression strain was increased (up to 4.5-fold) at all growth stages while growing on fructose when compared to the plasmid control strain. However, the increased *aor1* transcript of the overexpression strain did not result in significant changes in the growth and metabolite profiles on fructose.

Although the mRNA level of *aor1* was not examined in the presence of CO, it is anticipated that the promoter P_{acsA} used to drive *aor1* expression is highly active under autotrophic conditions based on the findings of Köpke *et al*. (2011) (53). While growing on 2 bar of CO, the *aor1* overexpression strain displayed an extended growth lag phase but generated similar amounts of ethanol compared to the control that carried only the empty vector. Moreover, overexpression of *aor1* resulted in 31% less acetate, 65% less 2,3-butanediol and the complete abolishment of lactate production.

Collectively, the growth experiments under both heterotrophic and autotrophic settings showed that overexpression of *aor1* has little effect other than prolonging the growth lag phase. The lack of positive effect on ethanol titre can be explained by the findings that *aor1* is already one of the most highly expressed genes (similar level as *rnf* complex) of *C. autoethanogenum* during bioreactor fermentation using H_2- and CO- rich gas mix (Dr. Michael Köpke, LanzaTech; unpublished data).

6.6.3 Inactivation of *aor2* Increased Ethanol Production under Autotrophic and Heterotrophic Conditions

In *C. autoethanogenum*, the two Aor enzymes are of the same length and share 78% AA identities. The *aor1* gene is followed by two σ_{54}–specific transcriptional regulators whereas the *aor2* gene is preceded by a putative σ_{54}–specific transcriptional regulator and followed by genes encoding thiamine S protein and UBA/THIF-type NAD/FAD binding protein (Figure 6.1). Given the different profile and lower expression level of *aor2* relative to *aor1* during H_2- and CO- rich gas fermentation (Dr. Michael Köpke, LanzaTech; unpublished data), it is hypothesized that they may have different significance in ethanol formation in *C. autoethanogenum*.

When growing on pure CO, the *aor2* KO mutant is similar to *aor1* KO mutant in that the growth lag phase is longer than that seen with the WT and the final OD_{600} of the culture is half that attained by the WT. In contrast to the *aor1* mutant, when growing on CO the *aor2* mutant produced, relative to the WT, increased titres of ethanol (170%) and reduced levels of acetate (36%) while retaining the same levels

of 2,3-butanediol and lactate. A similar trend was observed when the *aor2* mutant was grown on BOF gas, and the cultures produced 93% more ethanol and 16% less acetate than the WT. While growing on fructose, the *aor2* mutant achieved a slightly higher OD_{600} than the WT, but exhibited a slightly longer growth lag phase. Similar amounts of acetate and 2,3-butanediol, but 47% more ethanol, were recorded in the *aor2* mutant strain growing on fructose compared to the WT.

Based on these results, the inactivation of *aor2* in *C. autoethanogenum* consistently enhanced ethanol production in both autotrophic and heterotrophic settings, which is the opposite of what was observed with *aor1* mutant. One possible explanation for the contrasting phenotype is that Aor2 functions predominantly in the oxidation of acetaldehyde whereas Aor1 functions predominantly in the reduction of acetic acid. Alternatively, the inactivation of *aor2* may reduce competition for access to substrate by the highly expressed and presumably more efficient Aor1, resulting in increased ethanol production.

6.6.4 Generation of *aor1+2*KO Mutant

The multiplicity of *aor* genes in *C. autoethanogenum* makes it difficult to interpret the phenotype from single *aor* KO mutants, as the unperturbed *aor* genes may compensate for any loss of activity associated with the inactivated gene. Furthermore, the creation of a mutant that is completely deficient in Aor activity may have some industrial applications, for example the creation of an acetone-producing strain because acetate is a precursor for acetone synthesis, so the inactivation of Aor may eliminate the formation of the side product ethanol from acetate.

A combination of ClosTron mutagenesis and allelic-exchange was employed to construct a double *aor* KO mutant due to inability to recycle the ermB marker from ClosTron insertion in *C. autoethanogenum*. Starting from a Δ*pyrE* strain, *aor1* was first disrupted using ClosTron mutagenesis before *aor2* was (in-frame) deleted using *pyrE*-mediated allelic-exchange. During the construction of Δ*aor2* mutant, the identification of the 'correct' second recombination event from single crossover mutant was the most challenging step. PCR screening showed the majority of FOA^R colonies had the second recombination event at the same homology arm, resulting in

reversion back to WT allele. For some unknown reasons, there appeared to be a strong bias for recombination at this homology arm despite very similar lengths of the two homology arms. As a final step, pMTL84151-fixpyrE was conjugated into the double *aor* KO strain to restore Δ*pyrE* back to WT allele, resulting in mutant '*aor1+2KO*' which is uracil prototrophic.

Due to time constraints, the *aor1+2KO* mutant was not characterized in this study. For future studies, serum bottle growth experiments using different growth substrates (pure CO, H_2+CO_2, or fructose) can be conducted to evaluate the impact of Aor elimination on growth and product profile. Given the growth deficiency exhibited by single *aor* KO mutants, it is anticipated that the *aor1+2KO* mutant may grow poorly on CO. As *aor* genes are present in the genomes of prominent acetogenic ethanol producers such as *C. ljungdahlii*, *C. autoethanogenum*, *C. carboxidivorans*, and *C. ragsdalei*, the construction of an *aor* deficient strain provides a unique opportunity to assess the roles of Aor in acetogenic ethanol production. By reintroducing either of the *aor* genes into the *aor1+2KO* mutant, the relative importance of *aor1* and *aor2* in supporting autotrophic growth and/or ethanol formation can be investigated. Furthermore, exogenous carboxylic acids such as *n*-butyric acid, propionic acid, *n*-valeric acid and *n*-caproic acid can be added to the mutants in the presence of CO to determine whether the corresponding primary alcohols are produced.

6.7 Chapter Summary

Given that acetogens are considered to live on the thermodynamic edge of life and the challenges around ATP limitation during acetogenesis, it has been hypothesized that Aor plays a significant role in ethanol production by reducing acetic acid (the synthesis of which generates ATP via SLP) (106, 140). The two *aor* KO mutants generated in this study allowed the examination of the significance of these individual Aors on ethanol formation in *C. autoethanogenum* during both autotrophic and heterotrophic growth. Both *aor* mutants exhibited growth defects when growing on pure CO, which indicates difficulties in recycling reduced ferredoxin generated from the CODH reaction. Given the higher transcript levels of *aor1* than *aor2* in *C.*

autoethanogenum while metabolizing H_2- and CO- rich gas (Dr. Michael Köpke, LanzaTech; unpublished data), it is hypothesized that Aor1 is the predominant enzyme involved in acetogenic ethanol formation. In agreement with this hypothesis, the inactivation of *aor1* reduced ethanol titre by 57% during growth on pure CO and the plasmid expression of *aor1* in the *aor1* KO mutant successfully restored ethanol production. However, plasmid overexpression of *aor1* in *C. autoethanogenum* WT did not increase ethanol formation during either autotrophic or heterotrophic growth.

In contrast to the *aor1* mutant, the inactivation of *aor2* resulted in 170% more ethanol than the WT when growing on CO. Although the *aor2* mutant displayed a significant growth defect while growing on pure CO, this hyper-ethanol producing mutant can be subjected to a prolonged adaptive evolution growth experiments in the presence of CO to select for a fast growing strain. The contrasting phenotype of *aor1* and *aor2* KO mutants points toward divergent roles for the two Aor in *C. autoethanogenum* and further studies are warranted. For instance, the two Aor can be independently cloned, expressed, and purified for enzymatic assays to unambiguously determine their roles and enzyme kinetics.

In comparison to the WT under pure CO conditions, neither of the two *aor* KO mutants generated more 2,3-butanediol, although the *aor1* mutant did produce 11-fold higher lactate. Any excess in availability of reduced ferredoxin as a result of *aor1* inactivation could potentially drive the formation of pyruvate via the action of PFOR, and then lactate is preferentially formed over 2,3-butanediol. If the production of 2,3-butanediol is the preferred product (a valuable platform chemical) over ethanol and lactate, one strategy is to inactivate *aor1, aor2* and lactate dehydrogenase (CAETHG_1147). The successful generation of an *aor* double KO mutant and subsequent restoration of *pyrE* in *C. autoethanogenum* exemplified the combinatorial use of ClosTron mutagenesis and allelic-exchange for complex genetic manipulation in this acetogen. Although this *aor* deficient mutant was not characterized due to time constraints, future studies of this mutant are likely to reveal useful information regarding the roles of the Aor enzymes on autotrophic growth and product formation.

CHAPTER 7

EFFECT OF CHAPERONE OVEREXPRESSION ON PRODUCT FORMATION AND TOLERANCE TOWARDS ETHANOL, HEAT, AND SALINE

7 Effect of Chaperone Overexpression on Product Formation and Tolerance towards Ethanol, Heat, and Saline

7.1 Introduction

One of the major challenges of industrial production of biofuels and biochemicals from bacterial hosts is toxicity towards metabolic end-products, intermediates and potential fermentation by-products. With the exception of a few bacterial species such as *Zymomonas mobilis* (375) and *Lactococcus* strains (376) which can tolerate more than 10% ethanol, most bacteria can only tolerate up to 4-7% ethanol (377). Butanol exerts even greater toxicity as most microorganisms are unable to tolerate greater than 2.5 - 3% of the compound (378-380), except selected *Pseudomonas putida* strains which can grow in 6% butanol (381). The intrinsic low alcohol tolerance of biocatalysts represents a bottleneck for achieving high alcohol titre (or beer strength), which is required for energy efficient and economic product recovery via distillation (382).

The antimicrobial effect of alcohols strongly correlates with their level of hydrophobicity, which directly affects their affinity to associate with the cellular membrane. The octanol-water partition coefficient (logP) is a measure of relative hydrophobicity, and a more polar solvent/chemical will have a lower logP value. The relation between LogP and solvent toxicity is therefore derived from the tendency of a compound to partition in the cell membrane and is commonly used to assess solvent toxicity (379, 383-385). The accumulation of solvent in the phospholipid bilayer increases the permeability and fluidity of the membrane, impairs membrane protein function, diminishes energy transduction and disrupts energy homeostasis (379, 383, 386). Other mechanisms of solvent toxicity include chemical damage to macromolecules such as DNA, RNA and protein (384).

Solvent tolerance is a complex phenotype that involves the interaction of many cellular responses. One of the strategies employed by the stressed microbes is to fortify membrane structure by shifting from cis- to trans- fatty acids through the action of cis/trans isomerase (387), altering the ratio of saturated to unsaturated

fatty acids (385), and increasing the phospholipid chain length (388). The expression of efflux pumps is another avenue to excrete solvents from the cells but they are mainly studied in Gram negative microbes (379, 383, 389). Moreover, transcriptional regulators that mediate general stress response were also shown to participate in solvent tolerance by regulating respiration, ATP synthesis and consumption, signal transduction, and amino acid transport and metabolism (390). For instance, a transcriptional regulator (CA1869) that is predicted to regulate transitional-phase events, was shown to be implicated in *n*-butanol tolerance in *C. acetobutylicum* (391). Plasmid overexpression of this gene resulted in a 81% increase in *n*-butanol tolerance (391).

Heat shock proteins (HSP) are ubiquitous molecular chaperones that are involved in the synthesis, folding, transport and degradation of proteins. During cellular stress, chaperones target terminally misfolded proteins for proteolytic degradation, prevent protein aggregation, and assist in refolding of damaged proteins (392). Transcriptomic and proteomic studies consistently demonstrated that chaperones such as *groES, groEL, grpE, dnaK, dnaJ, clpB, tufA*, *tufB,* and *yacI* are generally upregulated when microorganisms are challenged with solvents (133, 169, 393), highlighting their roles in solvent tolerance.

The chaperone complexes GroESL, DnaKJE and chaperone protein ClpB form the core network machinery for the folding of both nascent and misfolded proteins in many microorganisms (394) (Figure 7.1). In *E. coli*, 10-15% of newly synthesized proteins were shown to interact with the GroESL chaperone, whereas the DnaKJE chaperone interacts with approximately 20 - 25% of the proteins (392, 395-397). The DnaK chaperone, often described as a ‘brick-shaped’ domain with an opening for the protein to be folded, functions with co-chaperone DnaJ and nucleotide exchange factor, GrpE, to protect nascent chains from aberrant interactions and assists in protein folding during- and post-translation in an ATP-dependent manner (383, 392). In addition, the DnaKJE chaperone complex also serves as a substrate filter and mediates the transfer of the polypeptide chains to downstream chaperones such as GroEL (396, 397). In *E. coli,* the chaperonin GroEL consists of two stacks of heptameric rings which create a hollow cavity for denatured proteins to be refolded

(398, 399). GroES, a ring of seven subunits, forms a lid to the GroEL cavity and generates a favourable environment for misfolded proteins to be refolded upon ATP hydrolysis (383, 400). The ClpB chaperone interacts specifically with the DnaKJE chaperone system to disaggregate proteins and permit protein refolding (401, 402).

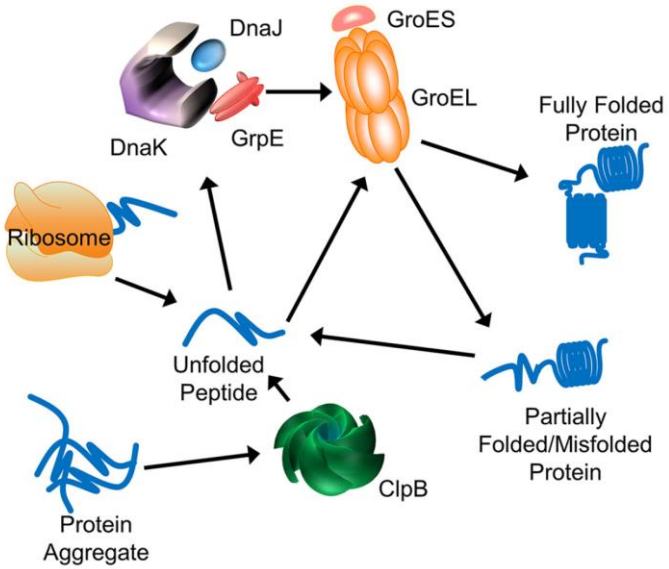


Figure 7.1. Schematic showing the involvement of chaperones in refolding nascent and misfolded proteins. Diagram was obtained from Zingaro and Papoutsakis (2012) (394).

In common with *C. acetobutylicum*, *C. beijerinckii*, *C. ljungdahlii*, and *B. subtilis*, the GroESL and DnaKJE chaperone complexes of *C. autoethanogenum* are encoded in operons of *groES-groEL* (CAETHG_1573-1572) and *grpE-dnaK-dnaJ* (CAETHG_2890-2892), respectively (Figure 7.2). Upstream of the *grpE-dnaK-dnaJ* operon lies a gene coding for a transcriptional repressor known as HrcA (heat shock regulation at CIRCE elements; CAETHG_2889), which binds to the operator CIRCE (controlling inverted repeat of chaperone expression) element and represses gene transcription (403, 404). The CIRCE elements are identified in both the *groES-groEL* and *hrcA-grpE-dnaK-dnaJ* operons in *C. autoethanogenum* (Figure 7.2). Inactivation of *hrcA* in *B. subtilis*, *L. lactis* and cyanobacteria led to the elevated expression of DnaK and GroESL operons at physiological temperature, confirming its role as a negative cis-element (403, 405-407).

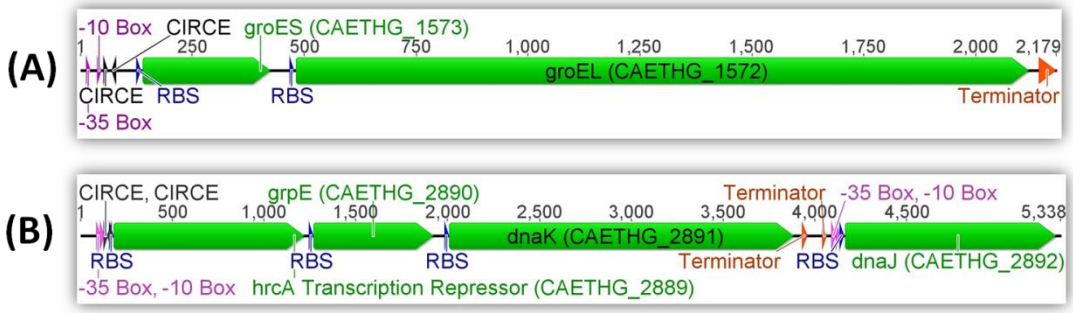


Figure 7.2. Gene organization of chaperones in *C. autoethanogenum*. (A) Gene arrangement of *groES-groEL* operon; (B) Gene arrangement of *hrcA-grpE-dnaK-dnaJ* operon. Putative ribosomal binding site (RBS; in blue), -10 and -35 box (in purple), controlling inverted repeat of chaperone expression (CIRCE; in black), and terminator (orange) are shown. Figure is generated using Geneious 6.1.7 (Biomatters Ltd).

Strain engineering through the overexpression of chaperones has been extensively investigated in microbes such as *E. coli*, *L. lactis*, *Lactobacillus plantarum*, *Cyanobacterium anabaena* and *C. acetobutylicum*, resulting in increased tolerance towards elevated and depressed temperatures, high salinity, acids, and solvents (176, 394, 408-415) (Table 7.1). The potential of chaperone overexpression in promoting growth at higher temperature should not be overlooked because the raising of gas fermentation temperature by a few degrees Celsius at the industrial scale leads to significant energy saving in cooling of the bioreactors, more efficient product removal and reduction of contamination risks. The enhancement of salt tolerance in the biocatalysts allows more of the water from the fermentation process to be recycled and reused without extensive water treatment (salts accumulate with each cycle). This not only reduces waste water treatment costs but also reduces the water footprint of the bioprocess.

To date the study and exploitation of chaperones for enhanced solvent, high temperature and salt tolerance remained unexplored in acetogens. In this study, the native chaperone operons *groES-groEL* and/or *grpE-dnaK-dnaJ* were cloned and overexpressed in *C. autoethanogenum*. The resulting chaperone overexpression strains were then assessed under both heterotrophic and autotrophic (ATP-limited) conditions to examine the impact on biomass, product formation and stress tolerance.

Table 7.1. The effect of chaperone overexpression on tolerance of microorganisms.

Chaperone Overexpression (Source)	Host	Effects	Reference
GroESL (native)	*Clostridium acetobutylicum*	85% less growth inhibition due to butanol stress, 30% improved *n*-butanol titre and prolonged metabolism	(176)
Hsp33 (*Bacillus psychrosaccharolyticus*)	*Clostridium acetobutylicum*	22% increased solvent titre but no change in growth inhibition when challenged with *n*-butanol (up to 16 g/L)	(416)
DnaK (*Bacillus pumilus*)	*Escherichia coli*	Growth up to 50^{o}C and survival up to 60^{o}C for 16 hours	(409)
DnaKJ and/or GroEL (native)	*Escherichia coli*	114 - 1060% increase in % viable cells upon freezing (-80^{o}C) relative to uninduced controls	(408)
GroESL (native)	*Escherichia coli*	12-fold increase in total growth in 4% ethanol, 2.8-fold increase in 0.75% *n*-butanol, 3-fold increase in 1.25% 2-butanol and 4-fold increase in 20% 1,2,4-butanetriol	(417)
DnaK (*Tetragenococcus halophilus*)	*Escherichia coli*	Shortened growth lag phase in 0.86 M NaCl and 1.2 M NaCl; Suppressed protein aggregation at 0.17 M and 0.86 M NaCl	(412)
GrpE, GroESL and ClpB (native)	*Escherichia coli*	200% and 390% increase in cfu after 24 hours in 7% ethanol, or 1% *n*-butanol, respectively	(394)
DnaK (*E. coli)*	*Lactococcus Lactis*	13.5-fold increased viability upon heat shock at 40^{o}C; 23% increased OD_{600} in 3% NaCl; 13% increased OD_{600} in 5% ethanol; 44% increased OD_{600} at 0.5% lactic acid	(414)
GroESL (*Lactobacillus paracasei*)	*Lactococcus Lactis*	1-log unit increase in cell viability compared to control upon heat shock at 54^{o}C; Able to grow in the presence of 0.5% [v/v] *n*-butanol for 5 hour while the viability of parent strain declined; No change in salt tolerance (5 M NaCl)	(411)
Hsp18.55 or Hsp19.3 (native)	*Lactobacillus plantarum*	Significant increase in survival (cfu/mL) upon heat shock, cold shock, ethanol (12% v/v) stress and *n*-butanol (1% v/v) stress	(415)
GroESL (native)	*Cyanabacterium anabaena*	Permitted growth at 42^{o}C whereas no growth was detected for WT control; ~35% increase in OD_{750} when challenged with 150 mM NaCl	(413)

7.2 Construction of Chaperone Overexpression Strains in *C. autoethanogenum*

In this study, three chaperone overexpression plasmids were constructed to increase expression of the native *groES-groEL* operon, *grpE-dnaK-dnaJ* operon, and a combination of both *groES-groEL* and *grpE-dnaK-dnaJ* operons. The native promoter of PFOR (P_{pfor}) (CAETHG_3029) was selected to drive chaperone overexpression because qRT-PCR experiments showed that this gene is stably and highly expressed under autotrophic conditions in *C. autoethanogenum* (53). As a first step, P_{pfor} was amplified from *C. autoethanogenum* gDNA using oligonucleotides 'P_{pfor}-NotI-F' and

'P_{pfor}-NdeI-R', followed by cloning into plasmid pMTL83151 using restriction sites *Not*I and *Nde*I to generate plasmid 'pMTL83156'.

Since the *groEL* CDS contains an internal *Nde*I site which interferes with the cloning procedure, SOE-PCR using primers 'SOE-groESL-a-NdeI', 'SOE-groESL-b', 'SOE-groESL-c' and SOE-groESL-d-EcoRI' was conducted to mutate the internal *Nde*I site from 'CATATG' to 'CTTATG' at nucleotide position 191 while retaining the same amino acid. The resulting SOE-PCR product was cloned into plasmid pMTL83156 using restriction sites *Nde*I and *Eco*RI to generate plasmid 'pMTL83156-groESL'. For the cloning of the *grpE-dnaK-dnaJ* operon, oligonucleotides 'grpE-NdeI-F' and 'dnaJ-SacI-R' were utilized to amplify the operon followed by cloning into plasmid pMTL83156 using restriction sites *Nde*I and *Sac*I to generate plasmid 'pMTL83156-grpE-dnaKJ'. To overexpress both *grpE-dnaK-dnaJ* and *groES-groEL* chaperones, a second promoter was introduced into plasmid 'pMTL83156-grpE-dnaKJ' before the cloning of the *groES-groEL* operon. P_{acs} was selected as the second promoter and was amplified using oligonucleotides 'P_{acsA}-KpnI-F' and 'P_{acsA}-BamHI-R', followed by cloning using restriction sites *Kpn*I and *Bam*HI to produce plasmid 'pMTL83156-grpE-dnaKJ-P_{acsA}'. As a next step, the *groES-groEL* operon was amplified using primers 'groESL-BamHI-F' and 'groESL-SalI-R' and cloned using restriction sites *Bam*HI and *Sal*I to generate plasmid 'pMTL83156-grpE-dnaKJ-P_{acsA}-groESL'. Sanger sequencing confirmed the cloned promoter(s) and chaperones were free of mutations.

Plasmid control pMTL83156 and chaperone overexpression plasmids were conjugated into *C. autoethanogenum* according to section 2.12.3. The resulting Tm^R colonies were subjected to plasmid rescue and restriction digest analysis to check if the appropriate plasmids were present in the transconjugants. As shown in Figure 7.3, the expected restriction digest bands were detected in the rescued plasmids from *C. autoethanogenum* transconjugants. The transconjugants with plasmids pMTL83156-groESL, pMTL83156-grpE-dnaKJ and pMTL83156-grpE-dnaKJ-P_{acsA}-groESL are termed '$GroESL^{over}$', '$DnaKJE^{over}$' and '$DnGr^{over}$' strains, respectively.

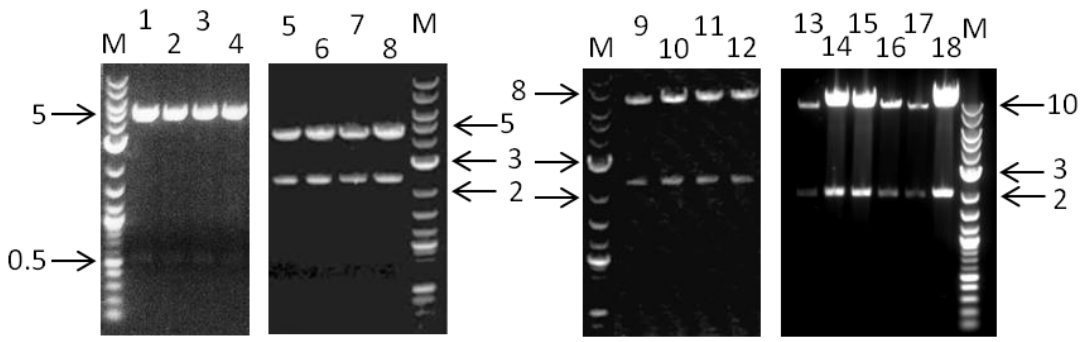


Figure 7.3. Gel electrophoresis showing the expected restriction digest bands from rescued plasmids of *C. autoethanogenum* transconjugants. M = NEB 2-log DNA ladder; 1 – 4 = *Nde*I + *Sbf*I digested pMTL83156 (expect 4.4 kb + 560 bp); 5 – 8 = *Pme*I + *Asc*I digested pMTL83156-groESL (expect 4.5 kb + 2.4 kb); 9 – 12 = *Pme*I + *Asc*I pMTL83156-grpE-dnaKJ (expect 6.6 kb + 2.4 kb); 13 – 18 = *Bam*HI + *Sal*I pMTL83156-grpE-dnaKJ-P_{acsA}-groESL (expect 9.5 kb + 2 kb).

7.3 Heterotrophic Growth Experiments and Chaperone Gene Expression Studies

Validated chaperone overexpression strains and the plasmid control were cultivated in triplicates of 500 mL Schott bottles containing 200 mL CGMY medium supplemented with 10 g/L fructose and 7.5 µg/mL thiamphenicol to assess the impact of chaperone overproduction on product formation during heterotrophic growth. In parallel, the mRNA level of the chaperones was investigated using qRT-PCR to examine the extent of increased chaperone transcript levels (if any) due to plasmid overexpression. In addition to routine sampling of liquid cultures for HPLC analysis and OD_{600} measurements, cells were harvested at early-exponential phase, mid-exponential phase, and late-exponential phase for gene expression analysis according to section 2.9.1. Total RNA was extracted from two of the three replicate cultures as described in section 2.9.2 and reverse transcribed into cDNA according to section 2.9.3. For qRT-PCR analysis, TaqMan primers and probes were employed for the two housekeeping genes (*gyrA* and *rho*) and genes of interest (*groES, groEL, grpE, dnaK,* and *dnaJ*). Standard curves using serially diluted cDNA were generated and the TaqMan primers and probes demonstrated excellent amplification efficiencies (section 2.9.4).

In comparison to the plasmid control, all three chaperone overexpression strains exhibited an increased growth lag phase but similar levels of OD_{600} were recorded while growing on fructose (Figure 7.4A). The acetate titre was not altered as a result of chaperone overexpression, except in the GroESL^{over} strain which generated 13% more acetate than the plasmid control strain (p-value = 0.003) (Figure 7.4B). Interestingly, both the DnaKJE^{over} and the DnGr^{over} strains synthesized approximately 80% higher ethanol titres when compared to the plasmid control strain (p-values = 0.007 and <0.0001, respectively), whereas the GroESL^{over} strain produced 12% less ethanol (p-value = 0.0003) (Figure 7.4C). In terms of 2,3-butanediol production, the DnaKJE^{over} strain generated 291% higher titre (p-value <0.0001) whereas the DnGr^{over} strain synthesized 48% higher titre (p-value = 0.0003) than the plasmid control strain while metabolizing fructose (Figure 7.4D). No change in 2,3-butanediol level was detected as a result of GroESL overexpression (Figure 7.4D).

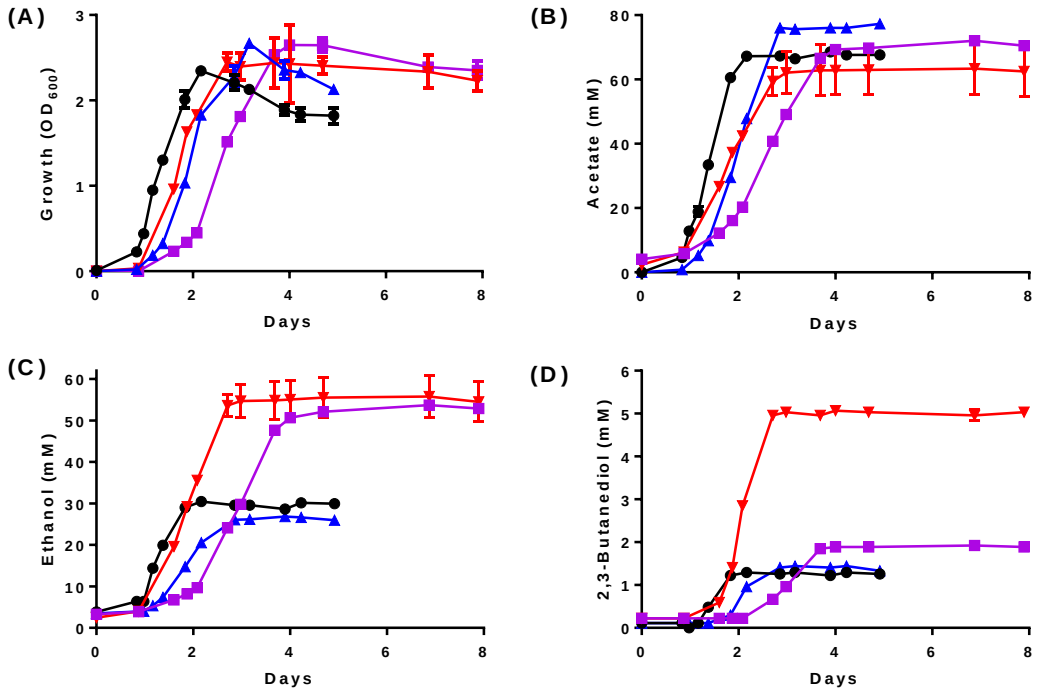


Figure 7.4. Growth and metabolite profiles of unchallenged *C. autoethanogenum* chaperone overexpression strains on fructose. (A) Growth profile; (B) Acetate profile; (C) Ethanol profile; and (D) 2,3-Butanediol profile. Black circles = plasmid control strain; Blue triangles = GroESL^{over} strain; Red inverted triangles = DnaKJE^{over} strain; Purple squares = DnGr^{over} strain; N = 3; Error bars = standard error of mean.

Following normalization for both housekeeping genes (*gyrA* and *rho*), the chaperone transcript levels were compared to the plasmid control at early-, mid- and late-growth phases during heterotrophic growth. In the GroESL^{over} strain, *groEL* mRNA was increased at early (3-fold) and late (106-fold) growth phases (p-values = 0.001 and <0.0001, respectively) whereas *groES* transcript was only increased at late growth phase (9-fold) when compared to plasmid control (p-value <0.0001) (Figure 7.5A & B). Surprisingly, the *groES* transcript level of the GroESL^{over} strain was lower than the plasmid control at early (p-value = 0.0015) and not significantly altered at mid growth phases (Figure 7.5A). For the *grpE-dnaK-dnaJ* chaperones, their gene expression levels were equal or reduced in early- and mid-growth phases relative to the plasmid control strain (Figure 7.5C-E). In contrast, the transcript levels of these genes were up-regulated in the GroESL^{over} strain at late-growth phase (Figure 7.5C-E).

For the DnaKJE^{over} strain, the transcript levels of chaperones *grpE* and *dnaK,* but not *dnaJ*, were consistently higher (3.1 – 9.7 fold) than the plasmid control at all the examined time points (Figure 7.5C, D & E). The mRNA abundance of *groES* was significantly down-regulated in early- growth phase (2.3 fold; p-value = 0.0048) of the DnaKJE^{over} strain but not significantly different from the plasmid control strain at mid- and late-growth phase (Figure 7.5A). During early-growth phase, the *groEL* transcript level was significantly up-regulated in the DnaKJE^{over} strain (3.1 fold; p-value <0.0001) when compared to the plasmid control strain (Figure 7.5B).

In the recombinant strain that carried the plasmid for overexpression of both GroESL and DnaKJE chaperone systems, the transcript abundance of *groES* (1.8 – 3.1 fold)*, groEL* (6.8 – 20.8 fold)*, grpE* (3.9 – 13.1 fold) and *dnaK* (2 – 7.8 fold) was consistently increased at the examined time points relative to the plasmid control strain (Figure 7.5A - D). In contrast, the transcript level of *dnaJ* was reduced (2.5 – 3.2 fold) in the DnGr^{over} strain in all three growth phases (Figure 7.5E). Comparison of *groES* and *groEL* transcript levels between DnGr^{over} and DnaKJE^{over} strain showed upregulation in the DnGr^{over} strain during early- and mid-growth phases (Figure 7.5A & B).

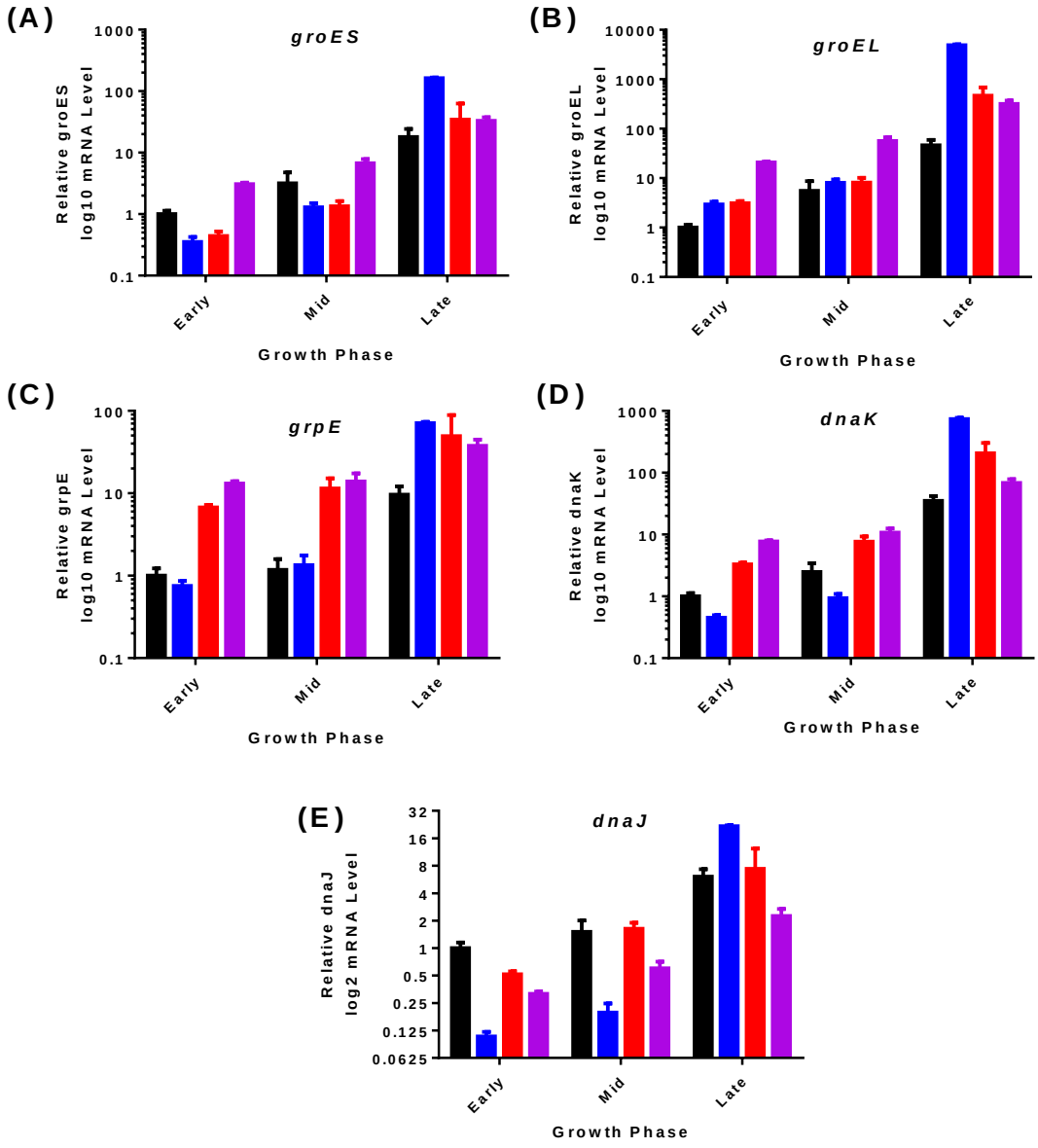


Figure 7.5. Normalized gene expression levels of chaperones during early-, mid- and late-growth phases of *C. autoethanogenum* chaperone overexpression strains growing on fructose. (A) *groES* mRNA level; (B) *groEL* mRNA level; (C) *grpE* mRNA level; (D) *dnaK* mRNA level; and (E) *dnaJ* mRNA level. Black = plasmid control strain; Blue = GroESL^{over} strain; Red = DnaKJE^{over} strain; Purple = DnGr^{over} strain; N = 6; Error bars = standard error of mean.

7.4 Autotrophic Growth Experiments

To examine the effect of chaperone overproduction on autotrophic growth and product formation, the chaperone overexpression strains were cultured in triplicates of 250 mL serum bottles containing 50 mL of CGMY medium containing 7.5 µg/mL

thiamphenicol with 2 bar CO in the headspace and incubated at 37°C with agitation for up to 24 days. In comparison to the plasmid control strain, the DnaKJE^{over} and DnGr^{over} strains displayed a slight increase in growth lag phase but peaked at a similar OD_{600} on pure CO (Figure 7.6A). Although the GroESL^{over} strain did not show prolonged growth lag phase, its peak OD_{600} was reduced by 33% relative to the plasmid control strain (p-value = 0.011) (Figure 7.6A).

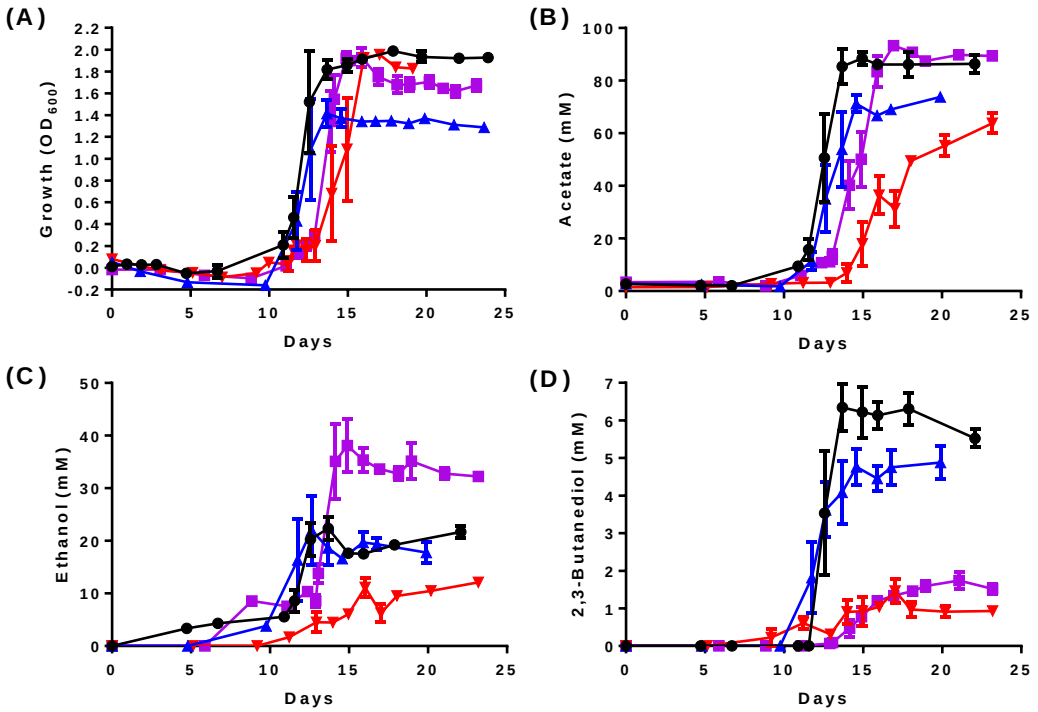


Figure 7.6. Growth and metabolite profile of unchallenged *C. autoethanogenum* chaperone overexpression strains on CO. (A) Growth profile; (B) Acetate profile; (C) Ethanol profile; and (D) 2,3-butanediol profile. Black circles = plasmid control strain; Blue triangles = GroESL^{over} strain; Red inverted triangles = DnaKJE^{over} strain; Purple squares = DnGr^{over} strain; N = 3; Error bars = standard error of mean.

While growing on CO, the DnGr^{over} strain generated a similar level of acetate to the plasmid control strain but the GroESL^{over} and DnaKJE^{over} strains synthesized 17% and 28% less acetate, respectively (p-values = 0.006 for both) (Figure 7.6B). Among the chaperone overexpression strains, only the DnGr^{over} strain produced more ethanol (71%; p-value = 0.0048) than the plasmid control strain (Figure 7.6C). The ethanol

titre of the DnaKJE^{over} strain was diminished by 50% (p-value = 0.011) but the ethanol level in the GroESL^{over} strain was unaffected (Figure 7.6C). The overexpression of chaperones in *C. autoethanogenum* had a negative impact on 2,3-butanediol titre during CO growth. In particular, the 2,3-butanediol level of the DnaKJE^{over} and DnGr^{over} strains was reduced by 77% and 73%, respectively, in comparison to the plasmid control strain (p-values = 0.0024 and 0.0025, respectively) (Figure 7.6D).

7.4.1 Ethanol Challenge Assay under Autotrophic Conditions

To determine whether chaperone overproduction has a positive effect on the ethanol tolerance of *C. autoethanogenum* under autotrophic conditions, both the plasmid control and chaperone overexpression strains were cultured in 250 mL serum bottles with 2 bar CO as described in section 7.4. When the culture OD_{600} reached 0.2, anaerobic ethanol (kept inside the anaerobic cabinet for >1 week) was injected in a drop-wise manner together with agitation to reach final ethanol concentrations of 20 g/L (434 mM) and 40 g/L (868 mM). The slow addition of ethanol is critical as quick injection of ethanol resulted in a localized 'sterilization zone' within the culture growth and prevented growth at 20 g/L ethanol challenge level (data not shown). As unchallenged controls, liquid medium from uninoculated culture was injected.

Following the injection of anaerobic ethanol or control medium, the bacterial cultures were allowed to incubate at 37^{o}C with agitation for 12 hours before 1 mL liquid sample was transferred into an anaerobic workstation for plating assay to determine the cell viability (cfu/mL). The samples were serially diluted with reduced YTF medium, and 150 µL of the diluted samples were plated onto triplicates of solid YTF medium supplemented with 7.5 µg/mL thiamphenicol. Colonies of typical *C. autoethanogenum* morphology emerged after 3-5 days, and microscope inspection was undertaken to check for contaminants using a selection of randomly picked colonies (data not shown). The challenged and unchallenged serum bottle cultures were returned to the 37^{o}C shaker and liquid samples were taken at regular intervals up to 50 days post ethanol challenge to monitor growth (OD_{600}).

As shown in Figure 7.7E, an ethanol challenge at 20 g/L and 40 g/L potently reduced the cell viability of the plasmid control strain after 12 hours incubation to only 0.071% and 0.035%, respectively, relative to unchallenged controls. In contrast, the three chaperone overexpression strains achieved between 8.2% to 23.8% cell viability at 20 g/L ethanol challenge level in comparison to unchallenged cultures (Figure 7.7E). The best performer at this level of ethanol challenge was the $DnGr^{over}$ strain, which recorded 23.8% cell viability (relative to unchallenged culture) and represents a 335-fold increase in cell viability over the plasmid control strain (p-value = 0.029) (Figure 7.7E). When challenged with 40 g/L ethanol, the $GroESL^{over}$ strain showed a decrease in cell viability of 41% in comparison to the plasmid control strain (p-value = 0.022) (Figure 7.7E). However, the $DnaKJE^{over}$ and $DnGr^{over}$ strains achieved 109-fold and 1083-fold, respectively, higher cell viability than the plasmid control strain (p-values = 0.002 and 0.019, respectively) (Figure 7.7E).

Within the first 7 days after a 20 g/L ethanol challenge, the serum bottle cultures of all three chaperone overexpression strains showed an increase of OD_{600} whereas the plasmid control strain experienced an initial decrease in OD_{600}, before an increase from day 7 onwards (Figure 7.7B). The $GroESL^{over}$ strain was able to immediately grow unperturbed by the ethanol stress and reached a peak OD_{600} of 1.18 – 1.42 three days after ethanol challenge (Figure 7.7B). Similarly the $DnGr^{over}$ strain was able to grow quickly but a lower peak OD_{600} of 0.76 – 0.83 was attained. Some variations were observed within the $DnaKJE^{over}$ strain triplicates but in general the strain was able to grow to OD_{600} of 1.1 – 1.3 within the first 6 days (Figure 7.7B). Beyond 7 days post 20 g/L ethanol challenge, the plasmid control strain was able to grow to an OD_{600} of 2.2 – 2.3, substantially outgrowing all three chaperone overexpression strains (Figure 7.7A).

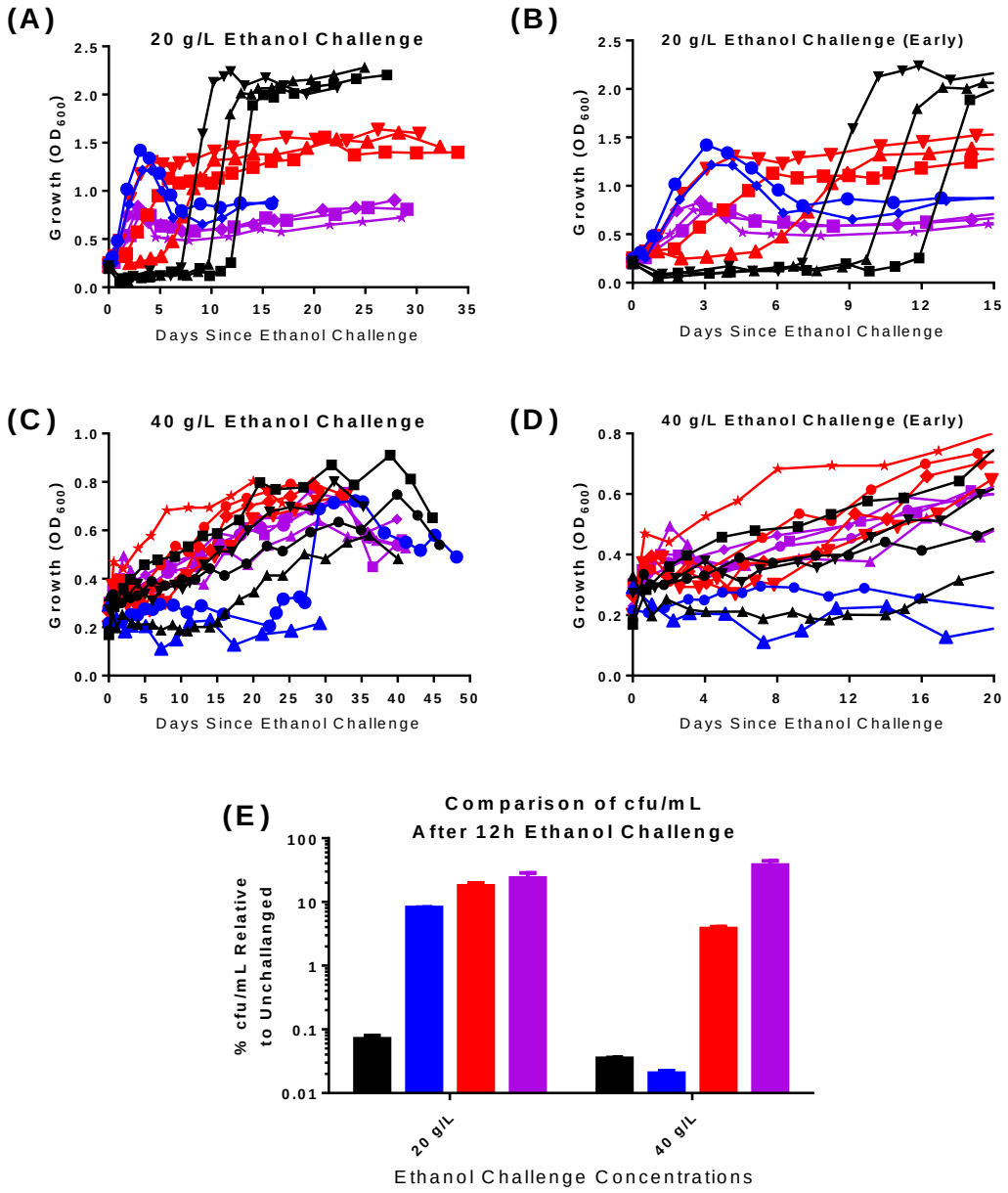


Figure 7.7. Effect of chaperone overexpression on growth and cfu/mL of *C. autoethanogenum* when challenged with ethanol on CO. (A) Growth profiles when challenged with 20 g/L ethanol; (B) The first 15 days of 20 g/L ethanol challenge; (C) Growth profiles when challenged with 40 g/L ethanol; (D) The first 20 days of 40 g/L ethanol challenge; (E) Comparison of percentage cfu/mL relative to unchallenged cultures after 12 hours of ethanol challenge. Anaerobic ethanol was administered into cultures to reach 20 g/L or 40 g/L ethanol when OD_{600} reached 0.2; Black = plasmid control strain (N = 3 - 4); Blue = GroESL^{over} strain (N = 2); Red = DnaKJE^{over} strain (N = 3 - 4); Purple = DnGr^{over} strain (N = 3); Error bars = standard error of mean.

In the presence of 40 g/L ethanol, more intra-replicate variations were observed for the serum bottle cultures, which complicate the analysis of impact of chaperone

overexpression (Figure 7.7C & D). After prolonged incubation, the plasmid control strain was able to reach a peak OD_{600} of 0.6 – 0.9, followed by the DnaKJE^{over} strain that achieved a peak OD_{600} of 0.7- 0.8 (Figure 7.7C). Similarly, the DnGr^{over} strain reached a peak OD_{600} of 0.6 – 0.7 whereas one of the replicates of the GroESL^{over} strain attained a peak OD_{600} of 0.7 (Figure 7.7C). Despite the substantial intra-replicate variations, it was observed that both the DnaKJE^{over} and DnGr^{over} strains achieved higher OD_{600} than the plasmid control strain in the first two days after a 40 g/L ethanol challenge (Figure 7.7D). In contrast, the GroESL^{over} strain struggled to grow in the first 20 days post 40 g/L ethanol challenge (Figure 7.7D).

7.4.2 Heat Stress Plating Assay

In addition to ethanol tolerance assay, the chaperone overexpression and the plasmid control strains were subjected to thermal stress to examine the effect of chaperone overproduction on the survival of *C. autoethanogenum* at elevated temperature. The recombinant strains were cultured in CGMCF liquid medium inside an anaerobic workstation for 1-2 days, where they achieved an OD_{600} of 0.43 – 0.68. From these, the cultures were standardized to an OD_{600} of 0.4 via dilution, before being serially diluted in 10-fold steps and 100 µL was plated onto YTF solid medium supplemented with 7.5 µg/mL thiamphenicol. These culture plates were housed inside anaerobic jars containing anaerobic atmosphere (CO_2) generating bags (Thermo Scientific) to minimize oxygen contamination, and incubated at 42^{o}C for 5 days and 45^{o}C for 14 days.

As shown in Figure 7.8, the chaperone overexpression strains generated a significantly greater number of colonies than the plasmid control strain following 5 days of incubation at 42^{o}C. The DnaKJE^{over} strain exhibited the highest viable cell count that is 238-fold higher than the plasmid control (p-value < 0.0001), followed by the DnGr^{over} strain that produced a 139-fold higher count than the plasmid control strain (p-value < 0.0001). The overexpression of GroESL enhanced survival by 42-fold relative to plasmid control (p-value < 0.0001). Despite prolonged incubation duration of 14 days at 45^{o}C, none of the strains showed any signs of colonies.

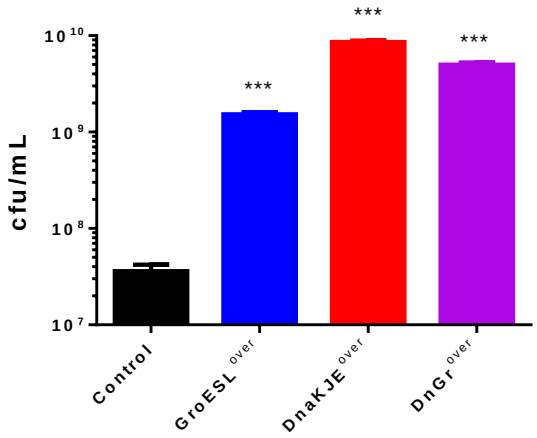


Figure 7.8. Chaperone overexpression enhances viable cell counts (cfu/mL) of *C. autoethanogenum* at 42°C following incubation for 5 days. N = 3; Error bars = standard error of mean. *** Indicates p-value < 0.0001 when compared to plasmid control.

7.4.3 Salinity Stress Growth Experiment

The plasmid control and chaperone overexpression strains were subjected to growth in the presence of high salt concentrations to investigate whether chaperone overexpression in *C. autoethanogenum* enhances salt tolerance. The growth experiment was conducted in triplicates of 4 mL tubes, each containing 3.5 mL of CGMCF medium with 7.5 µg/mL thiamphenicol and supplemented with 100 mM, 200 mM and 500 mM NaCl. After inoculation using 100 µL of 2 day old pre-culture (standardized to OD_{600} of 1.4 via dilution), static incubation at 37°C was undertaken inside an anaerobic workstation for up to 14 days. Culture growth was monitored by measuring OD_{600}.

In the presence of 100 mM NaCl, the GroESL^{over} and DnGr^{over} recombinant strains achieved significantly higher cell densities in terms of OD_{600} and growth rates relative to the plasmid control strain (Figure 7.9A). In particular, the GroESL^{over} strain achieved an 18% higher OD_{600} (p-value = 0.004) whereas the DnGr^{over} strain attained a 42% increased OD_{600} (p-value = 0.0001) (Figure 7.9A). In contrast, the DnaKJE^{over} strain exhibited a low growth rate and achieved a peak OD_{600} that was 47% lower than the plasmid control strain (p-value = 0.0008) (Figure 7.9A). At 200 mM NaCl level, the growth of the plasmid control strain was restricted to a peak OD_{600} of 0.23

while the DnGr^{over} strain reached 35% higher OD_{600} of 0.31 (p-value = 0.01) and exhibited a reduced growth lag phase (Figure 7.9B). Under the same conditions, the GroESL^{over} strain achieved a peak OD_{600} that was 3.65-fold higher than the plasmid control strain (p-value = 0.0173), followed by the DnaKJE^{over} strain that was 1.91-fold higher (p-value = 0.067) (Figure 7.9B). When challenged with 500 mM NaCl, all the examined strains grew poorly (Figure 7.9C). The DnGr^{over} strain showed some early growth and reached its maximum OD_{600} of 0.10 on day 5, whereas the DnaKJE^{over} strain appeared to reach a peak OD_{600} of 0.14 on day 14 relative to a peak OD_{600} of 0.09 by the plasmid control strain on day 11 (Figure 7.9C).

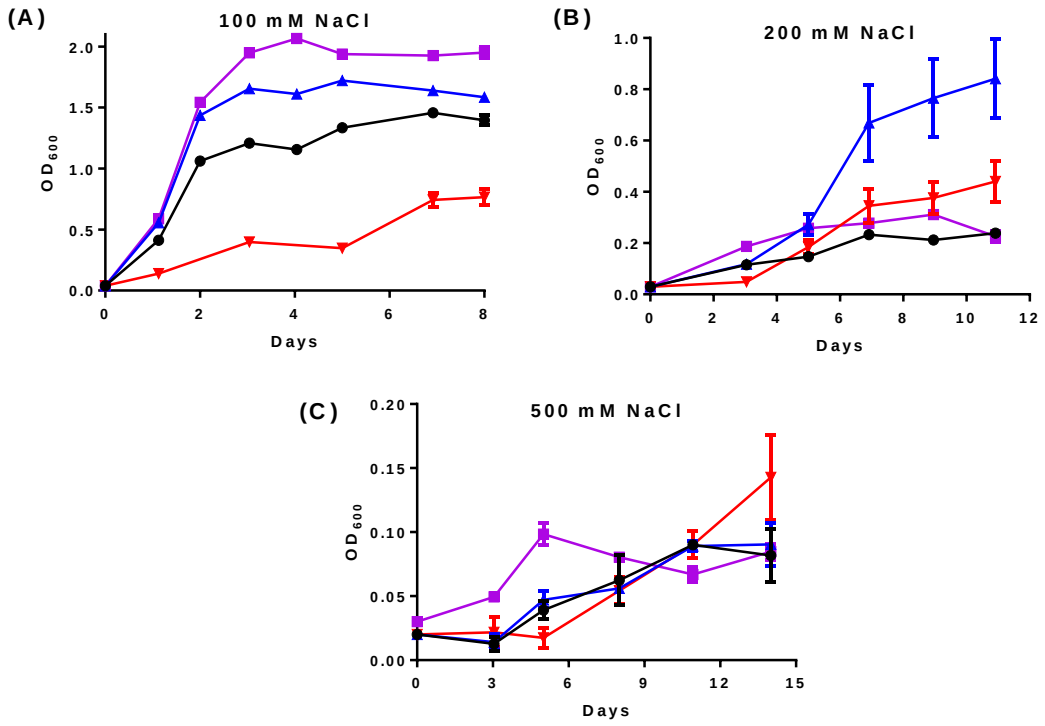


Figure 7.9. The effect of chaperone overexpression on growth of *C. autoethanogenum* in the presence of high salt concentrations under heterotrophic conditions. (A) 100 mM NaCl; (B) 200 mM NaCl; (C) 500 mM NaCl. Black = plasmid control strain; Blue = GroESL^{over} strain; Red = DnaKJE^{over} strain; Purple = DnGr^{over} strain; N = 3; Error bars = standard error of mean.

7.5 Discussion

7.5.1 Enhanced Ethanol and 2,3-Butanediol Titres from DnaKJE Overexpression During Fructose Growth on Fructose

During growth on fructose, all three chaperone overexpression strains exhibited an increased growth lag phase in comparison to the plasmid control strain. This can be explained by the additional metabolic burden imposed through the biosynthesis of these enzyme complexes and the subsequent ATP costs involved in protein folding (418, 419). Consistent with this notion, the strain overexpressing both DnaKJE and GroESL chaperones experienced the longest growth lag phase when compared to mono-chaperone overexpression systems. Despite the increased growth lag phase, these chaperone overexpression strains were eventually able to achieve equal or higher cell densities measured by OD_{600} than the plasmid control strain.

In *C. acetobutylicum*, the plasmid overexpression of native GroESL increased butanol titre by 30% without affecting ethanol levels while metabolizing glucose (176). In this work, the overexpression of native GroESL in *C. autoethanogenum* reduced ethanol titres by 12%, and increased acetate titre by 13% while the 2,3-butanediol level was unaffected during growth on fructose. Surprisingly, the overexpression of chaperone DnaKJE alone enhanced ethanol production by 82%, and elevated 2,3-butanediol titre by 291% relative to plasmid control. Interestingly, the addition of GroESL to the DnaKJE overexpression strain ($DnGr^{over}$) slightly reduced the ethanol level and substantially decreased 2,3-butanediol titre from 5.1 mM to 1.9 mM. The negative effect on ethanol level due to the addition of GroESL overexpression to $DnaKJE^{over}$ strain is consistent with the phenotype observed in the $GroESL^{over}$ strain.

GroEL has been demonstrated to negatively modulate both *dnaKJE* and *groESL* operons by stabilizing HrcA which binds to CIRCE elements in *B. subtilis* (420-422). The overexpression of GroESL in *C. acetobutylicum* has also been shown to reduce DnaKJ mRNA and protein levels (176). In a reverse manner, the plasmid-borne overexpression of DnaK resulted in a 2.3-fold reduction in GroEL protein level in *Haemophilus ducreyi* (423). The negative effect of GroESL on DnaKJ expression may explain why the overexpression of GroESL in *C. autoethanogenum* WT or DnaKJE

overexpression strains can reduce ethanol and 2,3-butanediol titres. The exact mechanism of how chaperone DnaKJE promotes ethanol and 2,3-butanediol production under heterotrophic conditions is unclear. One hypothesis is that the DnaKJE chaperone assists in the folding of enzymes responsible for ethanol and 2,3-butanediol biosynthesis. *C. autoethanogenum* enzymes such as AdhE, AOR (both required for ethanol production) and PFOR (required for 2,3-butanediol biosynthesis) fall outside the 60 kDa protein range that can be encapsulated by the GroESL chaperone (396, 424). In contrast, the DnaK chaperone assists protein folding by association with short linear peptide segments that are rich in hydrophobic residues (425-427). By using an algorithm which claimed to have a 77.2% true positive and 1% false positive prediction (428), DnaK binding sites were detected in proteins involved in ethanol formation and biosynthesis of 2,3-butanediol (Table 7.2).

Table 7.2. Putative DnaK binding sites within proteins that participate in biosynthesis of ethanol and 2,3-butanediol in *C. autoethanogenum*.

Protein	Amino acid Position	Sequence	Score
Butanediol dehydrogenase (CAETHG_0385)	1-7	MKAVLWY	17.1
	198-204	RIVIVFQ	13.7
	317-323	DGYITKR	11.5
Alpha-Acetolactate Decarboxylase (ALDC; CAETHG_2932)	32-38	SKLLKKG	14.7
	51-57	ELTLLNG	12.5
	58-64	TFYRTKP	11.9
	160-166	GYVVGFR	11.2
Acetolactate synthase (AlsS; CAETHG_1740)	37-43	NLEIMNA	11.5
	147-153	IIRLVFK	15.7
	148-154	IRLVFKY	14
	253-259	NKYSMWT	12.9
	276-282	DLVITIG	11.6
	331-337	NILRRTS	11.3
	377-383	RKVMGPH	11.1
	396-402	WIARHYN	11.1
	463-469	IVVLIFN	14
	464-470	VVLIFND	11.4
	473-479	YGLIKWK	19.7
	515-521	EDLIPTL	11.4

Protein	Amino acid Position	Sequence	Score
Pyruvate:ferredoxin oxidoreductase (PFOR; CAETHG_0928)	88-94	QGLLLMI	12.7
	89-95	GLLLMIP	17.3
	90-96	LLLMIPN	16.4
	223-229	DIYFQQR	11.7
	270-276	EYIIVAM	11.6
	287-293	VDYLRQN	13.3
	301-307	KVHLYRP	13.1
	303-309	HLYRPFS	14
	312-318	YFFKYLP	15.2
	314-320	FKYLPKT	16.6
	719-725	ENFLTKK	12.9
	720-726	NFLTKKP	12.3
	735-741	HYRIQIS	11.6
	779-785	EYAMKIT	11.9
	821-827	IKLLTQL	13.6
	822-828	KLLTQLY	14.4
	929-935	KILKILN	13
	947-953	EIFMKKD	13.6
	952-958	KDYLIKK	13.2
	953-959	DYLIKKS	13.9
	1100-1106	HLYRYNP	14.1
Aldehyde:ferredoxin oxidoreductase (AOR1; CAETHG_0092)	6-12	GKVLRIN	12.9
	8-14	VLRINLK	11.2
	57-63	NKFIIVT	12.1
	58-64	KFIIVTG	12.2
	75-81	GRFMVVT	11.5
	310-316	EYETLWC	12.9
	371-377	NLSKLWG	12
	386-392	IKRMVYS	13.2
	450-456	KGYMINP	11.9
	552-558	KRLLEEP	12.1
	572-578	DVLLPEY	12
Aldehyde:ferredoxin oxidoreductase (AOR2; CAETHG_0102)	6-12	GKVLRIN	12.9
	29-35	KKFIGAR	14.5
	57-63	NKFIIAA	11.8
	75-81	GRFMVVT	11.5
	310-316	EYETLWS	18.8
	572-578	DVLLPEY	12

Protein	Amino acid Position	Sequence	Score
Bi-functional Aldehyde/Alcohol Dehydrogenase (adhE1; CAETHG_3747)	125-131	LIALKTR	11.9
	164-170	EGIIGWI	13.8
	231-237	SILLSKT	14.4
	282-288	KIILKNG	11.8
	368-374	SLYINPM	14.9
	434-440	KHLLNIK	13.6
	451-457	WFRVPEK	16.2
	479-485	KVFIVTD	12
	485-491	DKVLYQL	13.5
	566-572	DLAMRFM	13.4
	569-575	MRFMDIR	13.6
	577-583	RVYVFPK	12.3
	586-592	EKAMMIS	11.6
	677-683	VKLIFEY	12.5
	790-796	KVQLLIN	14
	792-798	QLLINAI	13
	850-856	IKQMYIN	14.8
Bi-functional Aldehyde/Alcohol Dehydrogenase (adhE2; CAETHG_3748)	3-9	NLFIFNS	15.1
	146-152	LIALKTR	11.9
	185-191	EGIIGWI	13.8
	252-258	SILLSKT	14.4
	360-366	VLAMYKA	11.6
	456-462	KHLLNIK	13.6
	473-479	WFRVPEK	16.2
	491-497	LKELRIM	12.4
	493-499	ELRIMEK	11.1
	507-513	DKVLYQL	13.5
	588-594	DLAMRFM	13.4
	591-597	MRFMDIR	13.6
	599-605	RVYVFPK	12.3
	608-614	EKAMMIS	11.6
	644-650	DYELTPN	12.3
	699-705	TRLVFKY	13.9
	701-707	LVFKYLP	12.1
	703-709	FKYLPIA	16.1
	812-818	KVQLLIN	14
	814-820	QLLINAI	13
	872-878	IKQMYIN	14.8

Notes: Algorithm was developed by Van Durme *et al*. (2009) (428) and is available online via http://limbo.switchlab.org/limbo-analysis

7.5.2 Molecular Evidence for Increased Chaperone Gene Overexpression in Recombinant Strains While Metabolizing Fructose

In parallel to the heterotrophic growth experiment reported in section 7.5.1, the mRNA abundance of chaperone overexpression and plasmid control strains was examined at early-, mid- and late-growth phases using qRT-PCR to seek molecular evidence for any increase in chaperone transcript levels as a result of plasmid overexpression. Since the native chaperones of *C. autoethanogenum* were used for plasmid overexpression, the TaqMan probes and primers anneal to both the endogenously generated transcripts (from the chromosome) and plasmid-generated mRNA. Although a nucleotide within *groEL* was mutated using SOE-PCR to remove an interfering *Nde*I cloning site (while retaining the same encoded amino acid) (Section 7.2), the TaqMan probes and primers anneal to a different region of *groEL*. If the goal of the experiment is to distinguish between plasmid-borne chaperone mRNA and chromosome-borne chaperone mRNA, the forward primer can be designed to anneal to the promoter region since non-native promoters (P_{pfor} and P_{acsA} of *C. autoethanogenum*) were used to drive chaperone expression in the plasmid constructs. However, this strategy can only be applied to the first gene of the chaperone operons: *groES* and *grpE*.

In the recombinant strain that carried the GroESL overexpression plasmid, a significant increase in mRNA level of chaperonin *groEL* relative to the plasmid control strain was detected at early and late growth phases. In contrast, the first gene of the *groESL* operon, *groES* (encoding GroES, a cofactor of GroEL), only showed increased gene expression relative to the plasmid control strain in the late-growth phase but not during early- and mid-growth phases. In the $GroESL^{over}$ strain, the untargeted chaperones *grpE*, *dnaK*, and *dnaJ* were expressed at similar levels or down-regulated relative to the plasmid control strain during early- and mid-growth phases but expression of the former two genes was elevated during the late-growth phase. A similar phenomenon was observed by Tomas *et al.* (2003), who reported a decrease in transcript level of *dnaK* and *dnaJ* (but not *grpE*) in a recombinant *C. acetobutylicum* strain overexpressing GroESL in a bioreactor (176).

The gene expression data showed that the DnaKJE^{over} strain exhibited enhanced mRNA levels for *grpE* and *dnaK*, but not *dnaJ*, at all the examined time points relative to the plasmid control strain. The gene *dnaJ* of *C. autoethanogenum* is distally located in the *grpE-dnaK-dnaJ* operon and is preceded by two putative transcriptional terminators and a putative promoter region (Figure 7.2), which suggests it may be differentially expressed from *grpE* and *dnaK*. In support of this notion, the peptide molar ratio of *grpE*:*dnaK*:*dnaJ* in *E. coli* was determined as 20:30:1 using MS (397). The transcript level of the untargeted *groES* was not up-regulated in the DnaKJE^{over} strain at all the examined time-points, but *groEL* was up-regulated during early- and late-growth phases in comparison to plasmid control.

The DnGr^{over} strain carries a plasmid that overexpresses the *grpE-dnaK-dnaJ* operon from a P_{pfor} promoter, followed by a P_{acsA} promoter that drives *groES-groEL* operon expression. Gene up-regulation of *grpE*, *dnaK*, *groES*, and *groEL* was consistently detected at all the examined time-points in the DnGr^{over} strain relative to the plasmid control strain. Similar to the DnaKJE^{over} strain, the *dnaJ* mRNA level was not elevated in the DnGr^{over} strain. Given the difference in promoters driving the expression of *groES-groEL* between DnGr^{over} (P_{acsA}) and GroESL^{over} (P_{pfor}) strains, it is not surprising that both *groES* and *groEL* mRNA levels in the DnGr^{over} strain are 5.2- to 8.8-fold higher than the GroESL^{over} strain during early- and mid-growth phase. Under autotrophic conditions, *acsA* was more strongly expressed than *pfor* in *C. autoethanogenum* and the two genes displayed different expression profiles (53). During late growth phase, the mRNA levels of *groES* and *groEL* were 4.9- to 15.5-fold higher in the GroESL^{over} strain than in the DnGr^{over} strain.

Both the plasmid control and chaperone overexpression strains displayed increasing chaperone expression from early to late growth phases, which is consistent with their roles in response to stress. In the plasmid control strain, *dnaJ* showed the least amount of up-regulation (6.1 fold) from early to late growth phases, whereas *groEL* exhibited the largest magnitude of up-regulation at 46.4 fold during the same time frame. As a comparison, the *groEL* transcript level of the GroESL^{over} strain showed a 1669-fold increase from early- to late-growth phase, further demonstrating the effect of chaperone overexpression at the molecular level.

7.5.3 Co-Overexpression of DnaKJE and GroESL Chaperones Increases Ethanol Production during CO Growth

Unlike heterotrophic growth, autotrophic growth is predicted to be limited in ATP (106, 140), which poses challenges for chaperone overexpression strains because both the GroESL and DnaKJE chaperone systems are ATP-dependent. It has been determined that 130 ± 20 moles ATP are required for GroESL chaperonin of *E. coli* to fold one rhodanase (a 293 residue monomeric enzyme), which is 5 – 10% of the ATP cost for the degradation and resynthesis of a rhodanase (418). In contrast, the DnaKJE chaperone system of *E. coli* was shown to involve the hydrolysis of only 5 ATP for folding of one luciferase polypeptide (572 residue) (429). Consistent with the additional ATP burden, the GroESL^{over} strain of *C. autoethanogenum* was only able to achieve 67% of the peak OD_{600} of the plasmid control strain but without alteration in growth lag-phase while growing on pure CO. Under the same conditions, both the DnaKJE^{over} and DnGr^{over} strains exhibited a slight increase in growth lag phase but recorded similar peak OD_{600} as the plasmid control strain.

In the presence of pure CO, the recombinant strain co-overexpressing chaperones DnaKJE and GroESL generated 71% more ethanol, similar acetate titre but 73% less 2,3-butanediol than the plasmid control strain. The effect of chaperone overexpression on metabolites of acetogens growing autotrophically in CO has not been investigated in the literature. During glucose metabolism, the plasmid overexpression of GroESL in *C. acetobutylicum* increased butanol titre by 30% (176). Another example is the heterologous expression of Hsp33 from *B. psychrosaccharolyticus* in *C. acetobutylicum*, which increased the solvent titre by 22% (416). In *C. autoethanogenum*, the overexpression of GroESL had a neutral effect on the ethanol titre while the overexpression of DnaKJE diminished ethanol levels by 50% during autotrophic conditions. Based on these data, the over-production of DnaKJE alone in CO had a negative effect on ethanol production but the combined over-production of DnaKJE and GroESL significantly elevated ethanol levels. This phenomenon can be attributed to the relative abundance and interplay between the two chaperone systems. In particular, GroEL is known to negatively modulate the

expression of DnaKJE (as mentioned earlier) and both chaperone systems are known to interact with regulatory elements such as stress-specific sigma factor H (σ^H) (430).

Unlike during heterotrophic growth, the overexpression of DnaKJE with or without GroESL in *C. autoethanogenum* did not raise 2,3-butanediol titre under pure CO growth conditions. The 2,3-butanediol levels were diminished by 73 – 77% in DnaKJE^{over} and DnGr^{over} strains and reduced by 23% in the GroESL^{over} strain relative to the plasmid control strain in the presence of CO. It is likely that the flux at the pyruvate (a precursor of 2,3-butanediol) node is significantly different between the two growth conditions. Pyruvate has to be generated from acetyl-CoA and CO_2 using PFOR and Fd_{red} during acetogenesis but it is a metabolic intermediate during glycolysis. Furthermore, the promoters used to drive the chaperone expression are likely to display different expression profiles under the two growth conditions. Another explanation is that the additional metabolic and energetic burden of chaperone over-production under ATP-limiting conditions contributed to the reduced 2,3-butanediol levels.

7.5.4 Overexpression of Chaperones under Autotrophic Conditions Enhanced Tolerance towards Ethanol in the Early Phase of Ethanol Challenge Assay

During the design of a chemical stress experiment, careful considerations have to be given to the medium composition, inoculum age and density, chemical stress duration, and method of quantifying tolerance in the form of cell viability and growth (384). This is to ensure that the assay being undertaken best resembles the challenging conditions the microbe is likely to encounter during industrial bioprocessing. In this study, chaperone overexpression and plasmid control strains of *C. autoethanogenum* were allowed to grow in serum bottles containing 2 bar CO to early exponential growth phase (OD_{600} = 0.2) before anaerobic ethanol was injected to final concentrations of 20 g/L and 40 g/L. Ethanol tolerance was measured in the form of viability assay by comparing the % cfu/mL relative to unchallenged culture after 12 hour ethanol challenge, and by monitoring the culture growth (OD_{600}) for up

to 50 days post ethanol challenge. The addition of ethanol into molten agar medium prior to plating failed to reduce the number of cfu (data not shown), most likely due to evaporation of ethanol from the plates. Furthermore, ethanol stress of only 1 hour in serum bottles was insufficient to have an impact on viability of *C. autoethanogenum* (data not shown).

The viability of the plasmid control strain was drastically diminished to only 0.071% and 0.035% cfu/mL after 12 hours of ethanol challenge at concentrations of 20 g/L and 40 g/L, respectively, when compared to the unchallenged cultures. As a result of chaperone overexpression, this was increased to 8.2 for the GroESL^{over} strain, 17.9 for the DnaKJE^{over} strain and 23.8 for the DnGr^{over} strain at the 20 g/L ethanol challenge level. When challenged with 40 g/L, the GroESL^{over} strain recorded only 0.02% survival, which is 41% less than the plasmid control strain. In contrast, the DnaKJE^{over} and DnGr^{over} strains respectively generated 109-fold and 1083-fold improvement in % cfu/mL relative to the plasmid control strain at 40 g/L ethanol challenge concentration.

At both 20 g/L and 40 g/L ethanol challenge levels, the recombinant strains co-overexpressing both DnaKJE and GroESL chaperone systems displayed the greatest tolerance from the 12 hour viability assay. This positive effect of combined chaperone systems on alcohol tolerance has also been reported in the literature. For instance, the combined overexpression of ClpB, GrpE, GroESL in *E. coli* imparted a higher tolerance towards 7% (v/v) ethanol than strains overexpressing each chaperone (394). In terms of freeze tolerance, an *E. coli* strain over-producing both GroEL and DnaKJ chaperone systems also displayed greater viability than a strain over-producing only GroEL (408). Despite significant functional overlap between GroESL and DnaKJE chaperone systems (396, 397), it is not inconceivable that their combined over-production confers a higher tolerance towards alcohols.

Continued monitoring of the OD_{600} of the 20 g/L ethanol challenged cultures on CO revealed the plasmid control strain suffered a growth lag-phase of >7 days, before eventually reaching a peak OD_{600} of 2.2 – 2.3. In contrast, all three chaperone overexpression strains were able to grow within the first 7 days post ethanol

challenge but they reached substantially lower peak OD_{600} than the plasmid control strain. In particular, the GroESL^{over} strain managed to grow unperturbed by the challenge of 20 g/L ethanol and reached OD_{600} of 1.2 – 1.4 three days post ethanol stress. The ability of the chaperone overexpression strains to grow earlier than the plasmid control strain is consistent with results from the viability assay (% cfu/mL) at 20 g/L ethanol challenge level.

Despite the greater intra-replicate variations in growth response from the 40 g/L ethanol challenge, some observations can be made. Following prolonged incubation (up to 50 days post ethanol challenge), both the plasmid control and chaperone overexpression strains were able to achieve comparable cell densities. The DnaKJE^{over} and DnGr^{over} strains displayed stronger growth than the plasmid control strain in the first two days post 40 g/L ethanol challenge. The GroESL^{over} strain was unable to show significant increase in OD_{600} in the first 20 days following 40 g/L ethanol stress. Again, these results are in agreement with the higher viability (% cfu/mL) of DnaKJE^{over} and DnGr^{over} strains but lower viability of the GroESL^{over} strain when compared to the plasmid control strain at 40 g/L ethanol challenge level.

Interestingly the positive effect of chaperone overexpression on ethanol tolerance appears to be restricted to the early-phase of ethanol stress, as the plasmid control strain eventually outgrew the chaperone overexpression strains following prolonged incubation. Two hypotheses were proposed to explain this phenomenon. One is the promoter(s) used for chaperone overexpression may be more active at the early growth phase in the presence of pure CO. The second hypothesis is that the serum bottle cultures may be substrate limited, which translates into limited ATP availability to support the synthesis and folding actions of the chaperones. To test these hypotheses, the mRNA level of these chaperones can be examined using qRT-PCR under CO conditions, and the ethanol stress experiment can be performed in a bioreactor with continuously supplied gas to overcome substrate limitation.

7.5.5 Chaperone Overexpression Enhances Tolerance of *C. autoethanogenum* towards Thermal Stress and High Salinity

During the recycling of water in an industrial bioprocess, osmolarity increases as salts accumulate with every cycle so it is desirable to employ a biocatalyst that is tolerant towards high salt concentrations. Furthermore, the ability to operate a gas fermentation process at high temperature utilizing a heat tolerant biocatalyst not only lowers the cooling costs and facilitates product separation via distillation but also reduces risk of contaminations. Hence, the chaperone recombinant strains constructed in this study were assessed for their heat and salt tolerance capabilities. Viable cell count assay showed that the overexpression of chaperones in *C. autoethanogenum* profoundly enhanced viability at 42^{o}C. The DnaKJE^{over} strain displayed a viable cell count that was 238-fold higher than the plasmid control strain at this elevated temperature. In *L. lactis*, the heterologous expression of DnaK from *E. coli* resulted in 13.5-fold increase in viability upon heat shock at 42^{o}C (414). In *C. autoethanogenum*, the 42-fold improvement in cfu/mL relative to the plasmid control at 42^{o}C as a result of GroESL over-production is in congruence with literature findings. For instance, the overexpression of native GroESL in *Cyanobacterium anabaena* permitted growth at 42^{o}C (413) and the heterologous expression of GroESL from *L. paracasei* in *L. lactis* resulted in 1-log increase in cell viability at 54^{o}C (411). The co-overexpression of both DnaKJE and GroESL chaperone systems in *C. autoethanogenum* did not further enhance viable cell count. None of the chaperone recombinant strains or plasmid control strain in this study was able to form colonies at 45^{o}C after 14 days of incubation, which is consistent with the growth temperature range of 20^{o}C to 44^{o}C reported by Abrini *et al.* (1994) (52).

Both GroESL^{over} and DnGr^{over} recombinant strains, but not the DnaKJE^{over} strain, displayed higher tolerance towards 100 mM NaCl as evident in the significant increase in peak OD_{600} and growth rates relative to the plasmid control strain. The overexpression of GroESL raised peak OD_{600} by 18% whereas the co-overexpression of GroESL and DnaKJE chaperone systems enhanced peak OD_{600} by 42%. Surprisingly the overexpression of DnaKJE alone reduced growth rate and lowered peak OD_{600} by 47% relative to the plasmid control strain at 100 mM NaCl. When challenged with

200 mM NaCl, the growth of the plasmid control strain was significantly diminished to a peak OD_{600} of 0.23. In contrast, the GroESL^{over}, DnaKJE^{over} and DnGr^{over} strains were able to reach peak OD_{600} of 0.84 (3.65-fold increase), 0.44 (1.91-fold increase) and 0.31 (35% increase), respectively. Although the DnaKJE^{over} strain performed poorly at 100 mM NaCl level, it was significantly superior to the plasmid control strain at 200 mM NaCl concentration. One possible explanation for this discrepancy is that the positive effect of DnaKJE on cell growth outweighed its metabolic costs at extreme salt conditions of 200 mM but not 100 mM.

Negligible growth was recorded for all examined strains at 500 mM NaCl concentration over 14 days of incubation. It has been reported that 0.86 M to 1.2 M NaCl is sufficient to completely inhibit clostridia (431), which forms the basis for using salt as a food preservative. The positive impact of chaperone overexpression on salinity tolerance of *C. autoethanogenum* observed in this study is echoed elsewhere in the literature. For instance, the overexpression of native GroESL in *Cyanobacterium anabaena* increased OD_{750} by ~35% at 150 mM NaCl level (413) and the heterologous expression of DnaK from *E. coli* in *L. lactis* enhanced OD_{600} by 23% in the presence of 0.51 M NaCl (414). The heterologous expression of DnaK from *T. halophilus* in *E. coli* reduced growth lag phase in the presence of 0.86 M NaCl and 1.2 NaCl without increasing final OD_{600} (412).

7.6 Chapter Summary

Tolerance to toxic chemicals and stresses is a complex trait involving the actions of multiple genes and diverse cellular responses. Through the overexpression of chaperones, increased solvent tolerance was demonstrated in several saccharolytic microorganisms (176, 394, 411, 414, 416, 417) but this strategy has not been investigated in acetogens. This study demonstrated that the overexpression of chaperone system GroESL and/or DnaKJE in *C. autoethanogenum* enhanced survival and cell growth in the early stages of ethanol stress under autotrophic conditions. However, after prolonged incubation the plasmid control strain eventually outgrew the chaperone overexpression strains when challenged with 20 g/L ethanol. While

growing on CO without exogenous ethanol addition, the strain co-overexpressing GroESL and DnaKJE displayed significantly enhanced ethanol production. Besides ethanol tolerance, the overexpression of chaperones was shown to substantially improve thermal and salt tolerance in *C. autoethanogenum*, both of which are invaluable characteristics for an efficient industrial bioprocess.

Given the modulatory role of chaperones GroESL and DnaKJE on each other's expression, it is likely that optimization in their expressions via promoter selection/engineering can further enhance stress tolerance. Unbalanced overproduction of DnaK has been shown to be bactericidal in *E. coli* (432) and overproduction of GroEL can lead to undesired proteolytic activities (433). Transcriptomic studies will be very informative in revealing the impact of chaperone overexpression on global gene expression and allude to more detailed mechanisms of stress tolerance in *C. autoethanogenum*. As a next step of metabolic engineering, the chaperone genes should be codon altered (to prevent unintended recombination with genomic copy) and integrated into the genome for stable expression without the need for costly plasmid maintenance via antibiotic supplementation. Chaperones from microorganisms that naturally tolerate high ethanol concentrations (such as *Z. mobilis*) (434) and chaperones from thermophiles (409) are potential candidates for genetic engineering. Furthermore, bioreactor gas fermentations should be conducted to overcome any substrate limitation from the serum bottle studies in order to better assess the effect of chaperone production on product formation and stress tolerance.

CHAPTER 8

SUMMARY DISCUSSION

8 Summary Discussion

8.1 Introduction

The production of biofuels and commodity chemicals from waste gas fermentation is a unique technology that offers a range of advantages including the utilization of extremely low-cost, non-food feedstocks, and provides a mean to recycle waste carbon as part of humanity's concerted effort to tackle climate change. To bring this technology closer to commercial reality, metabolic engineering of the biocatalyst (an acetogenic bacterium) has the potential to address some of the limitations of the technology, such as low production rate and concentration, sub-optimal substrate utilization efficiency and product inhibition. Crucially, the ability to genetically modify the acetogen to synthesize new products permits the diversification of product streams to counter price volatility and reduce market risks.

This PhD project was initiated to develop genetic tools for targeted gene disruption and heterologous gene expression in gas-utilizing *C. autoethanogenum*. The following sections will address the objectives of this PhD study and provide a summary of the research outcomes. In particular, the construction of *cooS*, *adhE* and *aor* mutants using ClosTron mutagenesis and *pyrE*-mediated in-frame deletion (IFD) technique will be highlighted. Characterization of these mutants uncovered valuable insights into the roles of the inactivated genes in CO oxidation and fixation, and ethanol formation. Moreover, chaperone overexpression was attempted to engineer a recombinant strain for greater tolerance towards ethanol, heat and high salinity. Finally, a range of experiments is proposed as future work to generate a robust, hyper-ethanol producing *C. autoethanogenum* for industrial gas fermentation.

8.2 Development of Genetic Tools for *C. autoethanogenum*

One of the biggest obstacles to the development of genetic tools for any organism is to establish a reliable and efficient method of introducing foreign DNA into the cells. The thick peptidoglycan layer of Gram-positive bacteria and active RM systems have

frequently been held responsible for the inability to transform industrially important acetogens such as *C. carboxidivorans*, *C. ragsdalei*, *C. drakei*, and *E. limosum* (255). An efficient electroporation protocol for *C. ljungdahlii* was developed by Dr. Anne M. Henstra and Dr. Elizabeth Steiner in this laboratory (unpublished results), resulting in transformation efficiencies comparable to that reported by Leang *et al.* (2013) (229). Surprisingly, this electroporation procedure only resulted in limited success for the closely related *C. autoethanogenum* (100% nucleotide identity in 16S rRNA (38)). Comparison of the RM systems between the two acetogens revealed twelve unique RM systems in *C. autoethanogenum*, which are hypothesized to be a major contributor towards the genetic recalcitrance of the microbe. Very recently, genome-wide DNA methylation pattern of *C. autoethanogenum* was revealed using SMRT sequencing technologies (435). This information can be utilized to protect foreign DNA by *in vitro* or *in vivo* methylation, and the CDS of the RM systems can be genetically inactivated to significantly improve transformation efficiencies.

An alternative method of transformation is conjugation, which relies on direct cell-to-cell contact between the donor and recipient and therefore is restricted by the host range of the donor. Nonetheless, plasmids with three different Gram-positive replicons (pBP1, pCB102 and pCD6) were successfully conjugated into *C. autoethanogenum* using *E. coli* strain CA434 as the donor. The relatively high transfer efficiency and high reproducibility of conjugation in comparison to electroporation means conjugation was the method of choice for all genetic manipulations of *C. autoethanogenum* in this PhD study.

The establishment of a reliable DNA transfer protocol allowed genetic tools such as ClosTron mutagenesis and ACE to be exemplified in *C. autoethanogenum*. As a proof of concept, the EIIABC subunit of a fructose-specific PTS (*fruA*) was inactivated using ClosTron, resulting in a mutant that is unable to utilize fructose as a growth substrate. A *fruA* gene product was also investigated as a potential counter-selectable marker due to its ability to transport non-metabolizable sugar alcohols such as xylitol and D-mannitol into the cells, resulting in the accumulation of toxic phosphorylated intermediates. Growth experiments in pyruvate-based liquid medium showed that 100 mM D-mannitol did not inhibit growth of the WT whereas

100 mM xylitol reduced end-point OD_{600} of WT cells by 55% but only lowered end-point OD_{600} of a *fruA* mutant by 5%. A plating assay demonstrated that the WT was still able to form small colonies in the presence of 100 mM xylitol, but not at 200 mM and 300 mM concentrations. In contrast, the *fruA* mutant was able to form large colonies in the presence of 300 mM xylitol. These results demonstrated the potential of using *fruA* as a positive and negative selectable marker for *C. autoethanogenum*.

The genes *pyrE*/*pyrF*, whose encoded enzymes are involved in uracil biosynthesis but also convert the harmless pro-drug FOA into the cytotoxic compound FU, are frequently employed as positive and negative selectable markers in this laboratory (212, 214, 436) and others (237, 280). The *pyrE* gene of *C. autoethanogenum* was inactivated using ClosTron and the mutant was demonstrated to be uracil auxotrophic and tolerant to FOA, confirming its suitability as a selectable marker for future genetic works. Similar to *pyrE*, *codA* is also a potential counter-selectable marker due to its ability to convert the innocuous pro-drug FC into the cytotoxic compound FU. As expected, a ClosTron mutant of *codA* in *C. autoethanogenum* exhibited tolerance towards FC while the WT was growth inhibited by 50 µg/mL FC.

For precise genetic manipulations such as base substitutions, IFD and integration of large DNA fragments, allelic-exchange techniques such as ACE are employed. ACE utilizes non-symmetrical homology arms to direct the sequence of recombination events and also the activation/inactivation of gene(s) for selectable phenotype(s) (212). Although a counter-selectable marker is not a pre-requisite for ACE, the generation of a Δ*pyrE* mutant in *C. autoethanogenum* is useful for integration of biosynthetic pathways, IFD and substitution of bases by iterative alteration of the state of *pyrE*. Using ACE, a Δ*pyrE* mutant with 227 bp of 3` CDS deleted was successfully generated and subsequently restored back to WT allele. By cloning biosynthetic genes into the multiple cloning site (in *lacZα*) between the two homology arms of the *pyrE* restoration plasmid, heterologous pathways can be stably integrated into the genome of *C. autoethanogenum* to synthesize novel products such as butanol and isopropanol. During the IFD and subsequent restoration of *pyrE*, plasmid loss was achieved by replica plating on thiamphenicol containing solid medium.

8.3 Characterization of CODHs in *C. autoethanogenum*

Similar to other anaerobes such as *C. hydrogenoformans* (297), *M. acetivorans* (302), *M. thermoacetica* (73), and *C. ljungdahlii* (37), the genome of *C. autoethanogenum* encodes multiple CODHs: two mono-functional CODH (*cooS1* and *cooS2*) and one bi-functional CODH/ACS (*acsA*) (38). By employing ClosTron mutagenesis, these three CODHs were independently disrupted to assess their roles in supporting CO oxidation and carbon fixation.

As expected, the inactivation of *acsA* completely abolished autotrophic growth (CO or H_2+CO_2) and complementation by plasmid expression of functional *acsA* partially restored growth on pure CO. During growth on fructose, the *acsA* mutant accumulated 61% less biomass than WT, confirming the role of ACS in heterotrophic growth of *C. autoethanogenum*. Surprisingly, the mutant generated little or no acetate (a hallmark feature of acetogens), but 113% more ethanol and 138% more 2,3-butanediol than the WT. One explanation for these *acsA* mutant phenotypes is that disruption of *acsA* disabled the WLP, resulting in excess reducing equivalents which generated a driving force for the electron-consuming ethanol and 2,3-butanediol biosynthetic reactions. Again, complementation of the *acsA* mutant partially restored the biomass, acetate, ethanol and 2,3-butanediol levels back to WT. Plasmid overexpression of *acsA* in the presence of CO reduced the lag phase of growth by 4 days and appeared to increase the ethanol titre by 21% relative to plasmid control (not statistically significant). While growing on fructose, the *acsA* overexpression strain enhanced cell density by 24% without affecting acetate and ethanol levels. Collectively, *acsA* was demonstrated to be unequivocally essential for autotrophic growth in *C. autoethanogenum* and there is some evidence that overexpression of *acsA* enhances growth and ethanol formation during CO growth.

Unique to *C. autoethanogenum* is the presence of an internal 'TGA' stop codon within the *acsA* of this acetogen, splitting the gene into two CDS: CAETHG_1621 (1203 bp) and CAETHG_1620 (684 bp). The lack of an apparent RBS for the downstream CDS raised the suspicion that there may be a translational read-through mechanism which allows the synthesis of a full length AcsA ($AcsA^{full}$), instead of a truncated AcsA ($AcsA^{trunc}$). N-terminal and C-terminal FLAG-tagged *acsA* constructs

were transformed into *C. autoethanogenum*, *C. acetobutylicum* and *E. coli* to investigate the translational patterns of *acsA* in different hosts. No signals were detected in Western Blots containing crude lysates of transformed *C. acetobutylicum* (including a positive control that has the 'TGA' stop codon replaced by a 'TCA' serine codon) so it is hypothesized that the *acsA* promoter is not active in this *Clostridium*.

In *C. autoethanogenum*, Western Blots showed that there was no evidence of independent translation of the downstream CDS of *acsA*. Both N-terminal and C-terminal FLAG-tagged constructs clearly showed the presence of a full-length AcsA protein. In addition to the $AcsA^{full}$ protein, Western Blots also demonstrated the presence of the $AcsA^{trunc}$ band, which showed greater signal intensity than the $AcsA^{full}$ protein. These results indicated that although translational read-through occurs in *acsA* of *C. autoethanogenum*, the formation of the $AcsA^{full}$ protein is partial and inefficient. Given the pivotal roles AcsA has in acetogenesis, this inefficiency in synthesizing $AcsA^{full}$ may impose a handicap on autotrophic growth of *C. autoethanogenum*. Consistent with this notion, *C. ljungdahlii*, which does not have an internal stop codon in *acsA*, is reported to have a slightly shorter doubling time of 3.8 h instead of the 4 h observed for *C. autoethanogenum* under CO conditions (333).

Unlike *C. autoethanogenum*, *E. coli* is unable to form the $AcsA^{full}$ protein from either N-terminal or C-terminal FLAG-tagged *acsA* constructs. Instead, the $AcsA^{trunc}$ was detected, indicating that the promoter P_{acsA} is active in *E. coli*. Furthermore, a construct variant with a 'TCA' serine codon in place of the 'TGA' stop codon successfully produced the $AcsA^{full}$ protein. These results indicated that the translational read-through mechanism is unique to *C. autoethanogenum*. A putative bSECIS element was not detected by the algorithm developed by Zhang and Gladyshev (2005) (324) but was observed via manual inspection in the region immediately following the 'TGA' stop codon of *acsA* so the incorporation of selenocysteine is hypothesized to be the translational read-through mechanism. However, the absence of $AcsA^{full}$ protein in *E. coli*, which is one of the model organisms for selenocysteine biosynthesis and incorporation, suggests other mechanisms are responsible. Peptide sequencing using mass-spectroscopy could be

performed to identify the unknown amino acid corresponding to the 'TGA' stop codon.

In an attempt to examine the roles of *cooS1* and *cooS2* in *C. autoethanogenum*, the *acsA* KO mutant and WT were subjected to mixotrophic growth in the presence of both fructose and CO. The WT was able to consume fructose while oxidizing CO to CO_2, but the *acsA* mutant not only did not consume CO, it generated an additional 2.03 mmol CO. These results indicate that under the mixotrophic conditions tested, the physiological role of these mono-functional CODHs may lie in the direction of CO_2 reduction. During growth on pure CO (without fructose), the *cooS1* KO mutant exhibited a prolonged growth lag phase and reached lower cell density, but generated more ethanol than the WT. The elevated ethanol titre of the *cooS1* mutant was also observed during growth on BOF gas from a steel-making process (composition: 51.24% CO, 31.22% N_2, 11.98% CO_2, and 3.05% H_2). Surprisingly, the inactivation of *cooS1* had a profound, positive impact on H_2+CO_2 growth, as the mutant was able to grow without apparent lag phase and reached 2.2-fold higher cell density than the WT while acetate and ethanol production was unaffected. Since the mixotrophic growth experiments (CO and fructose) indicated that CODH1 and/or CODH2 may catalyze CO_2 reduction to CO, the elimination of these genes may improve growth on H_2+CO_2 by reducing competition for the CODH/ACS complex to access CO_2. Given the lack of negative impact of its mutation on autotrophic growth on CO or H_2+CO_2, the *cooS2* gene is unlikely to be heavily involved in autotrophy of *C. autoethanogenum*. For more definitive assessment of the roles of *cooS1* and *cooS2*, they could be cloned and purified for enzymatic studies.

8.4 Elucidation of Ethanologenic Pathway of *C. autoethanogenum*

The ethanologenic pathway of *C. autoethanogenum* and other prominent acetogenic ethanol producers such as *C. ljungdahlii*, *C. carboxidivorans*, and *C. ragsdalei* constitutes two metabolic routes (37-39, 141). One involves the direct reduction of acetyl-CoA to ethanol via acetaldehyde using a bi-functional AdhE enzyme. A second (indirect) route proceeds via acetate and employs an Aor enzmye to catalyze the

reduction of acetic acid to acetaldehyde followed by ethanol synthesis via an Adh enzyme. For each of the enzymes multiple copies are encoded in the genome of *C. autoethanogenum* (38). During acetogenic growth, the ATP yield is predicted to be limited so the generation of one mole of ATP (via SLP) per acetate synthesis is likely to make a significant difference. Due to this reason, it has been hypothesized that the indirect route of ethanol synthesis via acetate formation followed by subsequent reduction via an Aor enzyme is more favourable for acetogenic ethanol production. This is supported by stoichiometric and energetic analysis which predicted that very little ethanol production is possible from H_2+CO_2 without Aor due to severe ATP limitation (140). To enhance our understanding of the two ethanol formation routes, the two *adhE* genes (*adhE1* and *adhE2*) and *aor* genes (*aor1* and *aor2*) in *C. autoethanogenum* were targeted by ClosTron mutagenesis and IFD.

8.4.1 Characterization of *adhE* Mutants

The bi-functional AdhE enzymes consist of an upstream Ald domain and a downstream Adh domain. A ClosTron insertion in the Ald domain of *C. autoethanogenum* has been achieved in this study (*adhE1a* mutant) but there was concern that this may not be sufficient to disrupt the downstream Adh domain due to the insertional nature of intron-based mutagenesis. Furthermore, it has been shown that the related *adhE1* (*sol* operon) of *C. acetobutylicum* is translated into two peptides: one full length peptide and one truncated peptide encoding only the Adh domain (355). Hence, a separate ClosTron mutant targeting the Adh domain (*adhE1b* mutant) was also constructed. For the *adhE2* mutant, the ClosTron insertion site was located in the Ald domain. Serum bottle growth experiments with 2 bar CO showed that all three *adhE* mutants (*adhE1a*, *adhE1b* and *adhE2*) had significant growth retardation (reaching only half the cell density of WT), suggesting difficulty in recycling of reducing equivalents. Interestingly, all three *adhE* mutants generated 154 – 183% more ethanol but less 2,3-butanediol than WT. Increased ethanol production by the *adhE1a* mutant was further demonstrated using BOF gas as a substrate. The increase in ethanol production as a result of *adhE* inactivation can be explained by an increase in the availability of acetyl-CoA for acetate synthesis and

ethanol formation via Aor and Adh, which represents a viable strategy to manipulate the flux at acetyl-CoA towards the ATP-friendly, indirect ethanol biosynthetic route.

In comparison to the *adhE1a* mutant, the *adhE1b* mutant displayed a milder growth lag phase and was less affected in acetate synthesis during CO growth, which indicates that the function of the upstream Ald domain of *adhE1b* mutant is at least partially retained. To overcome the limitation of ClosTron mutagenesis, IFD of *adhE1* (both domains) and *adhE1+2* were undertaken. In the first attempt, an IFD mutant of *adhE1* was generated but an unintended deletion of 84 bp in the inter-genic region between *adhE1* and *adhE2* had also occurred, most likely due to homologous recombination between two 9 bp repeats. Following the loss of the IFD plasmid, the mutant was termed '$\Delta adhE1^{mut}$' and it was subjected to heterotrophic and autotrophic growth experiments. qRT-PCR studies showed that the $\Delta adhE1^{mut}$ mutant exhibited elevated *adhE2* mRNA levels compared to the WT during heterotrophic growth. This is likely because the IFD of *adhE1* together with the unintended removal of the promoter region of *adhE2* resulted in an arrangement in which the *adhE1* promoter can drive *adhE2* expression.

A second attempt at generating a Δ*adhE1* mutant without the unintended deletion of the *adhE2* promoter was successful but repeated attempts to lose the IFD plasmid were unsuccessful. Similarly, *adhE1+2* was deleted but the IFD plasmid was retained. The inability to isolate a 'clean' deletion mutant of *adhE1* and *adhE1+2* indicates that *adhE* may have some roles in supporting heterotrophic growth of *C. autoethanogenum*. In the case of the $\Delta adhE1^{mut}$ mutant, in which the IFD plasmid was lost in the first attempt, the overexpression of *adhE2* may compensate for the loss of activity of *adhE1*. This overexpression of *adhE2* in the $\Delta adhE1^{mut}$ mutant also appeared to dampen the increase in ethanol production to only 27% over the Δ*pyrE* control during CO growth, in comparison to the 171 – 183% increase in ethanol levels observed in ClosTron *adhE1a* and *adhE1b* mutants.

During heterotrophic growth on fructose, the *adhE1a* and *adhE1b* ClosTron mutants produced equal amounts of ethanol to the WT. This contradicts the findings of Leang *et al.* (2013), who showed that the replacement of part of Ald and Adh domains of

adhE1 in *C. ljungdahlii* with an *ermC* marker using homologous recombination resulted in a mutant that generated 6-fold less ethanol (229). As further evidence, the Δ*adhE1*^{mut} mutant also synthesized equal amounts of ethanol to the Δ*pyrE* control during growth on fructose. While growing on fructose, the *adhE2* ClosTron mutant attained 28% lower cell density than WT and was unable to completely utilize all the available substrate. Moreover, this mutant synthesized 63% less ethanol and 79% less 2,3-butanediol, but 39% more acetate than the WT. This repressed level of ethanol production in the *adhE2* mutant in *C. autoethanogenum* is again contradictory to a Δ*adhE2* mutant in *C. ljungdahlii*, where ethanol production was unaffected (229).

Comparison of AA sequence of AdhE1 and AdhE2 between *C. autoethanogenum* and *C. ljungdahlii* demonstrated that there are three substitutions in AdhE1 and eight substitutions in AdhE2. One of the AA changes in AdhE2 occurs in the NADH binding site of the Adh domain. It is possible that one of these substitutions results in modification of substrate and cofactor specificities, as demonstrated by the change of cofactor from NADH to NADPH in the AdhE of *C. thermocellum* due to one AA change in the Fe-Adh domain (357). Another possible explanation is that *C. autoethanogenum* may possess other ethanologenic enzymes that compensate for the loss of AdhE activities during growth on fructose. In order to fully elucidate the roles and potential differences of AdhEs between *C. autoethanogenum* and *C. ljungdahlii*, the *adhE* genes from both acetogens could be cloned, and the enzymes purified and subjected to enzymatic studies to compare their activities. Furthermore, transcriptomics and/or proteomics studies of *C. autoethanogenum* would also be informative in understanding the expression profiles of *adhEs*.

8.4.2 Characterization of *aor* Mutants

C. autoethanogenum possesses two *aor* genes (*aor1* and *aor2*), whose protein products are of the same length and which share 78% AA sequence identity. However, qRT-PCR studies of this acetogen growing in a bioreactor containing gas rich in H_2 and CO showed that the two *aor* genes displayed differential gene

expression and *aor1* (but not *aor2*) was one of the most highly expressed genes (Dr. Michael Köpke, LanzaTech; unpublished results). One of the main goals of this PhD project was to investigate the roles of Aor in supporting growth on CO and ethanol formation by characterizing *aor* KO mutants.

During growth on pure CO, the *aor1* ClosTron mutant displayed significant growth defects in the form of extended lag phase and it recorded half the cell density attained by the WT, indicative of difficulties in recycling reduced ferredoxins (from CO oxidation via CODH). Despite producing similar amounts of acetate as WT, the *aor1* mutant synthesized 57% less ethanol and 77% less 2,3-butanediol. Interestingly, this mutant also achieved 11-fold higher lactate titres than WT, suggesting that some of the excess reduced ferredoxins were used to catalyze the formation of pyruvate (a precursor of lactate) via PFOR. Complementation of the mutant by plasmid overexpression of *aor1* successfully restored ethanol and lactate levels, while improving cell density and 2,3-butanediol levels during CO growth.

Under heterotrophic conditions, the ethanol level of the *aor1* KO mutant was similarly reduced (by 33%), but without the significant reduction in cell density and elevated lactate production observed during CO growth. Recently, an *aor* deletion mutant in the hyperthermophilic archaeon *P. furiosus* was shown to generate 45-fold less ethanol than WT while metabolizing maltose (142). Both the autotrophic and heterotrophic growth experiments demonstrated that *aor1* is involved in ethanol formation in *C. autoethanogenum*. However, plasmid overexpression of *aor1* under CO conditions failed to raise ethanol levels, suggesting that *aor1* was not the bottleneck for ethanol biosynthesis under the conditions examined.

Similar to *aor1*, the inactivation of *aor2* resulted in a mutant that exhibited a prolonged growth lag phase and reached only half the cell density recorded by WT under pure CO conditions. However, the *aor2* mutant synthesized 170% more ethanol and 36% less acetate than WT, which is the opposite of what was observed with the *aor1* mutant in terms of ethanol production. The higher levels of ethanol production (93%) and lower titres of acetate (16%) shown by *aor2* mutant were also observed during cultivation in BOF gas. Furthermore, the *aor2* mutant was able to

generate 47% more ethanol than WT under heterotrophic conditions, but without displaying the growth defects observed under pure CO conditions.

The consistent higher ethanol production observed for the *aor2* mutant under both autotrophic and heterotrophic conditions suggests that inactivation of *aor2* exerts a positive effect on ethanol biosynthesis in *C. autoethanogenum*. Two explanations are provided to explain the contrasting phenotypes of *aor1* and *aor2* mutants. One is that Aor2 functions predominantly in the oxidation of acetaldehyde whereas Aor1 functions predominantly in the reduction of acetic acid. The other possibility is that the inactivation of *aor2* may reduce competition for access to substrate by the highly expressed and presumably more efficient Aor1, resulting in increased ethanol production. Further biochemical work is required to fully deduce the roles of the two Aor enzymes. For instance, the two *aor* genes could be cloned, expressed and purified for enzymatic assays to compare their activities with acetaldehyde and acetic acid. However, due to the dependency of Aor activity on the incorporation of tungsten and/or molybdenum (137, 371-373), the functional heterologous expression of Aor in *E. coli* may be challenging so native purification of Aor may be necessary.

Due to potential compensation of lost Aor activities from the remaining, unperturbed *aor* gene, a double KO mutant of *aor* (*aor1+*2KO) was constructed to fully assess the collective roles of both Aor enzymes on ethanol formation by *C. autoethanogenum*. As a first step of mutant construction, *aor1* was disrupted using ClosTron mutagenesis in a Δ*pyrE* strain. This was followed by the IFD of *aor2* using *pyrE*-mediated homologous recombination. As a final step, the Δ*pyrE* allele was restored to WT using ACE technique, resulting in an *aor1+2KO* mutant with a clean genotype background. The whole process of constructing this mutant fully exemplified the application and versatility of using *pyrE* as a selectable marker (positive and negative), ACE approaches and ClosTron mutagenesis in *C. autoethanogenum*. Due to time constraints, this mutant was not characterized. Future studies that include the examination of growth and product profiles under autotrophic and heterotrophic conditions would better elucidate the roles of Aor. Moreover, exogenous carboxylic acids such as *n*-butyric acid, propionic acid, *n*-valeric acid and *n*-caproic acid can be

added to the mutants in the presence of CO to determine whether the corresponding primary alcohols are generated (374).

8.5 Impact of Chaperone Overexpression on Ethanol, Heat and Saline Tolerance of *C. autoethanogenum*

In addition to the core ethanologenic enzymes responsible for ethanol production, ethanol tolerance is an important factor that determines the upper limit of ethanol synthesis in a microorganism. With few exceptions such as *Z. mobilis* (375) and *Lactococcus* strains (376), most bacteria can only tolerate 4 – 7% of ethanol (377). Engineering of ethanol tolerance has to be part of the strategies in the creation of a hyper-ethanol producing acetogenic biocatalyst so this PhD project investigated the effect of chaperone overexpression on product profile and stress tolerance. By cloning the native chaperone systems *groES-groEL* and/or *grpE-dnaK-dnaJ* into overexpression plasmids and then transformation into *C. autoethanogenum*, three recombinant strains were created: GroESL^{over}, DnaKJE^{over}, and DnGr^{over} (which overexpresses both chaperone systems).

To evaluate the efficacy of gene overexpression, qRT-PCR studies using cDNA samples generated from early-, mid- and late-growth phases of heterotrophic growth were undertaken. For the GroESL^{over} strain, the mRNA levels of *groEL* were higher than in theplasmid control strain during early- and late- growth phases. The transcript level of *groES* (encoding the cofactor of GroEL) was only higher than plasmid control at late growth phase but not during early- and mid-growth phases. The DnaKJE^{over} strain exhibited higher transcript levels of *grpE* and *dnaK* (but not *dnaJ*) than the plasmid control strain at all examined time-points. For the DnGr^{over} strain, gene up-regulation of *grpE*, *dnaK*, *groES*, and *groEL* (but not *dnaJ*) was consistently detected in all three growth phases relative to the plasmid control strain. Overall, there is molecular evidence for increased transcript levels of the targeted chaperones in *C. autoethanogenum* while growing on fructose.

From the same growth experiment used for qRT-PCR studies, cell density and metabolite profiles were also monitored to assess the impact of chaperone

overexpression under heterotrophic conditions. All three chaperone overexpression strains displayed increased growth lag phase but reached similar cell density to the plasmid control strain. The delay in growth of chaperone overexpression strains can be attributed to the additional metabolic burden imposed by the biosynthesis of these enzyme complexes and the subsequent ATP costs involved in protein folding. In *C. acetobutylicum*, the plasmid overexpression of GroESL resulted in a 30% increase in butanol titre but had no effect on ethanol level (176). In *C. autoethanogenum*, the GroESL^{over} strain showed a mild decrease of ethanol levels by 12%, together with a 13% increase in acetate while 2,3-butanediol production was unaltered relative to the plasmid control strain.

Surprisingly, the DnaKJE^{over} strain produced 82% more ethanol and 291% more 2,3-butanediol than the plasmid control strain while growing on fructose. Similar to the DnaKJE^{over} strain, the DnGr^{over} strain generated 76% more ethanol but only 46% more 2,3-butanediol than the plasmid control strain. Based on these results, it appeared that the overexpression of DnaKJE in *C. autoethanogenum* enhances the formation of ethanol and 2,3-butanediol under heterotrophic conditions. By employing an algorithm developed by Van Durme *et al.* (2009) (428), DnaK binding sites were detected for key enzymes (e.g., butanediol dehydrogenase, AdhE, Aor and PFOR) involved in ethanol and 2,3-butanediol formation. Coincidentally, these enzymes are larger than the 60 kDa size limit for encapsulation by chaperonin GroESL (396, 424), which may explain the lack of positive effect of GroESL overexpression on ethanol and 2,3-butanediol productions.

Under autotrophic conditions, ATP yield is predicted to be limited so the ATP costs associated with the biosynthesis and folding of proteins via chaperones are likely to be more pronounced than under heterotrophic conditions. For GroESL of *E. coli*, 130 ± 20 ATP was shown to be required for the folding of one 293 AA monomeric protein, rhodanase (418). In comparison, DnaKJE chaperone system of *E. coli* requires only 5 ATP for folding of one luciferase polypeptide (572 AA) (429). Consistent with the greater ATP costs associated with GroESL, the *C. autoethanogenum* GroESL^{over} strain achieved 33% lower cell density but showed asimilar growth lag phase to the plasmid control strain under pure CO conditions. In comparison, the DnaKJE^{over} and DnGr^{over}

strains reached similar cell densities but displayed prolonged lag phases than the plasmid control strain during growth on CO.

In terms of product formation under CO growth conditions, the overexpression of GroESL had no effect on ethanol production but reduced 2,3-butanediol and acetate by 23% and 17%, respectively. In comparison to the plasmid control strain, the DnaKJE^{over} strain generated 50% less ethanol and 77% less 2,3-butanediol. In contrast, co-overexpression of DnaKJE and GroESL chaperone systems resulted in a strain that synthesized 71% more ethanol but 73% less 2,3-butanediol than the plasmid control strain. Since neither mono-chaperone overexpressing strain but only the bi-chaperone overexpression strain generated more ethanol under CO growth conditions, it is likely that the relative abundance and interplay between the two chaperone systems contributed to the observed phenotypes. In *E. coli*, the combined overexpression of GrpE, GroESL and ClpB imparted a stronger tolerance towards 7% (v/v) ethanol than strains overexpressing each individual chaperone (394).

As assessment of ethanol tolerance, the chaperone overexpression strains and plasmid control strain were cultivated in serum bottles containing 2 bar CO. When the OD_{600} reached 0.2, anaerobic ethanol was injected to achieve final ethanol concentrations of 20 g/L (434 mM) and 40 g/L (868 mM). Following 12 h of ethanol challenge, plating assays were undertaken to compare the viable cell counts which were expressed as % cfu/mL relative to unchallenged cultures. The addition of 20 g/L and 40 g/L ethanol drastically reduced the % cfu/mL of the plasmid control strain to 0.071 and 0.035, respectively. At the 20 g/L ethanol challenge level, all three chaperone overexpression strains recorded % cfu/mL of 8.2 to 23.8, with the DnGr^{over} strain being the best performer with a 335-fold improvement in viability over the plasmid control strain. At 40 g/L ethanol challenge level, the DnaKJE^{over} and DnGr^{over} strains, respectively, showed 109-fold and 1083-fold enhancement in % cfu/mL over the plasmid control strain. However, the GroESL^{over} strain performed less well than the plasmid control strain (41% decrease) in terms of cell viability at this ethanol challenge concentration. Overall, the overexpression of chaperones in *C. autoethanogenum* had a strong positive effect on cell viability when challenged with ethanol under CO conditions. In particular, the recombinant strain co-overexpressing

both GroESL and DnaKJE chaperone systems performed best under both ethanol challenge conditions.

Beyond the 12 h post ethanol challenge period, the cell density of serum bottle cultures was monitored spectroscopically for up to 50 days. Consistent with the viable cell count results, all three chaperone overexpression strains showed early increase of cell density at the 20 g/L ethanol challenge level within the first 7 days. In contrast, the plasmid control strain displayed a prolonged growth lag phase of >7 days. It is important to note that the plasmid control strain eventually outgrew all three chaperone overexpression strains, indicating that the metabolic burden of chaperone overproduction can lead to reduced cell yield under substrate limited conditions. In order to overcome this substrate limitation and better assess the effect of chaperone overexpression, the ethanol challenge assays can be undertaken in bioreactors with continuously supplied CO and high endogenous ethanol production should be achieved. At a 40 g/L ethanol challenge, comparisons of the cell density achieved were complicated by the significant intra-replicate variations. However, there is some evidence that the DnaKJE^{over} and DnGr^{over} strains (but not GroESL^{over}) were able to accumulate cell biomass earlier than the plasmid control strain, consistent with the viable cell count assays. It should be emphasized that the addition of exogenous ethanol is only a good proxy to mimic ethanol stress and the physiological response towards endogenously synthesized ethanol may differ.

Besides the enhancement of ethanol tolerance, overexpression of chaperones in microorganisms had been shown to improve tolerance to salt (412-414) and extreme temperature (408, 409, 411, 415). The ability to tolerate heat allows the industrial gas fermentation process to operate at higher temperature to reduce cooling costs and facilitate product separation via distillation by allowing higher titres. Moreover, high salt tolerance is also a desired property of a biocatalyst in allowing less cost-intensive purification prior to fermentation medium recycling. To compare the heat tolerance of chaperone overexpression strains, fructose-grown cells were serially diluted and plated onto solid medium (fructose based) and cfu numbers recorded after 5 days of incubation at 42^{o}C and 14 days of incubation at 45^{o}C. At 42^{o}C, the DnaKJE^{over}, DnGr^{over} and GroESL^{over} strains generated 238-fold, 139-fold and 42-fold

higher cfu/mL than the plasmid control strain. However, no colonies were observed at 45^{o}C after 14 days of incubation for all the examined strains. For assessment of salt tolerance, the bacterial strains were cultured in liquid medium (fructose-based) supplemented with 100 mM, 200 mM and 500 mM NaCl. The monitoring of cell density showed that the DnGr^{over} and GroESL^{over} (but not DnaKJE^{over}) strains significantly outgrew the plasmid control strain at the 100 mM NaCl level. When challenged with 200 mM NaCl, all three chaperone overexpression strains (especially the GroESL^{over}) reached higher cell density than the plasmid control strain. Negligible growth was detected for all strains in the presence of 500 mM NaCl.

In summary, the overexpression of chaperones in *C. autoethanogenum* was shown to enhance ethanol tolerance, influence product formation, and improve heat and salt tolerance. The recombinant strain co-overexpressing the GroESL and DnaKJE chaperone systems is particularly interesting because it uniquely increased ethanol production while growing on CO. As future studies, the two chaperone systems could be codon-altered (to prevent unwanted homologous recombination with the chromosome) and integrated into the genome of *C. autoethanogenum* before strain assessment in bioreactors. Given the interplay between GroESL and DnaKJE, and their interactions with regulatory elements such as stress-specific sigma factor H (σ^{H}) (430), optimization of promoters is also likely to be crucial for the construction of a high ethanol-producing and stress tolerant strain for industrial gas fermentation.

8.6 Generation of Robust, Hyper-Ethanol Producing Strains and Future Studies

In this PhD study, the generation and characterization of *cooS*, *adhE*, *aor* and chaperone mutants have revealed some interesting targets that lead to enhanced ethanol production under CO conditions. In particular, the individual inactivation of *adhE*, *aor2* and co-overproduction of GroESL and DnaKJE chaperone systems enhanced ethanol production in the presence of CO. By combining multiple genetic manipulations in the same strain, it should be possible to engineer a robust, hyper-ethanol producing strain for industrial gas fermentation. For instance, the disruption

of *pta* and *buk* genes, coupled with the overexpression of a mutated *adhE* in *C. acetobutylicum* resulted in a recombinant strain that produced 160% higher butanol titre than WT (363). With ClosTron mutagenesis and ACE fully exemplified in *C. autoethanogenum*, genetic tools are available for complex engineering of stable multiple KO and/or insertion mutants.

The impact of gene KO or plasmid overexpression on the production of ethanol and 2,3-butanediol in *C. autoethanogenum* under pure CO conditions is summarized in Figure 8.1A-D. The disruption of both *adhE* and *aor2* elicited a particularly strong increase in ethanol titres (Figure 8.1A) so these three genes can be inactivated to divert carbon and electrons towards the ATP-generating ethanologenic pathway employing *pta, ack* and *aor1*. Although the plasmid overexpression of *aor1* in an *adhE* sufficient background resulted in no positive effect on ethanol production (Figure 8.1C), it is worthwhile to investigate the overexpression of *aor1* in an *adhE* and *aor2* deficient genetic background. Furthermore, the chaperone systems *groESL* and *grpE-dnaK-dnaJ* can be co-overexpressed in this *adhE1*, *adhE2* and *aor2* triple KO mutant to further improve ethanol production and enhance stress tolerance towards ethanol, heat and salts. Out of the mutants examined in this study, none generated significantly more 2,3-butanediol under CO conditions than WT (Figure 8.1B) or plasmid controls (Figure 8.1D).

It is important to realise that, although the individual gene disruption improves ethanol titres, their combinations may not necessarily have a cumulative effect and may even have detrimental consequences on the performance of the mutants. Genome scale models may prove to be very useful in predicting whether a specific genetic manipulation combination is viable and favourable for autotrophic ethanol production. The genome scale models for acetogens growing on CO are beginning to emerge (170, 437) and are predicted to play an increasingly important role in directing metabolic engineering efforts. The data of this thesis can be used to validate and optimize genome scale models. Furthermore, transposon-directed insertion site sequencing (TraDIS) may also be very useful in elucidating which genes or regulators are essential for acetogenesis. Recently, TraDIS was demonstrated in

acetogen *C. difficile* but the experiment was not conducted to investigate autotrophic growth (438).

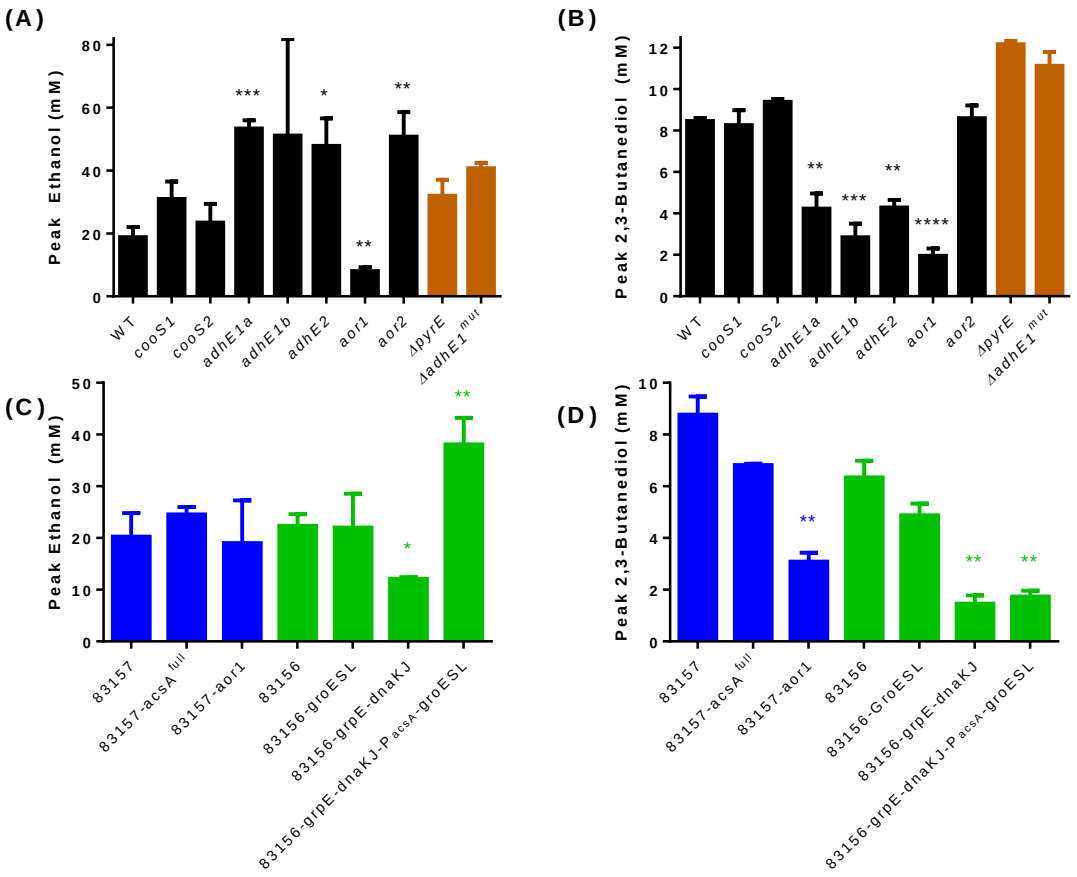


Figure 8.1. Comparison of peak ethanol and 2,3-butanediol production during growth of *C. autoethanogenum* mutants on pure CO. (A) Peak ethanol by ClosTron KO and in-frame deletion (IFD) mutants; (B) Peak 2,3-butanediol by ClosTron KO and IFD mutants; (C) Peak ethanol by plasmid overexpression strains; (D) Peak 2,3-butanediol by plasmid overexpression strains. Comparable mutants/strains and student's t-test statistical significance are colour-coded into black, brown, blue and green. N = 3-4; Error bars = standard error of mean; * p-value < 0.05; ** p-value < 0.005; *** p-value < 0.0005.

The balancing of fluxes of each enzyme reaction within the ethanologenic pathway is one of the main challenges in achieving high ethanol productivity. This approach aims to reduce accumulation of toxic intermediates (e.g., acetate and acetaldehyde), redox imbalance and metabolic burden from overproduction of enzymes. The

balancing of pathway flux can be achieved via modulation of enzyme expression at the level of DNA, RNA and protein by altering plasmid copy number, promoter selection and RBS strengths (439). At the post translational level, synthetic scaffolds offer great potential in co-localizing functionally related, multi-step pathway enzymes for spatial and temporal control over metabolic flux. For instance, three enzymes for the biosynthesis of mevalonate were tagged with binding motifs from metazoan signalling proteins to form a protein scaffold complex in *E. coli*, resulting in 77-fold improvement in mevalonate titre (440). As an extension to scaffold-based flux control, compartmentalization of substrates with functionally related enzymes in the form of bacterial micro-compartments (protein-based organelles) (360, 441, 442) can prevent the loss of volatile intermediates and insulate the cells from toxic compounds. Genes encoding putative micro-compartments are detected in the genome of *C. autoethanogenum* and their roles in supporting non-acetogenic growth of *A. woodii* on 1,2-propanediol have recently been reported (443).

To fully exploit the potential of *C. autoethanogenum* as a microbial chassis for generation of biofuels and platform chemicals from waste gases, more advanced synthetic biology tools are required. Fundamental to fine-tuning of expression is the development of constitutive and inducible promoters, RBS libraries, and codon optimization. For rapid generation of precise mutant libraries, Clustered Regularly Interspaced Short Palindromic Repeats (CRISPR)-based technologies have been successfully applied for *C. beijerinckii*, *E. coli*, *Streptococcus pneumoniae* and *S. cerevisiae* (444-446). Multiplex Automated Genome Engineering (MAGE) was developed to perform large-scale programming and evolution of cells by employing oligo-mediated allelic exchange and continuous directed evolution (447). Due to the scale of the genetic constructs and mutant libraries, automation will be an increasingly important part of modern synthetic biology approaches, from the assembly of plasmids to screening of mutants. Major challenges remains in the high throughput screening of mutant libraries under autotrophic conditions.

8.7 Conclusion

Prior to this PhD study, there had been no scientific publication on genetic manipulation of *C. autoethanogenum* so the overall goal of this work was to develop genetic tools to unlock the potential of this acetogen for commercial production of ethanol from waste gases. ClosTron mutagenesis and *pyrE*-mediated ACE were fully exemplified in this biocatalyst enabling the generation of stable KO and IFD mutants in the area of CO oxidation and fixation (*cooS* and *acsA*), and ethanologenic pathway (*adhE* and *aor*). Characterization of these mutants under autotrophic and heterotrophic conditions revealed new insights into their physiology and provided directions for further metabolic engineering of a hyper-ethanol producing strain. Individual disruption of *adhE*, *aor2* and co-overproduction of GroESL and DnaKJE chaperone systems were shown to increase ethanol production by 71 – 183% under CO conditions so these strains can serve as basis for future work. Finally, the overexpression of native chaperones was found to enhance ethanol production and improve tolerance towards ethanol, heat and salt. Recent advances in the field of genome scale models, synthetic biology and advanced genetic tools are predicted to revolutionize metabolic engineering efforts in this important acetogen.

CHAPTER 9

REFERENCES

9 References

1. **Lane J.** 2015. China Steel green-lights commercial-scale LanzaTech advanced biofuels project, *on* Biofuels Digest. http://www.biofuelsdigest.com/bdigest/2015/04/22/china-steel-green-lights-46m-for-commercial-scale-lanzatech-advanced-biofuels-project/.
2. **Lane J.** 2015. Steel's big dog jumps into low carbon fuels: ArcelorMittal, LanzaTech, Primetals Technologies to construct $96M biofuel production facility, *on* Biofuels Digest. http://www.biofuelsdigest.com/bdigest/2015/07/13/steels-big-dog-jumps-into-low-carbon-fuels-arcelormittal-lanzatech-primetals-technologies-to-construct-96m-biofuel-production-facility/.
3. **Demirbas A.** 2009. Political, economic and environmental impacts of biofuels: A review. Applied Energy **86:**S108-S117.
4. **REN21.** 2011. *Renewables 2011 Global Status Report*. REN21, Paris.
5. **Köpke M, Noack S, Dürre P.** 2011. The past, present, and future of biofuels – Biobutanol as promising alternative, p 451-486. *In* dos Santos Bernades MA (ed). InTech.
6. **Pernick R, Wilder C, Winnie T.** 2012. Clean Energy Trends 2012. Clean Edge Inc., Inc. CE,
7. **Dürre P.** 2007. Biobutanol: an attractive biofuel. Biotechnology Journal **2:**1525-1534.
8. **Jones DT, Woods DR.** 1986. Acetone-butanol fermentation revisited. Microbiological Reviews **50:**484-524.
9. **OECD-FAO.** 2011. OECD-FAO Agricultural Outlook 2011-2020.
10. **Murse T.** 2011. Understanding the ethanol subsidy. http://usgovinfo.about.com/od/moneymatters/a/The-Federal-Ethanol-Subsidy.htm.
11. **Pear R.** 2nd January 2012. After three decades, tax credit for ethanol expires, p *In* The New York Times.
12. **Carere CR, Sparling R, Cicek N, Levin DB.** 2008. Third generation biofuels via direct cellulose fermentation. International Journal of Molecular Sciences **9:**1342-1360.
13. **Datar RP, Shenkman RM, Cateni BG, Huhnke RL, Lewis RS.** 2004. Fermentation of biomass-generated producer gas to ethanol. Biotechnology and Bioengineering **86:**587-594.
14. **Abubackar HN, Veiga MC, Kennes C, Coruña L.** 2011. Biological conversion of carbon monoxide: rich syngas or waste gases to bioethanol. Biofuels, Bioproducts and Biorefining **5:**93-114.
15. **Siedlecki M, de Jong W, Verkooijen AHM.** 2011. Fluidized bed gasification as a mature and reliable technology for the production of bio-syngas and applied in the production of liquid transportation fuels-A review. Energies **4:**389-434.
16. **Mohammadi M, Najafpour GD, Younesi F, Lahijani P, Uzir MH, Mohamed AR.** 2011. Bioconversion of synthesis gas to second generation biofuels: A review. Renewable & Sustainable Energy Reviews **15:**4255-4273.
17. **Wei L, Pordesimo LO, Haryanto A, Wooten J.** 2011. Co-gasification of hardwood chips and crude glycerol in a pilot scale downdraft gasifier. Bioresource Technology **102:**6266-6272.
18. **Dudynski M, Kwiatkowski K, Bajer K.** 2012. From feathers to syngas - Technologies and devices. Waste Management **32:**685-691.
19. **Klasson KT, Ackerson MD, Clausen EC, Gaddy JL.** 1992. Bioconversion of synthesis gas into liquid or gasesous fuels. Enzyme and Microbial Technology **14:**602-608.
20. **Sipma J, Henstra AM, Parshina SM, Lens PN, Lettinga G, Stams AJM.** 2006. Microbial CO conversions with applications in synthesis gas purification and bio-desulfurization. Critical Reviews in Biotechnology **26:**41-65.
21. **Klasson KT, Ackerson MD, Clausen EC, Gaddy JL.** 1991. Bioreactor design for synthesis gas fermentations. Fuel **70:**605-614.
22. **Latif H, Zeidan AA, Nielsen AT, Zengler K.** 2014. Trash to treasure: production of biofuels and commodity chemicals via syngas fermenting microorganisms. Current Opinion in Biotechnology **27:**79-87.
23. **Bengelsdorf FR, Straub M, Dürre P.** 2013. Bacterial synthesis gas (syngas) fermentation. Environmental Technology **34:**1639-1651.
24. **Dürre P.** 2007. Clostridia, p *In* (ed), Encyclopedia of Life Sciences, ed vol John Wiley & Sons Ltd.
25. **Dürre P.** 2005. Handbook on Clostridia. CRC Press Taylor & Francis Group.
26. **Tracy BP, Jones SW, Fast AG, Indurthi DC, Papoutsakis ET.** 2011. Clostridia: the importance of their exceptional substrate and metabolite diversity for biofuel and biorefinery applications. Current Opinion in Biotechnology**:**1-18.
27. **Bahl H, Dürre P.** 2001. Clostridia: Biotechnology and medical applications. Wiley-VCH, Veinheim.
28. **Lincke T, Behnken S, Ishida K, Roth M, Hertweck C.** 2010. Closthioamide: An unprecedented polythioamide antibiotic from the strictly anaerobic bacterium *Clostridium cellulolyticum*. Angewandte Chemie-International Edition **49:**2011-2013.
29. **Minton NP.** 2003. Clostridia in cancer therapy. Nature Reviews Microbiology **1:**237-242.

30. **Desvaux M.** 2006. Unravelling carbon metabolism in anaerobic cellulolytic bacteria. Biotechnology Progress **22:**1229-1238.
31. **Drake HL, Gössner AS, Daniel SL.** 2008. Old acetogens, new light. Annals of the New York Academy of Sciences **1125:**100-128.
32. **Chen JS, Toth J, Kasap M.** 2001. Nitrogen-fixation genes and nitrogenase activity in *Clostridium acetobutylicum* and *Clostridium beijerinckii*. Journal of Industrial Microbiology & Biotechnology **27:**281-286.
33. **Nevin KP, Hensley SA, Franks AE, Summers ZM, Ou JH, Woodard TL, Snoeyenbos-West OL, Lovley DR.** 2011. Electrosynthesis of organic compounds from carbon dioxide is catalyzed by a diversity of acetogenic microorganisms. Applied and Environmental Microbiology **77:**2882-2886.
34. **Nevin KP, Woodard TL, Franks AE, Summers ZM, Lovley DR.** 2010. Microbial electrosynthesis: feeding microbes electricity to convert carbon dioxide and water to multicarbon extracellular organic compounds. Mbio **1:**e00103-00110.
35. **Nölling J, Breton G, Omelchenko MV, Makarova KS, Zeng Q, Gibson R, Lee HM, Dubois J, Qiu D, Hitti J, Wolf YI, Tatusov RL, Sabathe F, Doucette-Stamm L, Soucaille P, Daly MJ, Bennett GN, Koonin EV, Smith DR.** 2001. Genome sequence and comparative analysis of the solvent-producing bacterium *Clostridium acetobutylicum*. Journal of Bacteriology **183:**4823-4838.
36. **Sabathe F, Belaich A, Soucaille P.** 2002. Characterization of the cellulolytic complex (cellulosome) of *Clostridium acetobutylicum*. Federation of European Microbiological Society Microbiology Letters **217:**15-22.
37. **Köpke M, Held C, Hujer S, Liesegang H, Wiezer A, Wollherr A, Ehrenreich A, Liebl W, Gottschalk G, Dürre P.** 2010. *Clostridium ljungdahlii* represents a microbial production platform based on syngas. Proceedings of the National Academy of Sciences of the United States of America **107:**13087-13092.
38. **Brown SD, Nagaraju S, Utturkar S, De Tissera S, Segovia S, Mitchell W, Land ML, Dassanayake A, Köpke M.** 2014. Comparison of single-molecule sequencing and hybrid approaches for finishing the genome of *Clostridium autoethanogenum* and analysis of CRISPR systems in industrial relevant Clostridia. Biotechnology for Biofuels **7:**1-18.
39. **Bruant G, Lévesque M-J, Peter C, Guiot SR, Masson L.** 2010. Genomic analysis of carbon monoxide utilization and butanol production by *Clostridium carboxidivorans* strain P7. PloS ONE **5:**e13033.
40. **Paul D, Austin FW, Arick T, Bridges SM, Burgess SC, Dandass YS, Lawrence ML.** 2010. Genome sequence of the solvent-producing bacterium *Clostridium carboxidivorans* strain P7T. Journal of Bacteriology **192:**5554-5555.
41. **Genthner BRS, Bryant MP.** 1987. Additional characteristics of one-carbon-compound utilization by *Eubacterium limosum* and *Acetobacterium woodi*. Applied and Environmental Microbiology **53:**471-476.
42. **Poehlein A, Schmidt S, Kaster AK, Goenrich M, Vollmers J, Thurmer A, Bertsch J, Schuchmann K, Voigt B, Hecker M, Daniel R, Thauer RK, Gottschalk G, Müller V.** 2012. An ancient pathway combining carbon dioxide fixation with the generation and utilization of a sodium ion gradient for ATP synthesis. Plos ONE **7:**e33439.
43. **Kane MD, Breznak JA.** 1991. *Acetonema longum* gen nov SP-nov, an H2/CO2 acetogenic bacterium from the termite, *Pterotermes occidentis*. Archives of Microbiology **156:**91-98.
44. **Allen TD, Caldwell ME, Lawson Pa, Huhnke RL, Tanner RS.** 2010. *Alkalibaculum bacchi* gen. nov., sp. nov., a CO-oxidizing, ethanol-producing acetogen isolated from livestock-impacted soil. International Journal of Systematic and Evolutionary Microbiology **60:**2483-2489.
45. **Liu K, Atiyeh HK, Tanner RS, Wilkins MR, Huhnke RL.** 2012. Fermentative production of ethanol from syngas using novel moderately alkaliphilic strains of *Alkalibaculum bacchi*. Bioresource Technology **104:**336-341.
46. **Lynd L, Kerby R, Zeikus JG.** 1982. Carbon monoxide metabolism of the methylotrophic acidogen *Butyribacterium methylotrophicum*. Journal of Bacteriology **149:**255-263.
47. **Zeikus JG, Lynd LH, Thompson TE, Krzycki Ja, Weimer PJ, Hegge PW.** 1980. Isolation and characterization of a new, methylotrophic, acidogenic anaerobe, the marburg strain. Current Microbiology **3:**381-386.
48. **Grethlein AJ, Worden RM, Jain MK, Datta R.** 1991. Evidence for production of n-butanol from carbon monoxide by *Butyribacterium methylotrophicum*. Journal of Fermentation and Bioengineering **72:**58-60.
49. **Lux MF, Drake HL.** 1992. Reexamination of the metabolic potentials of the acetogens *Clostridium aceticum* and *Clostridium formicoaceticum* - chemolithoautotrophic and aromatic-dependent growth. Federation of European Microbiological Society Microbiology Letters **95:**49-56.
50. **Adamse AD.** 1980. New isoation of *Clostridium aceticum* (Wieringa). Antonie Van Leeuwenhoek Journal of Microbiology **46:**523-531.
51. **Braun M, Mayer F, Gottschalk G.** 1981. *Clostridium aceticum* (Wieringa), a microorganism producing acetic acid from molecular hydrogen and carbon dioxide. Archives of Microbiology **128:**288-293.
52. **Abrini J, Naveau H, Nyns EJ.** 1994. *Clostridium autoethanogenum*, sp. nov., an anaerobic bacterium that produces ethanol from carbon monoxide. Archives of Microbiology **161:**345-351.

53. **Köpke M, Mihalcea C, Liew FM, Tizard JH, Ali MS, Conolly JJ, Al-Sinawi B, Simpson SD.** 2011. 2,3-butanediol production by acetogenic bacteria, an alternative route to chemical synthesis, using industrial waste gas. Applied and Environmental Microbiology **77:**5467-5475.
54. **Liou JSC, Balkwill DL, Drake GR, Tanner RS.** 2005. *Clostridium carboxidivorans* sp nov., a solvent-producing clostridium isolated from an agricultural settling lagoon, and reclassification of the acetogen *Clostridium scatologenes* strain SL1 as *Clostridium drakei* sp nov. International Journal of Systematic and Evolutionary Microbiology **55:**2085-2091.
55. **Köpke M, Straub M, Dürre P.** 2013. *Clostridium difficile* is an autotrophic bacterial pathogen. Plos ONE **8:**e62157.
56. **Monot M, Boursaux-Eude C, Thibonnier M, Vallenet D, Moszer I, Medigue C, Martin-Verstraete I, Dupuy B.** 2011. Reannotation of the genome sequence of *Clostridium difficile* strain 630. Journal of Medical Microbiology **60:**1193-1199.
57. **Rieu-Lesme F, Dauga C, Fonty G, Dore J.** 1998. Isolation from the rumen of a new acetogenic bacterium phylogenetically closely related to *Clostridium difficile*. Anaerobe **4:**89-94.
58. **Küsel K, Dorsch T, Acker G, Stackebrandt E, Drake HL.** 2000. *Clostridium scatologenes* strain SL1 isolated as an acetogenic bacterium from acidic sediments. International Journal of Systematic and Evolutionary Microbiology **50 Pt 2:**537-546.
59. **Gössner AS, Picardal F, Tanner RS, Drake HL.** 2008. Carbon metabolism of the moderately acid-tolerant acetogen *Clostridium drakei* isolated from peat. Federation of European Microbiological Society Microbiology Letters **287:**236-242.
60. **Andreese.Jr, Gottscha.G, Schlegel HG.** 1970. *Clostridium formicoaceticum* nov spec - Isolation, description and distinction from *Clostridium aceticum* and *Clostridium thermoaceticum*. Archives of Microbiology **72:**154.
61. **Diekert GB, Thauer RK.** 1978. Carbon monoxide oxidation by *Clostridium thermoaceticum* and *Clostridium formicoaceticum*. Journal of Bacteriology **136:**597-606.
62. **Küsel K, Karnholz A, Trinkwalter T, Devereux R, Acker G, Drake HL.** 2001. Physiological ecology of *Clostridium glycolicum* RD-1, an aerotolerant acetogen isolated from sea grass roots. Applied and Environmental Microbiology **67:**4734-4741.
63. **Ohwaki K, Hungate RE.** 1977. Hydrogen utilization by clostridia in sewage sludge. Applied and Environmental Microbiology **33:**1270-1274.
64. **Tanner RS, Miller LM, Yang D.** 1993. *Clostridium ljungdahlii* sp. nov., an acetogenic species in clostridial rRNA homology group I. International Journal of Systematic Bacteriology **43:**232-232.
65. **Bomar M, Hippe H, Schink B.** 1991. Lithotrophic growth and hydrogen metabolism by *Clostridium magnum*. Federation of European Microbiological Society Microbiology Letters **83:**347-350.
66. **Schink B.** 1984. *Clostridium magnum* sp nov, a non-autotrophic homoacetogenic bacterium. Archives of Microbiology **137:**250-255.
67. **Kane MD, Brauman A, Breznak JA.** 1991. *Clostridium mayombei* sp nov, an H_2/CO_2 acetogenic bacterium from the gut of the African soil-feeding termite, C*ubitermes speciosus*. Archives of Microbiology **156:**99-104.
68. **Mechichi T, Labat M, Patel BK, Woo TH, Thomas P, Garcia JL.** 1999. *Clostridium methoxybenzovorans* sp. nov., a new aromatic o-demethylating homoacetogen from an olive mill wastewater treatment digester. International Journal of Systematic Bacteriology **49 Pt 3:**1201-1209.
69. **Huhnke R, Lewis RS, Tanner RS.** 2008. Isolation and characterization of novel Clostridial species. Patent WO2008/028055.
70. **Genthner BRS, Davis CL, Bryant MP.** 1981. Features of rumen and sewage sludge strains of *Eubacterium limosum*, a methanol-utilizing and H_2-CO_2-utilizing species. Applied and Environmental Microbiology **42:**12-19.
71. **Krumholz LR, Bryant MP.** 1985. *Clostridium pfennigii* sp nov uses methoxyl groups of monobenzenoids and produces butyrate. International Journal of Systematic Bacteriology **35:**454-456.
72. **Lorowitz WH, Bryant MP.** 1984. *Peptostreptococcus productus* strain that grows rapidly with CO as the energy source. Applied and Environmental Microbiology **47:**961-964.
73. **Pierce E, Xie G, Barabote R, Saunders E, Han CS, Detter JC, Richardson P, Brettin TS, Das A, Ljungdahl LG, Ragsdale SW.** 2008. The complete genome sequence of *Moorella thermoacetica* (f. *Clostridium thermoaceticum*). Environmental microbiology **10:**2550-2573.
74. **Daniel SL, Hsu T, Dean SI, Drake HL.** 1990. Characterization of the H2-dependent and CO-dependent chemolithotrophic potentials of the acetogens *Clostridium thermoaceticum* and *Acetogenium kivui*. Journal of Bacteriology **172:**4464-4471.
75. **Kerby R, Zeikus JG.** 1983. Growth of *Clostridium thermoaceticum* on H2/CO2 or CO as energy source. Current Microbiology **8:**27-30.
76. **Savage MD, Wu ZR, Daniel SL, Lundie LL, Drake HL.** 1987. Carbon monoxide-dependent chemolithotrophic growth of *Clostridium thermoautotrophicum*. Applied and Environmental Microbiology **53:**1902-1906.

77. **Drake HL, Küsel K, Matthies C.** 2006. Acetogenic prokaryotes, p 354-420. *In* Dworkin M, Falkow S, Rosenberg E, Schleifer K-H, Stackebrandt E (ed), The Prokaryotes, Third Edition ed. Springer New York.
78. **Ragsdale SW.** 2008. Enzymology of the Wood-Ljungdahl pathway of acetogenesis. Annals of the New York Academy of Sciences **1125:**129-136.
79. **Ragsdale SW.** 2004. Life with carbon monoxide. Critical Reviews in Biochemistry and Molecular Biology **39:**165-195.
80. **Ragsdale SW, Clark JE, Ljungdahl LG, Lundie LL, Drake HL.** 1983. Properties of purified carbon monoxide dehydrogenase from *Clostridium thermoaceticum*, a nickel, iron-sulfur protein. Journal of Biological Chemistry **258:**2364-2369.
81. **Pezacka E, Wood HG.** 1986. The autotrophic pathway of acetogenic bacteria - Role of CO dehydrogenase disulfide reductase. Journal of Biological Chemistry **261:**1609-1615.
82. **Müller V.** 2003. Energy conservation in acetogenic bacteria. Applied and Environmental Microbiology **69:**6345-6353.
83. **Schuchmann K, Müller V.** 2014. Autotrophy at the thermodynamic limit of life: A model for energy conservation in acetogenic bacteria. Nature Reviews Microbiology **12:**809-821.
84. **Calusinska M, Happe T, Joris B, Wilmotte A.** 2010. The surprising diversity of clostridial hydrogenases: a comparative genomic perspective. Microbiology **156:**1575-1588.
85. **Vignais PM, Colbeau A.** 2004. Molecular biology of microbial hydrogenases. Current Issues in Molecular Biology **6:**159-188.
86. **Vignais PM.** 2007. Hydrogenases and H^+-reduction in primary energy conservation. Results and Problems in Cell Differentiation **45:**223-252.
87. **Demuez M, Cournac L, Guerrini O, Soucaille P, Girbal L.** 2007. Complete activity profile of *Clostridium acetobutylicum* FeFe -hydrogenase and kinetic parameters for endogenous redox partners. Fems Microbiology Letters **275:**113-121.
88. **Schut GJ, Adams MWW.** 2009. The iron-hydrogenase of *Thermotoga maritima* utilizes ferredoxin and NADH synergistically: a new perspective on anaerobic hydrogen production. Journal of Bacteriology **191:**4451-4457.
89. **Wang S, Huang H, Kahnt HH, Mueller AP, Köpke M, Thauer RK.** 2013. NADP-specific electron-bifurcating [FeFe]-hydrogenase in a functional complex with formate dehydrogenase in *Clostridium autoethanogenum* grown on CO. Journal of Bacteriology **195:**4373-4386.
90. **Thauer RK, Jungermann K, Decker K.** 1977. Energy conservation in chemotrophic anerobic bacteria. Bacteriological Reviews **41:**100-180.
91. **Oelgeschläger E, Rother M.** 2008. Carbon monoxide-dependent energy metabolism in anaerobic bacteria and archaea. Archives of Microbiology **190:**257-269.
92. **Kumar M, Lu WP, Ragsdale SW.** 1994. Binding of carbon dislufide to the site of acetyl-CoA synthesis by the nickel-iron-sulfur protein, carbon monoxide dehydrogenase, from *Clostridium thermoaceticum*. Biochemistry **33:**9769-9777.
93. **Lindahl PA, Munck E, Ragsdale SW.** 1990. CO dehydrogenase from *Clostridium thermoaceticum* - EPR and electrochemical studies in CO2 and argon atmosphere. Journal of Biological Chemistry **265:**3873-3879.
94. **Biegel E, Schmidt S, Müller V.** 2009. Genetic, immunological and biochemical evidence for a Rnf complex in the acetogen *Acetobacterium woodii*. Environmental Microbiology **11:**1438-1443.
95. **Müller V, Imkamp F, Biegel E, Schmidt S, Dilling S.** 2008. Discovery of a ferredoxin:NAD^+-oxidoreductase (Rnf) in *Acetobacterium woodii*: a novel potential coupling site in acetogens. Annals of the New York Academy of Sciences **1125:**137-146.
96. **Mock J, Zheng Y, Mueller AP, Ly S, Tran L, Segovia S, Nagaraju S, Köpke M, Dürre P, Thauer RK.** 2015. Energy conservation associated with ethanol formation from H_2 and CO_2 in *Clostridium autoethanogenum* involving electron bifurcation. Journal of Bacteriology **Epub ahead of print**.
97. **Tremblay P, Zhang T, Dar SA, Leang C, Lovley DR.** 2012. The Rnf complex of *Clostridium ljungdahlii* is a proton-translocating ferredoxin:NAD oxidoreductase essential for autotrophic growth. mBio **4:**1-8.
98. **Herrmann G, Jayamani E, Mai G, Buckel W.** 2008. Energy conservation via electron-transferring flavoprotein in anaerobic bacteria. Journal of Bacteriology **190:**784-791.
99. **Schuchmann K, Müller V.** 2012. A bacterial electron-bifurcating hydrogenase. Journal of Biological Chemistry **287:**31165-31171.
100. **Wang S, Huang H, Kahnt J, Thauer RK.** 2013. A reversible electron-bifurcating ferredoxin- and NAD-dependent [FeFe]-hydrogenase (HydABC) in *Moorella thermoacetica*. Journal of Bacteriology **195:**1267-1275.
101. **Zheng Y, Kahnt J, Kwon IH, Mackie RI, Thauer RK.** 2014. Hydrogen formation and its regulation in *Ruminococcus albus*: involvement of an electron-bifurcating [FeFe]-hydrogenase, of a non-electron-bifurcating [FeFe]-hydrogenase, and of a putative hydrogen-sensing [FeFe]-hydrogenase. Journal of Bacteriology **196:**3840-3852.

102. **Wang SN, Huang HY, Moll J, Thauer RK.** 2010. NADP(+) reduction with reduced ferredoxin and NADP(+) reduction with NADH are coupled via an electron-bifurcating enzyme complex in *Clostridium kluyveri*. Journal of Bacteriology **192:**5115-5123.
103. **Wang S, Huang H, Kahnt J, Thauer RK.** 2013. *Clostridium acidurici* electron-bifurcating formate dehydrogenase. Applied and Environmental Microbiology **79:**6176-6179.
104. **Bertsch J, Parthasarathy A, Buckel W, Müller V.** 2013. An electron-bifurcating caffeyl-CoA reductase. Journal of Biological Chemistry **288:**11304-11311.
105. **Adamczack J, Hoffmann M, Papke U, Haufschildt K, Nicke T, Broring M, Sezer M, Weimar R, Kuhlmann U, Hildebrandt P, Layer G.** 2014. NirN protein from *Pseudomonas aeruginosa* is a novel electron-bifurcating dehydrogenase catalyzing the last step of heme d1 biosynthesis. Journal of Biological Chemistry **289:**30753-30762.
106. **Fast AG, Schmidt ED, Jones SW, Tracy BP.** 2015. Acetogenic mixotrophy: Novel options for yield improvement in biofuels and biochemicals production. Current Opinion in Biotechnology **33:**60-72.
107. **Roberts DL, Jameshagstrom JE, Garvin DK, Gorst CM, Runquist JA, Baur JR, Haase FC, Ragsdale SW.** 1989. Cloning and expression of the gene-cluster encoding key proteins involved in acetyl-CoA synthesis in *Clostridium thermoaceticum* - CO dehydrogenase, the corrinoid Fe-S protein, and methyltransferase. Proceedings of the National Academy of Sciences of the United States of America **86:**32-36.
108. **Loke HK, Bennett GN, Lindahl PA.** 2000. Active acetyl-CoA synthase from *Clostridium thermoaceticum* obtained by cloning and heterologous expression of *acsAB* in *Escherichia coli*. Proceedings of the National Academy of Sciences of the United States of America **97:**12530-12535.
109. **Al-Hinai MA, Fast AG, Papoutsakis ET.** 2012. Novel system for efficient isolation of *Clostridium* double-crossover allelic exchange mutants enabling markerless chromosomal gene deletions and DNA integration. Applied and Environmental Microbiology **78:**8112-8121.
110. **Al-Hinai MA, Fast AG, Indurthi D, Papoutsakis ET.** 2012. Installing the Wood-Ljungdahl (WL) pathway in *Clostridium acetobutylicum*, abstr Clostridium XII Conference, Nottingham, UK,
111. **Kaster AK, Goenrich M, Seedorf H, Liesegang H, Wollherr A, Gottschalk G, Thauer RK.** 2011. More than 200 genes required for methane formation from H(2) and CO(2) and energy conservation are present in *Methanothermobacter marburgensis* and *Methanothermobacter thermautotrophicus*. Archaea **2011:**973848.
112. **Alsaker KV, Papoutsakis ET.** 2005. Transcriptional program of early sporulation and stationary-phase events in *Clostridium acetobutylicum*. Journal of Bacteriology **187:**7103-7118.
113. **Köpke M.** 2009. Genetische Veränderung von *Clostridium ljungdahlii* zur produktion von 1-butanol aus synthesegas. PhD thesis. Ulm University, Germany.
114. **Sakai S, Nakashimada Y, Yoshimoto H, Watanabe S, Okada H, Nishio N.** 2004. Ethanol production from H_2 and CO_2 by a newly isolated thermophilic bacterium, *Moorella* sp HUC22-1. Biotechnology Letters **26:**1607-1612.
115. **Sakai S, Nakashimada Y, Inokuma K, Kita M, Okada H, Nishio N.** 2005. Acetate and ethanol production from H-2 and CO2 by *Moorella* sp using a repeated batch culture. Journal of Bioscience and Bioengineering **99:**252-258.
116. **Köpke M, Mihalcea C, Bromley JC, Simpson SD.** 2011. Fermentative production of ethanol from carbon monoxide. Current Opinion in Biotechnology **22:**320-325.
117. **Kundiyana DK, Wilkins MR, Maddipati P, Huhnke RL.** 2011. Effect of temperature, pH and buffer presence on ethanol production from synthesis gas by "*Clostridium ragsdalei*". Bioresource Technology **102:**5794-5799.
118. **Saxena J, Tanner RS.** 2011. Effect of trace metals on ethanol production from synthesis gas by the ethanologenic acetogen, *Clostridium ragsdalei*. Journal of Industrial Microbiology and Biotechnology **38:**513-521.
119. **Heiskanen H, Virkajärvi I, Viikari L.** 2007. The effect of syngas composition on the growth and product formation of *Butyribacterium methylotrophicum*. Enzyme and Microbial Technology **41:**362-367.
120. **Huang H, Liu H, Gan Y-R.** 2010. Genetic modification of critical enzymes and involved genes in butanol biosynthesis from biomass. Biotechnology Advances **28:**651-657.
121. **Lee SY, Park JH, Jang SH, Nielsen LK, Kim J, Jung KS.** 2008. Fermentative butanol production by clostridia. Biotechnology and Bioengineering **101:**209-228.
122. **Sauer U, Dürre P.** 1995. Differential induction of genes related to solvent formation during the shift from acidogenesis to solventogenesis in continuous culture of *Clostridium acetobutylicum*. Federation of European Microbiological Society Microbiology Letters **125:**115-120.
123. **Shi Z, Blaschek HP.** 2008. Transcriptional analysis of *Clostridium beijerinckii* NCIMB 8052 and the hyper-butanol-producing mutant BA101 during the shift from acidogenesis to solventogenesis. Applied and Environmental Microbiology **74:**7709-7714.
124. **Fischer RJ, Helms J, Dürre P.** 1993. Cloning, sequencing, and molecular analysis of the sol operon of *Clostridium acetobutylicum*, a chromosomal locus involved in solventogenesis. Journal of Bacteriology **175:**6959-6969.

125. **Chen C-K, Blaschek HP.** 1999. Effect of acetate on molecular and physiological aspects of *Clostridium beijerinckii* NCIMB 8052 solvent production and strain degeneration. Applied and Environmental Microbiology **65:**499-505.
126. **Kosaka T, Nakayama S, Nakaya K, Yoshino S, Furukawa K.** 2007. Characterization of the sol operon in butanol-hyperproducing *Clostridium saccharoperbutylacetonicum* strain N1-4 and its degeneration mechanism. Bioscience Biotechnology and Biochemistry **71:**58-68.
127. **Hollergschwandner C.** 2003. Unterschiede in der Regulation der Sporulation von C*lostridium acetobutylicum u*nd B*acillus subtilis*. PhD thesis. University of Ulm, Germany.
128. **Ravagnani A, Jennert KCB, Steiner E, Grunberg R, Jefferies JR, Wilkinson SR, Young DI, Tidswell EC, Brown DP, Youngman P, Morris JG, Young M.** 2000. Spo0A directly controls the switch from acid to solvent production in solvent-forming clostridia. Molecular Microbiology **37:**1172-1185.
129. **Köpke M, Dürre P.** 2011. Biochemical production of biobutanol, p 221-257. *In* Luque R, Campelo J, Clark JH (ed). Woodhead Publishing Ltd, Camebridge, UK.
130. **Gheshlaghi R, Scharer JM, Moo-young M, Chou CP.** 2009. Metabolic pathways of clostridia for producing butanol. Biotechnology Advances **27:**764-781.
131. **Seedorf H, Fricke WF, Veith B, Bruggemann H, Liesegang H, Strittimatter A, Miethke M, Buckel W, Hinderberger J, Li FL, Hagemeier C, Thauer RK, Gottschalk G.** 2008. The genome of *Clostridium kluyveri*, a strict anaerobe with unique metabolic features. Proceedings of the National Academy of Sciences of the United States of America **105:**2128-2133.
132. **Inui M, Suda M, Kimura S, Yasuda K, Suzuki H, Toda H, Yamamoto S, Okino S, Suzuki N, Yukawa H.** 2008. Expression of *Clostridium acetobutylicum* butanol synthetic genes in *Escherichia coli*. Applied Microbiology and Biotechnology **77:**1305-1316.
133. **Tomas CA, Beamish J, Papoutsakis ET.** 2004. Transcriptional analysis of butanol stress and tolerance in *Clostridium acetobutylicum*. Journal of Bacteriology **186:**2006-2018.
134. **Ismaiel AA, Zhu CX, Colby GD, Chen JS.** 1993. Purification and characterization of a primary-secondary alcohol dehydrogenase from two strains of *Clostridium beijerinckii*. Journal of Bacteriology **175:**5097-5105.
135. **Köpke M, Gerth ML, Maddock DJ, Mueller AP, Liew F, Simpson SD, Patrick WM.** 2014. Reconstruction of an acetogenic 2,3-butanediol pathway involving a novel NADPH-dependent primary-secondary alcohol dehydrogenase. Applied and Environmental Microbiology **80:**3394-3303.
136. **Toth J, Ismaiel aa, Chen JS.** 1999. The *ald* gene, encoding a coenzyme A-acylating aldehyde dehydrogenase, distinguishes *Clostridium beijerinckii* and two other solvent-producing clostridia from *Clostridium acetobutylicum*. Applied and Environmental Microbiology **65:**4973-4980.
137. **White H, Simon H.** 1992. Role of tungstate and/or molybdate in the formation of aldehyde oxidoreductase in *Clostridium thermoaceticum* and other acetogens; immunological distances of such. Archives of Microbiology**:**81-84.
138. **Simon H, White H, Lebertz H, Thanos I.** 1987. Reduction of 2-enoates and alkanoates with carbon monoxide or formate, viologens, and *Clostridium thermoaceticum* to saturated acids and unsaturated and saturated alcohols. Angewandte Chemie-International Edition in English **26:**785-787.
139. **Huber C, Skopan H, Feicht R, White H, Simon H.** 1995. Pterin cofactor, substrate specificity, and observations on the kinetics of the reversible tungsten-containing aldehyde oxidoreductase from *Clostridium thermoaceticum* - Preparative reductions of a series of carboxylates to alcohols. Archives of Microbiology **164:**110-118.
140. **Fast AG, Papoutsakis ET.** 2012. Stoichiometric and energetic analyses of non-photosynthetic CO_2-fixation pathways to support synthetic biology strategies for production of fuels and chemicals. Current Opinion in Chemical Engineering **1:**380-395.
141. **Isom CE, Nanny MA, Tanner RS.** 2015. Improved conversion efficiencies for n-fatty acid reduction to primary alcohols by the solventogenic acetogen "*Clostridium ragsdalei*". Journal of Industrial Microbiology & Biotechnology **42:**29-38.
142. **Basen M, Schut GJ, Nguyen DM, Lipscomb GL, Benn RA, Prybol CJ, Vaccaro BJ, Poole FL, Kelly RM, Adams MWW.** 2014. Single gene insertion drives bioalcohol production by a thermophilic archaeon. Proceedings of the National Academy of Sciences of the United States of America **111:**17618-17623.
143. **Bertram J, Kuhn A, Dürre P.** 1990. Tn916-induced mutants of *Clostridium acetobutylicum* defective in regulation of solvent formation. Archives of Microbiology **153:**373-377.
144. **Dürre P, Fischer RJ, Kuhn A, Lorenz K, Schreiber W, Sturzenhofecker B, Ullmann S, Winzer K, Sauer U.** 1995. Solventogenic enzymes of *Clostridium acetobutylicum* - catalytic properties, genetic organization, and transcriptional regulation. Federation of European Microbiological Society Microbiology Reviews **17:**251-262.
145. **Green EM, Bennett GN.** 1996. Inactivation of an aldehyde/alcohol dehydrogenase gene from *Clostridium acetobutylicum* ATCC 824. Applied Biochemistry and Biotechnology **57-58:**213-221.
146. **Nair RV, Papoutsakis ET.** 1994. Expression of plasmid-encoded aad in *Clostridium acetobutylicum* M5 restores vigorous butanol production. Journal of Bacteriology **176:**5843-5846.

147. **Petersen DJ, Welch RW, Rudolph FB, Bennett GN.** 1991. Molecular cloning of an alcohol (butanol) dehydrogenase gene cluster from *Clostridium acetobutylicum* ATCC 824. Journal of Bacteriology **173:**1831-1834.
148. **Feustel L, Nakotte S, Dürre P.** 2004. Characterization and development of two reporter gene systems for *Clostridium acetobutylicum*. Applied and Environmental Microbiology **70:**798-803.
149. **Fontaine L, Meynial-salles I, Girbal L, Yang X, Croux C, Soucaille P.** 2002. Molecular characterization and transcriptional analysis of *adhE2*, the gene encoding the NADH-dependent aldehyde/alcohol dehydrogenase responsible for butanol production in alcohologenic cultures of *Clostridium acetobutylicum* ATCC 824. Journal of Bacteriology **184:**821-830.
150. **Ukpong MN, Atiyeh HK, De Lorme MJM, Liu K, Zhu X, Tanner RS, Wilkins MR, Stevenson BS.** 2012. Physiological response of *Clostridium carboxidivorans* during conversion of synthesis gas to solvents in a gas-fed bioreactor. Biotechnology and Bioengineering **109:**2720-2728.
151. **Thauer RK, Jungerma.Ka, Kirchnia.Fh.** 1972. Properties and function of pyruvate-formate-lyase reaction in Clostridiae. European Journal of Biochemistry **27:**282-290.
152. **Schweiger G, Buckel W.** 1985. Identification of acrylate, the product of the dehydration of (R)-lactate catalyzed by cell-free-extracts from *Clostridium propionicum*. Federation of European Microbiological Society Letters **185:**253-256.
153. **Dalal RK, Akedo M, Cooney CL, Sinskey AJ.** 1980. A microbial route for acrylic acid production. Bioresource Dig **2:**89-97.
154. **Straathof AJJ, Sie S, Franco TT, van der Wielen LaM.** 2005. Feasibility of acrylic acid production by fermentation. Applied Microbiology and Biotechnology **67:**727-734.
155. **Obrien DJ, Panzer CC, Eisele WP.** 1990. Biological production of acrylic acid from cheese whey by resting cells of *Clostridium propionicum*. Biotechnology Progress **6:**237-242.
156. **Shaw AJ, Rajgarhia V.** 2010. Mesophilic and thermophilic organisms modified to produce acrylate, and methods of use thereof. Patent USPCT/US2010/027190.
157. **Johns AT.** 1952. The mechanism of propionicum acid formation by *Clostridium propionicum*. Journal of General Microbiology **6:**123-127.
158. **Renz M.** 2005. Ketonization of carboxylic acids by decarboxylation: Mechanism and scope. European Journal of Organic Chemistry **2005:**979-988.
159. **Gaertner CA, Serrano-Ruiz JC, Braden DJ, Dumesic JA.** 2009. Catalytic coupling of carboxylic acids by ketonization as a processing step in biomass conversion. Journal of Catalysis **266:**71-78.
160. **Steinbusch KJJ, Hamelers HVM, Plugge CM, Buisman CJN.** 2011. Biological formation of caproate and caprylate from acetate: fuel and chemical production from low grade biomass. Energy & Environmental Science **4:**216-224.
161. **Kenealy WR, Waselefsky DM.** 1985. Studies on the substrate range of *Clostridium kluyveri* - the use of propanol and succinate. Archives of Microbiology **141:**187-194.
162. **Ramachandriya KD, Kundiyana DK, Wilkins MR, Terrill JB, Atiyeh HK, Huhnke RL.** 2013. Carbon dioxide conversion to fuels and chemicals using a hybrid green process. Applied Energy **112:**289-299.
163. **Liu K, Atiyeh HK, Stevenson BS, Tanner RS, Wilkins MR, Huhnke RL.** 2014. Continuous syngas fermentation for the production of ethanol, n-propanol and n-butanol. Bioresource Technology **151:**69-77.
164. **Hemme CL, Mouttaki H, Lee Y-J, Zhang G, Goodwin L, Lucas S, Copeland A, Lapidus A, Glavina del Rio T, Tice H, Saunders E, Brettin T, Detter JC, Han CS, Pitluck S, Land ML, Hauser LJ, Kyrpides N, Mikhailova N, He Z, Wu L, Van Nostrand JD, Henrissat B, He Q, Lawson Pa, Tanner RS, Lynd LR, Wiegel J, Fields MW, Arkin AP, Schadt CW, Stevenson BS, McInerney MJ, Yang Y, Dong H, Xing D, Ren N, Wang A, Huhnke RL, Mielenz JR, Ding S-Y, Himmel ME, Taghavi S, van der Lelie D, Rubin EM, Zhou J.** 2010. Genome announcement - Sequencing of multiple clostridia genomes related to biomass conversion and biofuels production. Journal of Bacteriology **192:**6494-6496.
165. **Wang Y, Li X, Mao Y, Blaschek HP.** 2012. Genome-wide dynamic transcriptional profiling in *Clostridium beijerinckii* NCIMB 8052 using single-nucleotide resolution RNA-Seq. BMC Genomics **13:**102-102.
166. **Janssen H, Döring C, Ehrenreich A, Voigt B, Hecker M, Bahl H, Fischer R-J.** 2010. A proteomic and transcriptional view of acidogenic and solventogenic steady-state cells of *Clostridium acetobutylicum* in a chemostat culture. Applied Microbiology and Biotechnology **87:**2209-2226.
167. **Tan Y, Liu JJ, Chen XH, Zheng HJ, Li FL.** 2013. RNA-seq-based comparative transcriptome analysis of the syngas-utilizing bacterium *Clostridium ljungdahlii* DSM 13528 grown autotrophically and heterotrophically. Molecular Biosystems **9:**2775-2784.
168. **Haus S, Jabbari S, Millat T, Janssen H, Fischer R-J, Bahl H, King JR, Wolkenhauer O.** 2011. A systems biology approach to investigate the effect of pH-induced gene regulation on solvent production by *Clostridium acetobutylicum* in continuous culture. Bio-Med Central Systems Biology **5:**10-10.
169. **Alsaker KV, Paredes C, Papoutsakis ET.** 2010. Metabolite stress and tolerance in the production of biofuels and chemicals: gene-expression-based systems analysis of butanol, butyrate, and acetate stresses in the anaerobe *Clostridium acetobutylicum*. Biotechnology and Bioengineering **105:**1131-1147.

170. **Nagarajan H, Sahin M, Nogales J, Latif H, Lovley D, Ebrahim A, Zengler K.** 2013. Characterizing acetogenic metabolism using a genome-scale metabolic reconstruction of *Clostridium ljungdahlii*. Microbial Cell Factories **12:**118.
171. **Allcock ER, Reid SJ, Jones DT, Woods DR.** 1981. Autolytic activity of an autolysin-deficient mutant of *Clostridium acetobutylicum*. Appllied Environmental Microbiology **42:**929-935.
172. **Hermann M, Fayolle F, Marchal R, Podvin L, Sebald M, Vandecasteele JP.** 1985. Isolation and characterization of butanol-resistant mutants of *Clostridium acetobutylicum*. Applied Environmental Microbiology **50:**1238-1243.
173. **Van Der Westhuizen a, Jones DT, Woods DR.** 1982. Autolytic Activity and Butanol Tolerance of Clostridium acetobutylicum. Applied and Environmental Microbiology **44:**1277-1281.
174. **Baer SH, Blaschek HP, Smith TL.** 1987. Effect of butanol challenge and temperature on lipid composition and membrane fluidity of butanol-tolerant *Clostridium acetobutylicum*. Applied and Environmental Microbiology **53:**2854-2861.
175. **Soucaille P, Joliff G, Izard A, Goma G.** 1987. Butanol tolerance and autobacteriocin production by *Clostridium acetobutylicum*. Current Microbiology **14:**295-299.
176. **Tomas CA, Welker NE, Papoutsakis ET.** 2003. Overexpression of groESL in *Clostridium acetobutylicum* results in increased solvent production and tolerance, prolonged metabolism, and changes in the cell's transcriptional program. Applied and Environmental Microbiology **69:**4951-4965.
177. **Oultram JD, Peck H, Brehm JK, Thompson DE, Swinfield TJ, Minton NP.** 1988. Introduction of genes for leucine biosynthesis from *Clostridium pasteurianum* into *Clostridium acetobutylicum* by cointegrate conjugal transfer. Molecular and General Genetics **214:**177-179.
178. **Williams DR, Young DI, Young M.** 1990. Conjugative plasmid transfer from *Escherichia coli* to *Clostridium acetobutylicum*. Journal of General Microbiology **136:**819-826.
179. **Herbert M, O'Keeffe TA, Purdy D, Elmore M, Minton NP.** 2003. Gene transfer into *Clostridium difficile* CD630 and characterisation of its methylase genes. Federation of European Microbiological Society Microbiology Letters **229:**103-110.
180. **Theys J, Pennington O, Dubois L, Anlezark G, Vaughan T, Mengesha A, Landuyt W, Anne J, Blurke PJ, Dürre P, Wouters BG, Minton NP, Lambin P.** 2006. Repeated cycles of *Clostridium*-directed enzyme prodrug therapy result in sustained antitumour effects *in vivo*. British Journal of Cancer **95:**1212-1219.
181. **Oultram JD, Loughlin M, Swinfield TJ, Brehm JK, Thompson DE, Minton NP.** 1988. Introduction of plasmids into whole cells of *Clostridium acetobutylicum* by electroporation. Federation of European Microbiological Society Microbiology Letters **56:**83-88.
182. **Birrer GA, Chesbro WR, Zsigray RM.** 1994. Electrotransformation of *Clostridium beijerinckii* NRRL B-592 with shuttle plasmid pHR106 and recombinant derivatives. Applied Microbiology and Biotechnology **41:**32-38.
183. **Mermelstein LD, Welker NE, Bennett GN, Papoutsakis ET.** 1992. Expression of cloned homologous fermentative genes in *Clostridium acetobutylicum* ATCC 824. Bio-Technology **10:**190-195.
184. **Allen SP, Blaschek HP.** 1988. Electroporation induced transformation of intact cells of *Clostridium perfringens*. Applied and Environmental Microbiology **54:**2322-2324.
185. **Jennert KCB, Tardif C, Young DI, Young M.** 2000. Gene transfer to *Clostridium cellulolyticum* ATCC 35319. Microbiology-UK **146:**3071-3080.
186. **Reysset G, Hubert J, Podvin L, Sebald M.** 1988. Transfection and transformation of *Clostridium acetobutvlicum* Strain N1-4081 protoplasts. Biotechnology Techniques **2:**199-204.
187. **Dong H, Zhang Y, Dai Z, Li Y.** 2010. Engineering clostridium strain to accept unmethylated DNA. PloS ONE **5:**e9038-e9038.
188. **Mermelstein LD, Papoutsakis ET.** 1993. *In vivo* methylation in *Escherichia coli* by the *Bacillus subtilis* phage phi 3T I methyltransferase to protect plasmids from restriction upon transformation of *Clostridium acetobutylicum* ATCC 824. Applied and Environmental Microbiology **59:**1077-1081.
189. **Cui GZ, Hong W, Zhang J, Li WL, Feng Y, Liu YJ, Cui Q.** 2012. Targeted gene engineering in *Clostridium cellulolyticum* H10 without methylation. Journal of Microbiological Methods **89:**201-208.
190. **Heap JT, Pennington OJ, Cartman ST, Carter GP, Minton NP.** 2007. The ClosTron: A universal gene knock-out system for the genus *Clostridium*. Journal of Microbiological Methods **70:**452-464.
191. **Green EM, Boynton ZL, Harris LM, Rudolph FB, Papoutsakis ET, Bennett GN.** 1996. Genetic manipulation of acid formation pathways by gene inactivation in *Clostridium acetobutylicum* ATCC 824. Microbiology-UK **142:**2079-2086.
192. **Wilkinson SR, Young DI, Morris JG, Young M.** 1995. Molecular genetics and the initiation of solventogenesis in *Clostridium beijerinckii* (formerly *Clostridium acetobutylicum*) NCIMB 8052. Fems Microbiology Reviews **17:**275-285.
193. **Wilkinson SR, Young M.** 1994. Targeted integration of genes into the *Clostridium acetobutylicum* chromosome. Microbiology-UK **140:**89-95.
194. **Shimizu T, Bathein W, Tamaki M, Hayashi H.** 1994. The virr gene, a member of a class of 2-component response regulators, regulates the production of perfringolysin-O, collagenase, and hemagglutinin in *Clostridium perfringens*. Journal of Bacteriology **176:**1616-1623.

195. **Liyanage H, Kashket S, Young M, Kashket ER.** 2001. *Clostridium beijerinckii* and *Clostridium difficile* detoxify methylglyoxal by a novel mechanism involving glycerol dehydrogenase. Applied and Environmental Microbiology **67:**2004-2010.
196. **O'Connor JR, Lyras D, Farrow KA, Adams V, Powell DR, Hinds J, Cheung JK, Rood JI.** 2006. Construction and analysis of chromosomal *Clostridium difficile* mutants. Molecular Microbiology **61:**1335-1351.
197. **Awad MM, Bryant AE, Stevens DL, Rood JI.** 1995. Virulence studies on chromosomal alpha-toxin and theta-toxin mutants constructed by allelic exchange provide genetic evidence for the essential role of alpha-toxin in *Clostridium perfringens*-mediated gas gangrene. Molecular Microbiology **15:**191-202.
198. **Bannam TL, Crellin PK, Rood JI.** 1995. Molecular genetics of the chloramphenicol resistance transposon Tn4451 from *Clostridium perfringens* - The Tnpx site-specific recombinase excises a circular transposon molecule. Molecular Microbiology **16:**535-551.
199. **Tummala SB, Welker NE, Papoutsakis ET.** 2003. Design of antisense RNA constructs for downregulation of the acetone formation pathway of *Clostridium acetobutylicum*. Journal of Bacteriology **185:**1923-1934.
200. **Desai RP, Papoutsakis ET.** 1999. Antisense RNA strategies for metabolic engineering of *Clostridium acetobutylicum*. Applied and Environmental Microbiology **65:**936-945.
201. **Scotcher MC, Rudolph FB, Bennett GN.** 2005. Expression of abrB310 and sinR, and effects of decreased abrB310 expression on the transition from acidogenesis to solventogenesis, in *Clostridium acetobutylicum* ATCC 824. Applied and Environmental Microbiology **71:**1987-1995.
202. **Nakayama S-i, Kosaka T, Hirakawa H, Matsuura K, Yoshino S, Furukawa K.** 2008. Metabolic engineering for solvent productivity by downregulation of the hydrogenase gene cluster *hupCBA* in *Clostridium saccharoperbutylacetonicum* strain N1-4. Applied Microbiology and Biotechnology **78:**483-493.
203. **Sillers R, A-Hinai MA, Papoutsakis ET.** 2009. Aldehyde-alcohol dehydrogenase and/or thiolase overexpression coupled with CoA transferase downregulation lead to higher alcohol titers and selectivity in *Clostridium acetobutylicum* fermentations. Biotechnology and Bioengineering **102:**38-49.
204. **Tummala SB, Junne SG, Papoutsakis ET.** 2003. Antisense RNA downregulation of coenzyme A transferase combined with alcohol-aldehyde dehydrogenase overexpression leads to predominantly alcohologenic *Clostridium acetobutylicum* fermentations. Journal of Bacteriology **185:**3644-3653.
205. **Karberg M, Guo HT, Zhong J, Coon R, Perutka J, Lambowitz AM.** 2001. Group II introns as controllable gene targeting vectors for genetic manipulation of bacteria. Nature Biotechnology **19:**1162-1167.
206. **Heap JT, Kuehne Sa, Ehsaan M, Cartman ST, Cooksley CM, Scott JC, Minton NP.** 2010. The ClosTron: Mutagenesis in *Clostridium* refined and streamlined. Journal of Microbiological Methods **80:**49-55.
207. **Camiade E, Peltier J, Bourgeois I, Couture-Tosi E, Courtin P, Antunes A, Chapot-Chartier MP, Dupuy B, Pons JL.** 2010. Characterization of Acp, a peptidoglycan hydrolase of *Clostridium perfringens* with N-acetylglucosaminidase activity that is implicated in cell separation and stress-induced autolysis. Journal of Bacteriology **192:**2373-2384.
208. **Fabret C, Ehrlich SD, Noirot P.** 2002. A new mutation delivery system for genome-scale approaches in *Bacillus subtilis*. Molecular Microbiology **46:**25-36.
209. **Soucaille P, Rainer F, Christian C.** 2008. Process for chromosomal integration and DNA sequence replacement in clostridia. Patent EUEP2316952.
210. **von Abendroth G, Stripp S, Silakov A, Croux C, Soucaille P, Girbal L, Happe T.** 2008. Optimized over-expression of FeFe hydrogenases with high specific activity in *Clostridium acetobutylicum*. International Journal of Hydrogen Energy **33:**6076-6081.
211. **Soucaille P.** 2008. Process for the biological production of n-butanol at high yield. France. Patent WO 2008/052973.
212. **Heap JT, Ehsaan M, Cooksley CM, Ng YK, Cartman ST, Winzer K, Minton NP.** 2012. Integration of DNA into bacterial chromosomes from plasmids without a counter-selection marker. Nucleic Acids Research **40:**e59.
213. **LeBel M.** 1993. Pharmacokinetic properties of clarithromycin: A comparison with erythromycin and azithromycin. The Canadian Journal of Infectious Diseases **4:**148-152.
214. **Ng YK, Ehsaan M, Philip S, Collery MM, Janoir C, Collignon A, Cartman ST, Minton NP.** 2013. Expending the repertoire of gene tools for precise manipulation of the *Clostridium difficile* genome: Allelic exchange using *pyrE* alleles. Plos ONE **8**.
215. **Keis S, Shaheen R, Jones DT.** 2001. Emended descriptions of *Clostridium acetobutylicum* and *Clostridium beijerinckii*, and descriptions of *Clostridium saccharoperbutylacetonicum* sp nov and *Clostridium saccharobutylicum* sp nov. International Journal of Systematic and Evolutionary Microbiology **51:**2095-2103.
216. **Bertram J, Dürre P.** 1989. Conjugal transfer and expression ofstreptococcal transposons in *Clostridium acetobutylicum*. Archives of Microbiology **151:**551-557.
217. **Woolley RC, Pennock A, Ashton RJ, Davies A, Young M.** 1989. Transfer of Tn1545 and Tn916 to *Clostridium acetobutylicum*. Plasmid **22:**169-174.

218. **Blouzard JC, Valette O, Tardif C, de Philip P.** 2010. Random mutagenesis of *Clostridium cellulolyticum* by using a Tn1545 derivative. Applied and Environmental Microbiology **76:**4546-4549.
219. **Cartman ST, Minton NP.** 2010. A mariner-based transposon system for *in vivo* random mutagenesis of *Clostridium difficile*. Applied and Environmental Microbiology **76:**1103-1109.
220. **Lee J, Jang YS, Choi SJ, Im JA, Song H, Cho JH, Seung DY, Papoutsakis ET, Bennett GN, Lee SY.** 2012. Metabolic engineering of *Clostridium acetobutylicum* ATCC 824 for isopropanol-butanol-ethanol fermentation. Applied and Environmental Microbiology **78:**1416-1423.
221. **Lehmann D, Lutke-Eversloh T.** 2011. Switching *Clostridium acetobutylicum* to an ethanol producer by disruption of the butyrate/butanol fermentative pathway. Metabolic Engineering **13:**464-473.
222. **Siemerink MAJ, Kuit W, Contreras AML, Eggink G, van der Oost J, Kengen SWM.** 2011. D-2,3-butanediol production due to heterologous expression of an acetoin reductase in *Clostridium acetobutylicum*. Applied and Environmental Microbiology **77:**2582-2588.
223. **Cai XP, Bennett GN.** 2011. Improving the *Clostridium acetobutylicum* butanol fermentation by engineering the strain for co-production of riboflavin. Journal of Industrial Microbiology & Biotechnology **38:**1013-1025.
224. **Zhu LJ, Dong HJ, Zhang YP, Li Y.** 2011. Engineering the robustness of *Clostridium acetobutylicum* by introducing glutathione biosynthetic capability. Metabolic Engineering **13:**426-434.
225. **Higashide W, Li YC, Yang YF, Liao JC.** 2011. Metabolic engineering of *Clostridium cellulolyticum* for production of isobutanol from cellulose. Applied and Environmental Microbiology **77:**2727-2733.
226. **Atsumi S, Hanai T, Liao J.** 2008. Non-fermentative pathways for synthesis of branched-chain higher alcohols as biofuels. Nature **451:**86-89.
227. **Argyros DA, Tripathi SA, Barrett TF, Rogers SR, Feinberg LF, Olson DG, Foden JM, Miller BB, Lynd LR, Hogsett DA, Caiazza NC.** 2011. High ethanol titers from cellulose by using metabolically engineered thermophilic, anaerobic microbes. Applied and Environmental Microbiology **77:**8288-8294.
228. **Yu M, Zhang Y, Tang IC, Yang S-T.** 2011. Metabolic engineering of *Clostridium tyrobutyricum* for *n*-butanol production. Metabolic Engineering **13:**373-382.
229. **Leang C, Ueki T, Nevin KP, Lovley DR.** 2013. A genetic system for *Clostridium ljungdahlii*: A chassis for autotrophic production of biocommodities and a model homoacetogen. Applied and Environmental Microbiology **79:**1102-1109.
230. **Banerjee A, Leang C, Ueki T, Nevin KP, Lovley DR.** 2014. Lactose-inducible system for metabolic engineering of *Clostridium ljungdahlii*. Applied and Environmental Microbiology **80:**2410-2416.
231. **Ueki T, Nevin KP, Woodard TL, Lovley DR.** 2014. Converting carbon dioxide to butyrate with an engineered strain of *Clostridium ljungdahlii*. mBio **5:**e01636-14.
232. **Köepke M, Liew FM.** 2011. Recombinant microorganism and methods of production thereof. U.S. Patent US 2011/0236941 A1.
233. **Simpson SD, Koepke M, Liew FM.** 2011. Recombinant microorganisms and methods of use thereof. U.S. Patent US 2011/0256600.
234. **Lederle S.** 2011. Heterofermentative Acetonproduktion. PhD thesis. University of Ulm, Germany.
235. **Becker U, Grund G, Orschel M, Doderer K, Löhden G, Brand G, Dürre P, Lederle S, Bahl HJ, Fischer RJ, May A.** 2009. Zellen und Verfahren zur Herstellung von Aceton. Germany. Patent DE 10 2009 002 583 A1.
236. **Straub M, Demler M, Weuster-Botz D, Dürre P.** 2014. Selective enhancement of autotrophic acetate production with genetically modified *Acetobacterium woodii*. Journal of Biotechnology **178:**67-72.
237. **Kita A, Iwasaki Y, Sakai S, Okuto S, Takaoka K, Suzuki T, Yano S, Sawayama S, Tajima T, Kato J, Nishio N, Murakami K, Nakashimada Y.** 2013. Development of genetic transformation and heterologous expression system in carboxydotrophic thermophilic acetogen *Moorella thermoacetica*. Journal of Bioscience and Bioengineering **115:**347-352.
238. **Harris LM, Desai RP, Welker NE, Papoutsakis ET.** 2000. Characterization of recombinant strains of the *Clostridium acetobutylicum* butyrate kinase inactivation mutant: need for new phenomenological models for solventogenesis and butanol inhibition? Biotechnology and Bioengineering **67:**1-11.
239. **Kuit W, Minton NP, Lopez-Contreras AM, Eggink G.** 2012. Disruption of the acetate kinase (*ack*) gene of *Clostridium acetobutylicum* results in delayed acetate production. Applied Microbiology and Biotechnology **94:**729-741.
240. **Yu MR, Zhang YL, Tang IC, Yang ST.** 2011. Metabolic engineering of *Clostridium tyrobutyricum* for *n*-butanol production. Metabolic Engineering **13:**373-382.
241. **Li YC, Tschaplinski TJ, Engle NL, Hamilton CY, Rodriguez M, Liao JC, Schadt CW, Guss AM, Yang YF, Graham DE.** 2012. Combined inactivation of the *Clostridium cellulolyticum* lactate and malate dehydrogenase genes substantially increases ethanol yield from cellulose and switchgrass fermentations. Biotechnology for Biofuels **5:**1-13.
242. **Papoutsakis ET, AL-Hinai MA, Jones SW, Indurthi DC, Mitchell DK, Fast A.** 2012. Recombinant Clostridia that fix CO_2 and CO and uses thereof. U.S. Patent US 2012/0064587 A1.
243. **Strätz M, Sauer U, Kuhn A, Dürre P.** 1994. Plasmid transfer into the homoacetogen *Acetobacterium woodii* by electroporation and conjugation. Applied and Environmental Microbiology **60:**1033-1037.

244. **Heap JT, Pennington OJ, Cartman ST, Minton NP.** 2009. A modular system for *Clostridium* shuttle plasmids. Journal of Microbiological Methods **78:**79-85.
245. **Swinfield TJ, Oultram JD, Thompson DE, Brehm JK, Minton NP.** 1990. Physical characterisation of the replication region of the *Streptococcus faecalis* plasmid pAMβ1. Gene **87:**79-90.
246. **Weisburg WG, Barns SM, Pelletier DA, Lane DJ.** 1991. 16S ribosomal DNA amplification for phylogenetic study. Journal of Bacteriology **173:**697-703.
247. **Warrens AN, Jones MD, Lechlera RI.** 1997. Splicing by overlap extension by PCR using asymmetric amplification: an improved technique for the generation of hybrid proteins of immunological interest. Gene **186:**29-35.
248. **Sambrook J, Russell DW.** 2001. Molecular cloning: A laboratory manual, 3rd ed. Cold Spring Harbor Laboratory Press, New York.
249. **Liu J, Tan Y, Yang X, Chen X, Li F.** 2013. Evaluation of *Clostridium ljungdahlii* DSM 13528 reference genes in gene expression studies by qRT-PCR. Journal of Bioscience and Bioengineering **116:**460-464.
250. **Purdy D, O'Keeffe TAT, Elmore M, Herbert M, McLeod A, Bokori-Brown M, Ostrowski A, Minton NP.** 2002. Conjugative transfer of clostridial shuttle vectors from *Escherichia coli* to *Clostridium difficile* through circumvention of the restriction barrier. Molecular Microbiology **46:**439-452.
251. **Perutka J, Wang W, Goerlitz D, Lambowitz AM.** 2004. Use of computer-designed group II introns to disrupt *Escherichia coli* DExH/D-box protein and DNA helicase genes. Journal of Molecular Biology **336:**421-439.
252. **Kuehne SA, Minton NP.** 2012. ClosTron-mediated engineering of *Clostridium*. Bioengineered **3:**247-254.
253. ***Allcock ER, Reid SJ, Jones DT, Woods DR.*** 1981. Autolytic activity of an autolysin-deficient mutant of Cl*ostridium acetobutylicum*. Applied and Environmental Microbiology **42:**929-935.
254. **Hermann M, Fayolle F, Marchal R, Podvin L, Sebald M, Vandecasteele JP.** 1985. Isolation and characterization of butanol-resistant mutants of *Clostridium acetobutylicum*. Applied and Environmental Microbiology **50:**1238-1243.
255. **Pyne ME, Bruder M, Moo-Young M, Chung DA, Chou CP.** 2014. Technical guide for genetic advancement of underdeveloped and intractable *Clostridium*. Biotechnology Advances **32:**623-641.
256. **Ackermann G, Tang YJ, Henderson JP, Rodloff AC, Silva J, Cohen SH.** 2001. Electroporation of DNA sequences from the pathogenicity locus (PaLoc) of toxigenic *Clostridium difficile* into a non-toxigenic strain. Molecular and Cellular Probes **15:**301-306.
257. **Zhou YT, Johnson EA.** 1993. Genetic transformation of *Clostridium botulinum* hall A by electroporation. Biotechnology Letters **15:**121-126.
258. **Yu MR, Du YM, Jiang WY, Chang WL, Yang ST, Tang IC.** 2012. Effects of different replicons in conjugative plasmids on transformation efficiency, plasmid stability, gene expression and n-butanol biosynthesis in *Clostridium tyrobutyricum*. Applied Microbiology and Biotechnology **93:**881-889.
259. **Stratz M, Sauer U, Kuhn A, Durre P.** 1994. Plasmid transfer into the homoacetogen *Acetobacterium woodii* by electroporation and conjugation. Applied and Environmental Microbiology **60:**1033-1037.
260. **Reiner AM.** 1977. Xylitol and D-arabitol toxicities due to derepressed fructose, galactitol, and sorbitol phosphotransferases of *Escherichia coli*. Journal of Bacteriology **132:**166-173.
261. **Trahan L, Bourgeau G, Breton R.** 1996. Emergence of multiple xylitol-resistant (fructose PTS-) mutants from human isolates of mutans streptococci during growth on dietary sugars in the presence of xylitol. Journal of Dental Research **75:**1892-1900.
262. **Soderling E, Pihlantoleppala A.** 1989. Uptake and expulsion of C-14 xylitol by xylitol cultured streptococcus mutans ATCC 25175 in vitro. Scandinavian Journal of Dental Research **97:**511-519.
263. **Daniels GA, Drews G, Saier MH.** 1988. Properties of a Tn5 insertion mutant defective in the structural gene (*fruA*) of the fructose specific phosphotransferase system of *Rhodobacter capsulatus* and cloning of the Fru regulon. Journal of Bacteriology **170:**1698-1703.
264. **Berkowit D.** 1971. D-mannitol utilization in *Salmonella typhimurium*. Journal of Bacteriology **105:**232-&.
265. **Kalscheuer R, Syson K, Veeraraghavan U, Weinrick B, Biermann KE, Liu Z, Sacchettini JC, Besra G, Bornemann S, Jacobs WR.** 2010. Self-poisoning of *Mycobacterium tuberculosis* by targeting GlgE in an alpha-glucan pathway. Nature Chemical Biology **6:**376-384.
266. **Reyrat JM, Pelicic V, Gicquel B, Rappuoli R.** 1998. Counterselectable markers: Untapped tools for bacterial genetics and pathogenesis. Infection and Immunity **66:**4011-4017.
267. **Kast P.** 1994. pKSS - A 2nd-generation general-purpose cloning vector for efficient positive election of recombinant clones. Gene **138:**109-114.
268. **Boeke JD, Lacroute F, Fink GR.** 1984. A Positive selection for mutants lacking orotidine-5`-phosphate decarboxylase activity in yeast - 5-fluoro-orotic acid resistance. Molecular & General Genetics **197:**345-346.
269. **Gay P, Lecoq D, Steinmetz M, Berkelman T, Kado CI.** 1985. Positive selection procedure for entrapment of insertion-sequence elements in Gram-negative bacteria. Journal of Bacteriology **164:**918-921.
270. **Cartman ST, Kelly ML, Heeg D, Heap JT, Minton NP.** 2012. Precise manipulation of the *Clostridium difficile* chromosome reveals a lack of association between the *tcdC* genotype and toxin production. Applied and Environmental Microbiology **78:**4683-4690.

271. **Hartzog PE, Nicholson BP, McCusker JH.** 2005. Cytosine deaminase MX cassettes as positive/negative selectable markers in *Saccharomyces cerevisiae*. Yeast **22:**789-798.
272. **Zhu L, Phadtare S, Nariya H, Ouyang M, Husson RN, Inouye M.** 2008. The mRNA interferases, MazF-mt3 and MazF-mt7 from *Mycobacterium tuberculosis* target unique pentad sequences in single-stranded RNA. Molecular Microbiology **69:**559-569.
273. **Yamaguchi Y, Inouye M.** 2009. mRNA interferases, sequence-specific endoribonucleases from the toxin-antitoxin systems. Molecular Biology of RNA Processing and Decay in Prokaryotes **85:**467-500.
274. **Pritchett MA, Zhang JK, Metcalf WW.** 2004. Development of a markerless genetic exchange method for *Methanosarcina acetivorans* C2A and its use in construction of new genetic tools for methanogenic archaea. Applied and Environmental Microbiology **70:**1425-1433.
275. **Bochner BR, Huang HC, Schieven GL, Ames BN.** 1980. Positive selection for loss of tetracycline resistance. Journal of Bacteriology **143:**926-933.
276. **Bernard P, Couturier M.** 1992. Cell killing by the F-plasmid ccdB protein involves poisoning of DNA-topoisomerase-II complexes. Journal of Molecular Biology **226:**735-745.
277. **Toyn JH, Gunyuzlu PL, White WH, Thompson LA, Hollis GF.** 2000. A counterselection for the tryptophan pathway in yeast: 5-fluoroanthranilic acid resistance. Yeast **16:**553-560.
278. **Lederberg J.** 1951. Streptomycin resistance - a genetically recessive mutation. Journal of Bacteriology **61:**549-550.
279. **Murphy CK, Stewart EJ, Beckwith J.** 1995. A double counter-selection system for the study of null alleles of essential genes in *Escherichia coli*. Gene **155:**1-7.
280. **Tripathi SA, Olson DG, Argyros DA, Miller BB, Barrett TF, Murphy DM, McCool JD, Warner AK, Rajgarhia VB, Lynd LR, Hogsett DA, Caiazza NC.** 2010. Development of pyrF-based genetic system for targeted gene deletion in *Clostridium thermocellum* and creation of a *pta* mutant. Applied and Environmental Microbiology **76:**6591-6599.
281. **Nakayama S, Irie R, Kosaka T, Matsuura K, Yoshino S, Furukawa K.** 2007. New host-vector system in solvent-producing *Clostridium saccharoperbutylacetonicum* strain N1-4. Journal of General and Applied Microbiology **53:**53-56.
282. **Pyne ME, Moo-Young M, Chung DA, Chou CP.** 2013. Development of an electrotransformation protocol for genetic manipulation of *Clostridium pasteurianum*. Biotechnology for Biofuels **6**:1-20.
283. **Flusberg BA, Webster DR, Lee JH, Travers KJ, Olivares EC, Clark TA, Korlach J, Turner SW.** 2010. Direct detection of DNA methylation during single-molecule, real-time sequencing. Nature Methods **7:**461-U472.
284. **Fang G, Munera D, Friedman DI, Mandlik A, Chao MC, Banerjee O, Feng ZX, Losic B, Mahajan MC, Jabado OJ, Deikus G, Clark TA, Luong K, Murray IA, Davis BM, Keren-Paz A, Chess A, Roberts RJ, Korlach J, Turner SW, Kumar V, Waldor MK, Schadt EE.** 2012. Genome-wide mapping of methylated adenine residues in pathogenic *Escherichia coli* using single-molecule real-time sequencing. Nature Biotechnology **30:**1232-1239.
285. **Piffaretti JC, Arini A, Frey J.** 1988. pUB307 mobilizes resistance plasmids from *Escherichia coli* into *Neisseria gonorrhoeae*. Molecular & General Genetics **212:**215-218.
286. **Mitchell WJ, Tewatia P, Meaden PG.** 2007. Genomic analysis of the phosphotransferase system in *Clostridium botulinum*. Journal of Molecular Microbiology and Biotechnology **12:**33-42.
287. **Noelling J.** 2001. Genome sequence and comparative analysis of the solvent-producing bacterium *Clostridium acetobutylicum*. Journal of Bacteriology **183:**4823-4838.
288. **Shi Y, Li Y-X, Li Y-Y.** 2010. Large number of phosphotransferase genes in the *Clostridium beijerinckii* NCIMB 8052 genome and the study on their evolution. BMC Bioinformatics **11:**S9-S9.
289. **Ferry JG.** 1995. CO dehydrogenase. Annual Review of Microbiology **49:**305-333.
290. **Hugendieck I, Meyer O.** 1992. The structural genes encoding CO dehydrogenase subunits (cox L, M and S) in *Pseudomonas carboxydovorans* OM5 reside on plasmid pHCG3 and are, with the exception of *Streptomyces thermoautotrophicus*, conserved in Carboxydotrophic bacteria. Archives of Microbiology **157:**301-304.
291. **Schubel U, Kraut M, Morsdorf G, Meyer O.** 1995. Molecular characterization of the gene cluster *coxMSL* encoding the molybdenum-containing carbon monoxide dehydrogenase of *Oligotropha carboxidovorans*. Journal of Bacteriology **177:**2197-2203.
292. **King GM.** 2006. Nitrate-dependent anaerobic carbon monoxide oxidation by aerobic CO-oxidizing bacteria. Federation of European Microbiological Society Microbiology Ecology **56:**1-7.
293. **King GM, Weber CF.** 2007. Distribution, diversity and ecology of aerobic CO-oxidizing bacteria. Nature Reviews Microbiology **5:**107-118.
294. **Gonzalez JM, Robb FT.** 2000. Genetic analysis of *Carboxydothermus hydrogenoformans* carbon monoxide dehydrogenase genes *cooF* and *cooS*. Federation of European Microbiological Society Microbiology Letters **191:**243-247.
295. **Svetlitchnyi V, Peschel C, Acker G, Meyer O.** 2001. Two membrane-associated NiFeS-carbon monoxide dehydrogenases from the anaerobic carbon-monoxide-utilizing eubacterium *Carboxydothermus hydrogenoformans*. Journal of Bacteriology **183:**5134-5144.

296. **Svetlitchnyi V, Dobbek H, Meyer-Klaucke W, Meins T, Thiele B, Romer P, Huber R, Meyer O.** 2004. A functional Ni-Ni- 4Fe-4S cluster in the monomeric acetyl-CoA synthase from *Carboxydothermus hydrogenoformans*. Proceedings of the National Academy of Sciences of the United States of America **101:**446-451.

297. **Wu M, Ren Q, Durkin aS, Daugherty SC, Brinkac LM, Dodson RJ, Madupu R, Sullivan Sa, Kolonay JF, Haft DH, Nelson WC, Tallon LJ, Jones KM, Ulrich LE, Gonzalez JM, Zhulin IB, Robb FT, Eisen Ja.** 2005. Life in hot carbon monoxide: the complete genome sequence of C*arboxydothermus hydrogenoformans* Z-2901. PLoS Genetics **1:**e65-e65.

298. **Sokolova TG, Henstra AM, Sipma J, Parshina SN, Stams AJM, Lebedinsky AV.** 2009. Diversity and ecophysiological features of thermophilic carboxydotrophic anaerobes. Federation of European Microbiological Society Microbiology Ecology **68:**131-141.

299. **Grahame DA, Demoll E.** 1995. Substrate and accessory protein requirements and thermodynamics of acetyl-CoA synthesis and cleavage in *Methanosarcina barkeri*. Biochemistry **34:**4617-4624.

300. **Techtmann SM, Lebedinsky AV, Colman AS, Sokolova TG, Woyke T, Goodwin L, Robb FT.** 2012. Evidence for horizontal gene transfer of anaerobic carbon monoxide dehydrogenases. Frontiers in Microbiology **3:**1-16.

301. **Soboh B, Linder D, Hedderich R.** 2002. Purification and catalytic properties of a CO-oxidizing:H2-evolving enzyme complex from *Carboxydothermus hydrogenoformans*. European Journal of Biochemistry **269:**5712-5721.

302. **Matschiavelli N, Oelgeschlager E, Cocchiararo B, Finke J, Rother M.** 2012. Function and regulation of isoforms of carbon nonoxide dehydrogenase/acetyl coenzyme A synthase in *Methanosarcina acetivorans*. Journal of Bacteriology **194:**5377-5387.

303. **Matson EG, Gora KG, Leadbetter JR.** 2011. Anaerobic carbon monoxide dehydrogenase diversity in the homoacetogenic hindgut microbial communities of lower termites and the wood roach. Plos ONE **6:**1-15.

304. **Heo J, Skjeldal L, Staples CR, Ludden PW.** 2002. Carbon monoxide dehydrogenase from *Rhodospirillum rubrum* produces formate. Journal of Biological Inorganic Chemistry **7:**810-814.

305. **Lu WP, Ragsdale SW.** 1991. Reductive activation of the coenzyme A/acetyl-CoA isotopic exchange reaction catalyzed by carbon monoxide dehydrogenase from *Clostridium thermoaceticum* and its inhibition by nitrous oxide and carbon monoxide. Journal of Biological Chemistry **266:**3554-3564.

306. **Huang SQ, Lindahl PA, Wang CY, Bennett GN, Rudolph FB, Hughes JB.** 2000. 2,4,6-trinitrotoluene reduction by carbon monoxide dehydrogenase from *Clostridium thermoaceticum*. Applied and Environmental Microbiology **66:**1474-1478.

307. **Jeoung JH, Dobbek H.** 2012. n-Butyl isocyanide oxidation at the [NiFe4S4OH(x)] cluster of CO dehydrogenase. Journal of Biological Inorganic Chemistry **17:**167-173.

308. **Ragsdale SW, Pierce E.** 2008. Acetogenesis and the Wood-Ljungdahl pathway of CO(2) fixation. Biochimica et biophysica acta **1784:**1873-1898.

309. **Doukov TI, Iverson TM, Seravalli J, Ragsdale SW, Drennan CL.** 2002. A Ni-Fe-Cu center in a bifunctional carbon monoxide dehydrogenase/acetyl-CoA synthase. Science **298:**567-572.

310. **Darnault C, Volbeda A, Kim EJ, Legrand P, Vernede X, Lindahl PA, Fontecilla-Camps JC.** 2003. Ni-Zn-[Fe4-S4] and Ni-Ni-[Fe4-S4] clusters in closed and open subunits of acetyl-CoA synthase/carbon monoxide dehydrogenase. Nature Structural Biology **10:**271-279.

311. **Dobbek H, Svetlitchnyi V, Gremer L, Huber R, Meyer O.** 2001. Crystal structure of a carbon monoxide dehydrogenase reveals a [Ni-4Fe-5S] cluster. Science **293:**1281-1285.

312. **Drennan CL, Heo J, Sintchak MD, Schreiter E, Ludden PW.** 2001. Life on carbon monoxide: X-ray structure of *Rhodospirillum rubrum* Ni-Fe-S carbon monoxide dehydrogenase. Proceedings of the National Academy of Sciences of the United States of America **98:**11973-11978.

313. **Gong W, Hao B, Wei Z, Ferguson DJ, Tallant T, Krzycki JA, Chan MK.** 2008. Structure of the alpha(2)epsilon(2) Ni-dependent CO dehydrogenase component of the *Methanosarcina barkeri* acetyl-CoA decarbonylase/synthase complex. Proceedings of the National Academy of Sciences of the United States of America **105:**9558-9563.

314. **Ensign SA, Ludden PW.** 1991. Characterization of the CO oxidation/H2 evolution system of *Rhodospirillum rubrum*. Role of a 22-kDa iron-sulfur protein in mediating electron transfer between carbon monoxide dehydrogenase and hydrogenase. Journal of Biological Chemistry **266:**18395-18403.

315. **Doukov TI, Blasiak LC, Seravalli J, Ragsdale SW, Drennan CL.** 2008. Xenon in and at the end of the tunnel of bifunctional carbon monoxide dehydrogenase/acetyl-CoA synthase. Biochemistry **47:**3474-3483.

316. **Seravalli J, Kumar M, Lu WP, Ragsdale SW.** 1995. Mechanism of CO oxidation by carbon monoxide dehydrogenase from *Clostridium thermoaceticum* and its inhibition by anions. Biochemistry **34:**7879-7888.

317. **Menon S, Ragsdale SW.** 1996. Unleashing hydrogenase activity in carbon monoxide dehydrogenase/acetyl-CoA synthase and pyruvate: ferredoxin oxidoreductase. Biochemistry **35:**15814-15821.

318. **Kim BH, Bellows P, Datta R, Zeikus JG.** 1984. Control of carbon and electron flow in *Clostridium acetobutylicum* fermentations: Utilization of carbon monoxide to inhibit hydrogen production and to enhance butanol yields. Applied and Environmental Microbiology **48:**764-770.
319. **Braun K, Gottschalk G.** 1981. Effect of molecular hydrogen and carbon dioxide on chemo-organotrophic growth of *Acetobacterium woodii* and *Clostridium aceticum*. Archives of Microbiology **128:**294-298.
320. **Loubière P, Gros E, Paquet V, Lindley ND.** 1992. Kinetics and physiological implications of the growth behaviour of *Eubacterium limosum* on glucose/methanol mixtures. Journal of General Microbiology **138:**979-985.
321. **Thauer RK, Mollerzinkhan D, Spormann AM.** 1989. Biochemistry of acetate catabolism in anaerobic chemotropic bacteria. Annual Review of Microbiology **43:**43-67.
322. **Schauder R, Eikmanns B, Thauer R, Widdel F, Fuchs G.** 1986. Acetate oxidation to CO2 in anaerobic bacteria via a novel pathway not involving reactions of the citric acid cycle. Archives of Microbiology **145:**162-172.
323. **Spormann A, Thauer R.** 1988. Anaerobic acetate oxidation to CO2 by *Desulfotomaculum acetoxidans*. Archives of Microbiology **150:**374-380.
324. **Zhang Y, Gladyshev VN.** 2005. An algorithm for identification of bacterial selenocysteine insertion sequence elements and selenoprotein genes. Bioinformatics **21:**2580-2589.
325. **Zinoni F, Birkmann A, Stadtman TC, Bock A.** 1986. Nucleotide sequence and expression of the selenocysteine-containing polypeptide of formate dehydrogenase (formate-hydrogen-lyase-linked) from *Escherichia coli*. Proceedings of the National Academy of Sciences of the United States of America **83:**4650-4654.
326. **Zinoni F, Birkmann A, Leinfelder W, Bock A.** 1987. Cotranslational insertion of selenocysteine into formate dehydrogenase from *Escherichia coli* directed by a UGA codon. Proceedings of the National Academy of Sciences of the United States of America **84:**3156-3160.
327. **Yoshizawa S, Bock A.** 2009. The many levels of control on bacterial selenoprotein synthesis. Biochimica et biophysica acta **1790:**1404-1414.
328. **Soucaille P, Figge R, Croux C.** 2008. Process for chromosomal integration and DNA sequence replacement in clostridia. EU. Patent EP20070107017.
329. **Sattler C, Wolf S, Fersch J, Goetz S, Rother M.** 2013. Random mutagenesis identifies factors involved in formate-dependent growth of the methanogenic archaeon *Methanococcus maripaludis*. Molecular Genetics and Genomics **288:**413-424.
330. **Hendrickson EL, Kaul R, Zhou Y, Bovee D, Chapman P, Chung J, Conway de Macario E, Dodsworth JA, Gillett W, Graham DE, Hackett M, Haydock AK, Kang A, Land ML, Levy R, Lie TJ, Major TA, Moore BC, Porat I, Palmeiri A, Rouse G, Saenphimmachak C, Söll D, Van Dien S, Wang T, Whitman WB, Xia Q, Zhang Y, Larimer FW, Olson MV, Leigh JA.** 2004. Complete genome sequence of the genetically tractable hydrogenotrophic methanogen *Methanococcus maripaludis*. Journal of Bacteriology **186:**6956-6969.
331. **Liu X, Zhu Y, Yang ST.** 2006. Construction and characterization of ack deleted mutant of *Clostridium tyrobutyricum* for enhanced butyric acid and hydrogen production. Biotechnology Progress **22:**1265-1275.
332. **Chang DE, Shin S, Rhee JS, Pan JG.** 1999. Acetate metabolism in a pta mutant of *Escherichia coli* W3110: importance of maintaining acetyl coenzyme A flux for growth and survival. Journal of Bacteriology **181:**6656-6663.
333. **Schiel-Bengelsdorf B, Dürre P.** 2012. Pathway engineering and synthetic biology using acetogens. Federation of European Biochemical Society Letters **586:**2191-2198.
334. **Johansson L, Gafvelin G, Arner ES.** 2005. Selenocysteine in proteins-properties and biotechnological use. Biochimica et Biophysica Acta **1726:**1-13.
335. **Axley MJ, Böck A, Stadtman TC.** 1991. Catalytic properties of an *Escherichia coli* formate dehydrogenase mutant in which sulfur replaces selenium. Proceedings of the National Academy of Sciences of the United States of America **88:**8450-8454.
336. **Tate WP, Mansell JB, Mannering SA, Irvine JH, Major LL, Wilson DN.** 1999. UGA: A dual signal for "Stop" and for recoding in protein synthesis. Biochemistry (Moscow) **64:**1342-1353.
337. **Barrell BG, Bankier AT, Drouin J.** 1979. A different genetic code in human mitochondria. Nature **282:**189-194.
338. **Hirsh D.** 1971. Tryptophan transfer RNA as the UGA suppressor. Journal of Molecular Biology **58:**439-458.
339. **Inamine JM, Ho KC, Loechel S, Hu PC.** 1990. Evidence that UGA is read as a tryptophan codon rather than as a stop codon by *Mycoplasma pneumoniae*, *Mycoplasma genitalium*, and *Mycoplasma gallisepticum*. Journal of Bacteriology **172:**504-506.
340. **Blanchet S, Cornu D, Argentini M, Namy O.** 2014. New insights into the incorporation of natural suppressor tRNAs at stop codons in *Saccharomyces cerevisiae*. Nucleic Acids Research **42:**10061-10072.

341. **Citti C, Marechal-Drouard L, Saillard C, Weil JH, Bove JM.** 1992. *Spiroplasma citri* UGG and UGA tryptophan codons: sequence of the two tryptophanyl-tRNAs and organization of the corresponding genes. Journal of Bacteriology **174:**6471-6478.
342. **Feng YX, Copeland TD, Croszlan S, Rein A, Levin JG.** 1990. Identification of amino acids inserted during suppression of UAA and UGA termination codons at the gag-pol junction of Moloney leukemia virus. Proceedings of the National Academy of Sciences of the United States of America **87:**8860-8863.
343. **Maynard EL, Lindahl PA.** 1999. Evidence of a molecular tunnel connecting the active sites for CO2 reduction and acetyl-CoA synthesis in acetyl-CoA synthase from *Clostridium thermoaceticum*. Journal of the American Chemical Society **121:**9221-9222.
344. **Seravalli J, Ragsdale SW.** 2000. Channeling of carbon monoxide during anaerobic carbon dioxide fixation. Biochemistry **39:**1274-1277.
345. **Bar-Even A.** 2013. Does acetogenesis really require especially low reduction potential? Biochimica et Biophysica Acta **1827:**395-400.
346. **Peng H, Wu GG, Shao WL.** 2008. The aldehyde/alcohol dehydrogenase (AdhE) in relation to the ethanol formation in *Thermoanaerobacter ethanolicus* JW200. Anaerobe **14:**125-127.
347. **Membrillo-Hernandez J, Echave P, Cabiscol E, Tamarit J, Ros J, Lin EC.** 2000. Evolution of the *adhE* gene product of *Escherichia coli* from a functional reductase to a dehydrogenase. Genetic and biochemical studies of the mutant proteins. Journal of Biological Chemistry **275:**33869-33875.
348. **Arnau J, Jørgensen F, Madsen SM, Vrang A, Israelsen H.** 1998. Cloning of the *Lactococcus lactis adhE* gene, encoding a multifunctional alcohol dehydrogenase, by complementation of a fermentative mutant of *Escherichia coli*. Journal of Bacteriology **180:**3049-3055.
349. **Extance J, Crennell SJ, Eley K, Cripps R, Hough DW, Danson MJ.** 2013. Structure of a bifunctional alcohol dehydrogenase involved in bioethanol generation in *Geobacillus thermoglucosidasius*, p 2104-2115, Acta Crystallography Section D, Biological Crystallography, vol 69, United States.
350. **Lo J, Zheng T, Hon S, Olson DG, Lynd LR.** 2015. The bifunctional alcohol and aldehyde dehydrogenase gene, *adhE*, is necessary for ethanol production in *Clostridium thermocellum* and *Thermoanaerobacterium saccharolyticum*. Journal of Bacteriology **197:**1386-1393.
351. **Chen M, Li E, Stanley SL, Jr.** 2004. Structural analysis of the acetaldehyde dehydrogenase activity of *Entamoeba histolytica* alcohol dehydrogenase 2 (EhADH2), a member of the ADHE enzyme family. Molecular and Biochemical Parasitology **137:**201-205.
352. **Espinosa A, Yan L, Zhang Z, Foster L, Clark D, Li E, Stanley SL, Jr.** 2001. The bifunctional *Entamoeba histolytica* alcohol dehydrogenase 2 (EhADH2) protein is necessary for amebic growth and survival and requires an intact C-terminal domain for both alcohol dehydrogenase and acetaldehyde dehydrogenase activity. Journal of Biological Chemistry **276:**20136-20143.
353. **Kessler D, Leibrecht I, Knappe J.** 1991. Pyruvate-formate-lyase-deactivase and acetyl-CoA reductase activities of *Escherichia coli* reside on a polymeric protein particle encoded by *adhE*. Federation of European Biochemical Society Letters **281:**59-63.
354. **Henikoff S, Henikoff JG.** 1992. Amino acid substitution matrices from protein blocks. Proceedings of the National Academy of Sciences of the United States of America **89:**10915-10919.
355. **Thormann K, Feustel L, Lorenz K, Nakotte S, Dürre P.** 2002. Control of butanol formation in *Clostridium acetobutylicum* by transcriptional activation. Journal of Bacteriology **184:**1966-1973.
356. **Zheng T, Olson DG, Tian L, Bomble YJ, Himmel ME, Lo J, Hon S, Shaw AJ, van Dijken JP, Lynd LR.** 2015. Cofactor specificity of the bifunctional alcohol and aldehyde dehydrogenase (AdhE) in wild-type and mutant *Clostridium thermocellum* and *Thermoanaerobacterium saccharolyticum*. Journal of Bacteriology **197:**2610-2619.
357. **Brown SD, Guss AM, Karpinets TV, Parks JM, Smolin N, Yang S, Land ML, Klingeman DM, Bhandiwad A, Rodriguez M, Raman B, Shao X, Mielenz JR, Smith JC, Keller M, Lynd LR.** 2011. Mutant alcohol dehydrogenase leads to improved ethanol tolerance in *Clostridium thermocellum*. Proceedings of the National Academy of Sciences of the United States of America **108:**13752-13757.
358. **Alberts B, Johnson A, Lewis J, Raff M, Roberts K, Walter P.** 2002. Catalysis and the use of energy by cells, Molecular Biology of The Cell, 4th Ed ed. Garland Science, New York.
359. **Yao S, Mikkelsen MJ.** 2010. Identification and overexpression of a bifunctional aldehyde/alcohol dehydrogenase responsible for ethanol production in *Thermoanaerobacter mathranii*. Journal of Molecular Microbiology and Biotechnology **19:**123-133.
360. **Kerfeld CA, Heinhorst S, Cannon GC.** 2010. Bacterial microcompartments. Annual Review of Microbiology **64:**391-408.
361. **Kinney JN, Axen SD, Kerfeld Ca.** 2011. Comparative analysis of carboxysome shell proteins. Photosynthesis Research **109:**21-32.
362. **Yeates TO, Kerfeld Ca, Heinhorst S, Cannon GC, Shively JM.** 2008. Protein-based organelles in bacteria: carboxysomes and related microcompartments. Nature Reviews Microbiology **6:**681-691.
363. **Jang Y-S, Lee JY, Lee J, Park JH, Im JA, Eom M-H, Lee J, Lee S-H, Song H, Cho J-H, Seung DY, Lee SY.** 2012. Enhanced butanol production obtained by reinforcing the direct butanol-forming route in *Clostridium acetobutylicum*. mBio **3:**1-9.

364. **Maddox IS, Steiner E, Hirsch S, Wessner S, Gutierrez NA, Gapes JR, Schuster KC.** 2000. The cause of "acid-crash" and "acidogenic fermentations" during the batch acetone-butanol-ethanol (ABE-) fermentation process. Journal of Molecular Microbiology and Biotechnology **2:**95-100.
365. **Russell JB.** 1992. Another explanation for the toxicity of fermentation acids at low pH: anion accumulation versus uncoupling. Journal of Applied Bacteriology **73:**363-370.
366. **Heider J, Ma K, Adams MW.** 1995. Purification, characterization, and metabolic function of tungsten-containing aldehyde ferredoxin oxidoreductase from the hyperthermophilic and proteolytic archaeon *Thermococcus* strain ES-1. Journal of Bacteriology **177:**4757-4764.
367. **Mukund S, Adams MW.** 1991. The novel tungsten-iron-sulfur protein of the hyperthermophilic archaebacterium, *Pyrococcus furiosus*, is an aldehyde ferredoxin oxidoreductase. Evidence for its participation in a unique glycolytic pathway. Journal of Biological Chemistry **266:**14208-14216.
368. **Rauh D, Graentzdoerffer A, Granderath K, Andreesen JR, Pich A.** 2004. Tungsten-containing aldehyde oxidoreductase of *Eubacterium acidaminophilum*. European Journal of Biochemistry **219:**212-219.
369. **Chan MK, Mukund S, Kletzin A, Adams MW, Rees DC.** 1995. Structure of a hyperthermophilic tungstopterin enzyme, aldehyde ferredoxin oxidoreductase. Science **267:**1463-1469.
370. **Loach PA.** 1976. Oxidation-reduction potentials, absorbance bands and molar absorbance of compounds used in biochemical studies, p 122 - 130. *In* Fasman GD (ed), Handbook of biochemistry and molecular biology, vol 1. CRC Press, Cleveland.
371. **White H, Strobl G, Feicht R, Simon H.** 1989. Carboxylic acid reductase: a new tungsten enzyme catalyses the reduction of non-activated carboxylic acids to aldehydes. European Journal of Biochemistry **184:**89-96.
372. **White H, Feicht R, Huber C, Lottspeich F, Simon H.** 1991. Purification and some properties of the tungsten-containing carboxylic acid reductase from *Clostridium formicoaceticum*. Biological Chemistry Hoppe Seyler **372:**999-1005.
373. **White H, Huber C, Feicht R, Simon H.** 1993. On a reversible molybdenum-containing aldehyde oxidoreductase from *Clostridium formicoaceticum*. Archives of Microbiology **159:**244-249.
374. **Perez JM, Richter H, Loftus SE, Angenent LT.** 2013. Biocatalytic reduction of short-chain carboxylic acids into their corresponding alcohols with syngas fermentation. Biotechnology and Bioenginineering **110:**1066-1077.
375. **Seo JS, Chong H, Park HS, Yoon KO, Jung C, Kim JJ, Hong JH, Kim H, Kim JH, Kil JI.** 2005. The genome sequence of the ethanologenic bacterium *Zymomonas mobilis* ZM4. Nature Biotechnology **23:**63-68.
376. **Lucena BTL, dos Santos BM, Moreira KLS, Moreira APB, Nunes AC, Azevedo V, Miyoshi A, Thompson FL, Morais Junior MA.** 2010. Diversity of lactic acid bacteria of the bioethanol process. Bio-Med Central Microbiology **10:**1-8.
377. **Ingram LO.** 1990. Ethanol tolerance in bacteria. Critical Reviews in Microbiology **9:**305-319.
378. **Knoshaug EP, Zhang M.** 2009. Butanol tolerance in a selection of microorganisms. Applied Biochemistry and Biotechnology **153:**13-20.
379. **Dunlop MJ.** 2011. Engineering microbes for tolerance to next-generation biofuels. Biotechnology for Biofuels **4:**1-9.
380. **Li J, Zhao JB, Zhao M, Yang YL, Jiang WH, Yang S.** 2010. Screening and characterization of butanol-tolerant micro-organisms. Letters in Applied Microbiology **50:**373-379.
381. **Rühl J, Schmid A, Blank LM.** 2009. Selected *Pseudomonas putida* strains able to grow in the presence of high butanol concentrations. Applied and Environmental Microbiology **75:**4653-4656.
382. **Madson PW.** 2003. The Alcohol Textbook, 4th ed. Nottingham University Press.
383. **Nicolaou SA, Gaida SM, Papoutsakis ET.** 2010. A comparative view of metabolite and substrate stress and tolerance in microbial bioprocessing: From biofuels and chemicals, to biocatalysis and bioremediation. Metabolic Engineering **12:**307-331.
384. **Zingaro KA, Nicolaou SA, Papoutsakis ET.** 2013. Dissecting the assays to assess microbial tolerance to toxic chemicals in bioprocessing. Trends in Biotechnology **31:**643-653.
385. **Isken S, de Bont JA.** 1998. Bacteria tolerant to organic solvents. Extremophiles **2:**229-238.
386. **Sikkema J, de Bont JA, Poolman B.** 1995. Mechanisms of membrane toxicity of hydrocarbons. Microbiology Review **59:**201-222.
387. **Junker F, Ramos JL.** 1999. Involvement of the cis/trans isomerase Cti in solvent resistance of *Pseudomonas putida* DOT-T1E. Journal of Bacteriology **181:**5693-5700.
388. **Ramos JL, Duque E, Gallegos MT, Godoy P, Ramos-Gonzalez MI, Rojas A, Teran W, Segura A.** 2002. Mechanisms of solvent tolerance in Gram-negative bacteria. Annual Review of Microbiology **56:**743-768.
389. **Putman M, van Veen HW, Konings WN.** 2000. Molecular properties of bacterial multidrug transporters. Microbiology and Molecular Biology Review **64:**672-693.
390. **Rutherford BJ, Dahl RH, Price RE, Szmidt HL, Benke PI, Mukhopadhyay A, Keasling JD.** 2010. Functional genomic study of exogenous n-butanol stress in *Escherichia coli*. Applied and Environmental Microbiology **76:**1935-1945.

391. **Borden JR, Papoutsakis ET.** 2007. Dynamics of genomic-library enrichment and identification of solvent tolerance genes for *Clostridium acetobutylicum*. Applied and Environmental Microbiology **73:**3061-3068.
392. **Kim YE, Hipp MS, Bracher A, Hayer-Hartl M, Hartl FU.** 2013. Molecular chaperone functions in protein folding and proteostasis. Annual Review of Biochemistry **82:**323-355.
393. **Mao S, Luo Y, Zhang T, Li J, Bao G, Zhu Y, Chen Z, Zhang Y, Li Y, Ma Y.** 2010. Proteome reference map and comparative proteomic analysis between a wild type *Clostridium acetobutylicum* DSM 1731 and its mutant with enhanced butanol tolerance and butanol yield. Journal of Proteome Research **9:**3046-3061.
394. **Zingaro KA, Papoutsakis ET.** 2012. Toward a semisynthetic stress response system to engineer microbial solvent tolerance. mBio **3:**1-9.
395. **Fujiwara K, Ishihama Y, Nakahigashi K, Soga T, Taguchi H.** 2010. A systematic survey of in vivo obligate chaperonin-dependent substrates. European Molecular Biology Organization Journal **29:**1552-1564.
396. **Kerner MJ, Naylor DJ, Ishihama Y, Maier T, Chang HC, Stines AP, Georgopoulos C, Frishman D, Hayer-Hartl M, Mann M, Hartl FU.** 2005. Proteome-wide analysis of chaperonin-dependent protein folding in *Escherichia coli*. Cell **122:**209-220.
397. **Calloni G, Chen T, Schermann SM, Chang HC, Genevaux P, Agostini F, Tartaglia GG, Hayer-Hartl M, Hartl FU.** 2012. DnaK functions as a central hub in the *E. coli* chaperone network. Cell Reports **1:**251-264.
398. **Braig K, Otwinowski Z, Hegde R, Boisvert DC, Joachimiak A, Horwich AL, Sigler PB.** 1994. The crystal structure of the bacterial chaperonin GroEL at 2.8 A. Nature **371:**578-586.
399. **Boisvert DC, Wang J, Otwinowski Z, Norwich AL, Sigler PB.** 1996. The 2.4 A crystal structure of the bacterial chaperonin GroEL complexed with ATP[gamma]S. Nature Structural and Molecular Biology **3:**170-177.
400. **Ranson NA, White HE, Saibil HR.** 1998. Chaperonins. Biochemical Journal **333:**233-242.
401. **Lee S, Sowa ME, Watanabe YH, Sigler PB, Chiu W, Yoshida M, Tsai FTF.** 2003. The structure of clpB: A molecular chaperone that rescues proteins from an aggregated state. Cell **115:**229-240.
402. **Barnett ME, Zolkiewska A, Zolkiewski M.** 2000. Structure and activity of ClpB from *Escherichia coli* - Role of the amino- and carboxyl-terminal domains. Journal of Biological Chemistry **275:**37565-37571.
403. **Yuan G, Wong SL.** 1995. Isolation and characterization of *Bacillus subtilis groE* regulatory mutants: evidence for orf39 in the *dnaK* operon as a repressor gene in regulating the expression of both *groE* and *dnaK*. Journal of Bacteriology **177:**6462-6468.
404. **Minder AC, Fischer HM, Hennecke H, Narberhaus F.** 2000. Role of HrcA and CIRCE in the heat shock regulatory network of *Bradyrhizobium japonicum*. Journal of Bacteriology **182:**14-22.
405. **Zuber U, Schumann W.** 1994. CIRCE, a novel heat shock element involved in regulation of heat shock operon *dnaK* of *Bacillus subtilis*. Journal of Bacteriology **176:**1359-1363.
406. **van Asseldonk M, Simons A, Visser H, de Vos WM, Simons G.** 1993. Cloning, nucleotide sequence, and regulatory analysis of the *Lactococcus lactis dnaJ* gene. Journal of Bacteriology **175:**1637-1644.
407. **Nakamoto H, Suzuki M, Kojima K.** 2003. Targeted inactivation of the hrcA repressor gene in cyanobacteria. Federation of European Biochemical Society Letters **549:**57-62.
408. **Chow KC, Tung WL.** 1998. Overexpression of *dnaK/dnaJ* and *groEL* confers freeze tolerance to *Escherichia coli*. Biochemical and Biophysical Research Communications **253:**502-505.
409. **Kumar M, Prasanna R, Lone S, Padaria JC, Saxena AK.** 2014. Cloning and expression of *dnaK* gene from *Bacillus pumilus* of hot water spring origin. Applied and Translational Genomics **3:**14-20.
410. **Michel GP.** 1993. Cloning and expression in *Escherichia coli* of the *dnaK* gene of *Zymomonas mobilis*. Journal of Bacteriology **175:**3228-3231.
411. **Desmond C, Fitzgerald GF, Stanton C, Ross RP.** 2004. Improved stress tolerance of GroESL-overproducing *Lactococcus lactis* and probiotic *Lactobacillus paracasei* NFBC 338. Applied and Environmental Microbiology **70:**5929-5936.
412. **Sugimoto S, Nakayama J, Fukuda D, Sonezaki S, Watanabe M, Tosukhowong A, Sonomoto K.** 2003. Effect of heterologous expression of molecular chaperone DnaK from *Tetragenococcus halophilus* on salinity adaptation of *Escherichia coli*. Journal of Bioscience and Bioengineering **96:**129-133.
413. **Chaurasia AK, Apte SK.** 2009. Overexpression of the *groESL* operon enhances the heat and salinity stress tolerance of the nitrogen-fixing *Cyanobacterium anabaena* sp Strain PCC7120. Applied and Environmental Microbiology **75:**6008-6012.
414. **Abdullah Al M, Sugimoto S, Higashi C, Matsumoto S, Sonomoto K.** 2010. Improvement of multiple-stress tolerance and lactic acid production in *Lactococcus lactis* NZ9000 under conditions of thermal stress by heterologous expression of *Escherichia coli dnaK*. Applied and Environmental Microbiology **76:**4277-4285.
415. **Fiocco D, Capozzi V, Goffin P, Hols P, Spano G.** 2007. Improved adaptation to heat, cold, and solvent tolerance in *Lactobacillus plantarum*. Applied Microbiology and Biotechnology **77:**909-915.

416. **Bormann S, Baer ZC, Sreekumar S, Kuchenreuther JM, Dean Toste F, Blanch HW, Clark DS.** 2014. Engineering *Clostridium acetobutylicum* for production of kerosene and diesel blendstock precursors. Metabolic Engineering **25:**124-130.
417. **Zingaro KA, Terry Papoutsakis E.** 2013. GroESL overexpression imparts *Escherichia coli* tolerance to i-, n-, and 2-butanol, 1,2,4-butanetriol and ethanol with complex and unpredictable patterns. Metabolic Engineering **15:**196-205.
418. **Martin J, Langer T, Boteva R, Schramel A, Horwich AL, Hartl FU.** 1991. Chaperonin-mediated protein folding at the surface of groEL through a 'molten globule'-like intermediate. Nature **352:**36-42.
419. **Chapman E, Farr GW, Fenton WA, Johnson SM, Horwich AL.** 2008. Requirement for binding multiple ATPs to convert a GroEL ring to the folding-active state. Proceedings of the National Academy of Sciences of the United States of America **105:**19205-19210.
420. **Mogk A, Homuth G, Scholz C, Kim L, Schmid FX, Schumann W.** 1997. The GroE chaperonin machine is a major modulator of the CIRCE heat shock regulon of *Bacillus subtilis*. The European Molecular Biology Organization Journal **16:**4579-4590.
421. **Schulz A, Schumann W.** 1996. *hrcA*, the first gene of the *Bacillus subtilis dnaK* operon encodes a negative regulator of class I heat shock genes. Journal of Bacteriology **178:**1088-1093.
422. **Reischl S, Wiegert T, Schumann W.** 2002. Isolation and analysis of mutant alleles of the *Bacillus subtilis* HrcA repressor with reduced dependency on GroE function. Journal of Biological Chemistry **277:**32659-32667.
423. **Parsons LM, Limberger RJ, Shayegani M.** 1997. Alterations in levels of DnaK and GroEL result in diminished survival and adherence of stressed *Haemophilus ducreyi*. Infection and Immunity **65:**2413-2419.
424. **Saibil H.** 2013. Chaperone machines for protein folding, unfolding and disaggregation. Nature Reviews Molecular Cell Biology **14:**630-642.
425. **Rüdiger S, Buchberger A, Bukau B.** 1997. Interaction of Hsp70 chaperones with substrates. Nature Structural and Molecular Biology **4:**342-349.
426. **Rüdiger S, Germeroth L, Schneider-Mergener J, Bukau B.** 1997. Substrate specificity of the DnaK chaperone determined by screening cellulose-bound peptide libraries. The European Molecular Biology Organization Journal **16:**1501-1507.
427. **Zhu X, Zhao X, Burkholder WF, Gragerov A, Ogata CM, Gottesman ME, Hendrickson WA.** 1996. Structural analysis of substrate binding by the molecular chaperone DnaK. Science **272:**1606-1614.
428. **Van Durme J, Maurer-Stroh S, Gallardo R, Wilkinson H, Rousseau F, Schymkowitz J.** 2009. Accurate prediction of DnaK-peptide binding via homology modelling and experimental data. PLoS Computational Biology **5:**e1000475.
429. **Sharma SK, De Los Rios P, Christen P, Lustig A, Goloubinoff P.** 2010. The kinetic parameters and energy cost of the Hsp70 chaperone as a polypeptide unfoldase. Nature Chemical Biology **6:**914-920.
430. **Guisbert E, Herman C, Lu CZ, Gross CA.** 2004. A chaperone network controls the heat shock response in *E. coli*. Genes and Development **18:**2812-2821.
431. **Larsen H.** 1986. Halophilic and halotolerant microorganisms-an overview and historical perspective. Federation of European Microbiological Society Microbiology Letters **39:**3-7.
432. **Blum P, Ory J, Bauernfeind J, Krska J.** 1992. Physiological consequences of DnaK and DnaJ overproduction in *Escherichia coli*. Journal of Bacteriology **174:**7436-7444.
433. **Martinez-Alonso M, Garcia-Fruitos E, Ferrer-Miralles N, Rinas U, Villaverde A.** 2010. Side effects of chaperone gene co-expression in recombinant protein production. Microbial Cell Factories **9:**64.
434. **Yang SH, Pan CL, Tschaplinski TJ, Hurst GB, Engle NL, Zhou W, Dam P, Xu Y, Rodriguez M, Dice L, Johnson CM, Davison BH, Brown SD.** 2013. Systems biology analysis of *Zymomonas mobilis* ZM4 ethanol stress responses. Plos ONE **8:**1-14.
435. **Utturkar SM, Klingeman DM, Bruno-Barcena JM, Chinn MS, Grunden AM, Köpke M, Brown SD.** 2015. Sequence data for *Clostridium autoethanogenum* using three generations of sequencing technologies. Scientific Data **2:**1-9.
436. **Zhang Y, Grosse-Honebrink A, Minton NP.** 2015. A universal mariner transposon system for forward genetic studies in the genus *Clostridium*. PLoS ONE **10:**e0122411.
437. **Jeong J, Bertsch J, Hess V, Choi S, Choi I-G, Chang IS, Müller V.** 2015. A model for energy conservation based on genomic and experimental analyses in a carbon monoxide-utilizing, butyrate-forming acetogen, *Eubacterium limosum* KIST612. Applied and Environmental Microbiology**:**Published ahead of print.
438. **Dembek M, Barquist L, Boinett CJ, Cain AK, Mayho M, Lawley TD, Fairweather NF, Fagan RP.** 2015. High-throughput analysis of gene essentiality and sporulation in *Clostridium difficile*. mBio **6:**e02383-02314.
439. **Jones JA, Toparlak ÖD, Koffas MAG.** 2015. Metabolic pathway balancing and its role in the production of biofuels and chemicals. Current Opinion in Biotechnology **33:**52-59.

440. **Dueber JE, Wu GC, Malmirchegini GR, Moon TS, Petzold CJ, Ullal AV, Prather KLJ, Keasling JD.** 2009. Synthetic protein scaffolds provide modular control over metabolic flux. Nature Biotechnology **27:**753-759.

441. **Govindarajan S, Nevo-Dinur K, Amster-Choder O.** 2012. Compartmentalization and spatiotemporal organization of macromolecules in bacteria. Federation of European Microbiological Society Microbiology Review **36:**1005-1022.

442. **Cornejo E, Abreu N, Komeili A.** 2014. Compartmentalization and organelle formation in bacteria. Current Opinion in Cell Biology **26:**132-138.

443. **Schuchmann K, Schmidt S, Martinez Lopez A, Kaberline C, Kuhns M, Lorenzen W, Bode HB, Joos F, Müller V.** 2015. Nonacetogenic growth of the acetogen *Acetobacterium woodii* on 1,2-propanediol. Journal of Bacteriology **197:**382-391.

444. **Jiang W, Bikard D, Cox D, Zhang F, Marraffini LA.** 2013. CRISPR-assisted editing of bacterial genomes. Nature Biotechnology **31:**233-239.

445. **Ryan OW, Skerker JM, Maurer MJ, Li X, Tsai JC, Poddar S, Lee ME, DeLoache W, Dueber JE, Arkin AP, Cate JHD.** 2014. Selection of chromosomal DNA libraries using a multiplex CRISPR system. eLife **3:**e03703.

446. **Wang Y, Zhang ZT, Seo SO, Choi K, Lu T, Jin YS, Blaschek HP.** 2015. Markerless chromosomal gene deletion in *Clostridium beijerinckii* using CRISPR/Cas9 system. Journal of Biotechnology **200:**1-5.

447. **Wang HH, Isaacs FJ, Carr PA, Sun ZZ, Xu G, Forest CR, Church GM.** 2009. Programming cells by multiplex genome engineering and accelerated evolution. Nature **460:**894-898.